UNIVERSIDADE FEDERAL DE SANTA CATARINA

CAMPUS REITOR JOÃO DAVID FERREIRA LIMA

PROGRAMA DE PÓS-GRADUAÇÃO EM ENGENHARIA AMBIENTAL

Camyla Innocente dos Santos

Investigating physical controls of streamflow generation through baseflow campaigns

Florianópolis

2024

Camyla Innocente dos Santos

Investigating physical controls of streamflow generation through baseflow campaigns

Tese submetida ao Programa de pós-graduação em Engenharia Ambiental da Universidade Federal de Santa Catarina como requisito parcial para a obtenção do título de doutora em Engenharia Ambiental
Orientador: Prof. Pedro Luiz Borges Chaffe, Dr.
Co-orientador: Prof. Julian Klaus, Dr.

Florianópolis

2024

Camyla Innocente dos Santos

Investigating physical controls of streamflow generation through baseflow campaigns

O presente trabalho em nível de Doutorado foi avaliado e aprovado, em 28 de junho de 2024, pela banca examinadora composta pelos seguintes membros:

Profa. Aline de Almeida Mota, Dra.
Universidade Federal da Fronteira Sul

Prof. Gean Paulo Michel, Dr.
Universidade Federal Rio Grande do Sul

Prof. Leonardo Hoinaski, Dr.
Universidade Federal de Santa Catarina

Certificamos que esta é a versão original e final do trabalho de conclusão que foi julgado adequado para obtenção do título de Doutora em Engenharia Ambiental

_____
Coordenação do Programa de Pós-Graduação

_____
Prof. Pedro Luiz Borges Chaffe, Dr.
Orientador

Florianópolis, 2024

AGRADECIMENTOS

RESUMO

Os rios de cabeceira são essenciais para transporte de sedimentos e remoção de nutrientes, além de fornecerem água para consumo humano e irrigação. No entanto, ainda é necessário entender os fatores que controlam a geração de vazão nesses rios. Para isso, o monitoramento hidrológico de longo prazo em pequenas bacias hidrográficas é fundamental, mas tem diminuído, especialmente em regiões tropicais e subtropicais. Como alternativa, campanhas de escoamento de base, que fornecem informações detalhadas no espaço, mas não no tempo, podem ser usadas para testar hipóteses sobre controles de geração de vazão. O objetivo da tese é analisar a influência das estruturas da paisagem na geração de vazão na bacia experimental da Lagoa Peri por meio de campanhas de escoamento de base. A bacia, de 19 km², é coberta pela Mata Atlântica, sua geologia é caracterizada por granito e dique de diabásio. Mediu-se a vazão em 31 bacias e amostramos isótopos ($\delta^{18}O$) em 26 bacias (áreas variando de 0,02 a 5,33 km²). O modelo matemático fisicamente baseado ParFlow-CLM, validado por meio dos dados de vazão, foi utilizado como experimento virtual com diferentes configurações geológicas. Nossos resultados mostraram que a variação espacial dos dados de vazão não pode ser explicada por erros de medição, o que indica que a diferença de vazões entre as sub-bacias está relacionada à capacidade de armazenamento e liberação da água subsuperficial. Sendo assim, as características subterrâneas (ex.: porosidade, condutividade hidráulica e profundidade do solo) são as responsáveis por diferença de vazão. O coeficiente de Spearman entre a porcentagem de diabásio e a vazão específica é 0,68 (*p-value* < 0,05). Concluímos que, devido aos diques de diabásio serem mais rasos e terem maior permeabilidade, eles fornecem mais água aos rios durante o escoamento de base. Os dados de isótopos não puderam ser explicados por meio da topografia em sub-bacias com geologia heterogênea (granito e diabásio), e estão relacionados à área em bacias caracterizadas por geologia homogênea (granito), mostrando que uma geologia heterogênea resulta em caminhos subterrâneos mais diversificados. Kling–Gupta efficiency passou de -0,10 para 0,36 em uma série horária de vazão, apenas ao aumentar o grau de heterogeneidade subsuperficial no modelo ParFlow-CLM. Esse resultado destaca a importância da geologia e do solo para o entendimento da geração de vazão. Os resultados sugerem que as medições em bacias aninhadas durante condições de escoamento de base refletem a heterogeneidade das diferentes fontes que contribuem para os rios, sendo uma ferramenta poderosa para entender padrões de geração de escoamento em bacias subtropicais e tropicais, onde o monitoramento contínuo é difícil de implementar.

RESUMO EXPANDIDO

INTRODUÇÃO

Os rios de cabeceira desempenham um papel crucial na geração de escoamento, no transporte de sedimentos e na remoção de nutrientes em ambientes aquáticos. Além disso, a água desses rios é utilizada para consumo humano, irrigação e recreação. Portanto, compreender os processos de geração de escoamento e quantificar o armazenamento e a liberação de água em pequenas bacias é essencial para a gestão dos recursos hídricos. Para enfrentar desafios sociais críticos e avançar no entendimento hidrológico, é necessário expandir o trabalho de campo com monitoramento hidrológico, especialmente em regiões sub-representadas do mundo, como áreas tropicais e subtropicais. No entanto, esses estudos têm diminuído em comparação com os esforços de modelagem. No Brasil, por exemplo, um País vasto com 10 zonas climáticas e 6 biomas naturais, existem poucas bacias experimentais, e a continuidade da maioria dos monitoramentos tem sido prejudicada pela redução de recursos financeiros.

A falta de dados experimentais na hidrologia tem sido reconhecida como um grande obstáculo para avançar na pesquisa. Embora haja planos claros para conduzir redes de dados em diversas paisagens, como o Long Term Ecological Research (LTER), a rede Critical Zone Observatory (CZO) e os Observatórios Ambientais Terrestres (TERENO), manter essas redes em várias localidades é inviável, especialmente em regiões menos estudadas. Uma alternativa é equilibrar equipamentos de custo acessível, tecnologia simples e fontes de dados não convencionais para expandir a observação hidrológica. Breves campanhas de coleta de dados combinadas com o modelo físico ParFlow-CLM em rios com diferentes características de paisagem podem fornecer informações sobre como a água flui e é armazenada, além de estimativas das fontes nos cursos d'água. Essas campanhas podem complementar dados monitorados continuamente e ajudar a entender a relação entre as características da paisagem e os processos hidrológicos em diferentes ambientes. Portanto, o objetivo dessa tese é analisar a influência das estruturas da paisagem na geração de vazão na Bacia Experimental da Lagoa Peri por meio de campanhas de escoamento de base.

MATERIAIS E MÉTODOS

A área de estudo compreende a Bacia Experimental da Lagoa do Peri, situada no sul do Brasil. Esta bacia, abrangendo uma área de 19 km², é cercada por encostas cobertas por remanescentes de Mata Atlântica, com uma lagoa costeira de 5 km². Encontra-se na transição entre climas tropicais e temperados, apresentando uma precipitação média anual de 1700 mm, verões quentes e ausência de estação seca. A geologia da região é caracterizada por granito e diques de diabásio, sendo o granito consolidado posteriormente ao diabásio. Um aquífero de rochas fraturadas circunda a Lagoa do Peri. A profundidade do solo varia de acordo com a elevação, sendo que áreas mais elevadas e íngremes possuem um solo mais raso, com cerca de 1,0 m de profundidade, enquanto em áreas de menor elevação o solo atinge uma profundidade de aproximadamente 2,5 m. O solo residual do granito apresenta menor permeabilidade quando comparado ao solo residual de diabásio, o mesmo acontece quando comparado o granito ao diabásio. Ademais, regiões com a presença de diques de diabásio tendem a ter solos mais rasos.

Foram implementadas campanhas de medição espacialmente distribuídas durante o escoamento de base, para o monitoramento de: vazão, velocidade do fluxo e isótopos da água. Foram medidas um total de 31 seções transversais de rios diferentes para vazão utilizando diferentes métodos: diluição, volumétrico e velocidade *versus* área. Em 26 seções transversais de rios foram coletados isótopos. Foi coletada água para análise de isótopos da chuva em um pluviômetro e água subterrânea em quatro poços localizados em diferentes elevações. Ademais, dois sensores de níveis foram instalados e foram feitas as curvas-chave das seções, para obter um monitoramento contínuo. Também foram realizados ensaios para verificar a condutividade hidráulica e a taxa de infiltração em oito pontos diferentes da bacia hidrográfica.

Por meio dos dados coletados, verificou-se se a diferença entre as medições de vazão espacialmente distribuídas ocorria devido a erros de medição ou a diferenças nos processos hidrológicos. Por meio dos dados de isótopos e vazão, cruzando com dados das características das bacias hidrográficas (geologia, declividade, elevação e área), verificamos estatisticamente o papel da paisagem na geração de escoamento de base. Por fim, as medições de vazão espacialmente distribuídas, juntamente com a série de chuva-vazão, foram usadas para verificação do desempenho de um modelo fisicamente baseado, o ParFlow-CLM. Por meio dele, é possível entender o escoamento dos rios e o armazenamento da bacia hidrográfica continuamente no tempo e no espaço, o que facilita o entendimento do papel da paisagem na geração de vazão.

RESULTADOS E DISCUSSÃO

Os erros de medição de vazão, em média, foram menores que 10%, enquanto a diferença entre as vazões específicas (vazão dividido pela área da bacia) variaram 99 vezes entre o menor valor e o maior. O erro e as diferenças entre as medições de vazão foram compatíveis com outros trabalhos da literatura e mostraram que a diferença entre as medições refletem processos internos de armazenamento e liberação da água que estão relacionados à estrutura física da bacia hidrográfica.

Ao avaliar a relação estatística entre os dados de vazão específica e a geologia, observou-se que o coeficiente de Spearman foi de -0,68 (*p-value* < 0,05) entre a porcentagem de granito e a vazão específica. Enquanto isso, em sub-bacias caracterizadas apenas com granito, o coeficiente de Spearman foi de 0,72 (*p-value* < 0,05) entre a vazão específica e a elevação média. Ambas as correlações estão relacionadas à geologia. No primeiro caso, isso se justifica pelo fato de que o granito é mais antigo que o diabásio, e geologias mais antigas tendem a ter um escoamento superficial, enquanto geologias mais jovens têm um escoamento subsuperficial. A relação positiva com a elevação média está relacionada ao aquífero fraturado que circunda a lagoa, onde as áreas mais baixas das bacias direcionam água diretamente para a lagoa e não para os rios, resultando em uma vazão menor nos rios em lugares de baixa elevação. Os valores dos isótopos indicam que o escoamento de base é uma mistura de água da precipitação e do armazenamento local de água. No entanto, não foi possível detectar nenhuma correlação entre as características físicas das bacias e os isótopos em sub-bacias com diques de diabásio, o que indica que os fluxos de água subsuperficial são mais heterogêneos em geologias heterogêneas.

Por fim, por meio da aplicação do ParFlow-CLM, validando o *spin-up* pelas medições de vazão durante o escoamento de base e validando a resposta dos rios aos dados meteorológicos por meio de duas séries de chuva-vazão, foi possível verificar que a geologia é um fator determinante para a ativação da rede de drenagem e armazenamento de água na bacia. Comparando dois cenários – um que representa a realidade geológica da bacia hidrográfica e outro que representa uma subsuperfície homogênea – foi possível verificar que o KGE melhora de -0,10 para 0,36 apenas com a apresentação de uma geologia mais coerente.

CONCLUSÕES

As campanhas de escoamento de base mostraram variabilidade espacial significativa na vazão específica e nos valores de $\delta^{18}O$, que não pode ser explicada por erros de medição. Os padrões de $\delta^{18}O$ nos rios mostram que o subsolo pode alterar o $\delta^{18}O$ da chuva por meio de mistura. A complexidade geológica é crucial para prever tanto o $\delta^{18}O$ quanto a vazão onde há estruturas geológicas mais complexas dificultando a previsão dos padrões de escoamento. Modelos experimentais virtuais, como o ParFlow, fornecem *insights* sobre como a heterogeneidade do subsolo pode alterar os padrões de vazão em diferentes estados de saturação, destacando a importância de se concentrar na geologia como fator controlador primário no ciclo hidrológico em pequenas escalas. Isso enfatiza a necessidade de usar dados geológicos e hidrológicos detalhados para melhorar as previsões de vazão e desenvolver estratégias para tornar os recursos hídricos mais sustentáveis e resilientes em diferentes ambientes geológicos.

ABSTRACT

Headwater streams are essential for sediment transport and nutrient removal, as well as providing water for human consumption and irrigation. However, the factors controlling streamflow generation in these streams still need to be better understood. Long-term hydrological monitoring in small catchments is crucial for this understanding, but it has been declining, especially in tropical and subtropical regions. As an alternative, baseflow campaigns, which provide detailed spatial but not temporal information, can be used to test hypotheses about the controls of streamflow generation. The objective of this thesis is to analyze the influence of landscape structures on streamflow generation in the Peri Lake Experimental Catchment (PLEC) through baseflow campaigns. PLEC (19 km²) is covered by the Atlantic Forest, and its geology is characterized by granite and diabase dikes. Streamflow was measured in 31 subcatchments, and isotopes ($\delta^{18}O$) were sampled in 26 subcatchments (areas ranging from 0.02 to 5.33 km²). The physically-based model ParFlow-CLM, validated using baseflow data, was used to conduct a virtual experiment with different geological configurations. The spatial variation of baseflow data cannot be explained by measurement errors, indicating that the differences in flows between subcatchments are related to subsurface water storage capacity and release, thus, subsurface characteristics (e.g., porosity, hydraulic conductivity, and soil depth). The Spearman coefficient between the percentage of diabase and specific baseflow is 0.68 (p-value < 0.05), we concluded that, due to diabase dikes being shallower and having greater permeability, they deliver more water to stream during baseflow. Isotope data could not be explained by topography in subcatchments with diabase dikes and are related to area in subcatchments characterized by granite, showing that heterogeneous geology results in more heterogeneous subsurface pathways. The Kling–Gupta efficiency increased from -0.10 to 0.36 in a streamflow time series by simply increasing the degree of subsurface heterogeneity in the ParFlow-CLM model. This result highlights the importance of geology and soil for understanding streamflow generation. The results suggest that measurements in nested catchments during baseflow conditions reflect the heterogeneity of the different sources to streams, being a powerful tool for understanding streamflow generation patterns in subtropical and tropical catchment, where continuous monitoring is difficult to implement.

LIST OF FIGURES

LIST OF TABLES

LIST OF ABBREVIATION AND ACRONYMS

CASAN	Santa Catarina Sanitation Company
FLORAM	Florianópolis Environmental Foundation
GIUH	Geomorphologic Instantaneous Unit Hydrograph
IBGE	Brazilian Institute of Geography and Statistics
IPUF	Urban Planning Institute of Florianópolis
IWVVTTF	Input Weighted Variable Velocity Travel Time Function
PLEC	Peri Lake Experimental Catchment
RGC	Ribeirão Grande Catchment
SDS	Secretary of Sustainable Development of Santa Catarina
SMOW	Standard Mean Ocean Water
UH	Unit Hydrograph
WF	Width Function
WFIUH	Width Function Instantaneous Unit Hydrograph

SUMMARY

1. INTRODUCTION

Headwater streams control a significant portion of streamflow generation (Sidle *et al.*, 2000), sediment transport, and nutrient removal in aquatic environments (Alexander; Smith; Schwarz, 2000). Furthermore, water from headwater streams is used for human consumption, irrigation, and recreation (Freeman; Pringle; Jackson, 2007). Therefore, understanding streamflow generation processes (Egusa *et al.*, 2019; Uchida; Asano, 2010) and quantifying storage and release in small catchment is essential for water resource management (Miller *et al.*, 2016). To address critical societal challenges and advance hydrological understanding, expanding fieldwork with hydrological monitoring is necessary (Burt; McDonnell, 2015; Grant; Dietrich, 2017; Tetzlaff *et al.*, 2017), especially in underrepresented regions of the world, such as tropical and subtropical areas (Tetzlaff *et al.*, 2017; Wohl *et al.*, 2012). However, there has been a decline in such studies compared to modelling efforts (Burt; McDonnell, 2015). In Brazil, for example, a vast country within 10 climatic zones and 6 natural biomes, there are few experimental catchments, and the continuity of most monitoring has been hindered by reduced funding availability (Melo *et al.*, 2020). The aim of this work is improving streamflow generation knowledge through baseflow campaigns in an underrepresented small subtropical coastal catchment.

Streamflow generation depends on various landscape structures that control storage and release of water. Slopes are linked to water storage capacity: steeper hillslopes typically exhibit greater variations in catchments storage (McGuire *et al.*, 2005; Sayama *et al.*, 2011) and shorter water residence times (McGuire *et al.*, 2005). Convergent hillslopes with large contributing areas usually drain more water into the drainage network than divergent hillslopes with smaller contributing areas (Beven, 1978; Jencso *et al.*, 2009). In catchments with permeable bedrock, water falling on hillslopes infiltrates through the soil until it reaches the water table and is discharged into larger streams (Asano *et al.*, 2020). Land cover is related to water loss through evapotranspiration, reducing the availability of water to streams (Evaristo; Jasechko; McDonnell, 2015; Lyon *et al.*, 2012). Furthermore, water flow in a catchment is also dependent on the amount of water it stores (Ameli *et al.*, 2018).

During dry periods (i.e., without rainfall events), the water stored in the catchments is transpired by vegetation, and lateral flow sustains baseflow (Fan *et al.*, 2019). During baseflow, it is considered that the water delivered in the streams is predominantly sourced from the soil

and the from the bedrock (Egusa *et al.*, 2016). Under baseflow conditions, it can be assumed that there are scaling relationships between specific discharge and the catchment area (Asano; Uchida, 2010; Egusa *et al.*, 2016; Wolock, 1995; Woods; Sivapalan, 1997; Woods; Sivapalan; Duncan, 1995). The threshold at which these patterns are defined is referred to as the representative elemental area (Wood *et al.*, 1988). The assumed hypothesis is that local heterogeneity in streamflow generation is attenuated by increasing the contributing area, and the rainfall-runoff relationship becomes controlled by the macro-scale characteristics of the catchment (Wood *et al.*, 1988). However, the idea that a uniform specific discharge can be assumed in catchments within the same landscape is still debated, especially in cases related to rainfall events and overland flow (Karlsen *et al.*, 2016).

During rainfall events, classical hydrological theories describe three runoff generation processes (McDonnell, 2013): i) when infiltration capacity is less than rainfall intensity (Horton, 1933); ii) when the soil is saturated (Dunne; Black, 1970); and iii) when water infiltrates, and what dominates the hydrograph is subsurface flow, where water flows laterally (Hursh; Brater, 1941). In the first and second processes, surface runoff dominates the hydrograph, and it can be observed that channels extend longitudinally, increasing catchment connectivity and influencing the transport of water, nutrients, and sediments (Godsey; Kirchner, 2014; Mutzner *et al.*, 2016; Perez *et al.*, 2020). By using tracers, it was possible to observe that most of the water present in the streams during the rainfall event did not originate from the rainfall itself (McDonnell, 1990; Pearce; Stewart; Sklash, 1986; Sklash; Farvolden, 1979). The water in the stream had been stored within the catchment for a long time (months or years), and this effect is known as the "old-water paradox" (Kirchner, 2003). Therefore, there are velocity and celerity within the catchment: one that we can observe using tracers and another that occurs only during rainfall events and shapes the flood hydrograph (McDonnell; Beven, 2014).

The characteristics of overland flow and baseflow provide valuable insights into water storage and flow controls. Monitoring baseflow can provide information about the quantity of water available within the catchment and the source of this water (e.g., groundwater, subsurface). Spatial variability in specific baseflow can reveal the relationship between water availability and physical catchment characteristics, such as reduced water availability in areas with higher evapotranspiration (Lyon *et al.*, 2012) and steep hillslopes (Floriancic *et al.*, 2019), and increased water availability in locations with fractured (Tetzlaff; Soulsby, 2008) or permeable rocks (Asano *et al.*, 2020). On the other hand, analysing the spatial variability of water chemistry characteristics (e.g., isotopes) can provide insights into the source of baseflow

(Egusa *et al.*, 2016; Fischer *et al.*, 2015; Fischer; van Meerveld; Seibert, 2017; Peralta-Tapia *et al.*, 2015). In addition, the accurate determination of the expansion and contraction of the drainage network can provide information about the origin of water through an understanding of groundwater dynamics on the slopes (Godsey; Kirchner, 2014; Mutzner *et al.*, 2016; Perez *et al.*, 2020).

One way to connect the processes responsible for streamflow generation, during baseflow and runoff conditions, is through physical based models, as ParFlow (Ajami; McCabe; Evans, 2015; Condon; Maxwell, 2013; Ferguson *et al.*, 2016; Janus *et al.*, 2023; Kollet; Maxwell, 2008; Maxwell *et al.*, 2016). In physical models based on the Richards equations, it is possible to combine groundwater with surface water resulting a better understanding of different storages compartment, soil, and bedrock, thus improving our understanding of the significance of landscape within the terrestrial hydrological cycle (Hrachowitz *et al.*, 2016). Usually, studies that use Parflow are calibrated through a continuous series of rainfall-runoff data at the catchment, at a single stream. Baseflow campaigns can help verify the model's accuracy in multiple streams, thus ensuring that the model accurately describes the process not only in time but also in space.

In this study, we investigated the streamflow generation process. We combined baseflow discharge measurement campaigns and chemical characteristics of baseflow with landscape structure analysis and rainfall-runoff modeling. This study is related to question 5 of Unsolved Problems in Hydrology (Blöschl *et al.*, 2019): What causes spatial heterogeneity and homogeneity in runoff, evaporation, subsurface water and material fluxes, and in their sensitivity to their controls?

The study area is the Peri Lake Experimental Catchment (PLEC), which is coastal lake of 5 km² surrounded by headwaters covered with Subtropical Atlantic Forest, with a total catchment area of 19 km². PLEC is located on the island of Florianópolis-SC, in a transition region between tropical and temperate climates. Besides being an important ecosystem for biodiversity preservation, the PLEC serves as a crucial water reservoir for public water supply and a recreational destination. This productive yet vulnerable coastal habitat can provide a foundation for studying the interaction between society and water (Montanari *et al.*, 2013) and can also be used for environmental education (Sidle, 2006). Despite its clear social and economic significance, information about this ecosystem is scarce, particularly concerning the dynamics of the water balance and water quality.

1.1 GENERAL OBJECTIVE

Analyze the influence of landscape structures on the streamflow generation of the Peri Lake Experimental Catchment through baseflow campaigns of discharge and isotopes.

1.2 SPECIFIC OBJECTIVES

- Verify whether the difference in baseflow among different headwater streams is related to measurement errors or differences in the amount of water storage.
- Investigate how the physical characteristics of catchments (e.g., area, slope, elevation, geology) control the quantity and quality of baseflow.
- Verify how geology controls runoff generation through virtual experiments using a physical model (ParFlow) validated using baseflow campaigns and short-time rainfall-runoff data series.

1.3 STRUCTURE OF THE THESIS

This thesis is organized as follows: in chapter 2, a literature review is conducted, mainly addressing the relationship between landscape and the streamflow generation. In chapter 3, the study area and experimental design are presented. In Chapter 3, we verify whether the difference in baseflow among different headwater streams is related to measurement errors or differences in the amount of water storage. In Chapter 4, we investigate how the physical characteristics of catchments (e.g. area, slope, elevation, and geology) control the quantity and quality of baseflow. In Chapter 5, we verify how geology controls runoff generation through virtual experiments using a physical based model (ParFlow), validated with baseflow campaigns and short-term rainfall-runoff data series. Chapter 7 brings a general conclusion.

2. LITERATURE REVIEW

2.1 HYDROLOGICAL CYCLE

The hydrological cycle describes the path of water in nature. When water evaporates, condenses, and then precipitates, it falls in the surface, with some of it being stored in vegetation, which later evaporates (Brutsaert, 2008), the evaporated water is called as interception loss (Equation 1). As precipitation continues, part of it infiltrates the soil, and part flows over the surface as surface runoff. Surface runoff tends to accumulate locally and eventually ends up in a larger body of water (e.g., a lake, ocean). Some of the infiltrated water flows in the shallow soil layers to emerge as springs or streams, while some infiltrates more slowly and joins the groundwater, which sooner or later flows into open water bodies. Some of the infiltrated water is retained in the soil through capillarity and other factors, making it available for absorption by vegetation roots. The hydrological cycle is closed by evapotranspiration, which returns the water to atmosphere. The schematic representation of the hydrological cycle can be seen in Figure 1.

There are three scales to describe the hydrological cycle: micro, meso, and macro. The microscale refers to the path of water within a pedon (the smallest recognized volume as soil); the mesoscale involves water movement within a catchment; and finally, the macroscale refers to water movement at continental scales. At the meso and especially the macro scales, spatial variability leads to increasing complexity of hydrological processes. At the mesoscale, there are challenges in estimating the complete water balance, particularly regarding the path water takes within the soil (Botter; Bertuzzo; Rinaldo, 2010). From micro to macro scales, there is also the issue of coupling terrestrial hydrological processes with the atmosphere (Imbrie; McLntyre; Mix, 1989).

The water balance can be described by Equation 1. The change in water storage (ΔS) within a volume of control, generally a catchment (Figure 1) over a period of time (Δt) can be written as the difference between the input-net precipitation: total precipitation (P_T), minus interception loss (I) – and the output: overland flow (Q_S) baseflow (Q_B), soil evaporation (E_s), and vegetation transpiration (E_t).

$$\Delta S = \int_{\Delta t}^{0} [(P_T - I) - Q_B - Q_s - E_s - E_t] \, dt \qquad (1)$$

Figure 1 - Schematic representation of the control volume (V), within which hydrological processes can be analysed. $S_T(t)$ is the storage over time, $Q_T(t)$ is the flow over time, $J(t)$ is precipitation over time, and $ET(t)$ is evapotranspiration over time. (a) a catchment where individual travel times (T) are additive. (b) monitored hillslope where hydrological processes can be isolated. (c) cross-section emphasizing the main components responsible for the time it takes for water to deliver a catchment, the time for water to output through evapotranspiration (T_e), and the travel time for water to leave the catchment through streamflow (T_t). Source: Botter, Bertuzzo, and Rinaldo (2010).
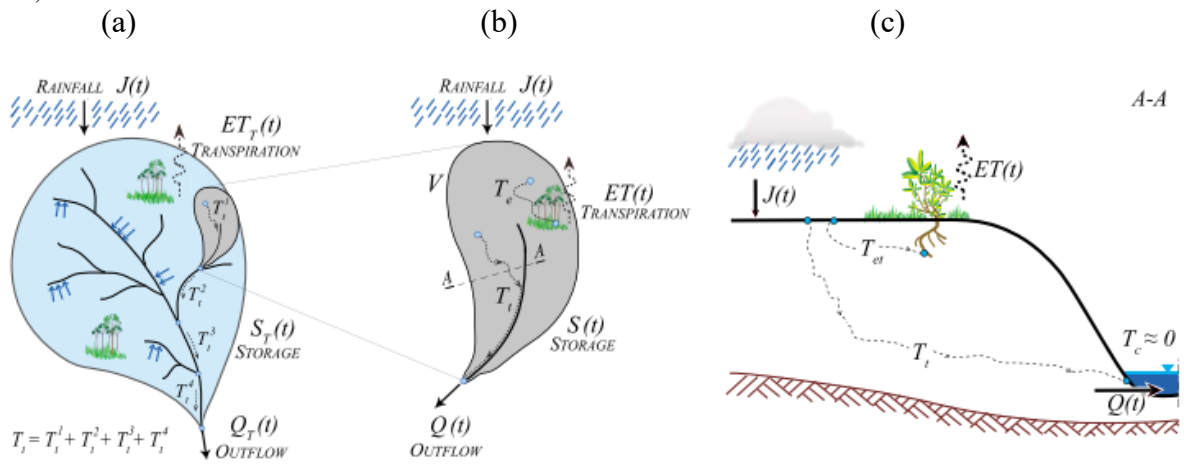
2.1.1 Isotopes of water and the water balance

Given the difficulty in estimating the water balance (Equation 1) through conventional methods that directly measure water volume, isotopes are used to assist in estimating the water balance (Araguás-Araguás; Froehlich; Rozanski, 2000; Camacho Suarez et al., 2015; Gibson; Birks; Moncur, 2019; Sacks; Lee; Swancar, 2014; Skrzypek et al., 2015). Each rain event has a unique isotopic signature for both oxygen ($\delta^{18}O$) and hydrogen ($\delta^{2}H$), which can vary in time and space (Fischer; van Meerveld; Seibert, 2017). By tracking the input of different rain isotope signatures, it is possible to trace the path of the water.

The behavior of isotopes is well exemplified by (Turekian, 2016): when seawater evaporates ($\delta^{18}O = 0$), the water vapor becomes enriched in ^{16}O, resulting in a negative $\delta^{18}O$. On a macro scale, water evaporates at low latitudes and is transported to higher latitudes by atmospheric circulation. The formation of precipitation leads to a rapid depletion of ^{18}O in the water vapor because water molecules with ^{18}O tend to fall out earlier due to their higher atomic weight. $\delta^{18}O$ becomes even more negative, and new raindrops also exhibit increasingly negative $\delta^{18}O$ values during transport (Figure 2). The $\delta^{18}O$ value of 0 for seawater is a convention based

on the relationship between $\delta^{18}O$ and $\delta^{16}O$ in standard mean ocean water (SMOW). The same process occurs for hydrogen.

Figure 2 - Evolution of $\delta^{18}O$ in precipitation. Atmospheric circulation transports water vapor from low latitudes to high latitudes. Source: Turekian (2016).
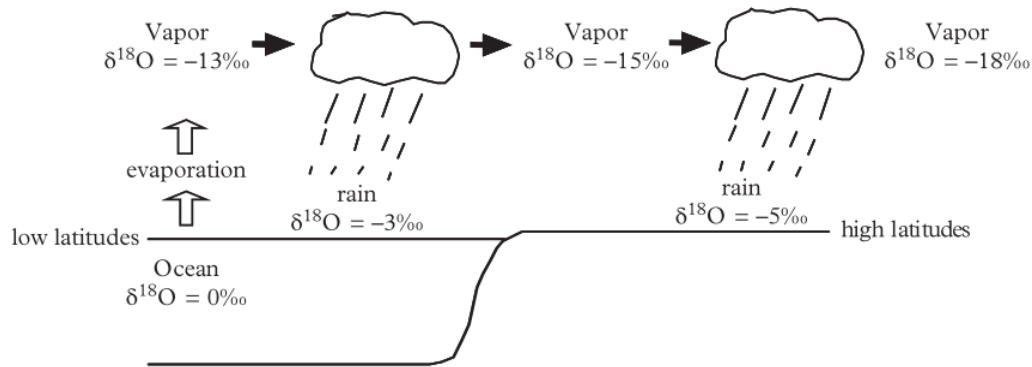
Each rain event has a unique ^{18}O enrichment process, and in a simplified manner, it is expected that we can trace the rainfall within the catchment through these different signatures. Since streams water is a mixture of waters that were stored within the catchment at different times, the variation in the isotopic signature of the streams will be less than the variation in the isotopic signature of the rainfall. The longer the water transit time in a compartment of the catchment, the less variability there will be in the isotopic signature over time.

When water is within the catchment, continuous evapotranspiration of water is expected. As ^{16}O tends to evaporate more easily due to its lighter nature, the water tends to have a more positive $\delta^{18}O$ compared to rainwater (Gibson; Birks; Moncur, 2019; Peralta-Tapia *et al.*, 2015; Sacks; Lee; Swancar, 2014). From the dataset of soil profile water during baseflow or lake discharge, it is possible to determine the slope of the local evaporation line (LEL). It is expected that for lakes, the angular coefficient of the LEL is less than 5 and less than 3 for the upper soil layers (Gibson; Birks; Edwards, 2008).

The scheme of the local evaporation line (LEL) is shown in Figure 3, along with the local meteoric water line (LMWL), which generally has an angular coefficient equal to 8. Both LEL and LMWL are subject to atmospheric conditions and the climate of the latitude and longitude where they are located (Figure 4).

Figure 3 - Plot of isotopic signature variation. Source: Stumpp et al. (2014).
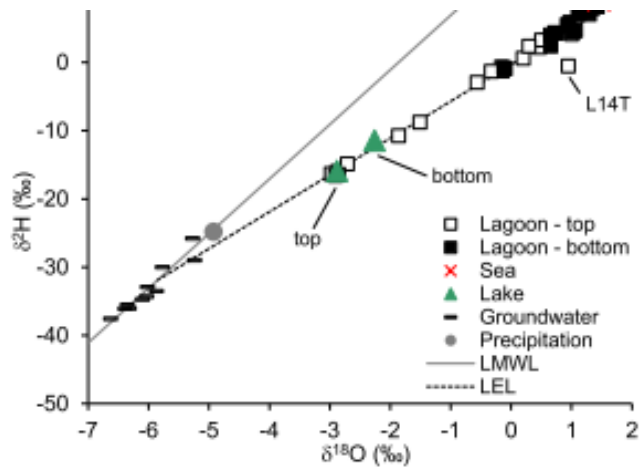
For the latitude and longitude of Peri Lake Experimental Catchment, it is expected to have a Local Evaporation Line (LEL) value for surface water (e.g., lakes) between 3 and 4, and for water from the soil (e.g., baseflow), values between 2 and 3. Figure 4 is derived from a modelling result conducted by Gibson, Birks, and Edwards (2008). To calibrate the model, they used isotopic signatures from South America from the work of Wolfe et al. (1997), which found an LEL slope of 5.1 for streams in the Andes. The higher the latitude, the steeper the slope of the LEL.

Figure 4 - Slopes of local evaporation lines calculated for surface water. Source: Gibson, Birks, and Edwards (2008).
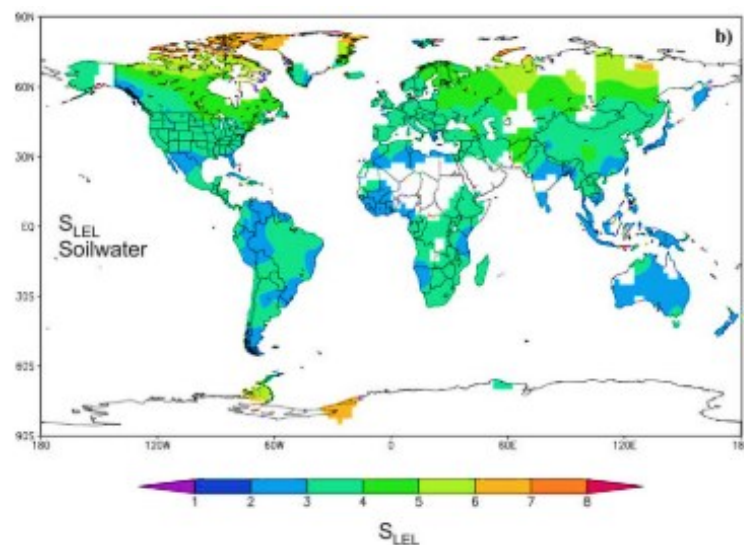
2.2 STREAMFLOW GENERATION MECHANISMS

The runoff of water in a catchment is typically described by a hydrograph, which represents the water flowing through a gauge level station over time. Based on the current

understanding of runoff generation, a hydrograph can be divided into three sources: i) surface runoff, which includes overland flow and flow in the root zone; ii) subsurface flow, which encompasses flow within the soil profile; iii) groundwater flow, originating from the water table (Egusa *et al.*, 2016). Another way to simplify a hydrograph is to separate it into just two components: i) new water (from precipitation); and ii) old water (previously stored in the catchment) (e.g., (Peralta-Tapia *et al.*, 2015).

Traditional rainfall-runoff models consider that the majority of the water comprising the storm hydrograph originates from overland flow (Clark, 1945; Gray, 1961; Nash, 1957; Rodríguez-Iturbe; Valdés, 1979). These models disregard a significant portion of the interaction between water with the critical zone. This perspective is based on the quick response of the system (runoff at the catchment outlet) to a stimulus caused by a rainfall event. According to this understanding, infiltration is the mechanism that divides water into surface runoff and infiltration. Therefore, surface runoff is generated when the infiltration capacity of the soil is exceeded by the intensity of the rainfall, called Hortonian runoff generation (Horton, 1933).

Hewlett (1961) introduced the concept of Variable Source Area (VSA), in which the generation of overland flow varies in location and size over time. Hewlett and Hibbert (1963) suggested that overland flow was not responsible for the entire increase in stream discharge, as a significant portion of the rainfall infiltrated into the soil. Hewlett and Hibbert (1963) concluded that, although the hydrograph is often treated as a product primarily of overland flow, this mechanism is the exception in forests, where the predominant mechanism is subsurface flow. Furthermore, Horton and Hawkins (1965) concluded that the longest travel time of water occurs within the soil profile.

Sklash and Farvolden (1979), using tracers, demonstrated that the water in the streams is a mixture of new water from the precipitation event and old water that was stored in the catchment. Mosley (1979) monitored overland flow and baseflow in a 0.30-hectare forested catchment in a temperate region covered with uniform and spaced vegetation. Mosley (1979) observed a rapid displacement of the applied tracer, which he interpreted as the generation of quick flow, where responses were 300 times faster than the measured saturated hydraulic conductivity. Mosley (1979) interpreted the water movement as Darcy flow. However, the water was not passing through soil pores but through preferential pathways in the soil (McDonnell; Beven, 2014).

The theory of Mosley (1979) predominated for many years in the understanding of runoff generation, which considered that the majority of the hydrograph comes from new water.

McDonnell (1990), using isotopes as tracers, demonstrated that most of the hydrograph is composed of water that was confined within the catchment before the precipitation event. Egusa *et al.* (2016) shown that the proportion of new and old water is not constant throughout the catchment, but rather strongly related to the physical characteristics of the catchment, namely the critical zone. This relationship is influenced by climate, vegetation, and land use (Figure 5).

Figure 5 - Understanding of dominant runoff generation mechanisms according to topography, soils, climate, vegetation, and land use. Source: McDonnell (2013)
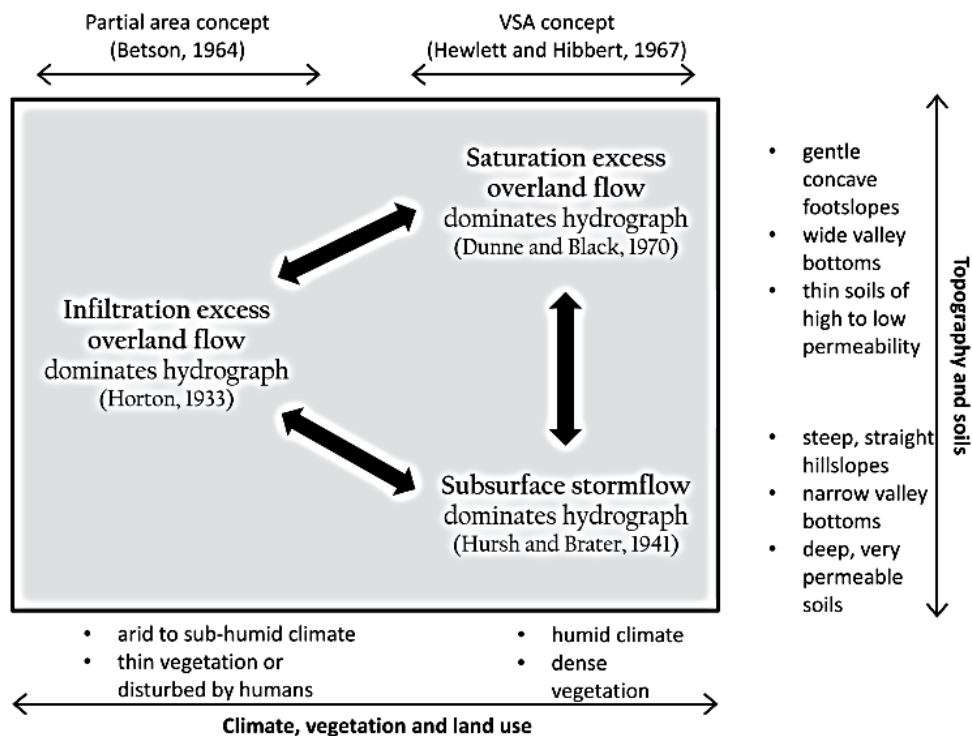
2.3 UNIT HYDROGRAPH, WATER TRAVEL TIME IN THE DRAINAGE NETWORK, AND AVERAGE RESIDENCE TIME

Some mathematical models have been created to assist in estimating the travel or transit time of water within the catchment, such as the unit hydrograph (HU) (Rigon *et al.*, 2016), Mean Transit Time (MTT) (McGuire; McDonnell, 2006), and water travel time in the drainage network (Bergstrom *et al.*, 2016). The HU, MTT, and drainage network travel time are mathematically represented by a Probability Density Function (PDF) that shows the water travel time. However, these three PDFs represent different water movements. The difference between the HU and MTT is related to the concept of celerity and velocity. While celerity represents the propagation of the flood wave in the channel, velocity represents the time it takes

for the water to leave a catchment after its input, including its path within the soil. It is considered that velocity ensures much longer travel times than celerity (McDonnell; Beven, 2014).

Figure 6, from Hrachowitz et al. (2016), schematically illustrates the difference between velocity and celerity. Figure 6a shows the analogy of a billiards game. Each ball represents a water input into the catchment. A new input at t1 (red ball) disrupts the system, propagates with celerity, and generates a response (blue ball) at t2. However, the red ball itself is released from the system only at t5 because it moves at a much slower velocity than celerity. In Figure 6b, it shows a slope where flow generation is dominated by subsurface runoff. In this system, the hydrograph is controlled by wave celerity and active storage, while the path of most of the water in the catchment is controlled by velocity and the length of the flow path through a hydrologically passive storage volume (Sp).

Figure 6 - (a) Conceptualization of the difference between hydrological responses driven by celerity and those driven by velocity using the analogy of a billiards game. (b) Water propagation in a system dominated by groundwater. Source: Hrachowitz *et al.* (2016).
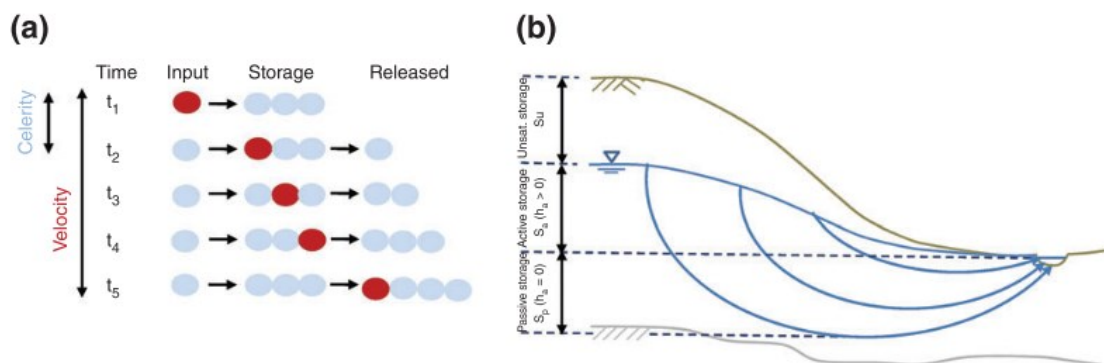
The Unit Hydrograph (UH) represents the flow response of catchment in the form of discharge to a unit of rainfall. Therefore, the UH is related to runoff generation, and thus, it is related to the celerity of water in the channels (Collischonn *et al.*, 2017). The estimation of UH is connected with the concept of time of concentration (Beven, 2020). However, there are various definitions and estimation methods for time of concentration reported in the literature (Grimaldi *et al.*, 2012; Mccuen, 2009). The theoretical definition of time of concentration is the time it takes for water to travel from the farthest point in the drainage network to the outlet. Nevertheless, identifying this time interval on the hydrograph and hyetograph graphs (e.g., time between the end of precipitation and the end of surface runoff, or time between the centroid of precipitation and the centroid of the hydrograph) can differ by up to 500% (Grimaldi *et al.*,

2012). Various models have been conceptualized to estimate time of concentration through empirical formulations that relate the time of concentration found in events to catchment characteristics (de Almeida *et al.*, 2014), and by calculating the water velocity in the channels during precipitation (USDA-NRCS, 2010). However, the model responses still vary widely.

The most robust used UH models in research are calculated based on the geomorphology of the catchment (Singh; Mishra; Jain, 2014). In these models, UH does not have a time scale, as they are based on Horton's laws or catchment shape (Kirkby, M. J., 1976; Rodríguez-Iturbe; González-Sanabria; Bras, 1982; Rodríguez-Iturbe; Valdés, 1979). However, the time scale is considered when using the length of the mainstream divided by the average flow velocity of the catchment. As stream velocities increase only slowly with drainage area and stream order (Leopold, 1953; Leopold; Maddock, 1953), it is possible to relate the length characteristics to time under the simple assumption of a constant average velocity (Beven, 2020). Nevertheless, there are still problems related to the formulation of the Geomorphological Instantaneous Unit Hydrograph (GIUH), which does not assume that the time to equilibrium involves a wave celerity but rather velocities and travel times of water droplets over the terrain, instead of wave velocities or celerities (Beven, 2020).

The calculation of the distribution of water travel time in the drainage network was proposed by Bergstrom *et al.* (2016). It is used in studies focused on the transport of water and solutes under baseflow conditions. Despite describing the travel time of water in channels during baseflow, its formulation has origins in rainfall-runoff studies. This model considers a varying velocity based on the catchment area, assuming that discharge is linearly related to the area (Karlsen *et al.*, 2016), and that velocity is potentially related to discharge (Leopold, 1953; Leopold; Maddock, 1953).

The distribution of transit time provides information about storage, flow paths, and water source in a single feature, as it shows the actual velocity of water travel within the catchment. However, it is not as straightforward to calculate. The main models for MTT distribution are related to the intersection of the isotopic signature of rainfall and runoff (McGuire; McDonnell, 2006). It is still not clear the relationship between MTT and critical zone characteristics, or even the relationship between the main characteristic of a catchment, as drainage area (Figure 7).

Figure 7 - Mean transit time relative to the catchment area. Based on Table 1 from the work of McGuire and McDonnell (2006).
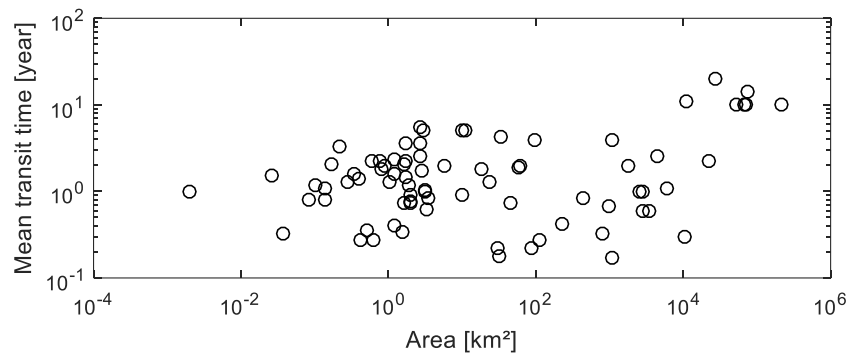
2.4 INVESTIGATION OF HYDROLOGICAL CYCLE THROUGH BASEFLOW CAMPAIGNS

Baseflow is the portion of streamflow between rainfall-runoff events, originating from delayed pathways of rainfall. Baseflow comes from water stored within rocks and/or in the soil profile (Egusa *et al.*, 2016). The storage of water that maintains baseflow functions as a buffer against changes caused by climate and/or land use and occupancy (Van Loon; Van Huijgevoort; Van Lanen, 2012), which is why it is important to understand the recession period. Baseflow also has ecological significance, as some chemical elements are better fixed under low flow conditions, leading to increased biota reproduction (Doyle *et al.*, 2005). It is crucial for water resource management, directly related to reference flows for water management, Q95, Q7,10, and considered critical for sustaining water demand, as population growth leads to predicted imbalances between water supply and demand (Miller *et al.*, 2016).

There is a difference in baseflow between dry and wet conditions. The article of Adji et al. (2017) showed that in drier seasons, the chemical properties of water indicate a more intense interaction between water and rocks. This can be attributed to a greater contribution of water directly from the groundwater table (Egusa *et al.*, 2016). The points where streamflow emerges in the catchment is not permanent, suggesting that quantifying baseflow is related to geological characteristics (Godsey; Kirchner, 2014; Whiting; Godsey, 2016). Whiting and Godsey (2016) demonstrated that drainage where flows are less stable are on slopes, in high latitudes, concluding that permanent drainage networks originate from groundwater. Therefore, the relationship between baseflow and area, both in terms of volume and water source, cannot

be directly applied, as it depends on whether, at the measured point, the water table has the freedom to emerge or not.

Baseflow discharge can be expressed as specific discharge. This is useful for mass balance between precipitation and streamflow, i.e., dividing baseflow by the catchment area. The area is determined by the catchment divide, based on topography, without considering that rock structure may direct groundwater to another catchment (Uchida; Asano, 2010).

Woods, Sivapalan, and Duncan (1995) investigated the existence of a Representative Elementary Area (REA) for baseflow, hypothesizing that the catchment is composed of subcatchments, and that beyond a certain area, the subcatchment will behave, on average, in the same way, with an REA between 0.5 and 2 km². After the REA, groundwater exchange between catchments can be neglected. The work of (Karlsen *et al.*, 2016) showed that assuming a uniform specific discharge for all points in a catchment can introduce errors of up to 33% on a daily scale. Egusa *et al.* (2016) demonstrated, through chemical differences between groundwater and sub-surface flow, that the REA for subsurface flow is 0.1 km², and the REA for groundwater is 1 km².

Baseflow velocity is an important characteristic, as it influences the amount of dissolved oxygen, which enhances solute purification, crucial for catchment contributions to lakes. Wondzell, Gooseff, and McGlynn (2007) analyzed data from 241 velocity measurements under baseflow conditions, relating them to the flow of eight catchments, and found a nonlinear relationship. Bergstrom *et al.* (2016), studying six catchments ranging from 11.64 to 62.8 km², showed that velocity is related to area.

Some chemical characteristics of surface waters can provide insight into the history of the catchment. For example, a high percentage of dissolved oxygen indicates a rocky streambed, shallow waters, and a large water-to-air contact surface. A high percentage of dissolved organic carbon indicates that the water has a strong interaction with the soil layer, a characteristic of sub-surface waters. Electrical conductivity indicates the presence of ions and cations, which result from the interaction between rocks and water, as does pH (Peralta-Tapia *et al.*, 2015).

However, with these characteristics alone, it is not possible to directly determine the source of water in the streams because they are non-conservative flow attributes. There are basically two ways to approach the source of the water studied: i) a mass balance between new water (from precipitation) and old water (present in the catchment after the event) (Peralta-Tapia *et al.*, 2015), or ii) groundwater, sub-surface water, and surface water (Camacho Suarez *et al.*, 2015; Egusa *et al.*, 2016; Hooper; Christophersen; Peters, 1990).

Among the conservative components used as tracers are the isotopes $\delta^{18}O$ and δ^2H, which are variants of a chemical element, having the same number of protons as the chemical element but varying in the number of neutrons. Concentrations of Na^+, HCO^{3-}, K^+, Mg^{2+}, Ca^{2+}, Cl^-, NO^{3-}, and SO_4^2 are also used for the same purpose. To analyze this composition, the End-Member Mixing Analysis (EMMA) method is widely used (Camacho Suarez *et al.*, 2015; Christophersen *et al.*, 1990; Hooper; Christophersen; Peters, 1990; Lohse *et al.*, 2009; Stumpp *et al.*, 2014). There are four assumptions for using this method (Barthold *et al.*, 2011): i) stream water is a mixture of solutions with a fixed composition; ii) the mixing process is linear and hydrodynamically dependent; iii) the tracers are conservative; iv) the solutions that originate the mixture have extreme concentrations.

2.5 FIELD MONITORING STUDIES IN BRAZIL

The humid tropics experience higher energy inputs and rates of environmental change, including human-induced changes. However, there is less monitoring in humid tropics compared to other regions (Wohl *et al.*, 2012). Brazil has a vast area within the humid tropics. Melo et al. (2020) provides a review of field monitoring studies in hydrology in Brazil. In an attempt to answer questions such as "How comprehensive and extensive are these field studies?" and "Where are they located?", the main conclusions drawn from the study include:

- Streamflow and precipitation are the most monitored hydrological variables, found in 98% of field studies.
- Soil moisture content, water quality, sediment transport, and erosion are poorly monitored.
- Traditional hydrology topics (e.g., water budget and hydrologic modeling) are more common, while interdisciplinary topics (e.g., extreme hydrology and ecohydrology) are neglected (Figure 8).
- Emerging research areas include "fluid dynamics", "transport phenomena in porous media", "biogeochemical monitoring", "hydrogeophysical monitoring and assessment", "extreme events" and "water quality monitoring".

Regarding the spatial distribution of field studies, although the subtropical zone represents 15% of the national territory, it contains 35% of the experimental catchments. The tropical zones (81% of the country's area) have 52% of the experimental catchments. Semi-arid

regions (8.4% of the country's area), characterized by water scarcity, account for 13% of the experimental catchments. Thus, there is a disparity in the number of experimental catchments in different climatic conditions found in Brazil (Melo *et al*., 2020).

Regarding the drainage area of the experimental catchment, they range from 0.02 km² to 563 km². Out of a total of 60 experimental catchments, 41 have drainage areas less than 20 km². The high number of small catchments is due to the need for better control of hydrological processes at this scale (Birkel *et al.*, 2020; Melo *et al.*, 2020).

Figure 8 - Frequency of hydrological research topics in Brazilian experimental catchments (MB) for the period 1970-2018. M&A: monitoring and assessment, M&M: monitoring and modelling. Source: Melo *et al.* (2020).
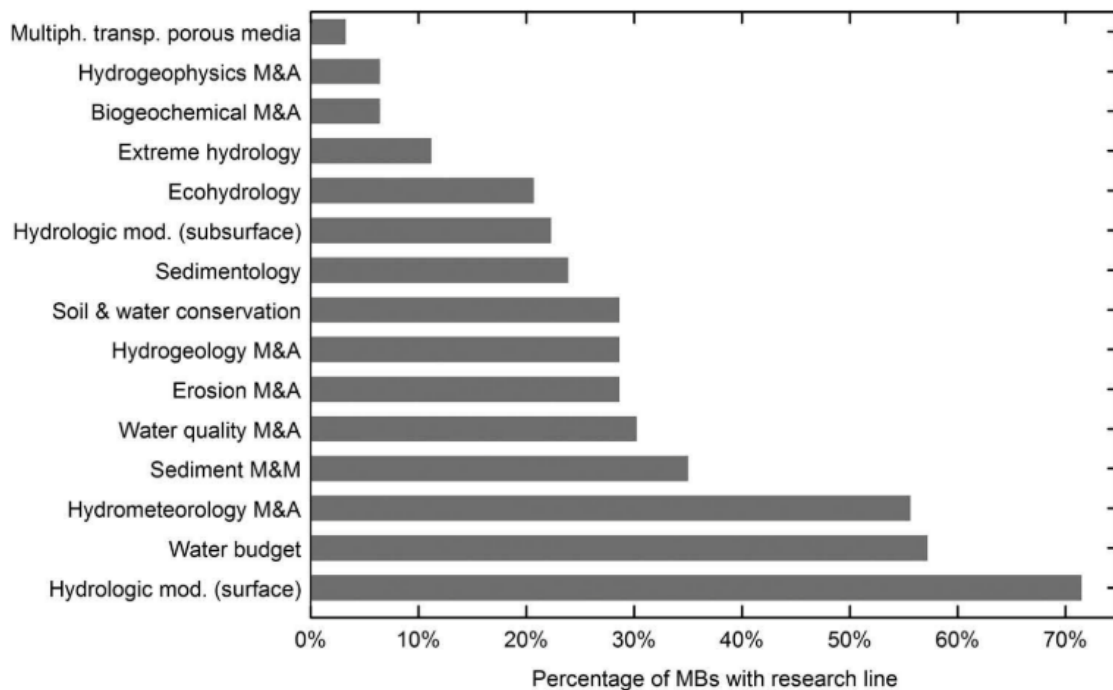
2.6 IMPACT OF CATCHMENT CHARACTERISTICS ON THE STREAMFLOW GENERATION

Hydrological processes are traditionally studied at micro and meso scales (from meters to kilometers). According to Fan *et al.* (2019), at these scales, it can be said that topography is responsible for directing the flow of water, which in turn quantifies various hydrological variables such as overland flow and baseflow, a fact that has been corroborated by many studies (Bárdossy *et al.*, 1999; Bergstrom *et al.*, 2016; Dunne; Black, 1970; Hrachowitz *et al.*, 2013; McDonnell, 1990). For many decades, and with the advent of digital elevation model

technology, scientific research has focused on studying the impact of topography on water pathways (Shen *et al.*, 2016).

Recently, in the 2000s, Critical Zone (CZ) science emerged strongly (White et al., 2015). To study the interaction between the CZ and the hydrological cycle, it is necessary to consider vegetation, the root zone, soil, and rock. In the CZ, there is a division between two types of flow separated by vegetation: "green" water flows, which sustain biomass, and "blue" water flows, which provide recharge and groundwater flow (Evaristo; Jasechko; McDonnell, 2015). This separation between flows shows that the catchment is compartmentalized, meaning that the water we see in the stream does not necessarily come from the same source as the evaporated water. This implies challenges in calculating the water balance (on an annual basis), as groundwater may originate from a process that occurred more than a year ago (McDonnell, 2017).

To study the critical zone, the concept of ecohydrology is often used, which explores the interactions between ecological systems and the movement and quality of freshwater (Guswa *et al.*, 2020). Guswa *et al.* (2020) provide a literature review of advances in ecohydrology, showing that there are still some open scientific questions that can be answered with advances in monitoring and modeling of ecohydrological aspects. These questions include: i) How do vegetation canopies interact with precipitation to affect the quantity and quality of water in space and time? ii) How do ecosystem processes in the CZ (Grant; Dietrich, 2017) affect the partitioning of water between that which constitutes transpiration and that which eventually becomes groundwater and streamflow? iii) How do changes in the landscape affect the quantity, distribution, and quality of streamflow? In the following, the relationship between landscape or CZ characteristics in the hydrological cycle at a meso scale will be described, addressing aspects of ecohydrology.

2.6.1   Vegetation

Vegetation alters the path that rainfall takes before reaching the ground, influencing both the quantity and quality of water available for other processes in the hydrological cycle. A portion of the rainfall intercepted by the forest elements is temporarily retained, and part of it evaporates, returning to the atmosphere. This is called interception loss, which was found to be 33% in the Peri Lake Experimental Catchment (Sá, 2019), considering only the tree canopy. In contrast, in temperate forests, interception loss averages around 40%, considering both the

canopy and forest floor (Gerrits; Pfister; Savenije, 2010). The portion of water not retained by vegetation is directed to the soil.

When rainfall comes into contact with vegetation, the distance traveled by water droplets to reach the ground becomes greater than if they fell directly without being intercepted. This extended distance results in a longer duration of water availability for evaporation. Besides reducing the amount of water that reaches the soil and altering its temporal distribution, vegetation also redistributes rainfall in space (Gerrits; Pfister; Savenije, 2010; Lloyd; Marques, 1988). This redistribution influences other processes in the hydrological cycle, such as infiltration and the generation of overland flow, as the intensity of water reaching the forest floor in areas where rainfall is funneled, such as near tree trunks and at canopy drip points, can exceed infiltration rates. On the other hand, tree roots can create preferential paths for water in the soil, increasing infiltration capacity in those locations.

Although one of the simplest concepts in ecohydrology, controls on canopy water storage and interception loss are not fully understood. Interception models like Rutter-Gash (apud: (Dingman, 2015) (Cooke; Buttle, 2020) embed invalid assumptions when compared to experimental data. One assumption concerns how the canopy functions during small events that lack the volume to saturate it, or during the initial phases of larger events. In both cases, the canopy is represented as a linearly filling reservoir where no flow, trunk flow, or throughfall occurs until the reservoir is full. However, interception theory has long recognized that canopy storage fills exponentially (Guswa *et al.*, 2020).

Additionally, interception loss may be related to raindrop size. Larger raindrops tend to splash more upon impact, increasing evaporation capacity, and they can also ventilate the canopy due to the impact of raindrops on leaves, further enhancing evaporation (Dunkerley, 2009). Another crucial point to consider is that the use of conventional theories like Penman-Monteith (apud: (Dingman, 2015) to estimate maximum event evaporation results in less interception loss than expected based on experimental evidence (Cisneros Vaca; Van Der Tol; Ghimire, 2018). In addition to altering the path of water and the volume of water stored within the catchment, vegetation is also responsible for another water output within catchments through evapotranspiration.

Therefore, removing vegetation for construction reduces local evapotranspiration as there is a decrease in water demand by plants. As a result, streamflow tends to increase during rainfall events where there is no forest to intercept the rain and increase during recessions unless land uses reduce rainfall infiltration rates (Wohl *et al.*, 2012). The magnitude of the effect

depends on rainfall rate and changes in land cover that occur, but observations from small catchments show an increase of 10-25% in the amount of water that reaches the ground (Hayhoe *et al.*, 2011) and a threefold increase in flow (Coe *et al.*, 2011).

2.6.2   Soil

The longest and slowest pathway for water within the catchment occurs within the soil (Botter; Bertuzzo; Rinaldo, 2010). Soil characteristics are critical parameters in hydrological models designed to determine the amount of water storage in the soil necessary to support evapotranspiration during dry periods between rainfall events (Fan *et al.*, 2019). However, as soil is not visible and highly heterogeneous, accurately estimating what happens in the soil profile is challenging. Typically, tensiometers are used to measure changes in water pressure in the soil (Liang; Chan, 2017; Mota et al., 2017; White et al., 2015). Piezometers are also used (Anderson; Burt, 1977). Nevertheless, both measurements provide only punctual data.

There is evidence that soil depth is correlated with topography, which largely drives water and sediment flows and rates of weathering and erosion that shape the Critical Zone (Fan *et al.*, 2019). From the valley floor to the hillslope, the porous-permeable layer becomes thicker (Figure 9).

Figure 9 - Examples of cross-sections showing hillslope soil thickness in Critical Zone observatories located in the USA: (a) rock with water storage capacity and groundwater in the Eel Stream. (b) total water storage and porosity (ϕ). Source: Fan *et al.* (2019).
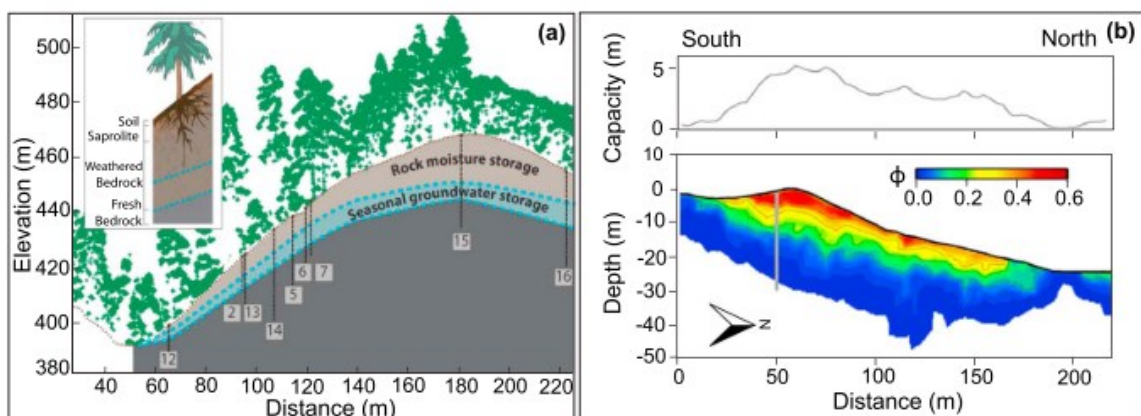
The source of baseflow has two main origins: subsurface water (from the soil matrix) and groundwater (water from fractured rock aquifers) (Egusa *et al.*, 2016). Soil depth becomes crucial in understanding the source of baseflow, depending on the outlet height and the

catchment area. Nevertheless, Ali et al. (2014) showed that soil depth is not directly related to the surface connectivity between the saturated areas of the catchment.

Virtual experiments by Hopp and McDonnell (2009) demonstrated that rock permeability or the contrast in hydraulic conductivity between soil and rock are the primary factors controlling the connectivity between the hillslope and the streams.

Field studies with tensiometers, such as those by Liang and Chan (2017), revealed that soil depth is inversely related to the increase in soil water pressure after soil saturation, and this increase persists for a short period around the initial rainfall peaks when the average soil water pressure sharply increased. Furthermore, Liang and Chan (2017) analyzed the relationship between water pressure and the topographic index (Beven; Kirkby, 1979) and observed that the topographic index is positively correlated with water pressure at all points that are not ephemeral or permanently saturated.

2.6.3   Drainage network

The fastest water flow within a catchment occurs in the drainage network. The morphology of the drainage network and the characteristics of the cross-sections are related to the shape of the hydrograph during the rainfall-runoff process (Beven, 2020; Chen *et al.*, 2019; Gad, 2013; Merz; Blöschl, 2009; Pan; Wang, 2004; Pradhan; Ogden, 2010; Rodriguez; Andrieu; Creutin, 2003; Saravanan; Manjula, 2015; van Meerveld *et al.*, 2019; Yoo *et al.*, 2014).

According to Montgomery and Buffington (1997), there are seven types of cross-sections commonly found in headwater catchments: cascade, pool and riffle, plane bed, pool-step, dune ripple, and colluvium.

Cascade is described as streams where energy dissipation is dominated by continuous oscillations and jet flow over and around large rock blocks (Kondolf; Piégay, 2016). Cascade channels typically occur on hillslopes and are characterized by longitudinally and laterally disorganized bed material. Comprehensive sets of partially small channels, less than one channel width wide, are common in cascade channels (Montgomery; Buffington, 1997).

Channels classified as pool and riffle are located in streams with large drainage areas. In pool-riffle channels, water in the stream spills over logs and/or rock steps crossing the channel into downstream pools (Wilcox *et al.*, 2011). The morphology results in alternating between critical and supercritical flow between the pools and subcritical within the pools, with

typical spacing between pools being 1 to 4 times the channel width (Montgomery; Buffington, 1997).

Streams characterized by cascades and step-pool patterns transform into dune ripple channels. The morphology of dune ripple channels is associated with low-gradient sand channels (Montgomery; Buffington, 1997). Colluvial channels are small streams that flow over a colluvial valley and exhibit weak or ephemeral streamflow (Montgomery; Buffington, 1997) and are present on hillslopes (Perez *et al.*, 2020).

One of the greatest challenges in using rainfall-runoff prediction models is identifying where the channels start. The results of Montgomey and Dietrich (1988) indicate that spring locations are primarily related to accumulated area and slope, where the relationship between area and gradient changes depending on the moisture content. The definition of drainage also leads to the definition of zero-order catchments. Zero-order catchments are defined as catchments that have no streams and are delimited from the spring, the beginning of a drainage network. The geometry of these catchments controls how sediments can be carried and governs water movement from slopes (Godsey; Kirchner, 2014; Grieve *et al.*, 2018; Mutzner *et al.*, 2016; Sidle *et al.*, 2000).

The drainage network is also important for classifying catchments. The width function, proposed by Kirkby (1976), shows the frequency distribution of water flow. It is a useful tool for comparing catchments (Di Lazzaro, 2009) and is often used to support unit hydrograph models (Grimaldi; Petroselli; Nardi, 2012; Grimaldi *et al.*, 2010; Rigon *et al.*, 2016). The width function also represents flow travel distances that solutes take to reach the catchment outlet. Often, when using the width function, a uniform velocity is assumed for the entire drainage network. However, velocity is not uniform throughout the stream network and can be influenced by differences in stream section geometry and flow rate (Collischonn *et al.*, 2017; Leopold, 1953).

Given that the catchment is formed by two well-defined systems, the hillslope and the streams, it would be necessary to assign a different velocity to each system. Rigon *et al.* (2016) proposed modifying this function, having a different velocity for the hillslope and the drainage network. The physical and chemical characteristics of water measured at the catchment outlet are influenced by the spatial distribution of the drainage network. Recently, many studies have been conducted with a focus on understanding water flow from the perspective of its chemical properties (Egusa *et al.*, 2016; Peralta-Tapia *et al.*, 2015). However, the influence of velocity within the drainage network is not considered, even when dealing with non-conservative

parameters, such as how it would affect dissolved oxygen and, consequently, organic matter degradation.

Lastly, the drainage network is not fixed in time and space; it exhibits expansion and contraction, connection and disconnection according to catchment conditions. When a spring moves to higher points, the drainage network and, consequently, the drainage density increase. By definition, drainage density is the sum of the drainage network length divided by the catchment area. Studies have shown that drainage density is exponentially related to specific discharge (Gregory; Walling, 1968). A saturated catchment tends to have a much denser drainage network than the same catchment during dry periods, potentially having up to two additional Strahler orders (Godsey; Kirchner, 2014).

It is not precisely known which characteristics of the catchment cause it to have a varying drainage density. Whiting and Godsey (2016) suggested that springs located at lower altitudes were more stable because they are located at the height of the bedrock that supports the water table. Various field measurements have found drainage density values ranging from 0.5 to 5.3 (Day, 1978; Godsey; Kirchner, 2014; Gregory; Walling, 1968; Roberts; Archibold, 1978; Whiting; Godsey, 2016).

2.6.4 Elevation

The analysis of elevation is important for several objectives, including the identification of floodplains, hydrological rainfall-runoff models, hydrodynamic models, and erosion models. Through elevation data, three significant terrain descriptors can be generated: the contributing area, slope, and topographic index.

The catchment area is a crucial characteristic. Hydrologists often use mass conservation principles to study the hydrological cycle, for which defining a control volume is necessary. The catchment area is defined as the entire area that, due to the topography, appears to drain to a lower point (Dingman, 2015). However, this area may be poorly estimated as there can be underground water exchanges between catchments (Egusa *et al.*, 2016). Despite documented variations in specific discharge (total discharge divided by the area) within sub-catchments of the same landscape (Egusa *et al.*, 2016; Karlsen *et al.*, 2016; Lyon *et al.*, 2012; Woods; Sivapalan; Duncan, 1995), it is often assumed that nearby catchments within a similar landscape have similar specific discharge (Archfield; Vogel, 2010).

The source of stream water can be related to the terrain slope. Under baseflow conditions, there are two main sources: subsurface water (from the soil matrix) and groundwater (from fractured rocks) (Egusa *et al*., 2016). Whiting and Godsey (2016) demonstrated that points where flows are less stable are found at high slopes, suggesting that permanent drainage networks originate from groundwater in areas with lower slopes. Additionally, slope directly influences the velocity of water in the stream (e.g., Leopold (1953), and Leopold, and Maddock (1953)). Slope is also related to the hydraulic geometry of the channels (Palucis; Lamb, 2017).

The topographic index, proposed by Beven and Kirkby (1979), which considers both slope and the contributing area, is important because it indirectly relates to soil moisture. The topographic index has been used to investigate scale influences within a single catchment by Woods and Sivapalan (1997), concluding that in sub-catchments with well-developed drainage networks, the topographic index follows a similar behavioral pattern, regardless of the area.

3.   STUDY AREA AND EXPERIMENTAL DESIGN

3.1   STUDY AREA

The Peri Lake Experimental Catchment (PLEC) is located in the southern Brazil (Figure 10a), in the south of Santa Catarina Island (Figure 10b). The elevation of the hillslopes ranges from 2 to 442 meters (Figure 10c). The 19 km² catchment is surrounded by hillslopes covered with remnants of Atlantic rainforest (Figure 10d) with a coastal lake of 5 km². It is situated in the transition between tropical and temperate climates, with an average annual precipitation of 1700 mm, a hot summer, and no dry season.

PLEC was designated as a Natural Patrimony site in 1976, and the Municipal Park of Peri Lake was created and regulated between 1981 and 1982. In 2019, the Municipal Park became a Natural Monument (Floram, 2019). Peri Lake is the largest source of water supply for the island, covering approximately 5% of the island's area. In 1989, the Santa Catarina Sanitation Company (CASAN) initiated works to use the water source for public water supply (Santos e Silva, 1989). The only outlet from the lake to the Atlantic Ocean is the Sangradouro Stream, which is the main supply of freshwater of Santa Catarina Island. The primary concern is that the drinking water may be contaminated with *trihalomethanes*. These highly carcinogenic substances are formed due to the combination of organic matter and filamentous cyanobacteria (Fontes *et al.*, 2013). The extensive flow of organic matter associated with runoff has the potential to substantially alter biogeochemical nutrient and energy balances, affecting water quality downstream (Rowland; Inamdar; Parr, 2017).

The geological formation of the PLEC is primarily granitic, with diabase dike formations throughout its structure and sedimentary deposits at lower altitudes (Figure 10e) (Universidade Federal de Santa Catarina, 2018). The hydrogeology of PLEC has three zones (SDS, 2013; Figure 10f): i) non-aquifer zone, the largest in extent, where shallow groundwater from recent rainfall infiltration can be found, creating a dense drainage network; ii) fractured aquifers, which are unconfined to semi-confined, with medium to low water productivity; and iii) marine and coastal sediment aquifers, which are unconfined and have sandy layers (Machado, 2013).

Regarding soil, PLEC has three distinct units, according to (Embrapa, 2004) (Figure 10g). In all three units, the depth of the first horizon varies between 60 and 150 cm. The most

extensive unit is clayey cambisol, with the depth of the second horizon reaching up to 150 cm, and the terrain is strongly undulating and mountainous. In the medium-textured cambisol soil unit, the depth of the second horizon reaches up to 60 cm, and the terrain is strongly undulating. The soil composed of marine quartz sand is the shallowest, present in a 250-meter-wide strip towards the sea, where the soil is nutrient-poor, with high sand and clay content, low fertility, and no support for a more lush cover, with its vegetation being of the restinga type (Santos e Silva, 1989).

Due to the history of occupation and land use in the PLEC, Sbroglia and Beltrame (2012) divided PLEC into three areas (Figure 10h): i) Biological reserve area, which contains remnants of advanced Atlantic rainforest (Figure 10i); ii) Cultural area, preserving the history of the local sugar cane and cassava mills, with the presence of residences and at least two sugar cane mills; there are advanced, intermediate, and initial forests in this region (Figure 10j); and iii) Recreation area, centered around the Peri Lake Park headquarters, in the restinga area, where many visitors come to enjoy the facilities and swim in the lake (Figure 10k).

Historically, the first inhabitants of PLEC settled in the Sertão do Peri, in the cultural landscape area (Figure 10h), establishing residence in 1971. These inhabitants survived through agriculture, primarily cultivating cassava, which led to significant deforestation. In 1978, there were 19 mills, which came in two types: cassava flour mills and cachaça distilleries. The latter also produced coarse sugar and sugarcane molasses. By 2006, only 5 mills remained (Batista, 2006). Due to the lack of land rotation, agriculture gradually replaced exhausted soil areas, leading to deforestation towards the hillslopes. The deforestation process even affected the vegetation along the streams, posing serious problems for the local population as the stream were their main source of water (Batista, 2006; Santos; Silva, 1989).

Figure 10 - Peri Lake Experimental Catchment (PLEC): (a) Global Location; (b) Location within the city of Florianópolis; (c) Terrain Elevation and Drainage Network (data source: SDS, 2013); (d) Land Cover (data source: IPUF, 2018), where A stands for advanced and I stands for initial or intermediate; (e) Geology (data source: UFSC, 2018); (f) Hydrogeology (data source: Machado, 2013); (g) Soil Types (data source: EMBRAPA, 2004); (h) Historical Division (data source: Sbroglia and Beltrame, 2012); (i) Biological reserve area; (j) Cultural area; and (k) Recreation area.
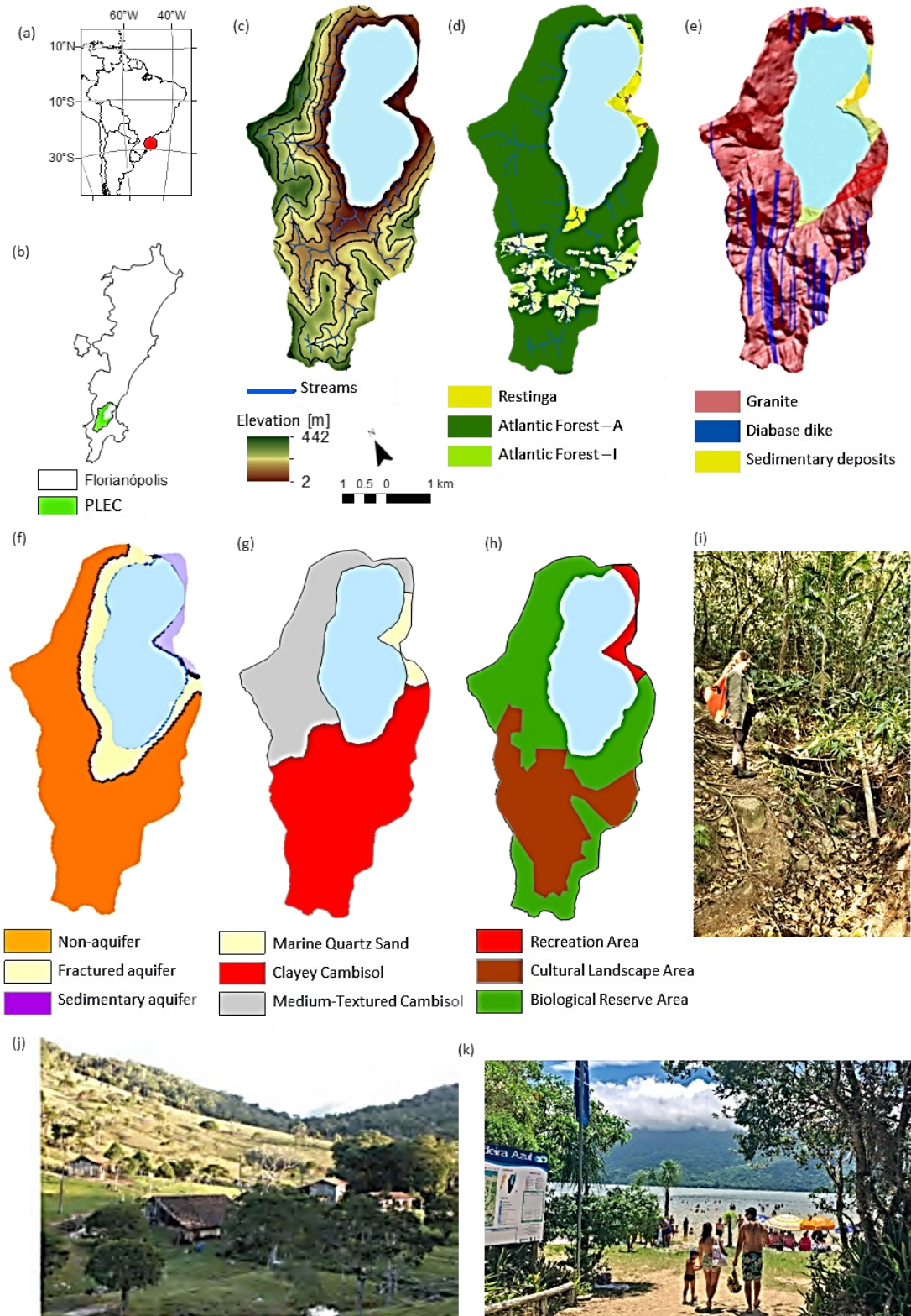
In 1989, farming slowed down, but people continued to cut down trees for wood. They used this wood as fuel for bakeries, restaurants with wood-burning ovens, for building things, and even for making small boats (Santos; Silva, 1989). Because of this, by 1989, only native plants and trees could be found in the special area reserved for them (Figure 10i).

In 1978, 214 people lived in the region, grouped into 54 families (Santos; Silva, 1989). According to Sbroglia and Beltrame (2012), between 1977 and 1978, the population of PLEC increased by 330%. But the grown was not homogeneous. Some families left the Sertão do Peri, high area, and moved to low areas where is characterized by restinga. In 2010, according to a survey by the Brazilian Institute of Geography and Statistics (IBGE), there were 23 people who lived in the cultural landscape area all the time.

3.1.1 Catchments physical characteristics

Twenty physical characteristics were calculated for each catchment of PLEC (Table 1). These calculations were performed using an algorithm developed by the author and implemented in the MATLAB software. The algorithm is available in the database, as described in Appendix A and presented in Appendix B. Spatial information was obtained from a Digital Elevation Model (DEM) with a 1-meter resolution, provided by (Secretary of State for the Economic and Sustainable Development (SDS), 2013). The vectorized geological map of Florianópolis Island was made available by the Microscopy Laboratory of the Federal University of Santa Catarina (UFSC, 2018), and land cover data is provided by the Florianópolis Municipal Government (Prefeitura de Florianópolis, [s.d.]). Regarding the land cover map, areas classified as early-stage Atlantic Forest were considered equivalent to pasture, as observed during fieldwork.

Table 1- Physical Characteristics of the Catchments

Var.	Dim.	Description	Definition	Reference
A	[L²]	Drainage area	An area delimited by the catchment boundary that drains into an outlet	Horton (1945)
E_P	[L]	Elevation of outlet	Elevation of outlet	-
S_P	[°]	Slope of outlet	Slope of outlet	-
Cur_P	[-]	Curvature of outlet	Curvature of outlet	-
P	[L]	Perimeter	Length of the catchment boundary	Schumm (1956)
O	[-]	Catchment order	The highest-order stream within the catchment	Strahler (1952)
L_{MS}	[L]	Length of the mainstream	Length of the longest stream within the catchments, which extends from the outlet to some spring	Mueller (1968)
L_W	[L]	Length of the catchment	Longest straight-line distance from the outlet to the catchment boundary of the catchment	Gregory and Walling (1968)
S_{MS}	[L/L]	Slope of mainstream	$S_{MS} = {H_{máx} - H_{mín}}/{L_s}$, where $H_{máx}$ and $H_{mín}$ is respectively the elevation of the spring and the elevation of the outlet.	Schumm (1956)
R_C	[-]	Circularity ratio	$R_c = {4\pi A}/{P^2}$	Miller e Summerson (1960)
C_C	[-]	Compactness coefficient	$Cc = {0,2841P}/{A^{0,5}}$	
R_B	[L]	Catchment relief	Difference between the elevation of the outlet and the highest elevation of the catchment boundary	Schumm (1956)
Ff	[-]	Form factor	$R_c = {A}/{L_w}$	Horton (1932)
Dd	[L/L²]	Drainage density	$Dd = {\sum L_s}/{L_w}$, where L_s is the sum of streams length	Gregory and Walling (1968)
E	[L]	Mean elevation	Mean elevation among all the points delimited by the catchment boundary	-
S	[°]	Mean slope	Mean slope among all the points delimited by the catchment boundary	Miller and Summerson (1960)
TWI	[-]	Median topographic index	Median topographic index among all the points delimited by the catchment boundary. The topographic index is defined as: $TWI = \ln\left(\frac{A}{\tan S}\right)$	Beven and Kirkby (1979)
G	[%]	Percentage of the total area with granite	Percentage of the total area on granite, based on the geological survey of the UFSC (2018)	UFSC (2018)
Pasture	[%]	Percentage of the total area of the catchment covered by pastures	Percentage of the area covered by pasture. Based on the survey conducted by Florianópolis Municipal Government	Prefeitura de Florianópolis [s.d.]
Cur_m	[-]	Curvature	Median curvature among all the points delimited by the catchment boundary	Evans (1980)

3.2   EXPERIMENTAL DESIGN

During the years 2017 and 2018, monitoring campaigns were conducted in the PLEC, where the following parameters were monitored: discharge, flow velocity, and isotopes (Figure 11). Soil measurements were conducted in the end of the 2022. All the data are available in the qualification database (Appendix A).

Figure 11 - Monitoring map.
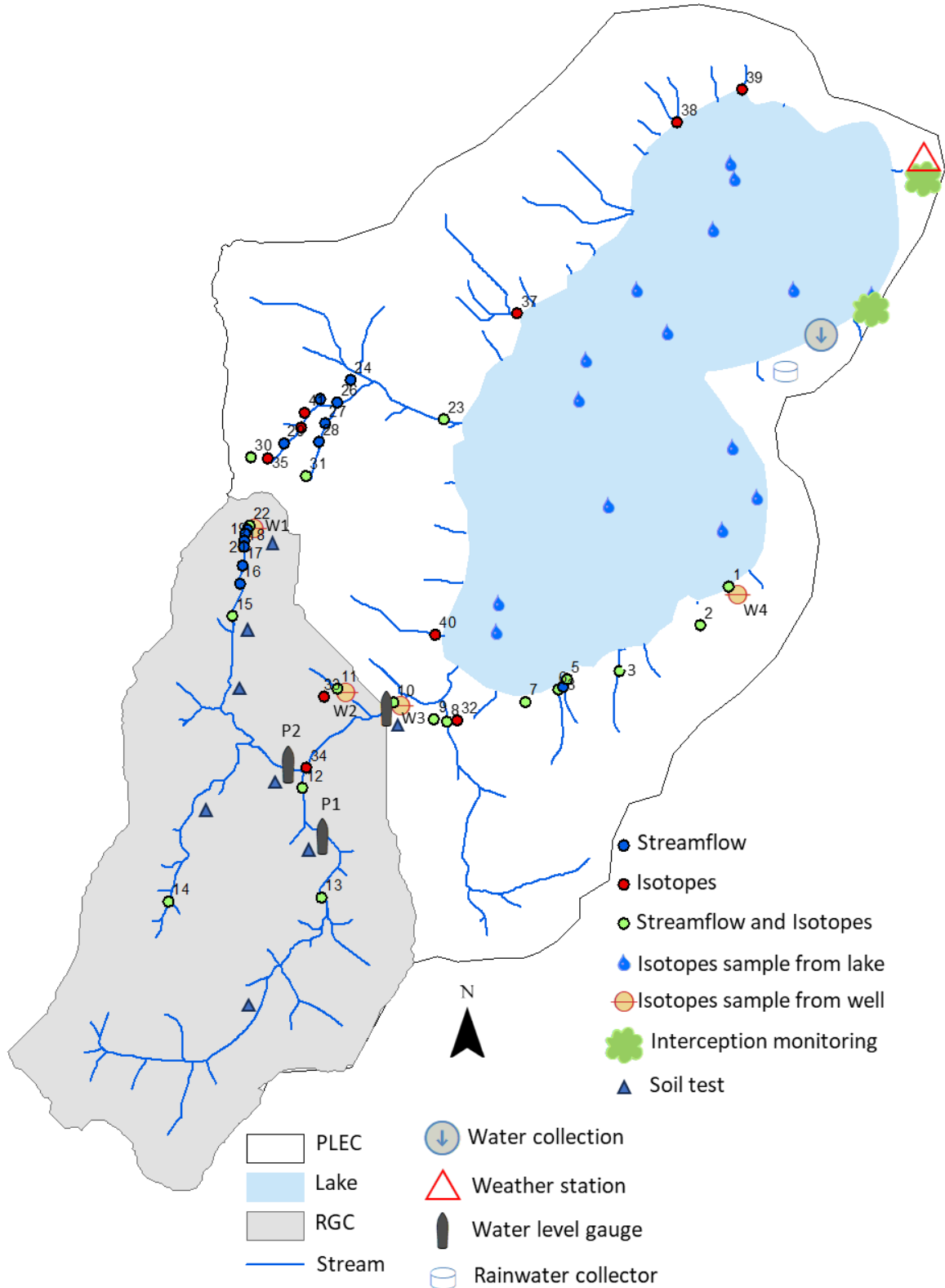
3.2.1   Streamflow and flow velocity

In total, 78 streamflow measurements were done in 31 different cross-sections of the PLEC (Figure 11). Four different alluvial channel morphologies were identified (Figure 12), visually classified according to Montgomery and Buffington (1997). There are six alluvial cross-sections in first-order channels. Cascade is the most common channel reach morphology (22 cross-sections), with drainage area ranging from 0.13 to 1.13 km² in streams from first to third order. Three cross-sections can be classified as step-pool. Streams characterized by cascade and step-pool transitions into dune ripple near Peri Lake are associated with alluvial deposits (Figure 12) and low-gradient sandy channels (Montgomery; Buffington, 1997).

Figure 12 - Alluvial channel morphology.

Aluvial channel morphology	Coluvial	Cascate	Step-pool	Dune ripple
Area [km²]	0,02 – 0,08	0,03 – 1,13	2,64 – 5,33	5,45
Order	1°	1° 2° 3°	3° 4°	4°
Width [m]	0,1 – 0,3	0,3 – 1,2	3,0 – 4,5	6,0

Streamflow was measured using three different methods depending on the cross-section: the volumetric method, the current meter, and the dilution method. The monitoring occurred on 17 different days (Table 2), during baseflow. We adopted one or more days without rainfall as baseflow conditions. Since the time of concentration of the largest contributing catchment is on the order of 1h (estimated using the formula of (Dooge, 1973), we considered that after a day without rainfall there would be only baseflow in the stream.

Table 2 - Description of the monitoring campaign.

Date	Cross-section	Number of measurements	Number of people working	Time spent [h]
14/03/2017	1, 2, 3, 4, 5, 6, 7, 8, 9 and 10	11	3	8
01/04/2017	1, 2, 3, 4, 6, 7, 8 and 9	8	2	7
10/04/2017	4	2	3	4
22/04/2017	1, 4, 5, 7, 8 and 9	6	4	6
19/07/2017	23 and 24	2	4	8
13/12/2017	12, 19, 25, 26, 27, 28 and 31	7	4	8
18/12/2017	4 and 10	2	2	6
05/02/2018	10, 16, 18 and 21	4	2	8
17/02/2018	29 and 30	2	2	4
20/02/2018	17, 18, 19, 20 and 21	5	2	8
06/06/2018	8, 10, 11, 13, 14, 15 and 21	8	4	5
26/06/2018	8, 10, 12, 13, 14 and 15	6	4	5
05/07/2018	10	2	2	3
14/08/2018	10	2	3	3
04/09/2018	10	1	4	2
12/09/2018	10	3	3	5
04/10/2018	10	1	1	2
18/06/2020	10, 12 and 13	6	3	6

For the volumetric method we used plastic containers with a volume of 0.25 L and 7 L (Figure 13a). The streamflow was estimated according to the following equation:

$$Q_v = \frac{V}{T} \tag{2}$$

where Q_v is streamflow by the volumetric method [L s^{-1}], V is the collected volume [L] and T is the total time of volume collection [s]. The verification that all the water of the cross-section flowed into the container was done visually.

We used a mechanical current meter to estimate streamflow (Figure 13b). The total streamflow is approximated by measuring the width, depth, and velocity at discrete points along the channel cross-section. The total streamflow in a cross-section is given by:

$$Q_{CM} = \sum_{i=1}^{n} \frac{A_i v_i}{1000} = \sum_{i=1}^{n} \frac{b_i d_i v_i}{1000} \tag{3}$$

where Q_{CM} is the streamflow [L s^{-1}] obtained with the current meter; n is the number of verticals i across the channel; A_i is the cross-section area [m²]; b_i is the width of the vertical i [m]; d_i is the average depth of the vertical i [m], and v_i is the average downstream velocity in vertical i [m s^{-1}]. The width of the vertical is estimated as $(x_{i-1} + x_{i+1})/2$, where x is the horizontal

distance of the vertical from the edge of the water (Cohn; Kiang; Mason, 2013). To estimate the average velocity at a vertical, velocity was measured at 60% of the height of the vertical, according to the method described in (Santos *et al.*, 2001).

Figure 13 - Streamflow measurement equipment: (a) Container of 7 L. (b) Mechanical current meter (OTT C2, OTT HydroMet, Ludwigstrasse, Munich, Germany). (c) Conductivity probe (Orion 4 Star, Thermo Scientific, Beverly, Massachusetts, USA).
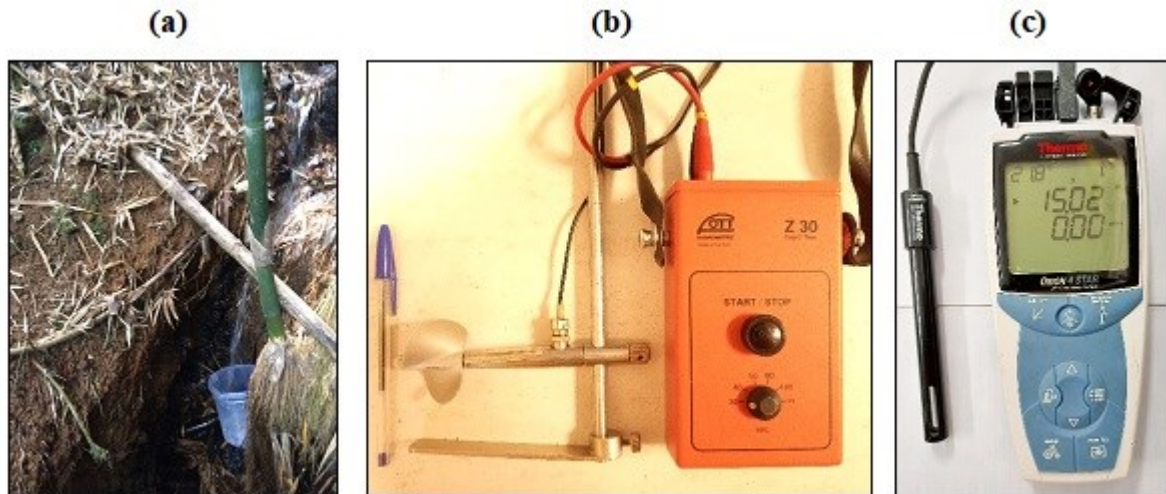
According to Hudson and Fraser (2002) there are four assumptions for the slug dilution method: (i) the salt must be completely mixed with the flow at the in-stream measurement point; (ii) the salt must be added to the channel instantaneously; (iii) there must be no local inflows between the injection and measurement points and; (iv) the measured reach should be straight with no pools where the salt can become retarded and separated from the main flow. We used table salt as a tracer for the dilution method. Salt concentration conductivity was measured using a conductivity probe (Figure 13c). The streamflow was calculated as:

$$Q_D = \frac{V(Ct)}{\sum_0^\tau (Cr(\tau) - Cr_0)d\tau} \tag{4}$$

where Q_D is the streamflow [L s^{-1}] obtained with the dilution method, V is the volume of tracer solution [L], Ct is the concentration of the applied salt solution [g L^{-1}], $Cr(\tau)$ is the concentration of salt in the stream [g L^{-1}] at time τ, Cr_0 is the concentration of salt in the stream [g L^{-1}] at the time of salt injection, and $d\tau$ is the time step (here 5 seconds).

The flow velocity was estimated as:

$$v_D = \frac{Ml}{t_{in} - t_e} \tag{5}$$

where v_D is the flow velocity [m s^{-1}] obtained with the dilution method, Ml is the mixing length (distance along the stream between the point of salt injection and the location of the probe in the stream) [m], t_{in} is the moment of salt injection [s] and t_e is the time [s] when 50% of the salt has passed by the probe.

Various strategies were adopted to ensure the complete mixing of the salt in the streams: (i) food coloring was injected into the water and its dilution observed; (ii) in cascade channels the salt injection point and the probe location were at sites where the water flows in a small cross-section; and (iii) in a step-pool channel the salt was injected after the pool.

3.2.2   Isotopes

In 2018, between June and September, we carried out five water sampling campaigns (C1, C2, C3, C4, and C5) (Figure 11; Table 3), all of which took place during baseflow conditions. Water level exceedance probabilities for these campaigns are presented in Figure 14. During these campaigns, we sampled streamflow for isotope analysis 26 subcatchments.

Not every site was sampled at every campaign due to flow intermittency and site access. This resulted in a total of 91 water samples ranging from 2 to 5 per site (Figure 1e). As we aimed at baseflow, we waited at least 24 hours after rainfall events before the measurements, which is feasible at PLEC with concentration times of around 1 hour. Throughout all campaigns days, the water level in the Ribeirao Grande Catchment (RGC) remained below Q90 (based on 2016 streamflow data; Figure 14). The discharge reached Q99 on the day with the lowest baseflow among the campaigns (Figure 14). On this particular day alone, W4 was empty (Figure 1f), and the water table level was the lowest of all campaign days. We assume that the $\delta^{18}O$ values in groundwater from the day with the lowest baseflow, and the weighted average $\delta^{18}O$ values in precipitation, represent deep and shallow groundwater, respectively.

Table 3 - Measured subca/tchments. Where C1 is the first campaign, C2 is the second campaign, C3 is the third campaign, C4 is the fourth campaign, C5 is the fifth campaign, WS is standing water and access is inability to access the collection location.

Stream	A [km²]	E [m]	S [°]	Caracterized by diabase dikes	$\delta^{18}O$					
					C1	C2	C3	C4	C5	Median
1	0.035	81	19.00	No	-3.85	-3.02	SW	SW	-3.30	-3.30
2	0.038	152	21.80	No			-3.62	-3.65	-3.78	-3.65
3	0.020	192	23.95	No			-3.40	-3.61	-3.62	-3.61
4	0.260	138	22.80	No	-3.58		-3.38	-3.50	-3.53	-3.52
5	0.070	176	23.90	No	-3.44		-3.64	-3.70	-3.75	-3.67
8	1.140	185	15.40	Yes	-3.70	-3.72	-3.72	-3.83	-3.76	-3.72
9	0.050	142	15.90	No	-3.79		-3.37	-3.56	-3.50	-3.53
10	5.330	200	16.70	Yes	-3.68	-3.25	-3.29	-3.70	-3.62	-3.62
11	0.130	165	20.50	Yes	Lost	-3.84	-3.74	-3.79	-3.66	-3.77
13	2.220	228	15.60	Yes	-3.76	-3.76	-3.86	-3.79	-4.00	-3.79
12	2.640	220	15.50	Yes	-3.94	-3.78	-3.87	-3.68	-3.86	-3.86
14	0.220	243	20.90	Yes	-3.79	-3.30	Access	Access	Access	-3.55
15	0.290	264	18.03	Yes	-3.51	-3.84	-3.87	-3.54	-3.60	-3.60
20	0.165	280	16.65	No	Access	-3.57	-3.88	-3.88	-3.77	-3.83
21	0.280	291	17.34	No	Access	-3.64	-3.88	SW	-3.80	-3.80
22	0.050	302	15.25	Yes	-2.46	-2.77	-2.88	-2.91	-3.17	-2.88
23	1.570	267	17.87	No	Access	Access	-3.28	Access	-3.73	-3.51
30	0.026	314	14.28	No	Access		-3.90	-4.20	-3.93	-3.93
31	0.015	304	13.11	No	Access	-3.90	-3.55	SW	-3.81	-3.81
32	0.030	92	21.25	No	-3.59		SW	-3.74	-3.62	-3.62
34	2.160	196	17.49	Yes	-3.51	-3.42	-3.51	-3.65	-3.59	-3.51
35	0.030	288	15.23	No	Access	-3.85	-3.85	SW	-3.82	-3.85
37	0.340	266	21.45	No	Access	Access	-3.01	Access	-3.51	-3.26
38	0.200	161	23.63	Yes	Access	Access	-3.46	Access	-3.52	-3.49
39	0.098	98	20.68	Yes	Access	Access	-3.67	Access	-3.51	-3.59
40	0.209	209	17.23	Yes	Access	Access	-3.58	Access	-3.76	-3.67

Figure 14 - Water level of Peri Lake Experimental Catchment: (a) Water level of Ribeirão Grande Catchment in 2016; and (b) permanence curve of stream water level of Ribeirão Grande Catchment. The vertical dashed black lines indicate water level at the sampling campaigns.
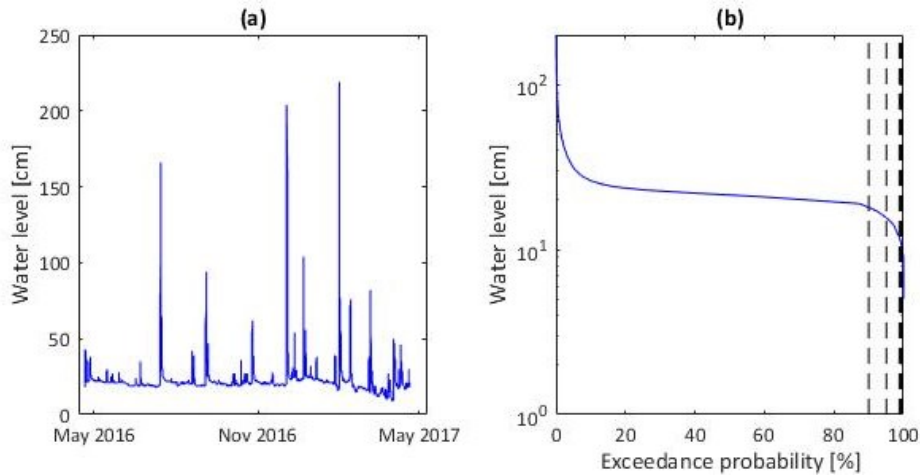
The sampled subcatchments (Table 3) provide a representative subset of the entire PLEC (Figure 15). Histograms for the entire PLEC are displayed in Figure 15 (e, f, g, h), while histograms for the sampled catchments can be found in Figure 15 (i, j, k, l). The mean drainage area for all subcatchments within PLEC is 0.38km², whereas it is 0.68km² for the monitored subcatchments. Similarly, the mean elevation for all PLEC subcatchments is 218m, while it is 208m for our monitored subcatchments. The mean slope for all PLEC subcatchments is 18.54° and 18.45° for our monitored subcatchments. Additionally, the average granite composition for all PLEC subcatchments is 85%, while for our monitored subcatchments, it is 90%.

Figure 15 - Landscape distribution of Peri Lake Experimental Catchment: (a) Drainage area; (b) Mean elevation; (c) Mean slope; (d) Mean percentage of granite; (e) Histogram of drainage area variability of PLEC; (f) Histogram of mean elevation variability of PLEC; (g) Histogram of mean slope variability of PLEC; (h) Histogram of percentage of granite variability of PLEC; (i) Histogram of drainage area of subcatchments sampled; (j) Histogram of mean elevation of subcatchments sampled; (k) Histogram of mean slope of subcatchments sampled; and (l) Histogram of percentage of granite of subcatchments sampled.
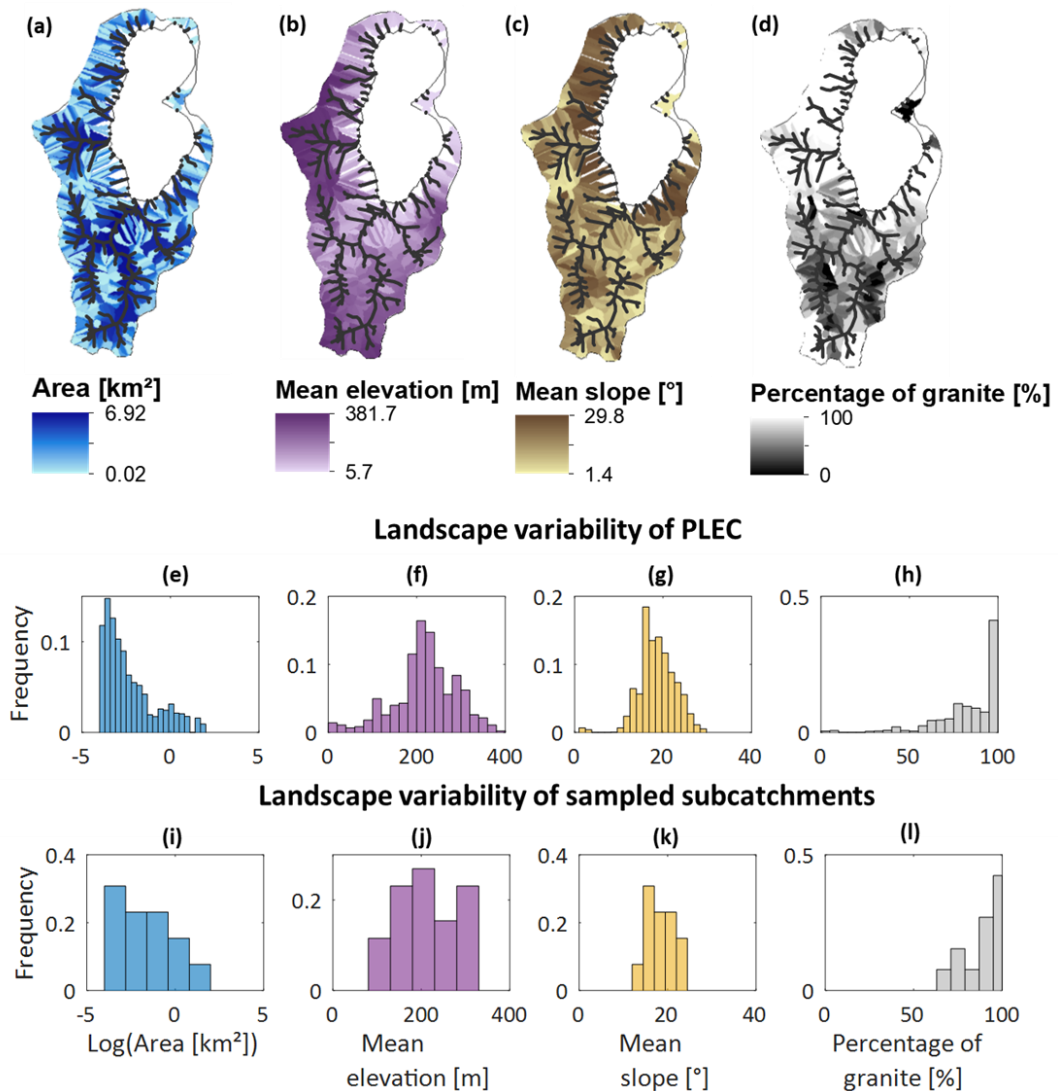
Additionally, we sampled groundwater and rainfall. Groundwater sampling was carried out during the streamflow sampling campaigns at four wells by emptying the well before the measurement. This resulted in 18 samples (two different wells were dry at two different campaigns). The wells (W1, W2, W3, and W4, Figure 11) were hand-drilled until resistance (bedrock) and installed to depths of 1.2, 0.6, 2.1 and 1.2 meters. They were screened for the lowest 20 cm and their locations were selected to cover the catchment elevation range.

We sampled rainfall (March to December 2018) at the hydro-meteorological station (Figure 11) within approximately 24-48 hours after rainfall events. We used a rainfall sampler

made from a PVC pipe with 5 cm of diameter and 60 cm of height topped by a funnel made with 20 cm in diameter. Collected water was protected against evaporation by a ping-pong ball inside the PVC pipe.

All water samples were analyzed for $\delta^{18}O$ with a Liquid Water Isotope Analyzer (LWIA; model 912-0008) manufactured by Los Gatos Research (LGR) and given in parts per thousand against the reference of Vienna Standard Average Ocean Water (VSMOW) (e.g., Stumpp et al., 2014). Throughout the calibration, correction, and determination of stable isotope signatures for the analyzed samples, we employed the LIMS 10.083 software for lasers developed by Coplen in 2000.

3.2.3   Network streams mapping

During the month of March in the year 2020, three campaigns were conducted to mapping springs during baseflow. Two types of springs were marked following the methodology of Mutzner et al. (2016). The route was traveled downstream to upstream along the streambed. The location of the last cross-section where there was water in the stream (Figure 16a) was considered an active spring during baseflow. Active springs with overland flow were determined by moving upstream along the stream channel until it was no longer possible to identify the channel formation (Figure 16b). In channels formed by large rocks, the point of the active spring with overland flow is where the rocks no longer follow an alignment. The GPS error used was about 7 meters, and the position chosen for the spring was the point within the 7-meter limit with the highest accumulated area. In total, six baseflow springs (permanent) and eight overland flow springs (temporary) were mapped (Figure 16c). All of the springs were mapped in catchments characterized by granite.

Figure 16 - Springs: (a) permanent springs; (b) temporary springs; (c) positions of the springs collected in the field. The red arrows indicate the sheath of a 25cm machete.
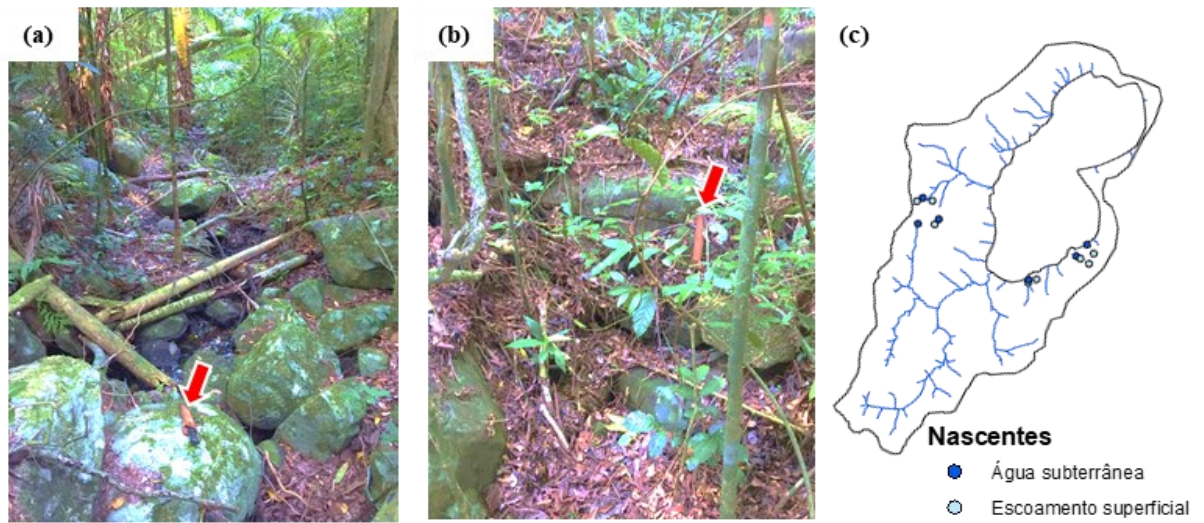
3.2.4 Soil characterization

Two soil test were employed in eight different points of the Ribeirão Grande Catchment (Figure 11) in November and December of 2022: concentric cylinders and inverted well. The equipment used was developed by (Perez, 2019) (

Figure 17). From concentric cylinders we determined the infiltration rate (e.g., Cauduro and Dorfman (1986)). Two cylinders were intersected, one with a 50 cm radius and another with a 25 cm radius, both 30 cm in height, both were buried in the soil simultaneously until reaching a depth of 10 cm. The cylinder with the larger diameter was utilized to saturate the soil surrounding the central cylinder, flowing the water vertically and eliminating the need for lateral infiltration measurements. A measuring tape was employed to monitor the water level fluctuations within the inner cylinder. Test durations varied between 20 to 40 minutes, until the water level fluctuations stabilized over time.

The instantaneous infiltration rate is, by definition, the amount of water that infiltrates during each time step. Therefore, the infiltration rate corresponds to the derivative of the accumulated infiltrated water:

$$\frac{dZ}{dt} = \frac{d(m \, t^a)}{dt} \tag{6}$$

$$\text{IR} = m \, a \, t^{(a-1)} = C \, t^{(a-1)} \tag{7}$$

where IR is the infiltration rate [mm h^{-1}], C is the instantaneous infiltration rate [mm h^{-1}], and t is the time [min].

The volume of water used in each test was calculated as the sum of the infiltrated volume at each time step, divided by the area of the cylinder:

$$\text{Vol} = \frac{\sum_0^i \Delta h \, r^2}{\pi \, r^2}$$
(8)

where Vol is the infiltrated volume in mm, Δh is the change in water level within the cylinder during time interval i [mm], and r is the radius of the inner cylinder [mm].

Inverted well described by Cauduro and Dorfman (1986) was used for the determination of saturated hydraulic conductivity ($Ksat$). The inverted well method assumes that the soil is almost saturated, and according to law of Darcy, the average velocity of the groundwater flow approximates the hydraulic conductivity:

$$Ksat = \frac{\Delta h}{\Delta t}\left(\frac{r}{R}\right)^2$$
(9)

where Δh r is the well's radius; R is $\frac{\sqrt{1+4h}-1}{2}$.

Figure 17 - Equipment utilized to do the soil test (a) cylinder concentric; and (b) invert well. Source of the pictures: Perez et al., 2018.

(a)   (b)
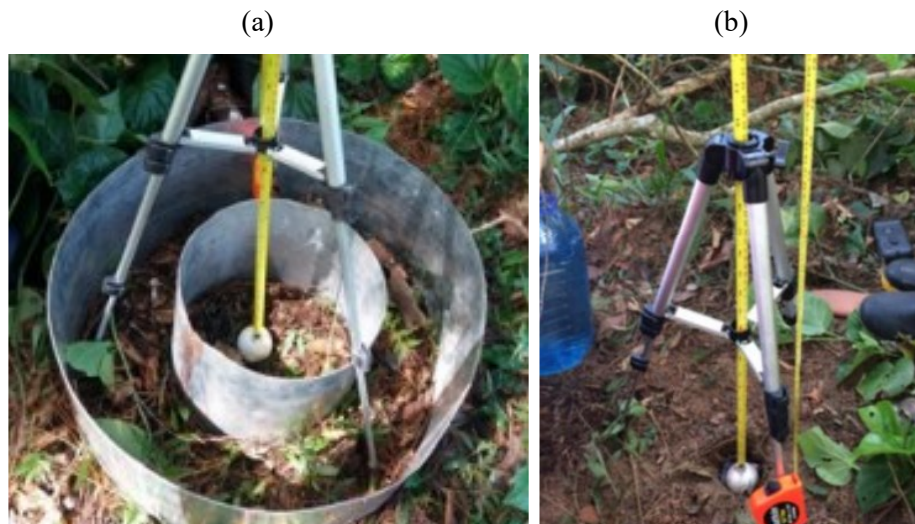
In order to make the inverted well test the wells were hand-drilled until resistance (bedrock or water). Through soil characterization, it was possible to describe soil depth in relation to elevation and $Ksat$ concerning depth (Figure 18 a,b,c). Thus, it was possible to characterize different layers of the Ribeirão Grande Catchment, from the surface to the bedrock (Figure 18, d, e) with different hydraulic conductivity. The soil in step hillslope is shallow and characterized by rock outcrop. Some studies of landslides determined main four classes of

hydraulic characteristics of the subsurface, residual soil of granite, residual soil of diabase, diabase, and granite (Oliveira *et al.*, 2012; Figure 18f).

Figure 18 - Geological information used to set up ParFlow. (a) Relationship between saturated conductivity and soil depth; (b) Relationship between soil depth and elevation; (c) Spatial distribution of soil depth; (d) Typical view in grasslands areas; (e) Typical soil profile structure; and (f) Geological section parametrized at ParFlow, where arrows at geology indicate the preferential flux of water during a storm. Adapted from: Oliveira et al., 2012.
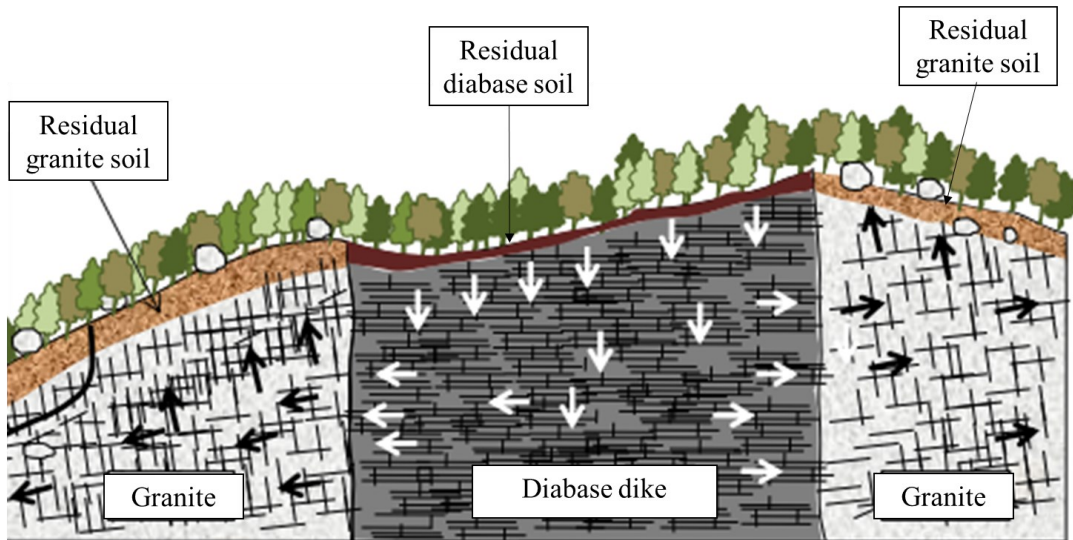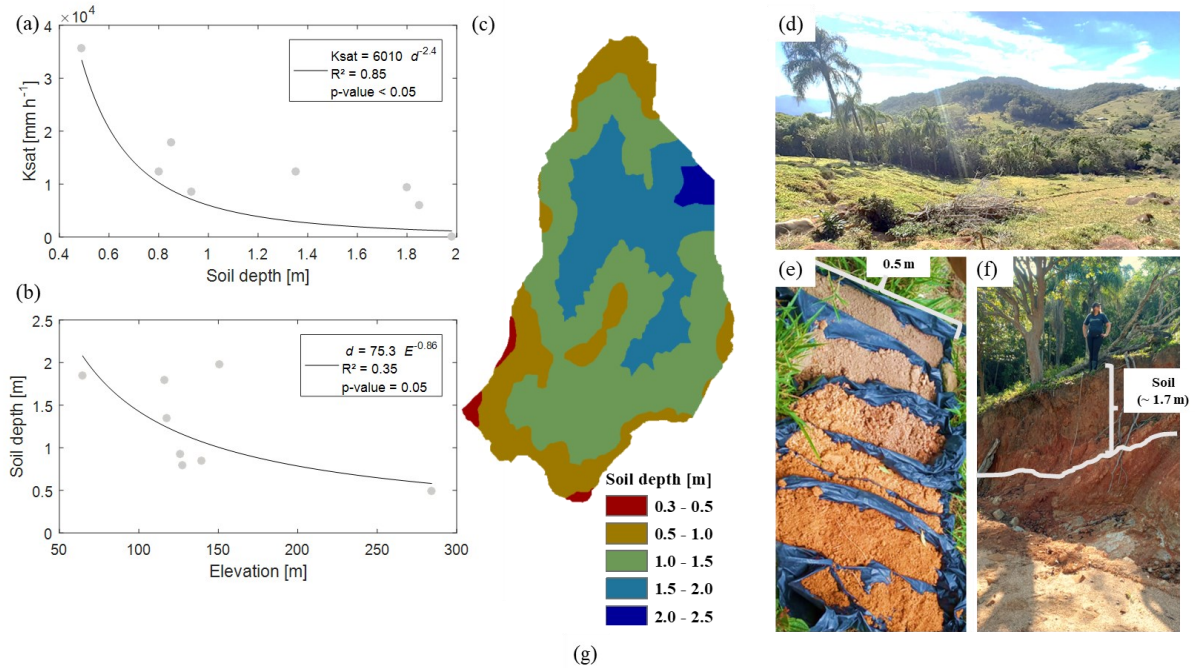
3.2.5   Continuous data

The RGC (Figure 11) had automatic water level monitoring at the outlet from December 2015 to July 2017, conducted by the Santa Catarina Sanitation Company (CASAN). Two more cross-sections have automatic water level monitoring installed by the author in November of 2022, P1 and P2 (Figure 11). There has also been automatic monitoring of rainfall, wind speed and direction, air temperature, radiation, and air humidity at the meteorological station since 2016 (Table 4). Atmospheric pressure data were obtained from the Institute of Meteorology (INMET) at the Florianópolis station "A806". The radiation data gaps from the Peri meteorological station were replaced with data from the INMET dataset. All of the equipment is shown at Figure 19.

Table 4 - Automatic monitoring of hydrological variables

Data	Equipement	Period of data collection
Meteorological station	Temperature: Thermistor Temperature Probe H377[1] Wind direction and speed: S[2] Sonic Anemometer Solar radiation: CMP[3]-L Pyranometer Relative humidity: HygroClip S3[4]	Solar radiation, relative humidity, and temperature since 10/20/2016. Wind speed and direction since 04/30/2020
Ribeirão Grande water level gauge	Data provided by CASAN	From 15/12/2015 until 22/07/2017
P1 water level gauge	AgSolve LEVELOGGER 5 M5	From November of 2022
P2 water level gauge	AgSolve LEVELOGGER 5 M5	From November of 2022
Meteorological station INMET	Atmospheric pressure and solar radiation data provided by INMET from station A806	From: 01/01/2015
Rainfall gauge	Tipping Bucket Rain Gauge - 260-2501-A[6]	From: 17/06/2016

[1] Manufactured by WaterLog, Yellow Springs, Ohio, United States of America
[2] Manufactured by Climatronics, Hamilton, Ohio, United States of America
[3] Manufactured by Campbell Scientific, Logan, Utah, United States of America
[4] Manufactured by Rotronic, Grindelstrasse, Bassersdorf, Switzerland
[5] Manufactured by Sollinst, Georgetown, Ontário, Canada
[6] Manufactured by Nova Lynx Corporation, Grass Valley, California, United States of America

The rating curve was developed to three cross-sections: outlet of RGC, P1 and P2 where water level gauges are located (Figure 11). The rating curves were calculated by the best fit of the power relationship between discharge and water level (Figure 20):

$$Q_{RC} = a_{RC}H^{b_{RC}} \tag{10}$$

where Q_{RC} is the estimated discharge by the rating curve [L s^{-1}], H is the water level [cm], and a_{RC} and b_{RC} are regression constants. At RGC the discharge measurements were done by

dilution and current meter (Figure 23). At P1 and P2 the discharge measurements were done by FlowTracker (Figure 20).

Figure 19 - Continuous data collection. (a) cross-section monitored with sensor level at P2; (b) cross-section monitored with sensor level at P1; (c) cross-section monitored with sensor level at Ribeirão Grande outlet; (d) meteorological station; and (e) rainfall gauge
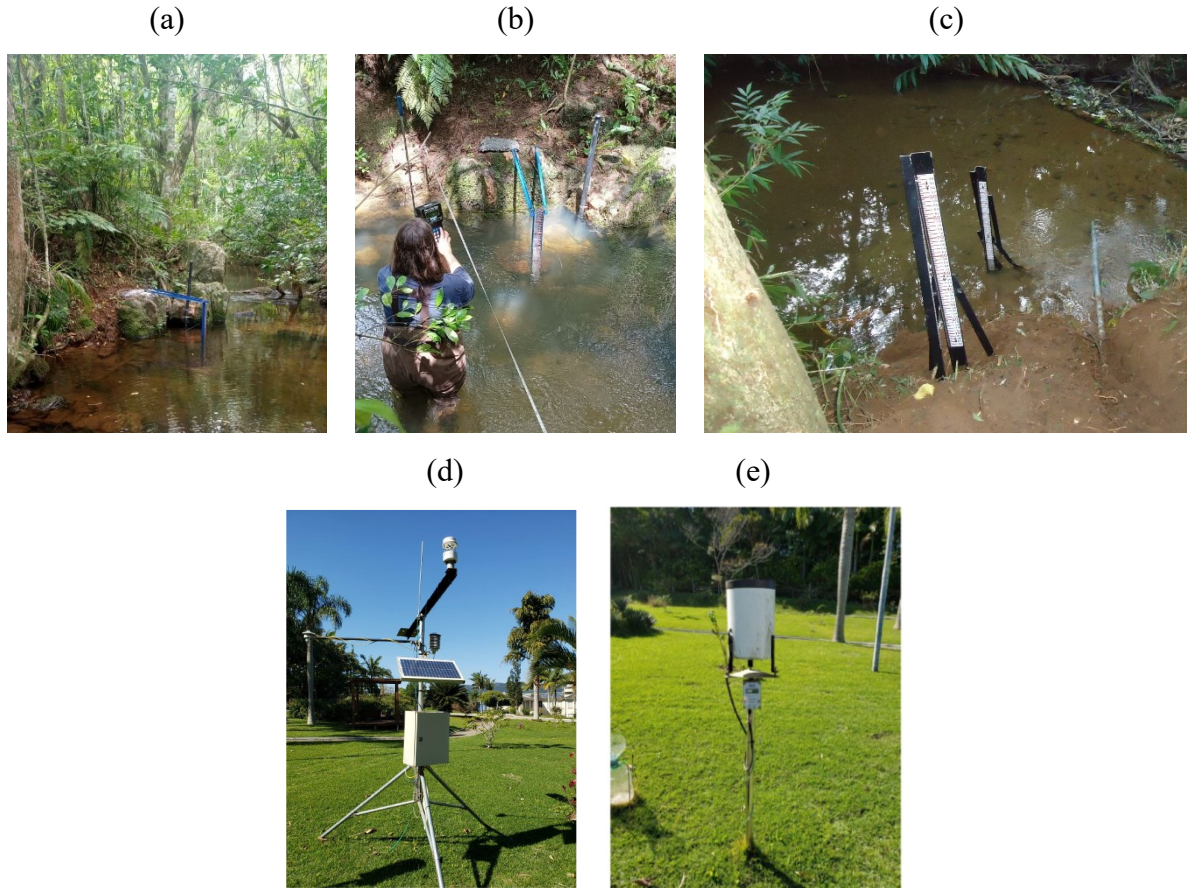
Figure 20 - Rainfall-runoff data (a) Rainfall-runoff data series at P1 and P2; (b) ratting curve at P1; and (c) ratting curve at P2.
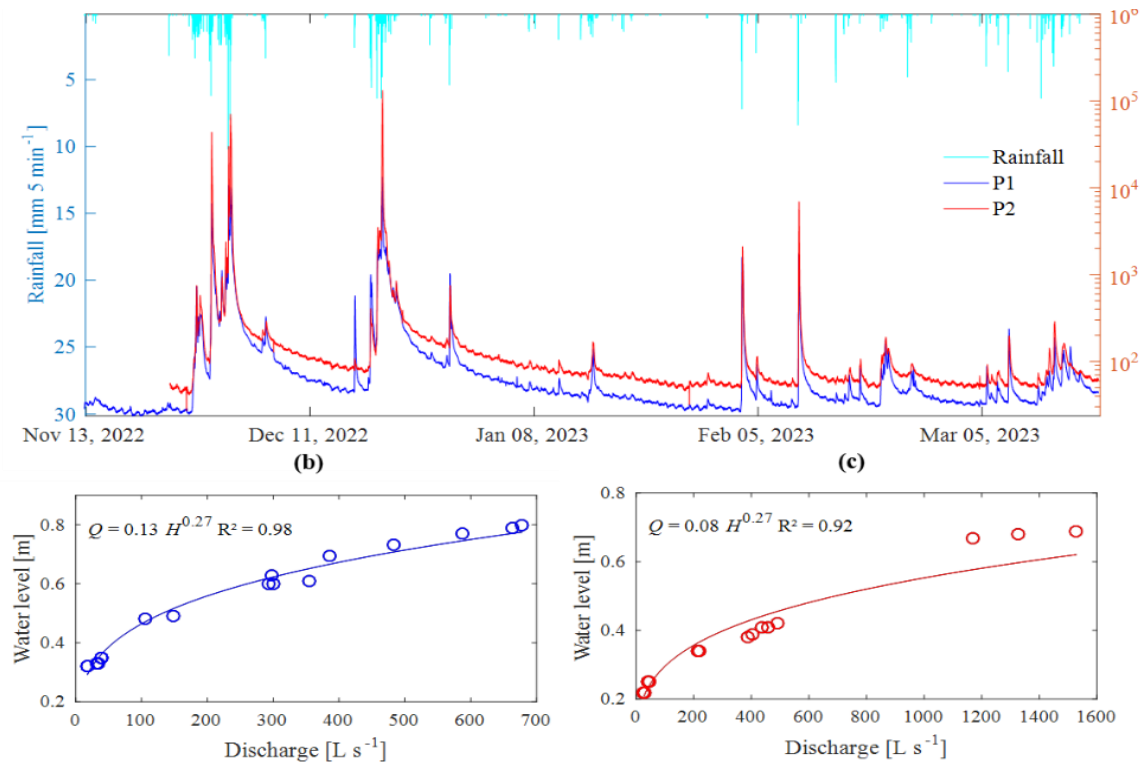
3.3 USE OF THE DATA

The collected data were used in various sections in the following chapters. To facilitate the understanding of the reader, Table 5 indicates where each dataset was employed. Chapter 4 has a specific objective: to determine whether the variations in baseflow among different headwater streams are attributable to measurement errors or differences in the water storage process. To achieve this objective, we utilized data from discharge and velocity flow measurements during baseflow.

Chapter 5 aims to investigate how the physical characteristics of catchments (e.g., area, slope, geology) influence the quantity and quality of baseflow. To accomplish this specific objective, we used data from the discharge campaign, including the discharge at the outlet of the Ribeirão Grande Catchment for normalizing specific baseflow. Additionally, isotopic data was employed.

Chapter 6 has the specific objective of using baseflow campaigns to assist in calibrating a physical model (ParFlow) to investigate how the physical characteristics of the landscape control runoff generation. To verify the spin-up process, we used data from the

baseflow campaign. To run the model, we relied on data from a meteorological station to estimate evapotranspiration, and rainfall and runoff data to validate the model.

Table 5 – Description of the use of the dataset

Data	Used in
Campaign discharge during baseflow	Chapter 4, Chapter, 5, Chapter 6 and APPENDIX C
Campaign flow velocity during baseflow	Chapter 4 and APPENDIX C
Campaign isotopes during baseflow	Chapter 5
Spring mapping	APPENDIX D
Meteorological dataset	Chapter 6
Discharge dataset at Ribeirão Grande Catchment	Chapter 4 and APPENDIX C
Discharge series at P1 and P2	Chapter 6
Rainfall data	Chapter 4, Chapter 6 and APPENDIX C

APPENDIX C aims to verify if velocity and discharge values measured during baseflow can improve the estimation of the geomorphological instantaneous unit hydrograph. We also utilized rainfall-runoff series to identify events and calibrate the GIUH based on the relationship between discharge and velocity during baseflow.

APPENDIX D is dedicated to exploring how the longitudinal dynamics of the drainage network change under different states of saturation. To address this objective, we relied on data from springs.

4. PRECISION AND ACCURACY OF STREAMFLOW MEASUREMENTS IN HEADWATER STREAMS DURING BASEFLOW

ABSTRACT

The quantification of baseflow is key for water resources management. However, there are few reports on the precision and accuracy in low streamflow measurements. In this paper, we systematically analyze the precision and accuracy of dilution streamflow measurements in headwater channels during baseflow. Precision refers to the variability of the values for repeated measurements and accuracy is how much the measured value approximates the reference one. We measured streamflow in 31 different cross-sections with contributing areas ranging from 0.02 to 5.33 km². Streamflow measurements with the current meter were adopted as reference for accuracy estimation. A precision error of ±5.0% was found for the measurements. The percent errors compared to reference streamflow ranged from 0.7 to 15.8%, with a median of 6.1%. Precision and accuracy are in the same order of magnitude found in the literature for larger streams. These results can be used for constraining the uncertainty of streamflow measurements and rainfall-runoff modeling of headwater streams.

4.1 INTRODUCTION

Streamflow from headwater is used for drinking water, irrigation, and recreation (Freeman; Pringle; Jackson, 2007). Headwater streams control a large part of streamflow generation (Sidle *et al.*, 2000) and they remove more nutrients than big streams (Alexander; Smith; Schwarz, 2000). Most of the time the water that flows in these streams is baseflow, coming from water stored in the soil and rock profiles (Egusa *et al.*, 2016). The baseflow is of ecological importance since some chemical elements important for the biota are better fixed in low flow conditions (Doyle *et al.*, 2005) and it acts as a buffer for changes caused by climate and land use (Van Loon; Van Huijgevoort; Van Lanen, 2012). Therefore, the quantification of the water stored and released as baseflow is key for water resources management (Miller *et al.*, 2016) as well as for the understanding of runoff generation processes in catchments (e.g.Egusa et al. (2019), and Uchida and Asano (2010)).

There are three main methods to measure streamflow in natural channels: the velocity-area method; the dilution method; and the use of hydraulic structures such as weirs or flumes

(Kondolf; Piégay, 2016). The most common procedure for measuring streamflow is to calculate the average velocity in a cross-section using a current meter along the stream width and depth profile (Mcmillan; Krueger; Freer, 2012). The main types of instruments of the current meter are mechanical (rotations of a propeller) or acoustical (ADCP - acoustic Doppler current profiler). However, it requires a cross-section where the water depth is sufficient for the equipment to work. The use of weirs or flumes requires ad hoc hydraulic works. The dilution method is particularly effective for small streams with irregular channel cross-sections (Bergstrom *et al.*, 2016), its only requirement being that the tracer should be completely mixed with the flow.

Quantifying streamflow measurement errors is crucial as they will be directly translated into uncertainty in hydrologic models (McMillan *et al.*, 2010) and may lead to unnecessary costs due to poor ecological or social decisions (McMillan *et al.*, 2017). Two types of errors in data measurement can be listed: errors related to precision and errors related to accuracy. Precision refers to the variability of the values found for repeated measurements (Day, 1976), which is a measure of ''the statistical variance of an estimation procedure'' (West, 1999). Accuracy is how much the measured value approximates a reference taken as the correct value (Walther; Moore, 2005).

Streamflow measurement in headwaters is challenging as the channels are usually highly heterogeneous with exposed bedrock, woody debris, cascades, and step-pools (Montgomery; Dietrich, 1989). Even for large-scale streams, where cross-sections are generally uniform, there is still a lack of information on the expected distributions and magnitudes of error in streamflow observational data (Mcmillan; Krueger; Freer, 2012). Most streamflow measurement errors were estimated for streams with streamflow in the orders of 10^2 to 10^5 L s^{-1} (Benischke; Harum, 1990; Clow; Fleming, 2008; Day, 1976, 1977; Kite, 1993), while little is known for headwater streams on the order of 10^{-1} to 10^2 L s^{-1} (Bjerve; Grosterrud, 1980; Hudson; Fraser, 2002).

The accuracy is generally estimated by comparing different measurement techniques (Benischke; Harum, 1990; Bjerve; Grosterrud, 1980; Davids *et al.*, 2019; Gees, 1990; Kite, 1989). Most of the time in headwater streams is not possible to use different techniques in the same cross-section. To overcome a such challenge one can resort to flow scaling, because streamflow is usually linearly related to the drainage area (Asano; Uchida, 2010; Egusa et al., 2016; Karlsen et al., 2016; Peralta-Tapia et al., 2015; Uchida; Asano, 2010; Woods; Sivapalan;

Duncan, 1995b) and velocity is a power-law function of streamflow (D'Angelo *et al.*, 1993; Leopold, 1953; Morrice *et al.*, 1997; Wondzell; Gooseff; McGlynn, 2007).

In this chapter, we systematically analyze the precision and accuracy of streamflow measurements in headwater channels under baseflow conditions. We used field data of first to fourth order catchments with areas ranging from 0.02 to 5.33 km². Measurement errors were estimated using three analyses: (i) the variance of repeated measurements; (ii) the comparison between the streamflow measured using the dilution method and the current meter and; (iii) the errors in relation to the rating curve. In addition, we looked at the relationships between streamflow, drainage area and flow velocity in our data and compared the results with those found in the literature.

4.2   MATERIALS AND METHODS

Precision and accuracy analysis of the dilution method was performed for streamflow measurements of each cross-section (Figure 11). Precision refers to the variability of the values found for repeated measurements (yellow box in Figure 21). The precision can be estimated when there are multiple streamflow measurements (Day, 1976).

Accuracy is the deviation of a measurement from a reference one. Most of the literature uses the streamflow measured with another method as the reference (or real) value. However, in headwater cross-sections it may not be possible to measure streamflow by more than one method. Therefore, we analyzed the accuracy of the data set in two different ways (grey boxes in Figure 21): (i) in the case that streamflow was measured with more than one method in the same cross-section, the differences between the streamflow measured with salt dilution and the other method were calculated (Benischke; Harum, 1990; Bjerve; Grosterrud, 1980; Davids *et al.*, 2019; Gees, 1990; Kite, 1989); (ii) in cross-section 10 we calculated it as the difference between the streamflow measured with the dilution method and the best fit of the rating curve derived using current meter measurements (e.g., Clow and Fleming (2008), and Hudson and Fraser (2002)).

In addition, we looked at the relationships between streamflow and drainage area, and between specific streamflow and drainage area on various days of measurement and for all our data combined. Lastly, we illustrated the relationship between streamflow and flow velocity we found using the dilution method and the current meter, respectively, and compared our results to data reported in the literature (quoted in Figure 26).

Figure 21 - Flowchart showing systematically how we calculated the measurement error.
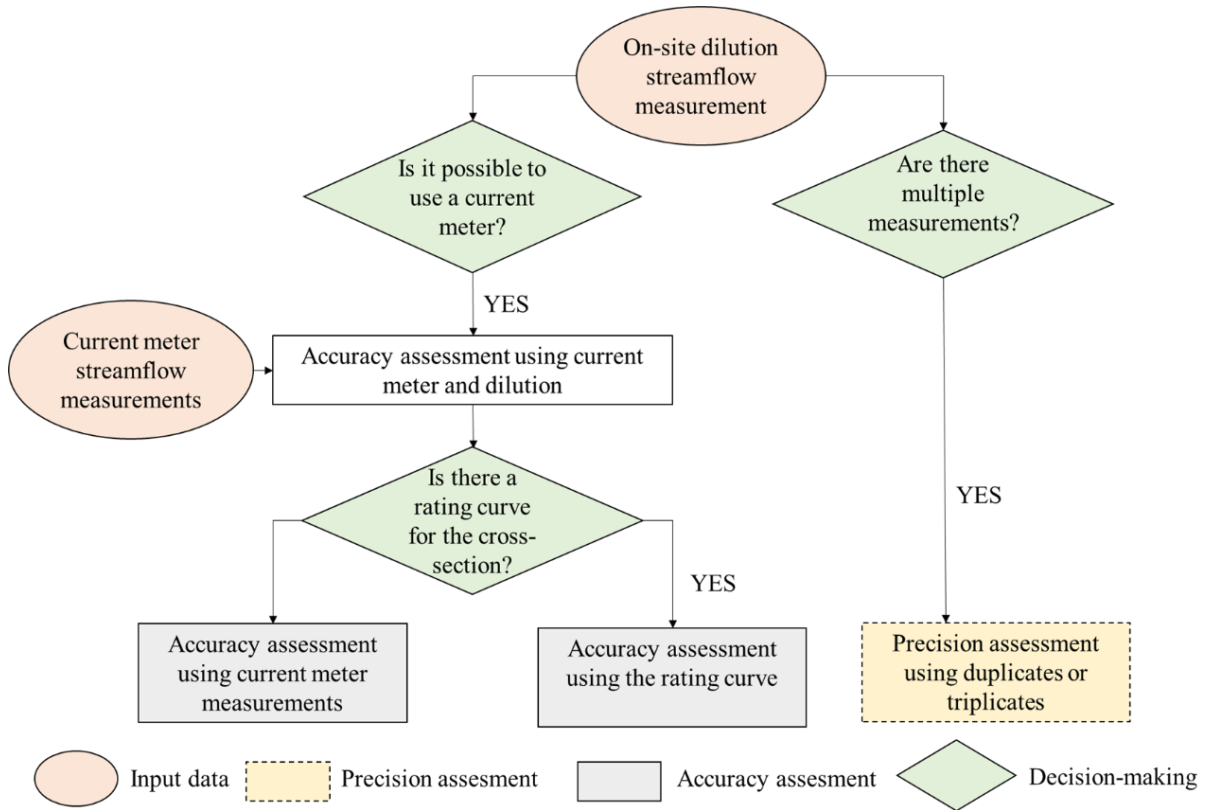
The precision is assessed through the percent error about the mean of duplicates and triplicates (Day, 1976). The greater the precision, the lower the error:

$$error_P = \frac{Q_j - \overline{Q_m}}{\overline{Q_m}} \cdot 100 \tag{11}$$

where Q_j is streamflow measurement j [L s^{-1}], $\overline{Q_m}$ is the mean value of all the measurements [L s^{-1}].

The accuracy is assessed through the absolute percent error compared to the reference streamflow. The greater the accuracy, the lower the error. In this paper the reference streamflow is either the streamflow measured with the current meter (Q_{CM}, Equation 6) or the streamflow estimated from the rating curve (Q_{RC}, Equation 7):

$$error_{CM} = \left| \frac{Q_D - Q_{CM}}{Q_{CM}} \right| \cdot 100 \tag{12}$$

$$error_{RC} = \left| \frac{Q_D - Q_{RC}}{Q_{RC}} \right| \cdot 100 \tag{13}$$

where Q_D is the streamflow measured using the dilution method [L s^{-1}].

The rating curve was derived in cross-section 10 where the water level gauge is located (Ribeirão Grande Catchment; Figure 11). The rating curve was obtained from the best fit of a

power-law relationship between streamflow measurements with the current meter and the corresponding water levels (Equation 10).

Streamflow, flow velocity, and drainage area scaling relationships were assessed. Relating (i.e. scaling) streamflow to the catchment area, which is called "drainage area ratio method", is commonly used to estimate the streamflow in ungauged catchments (Archfield; Vogel, 2010). Nearby catchments in the same landscape are often assumed to have similar specific streamflows:

$$q = \frac{Q}{A} \tag{14}$$

where q is specific streamflow [L s^{-1} km^{-2}], Q is streamflow and A is catchment area [km²]. Equation 9 implies that the relationship between streamflow and area is linear. This seems to be the case above an area of around 1 to 2 km² (e.g., (Archfield; Vogel, 2010; Egusa et al., 2016; Karlsen et al., 2016; Lyon et al., 2012; Woods; Sivapalan; Duncan, 1995b). In order to verify the variation in the specific streamflow of different monitoring campaigns, we normalized the specific streamflow of each cross-section (qn_i) by dividing the specific streamflow of each cross-section by the specific streamflow of the day (q_d):

$$qn_i = \frac{q_i}{q_d} \tag{15}$$

where qn is the normalized specific streamflow at cross-section i [L s^{-1} km^{-2}/L s^{-1} km^{-2}], q is the specific streamflow at cross-section i [L s^{-1} km^{-2}] and q_d is the specific streamflow on the day [L s^{-1} km^{-2}]. The specific streamflow for each day was obtained by Equation 9.

According to Leopold and Maddock (1953), the relationship between streamflow and velocity can be described with a power-law (e.g. Bergstrom et al. (2016), Edwardson et al. (2003), Leopold (1953), and Wondzell, Gooseff, and McGlynn (2007)):

$$v = aQ^b \tag{16}$$

where v is the velocity [m h^{-1}], a and b are regression constants.

4.3   RESULTS

We analyzed a total of 75 streamflow measurements, 12 measurements using the volumetric method (Q_V) (Table 6), 57 measurements using the dilution method (Q_D) (Table 7), and 9 measurements using the current meter (Q_{CM}) (Table 8). We observed that the volumetric method works well for small colluvial channels (Table 7), while the dilution method is ideal for

cascades (Table 7), and a step-pool channel supports the dilution and current method in different cross-sections (Table 7 and Table 8).

With the volumetric method we measured streamflows between 0.01 and 0.29 L s^{-1} in channels with drainage areas ranging from 0.02 to 0.05 km² (Table 2). With the dilution method we measured streamflows between 0.12 and 337.45 L s^{-1} in channels with drainage areas ranging from 0.02 to 5.33 km² (Table 3). Lastly, with the current meter we measured streamflows between 6.0 and 410 L s^{-1} in channels with drainage areas ranging from 0.26 to 5.33 km² (Table 8). The flow velocity of the fourth column was calculated as the total streamflow divided by the area of the cross-section. Two flow velocities are below the minimum suggested by the manufacturer (0.02 m s^{-2}) because the verticals where the propeller did not rotate were counted as zero flow velocity.

Table 6 - Description of streamflow measurements with the volumetric method. Due to the resolution of the digital elevation model, it was not possible to calculate the area for cross-section 1.

Cross-section	Date	Mean streamflow [L s^{-1}]	Container [L]	Number of measurements	Area [km²]	Order [-]	Channel type
1	14/03/2017	0.04	0.25	7	-	-	Colluvial
2	14/03/2017	0.04	0.25	5	0.033	1°	Cascade
3	14/03/2017	0.35	7.00	3	0.078	1°	Colluvial
5	14/03/2017	0.08	0.25	6	0.018	1°	Colluvial
7	14/03/2017	0.09	0.25	6	0.016	1°	Colluvial
9	14/03/2017	0.24	7.00	5	0.047	1°	Cascade
1	01/04/2017	0.07	7.00	3	-	-	Colluvial
2	02/04/2017	0.02	0.25	7	0.033	1°	Cascade
1	22/04/2017	0.01	0.25	6	-	-	Colluvial
5	22/04/2017	0.28	7.00	4	0.018	1°	Colluvial
7	22/04/2017	0.06	0.25	4	0.015	1°	Colluvial
31	13/12/2017	0.29	7.00	3	0.047	1°	Colluvial

Table 7 - Description of streamflow measurements with the dilution method. NC is the number of campaigns that streamflow was measured in a cross-section. Due to the resolution of the digital elevation model, it was not possible to calculate the area for cross-section 27.

Cross-Section	NC	Mean streamflow [L s^{-1}]	Velocity [m s^{-1}]	Width [m]	Mixing length [m]	Amount of salt added [g L^{-1} s]	Area [km²]	Order [-]	Channel type
3	1	0.49	-	0.30	-	16.2	0.078	1°	Colluvial
4	5	0.84 - 27.05	0.02 – 0.10	-	6.3 - 9.7	1.9 - 15.7	0.255	1°	Cascade
6	2	0.57 - 0.61	-	-	-	12.9 - 14.4	0.121	1°	Cascade
7	1	0.12	-	0.20	-	4.1	0.015	1°	Colluvial
8	5	7.33 - 9.68	0.07 – 0.12	-	10.1	3.1	1.136	3°	Cascade
9	2	0.24 - 0.60	0.01	-	3.6	10.0	0.047	1°	Cascade
10	11	9.09 - 337.45	0.13 - 1.33	3.90	6.6-16.5	0.3 - 3.5	5.331	4°	Step-pool
11	1	0.73	0.04	-	3.2	7.5	0.133	1°	Cascade
12	4	6.00 - 27.00	0.08 - 0.21	3.00	13.7	2.4 - 5.4	2.646	3°	Cascade
13	3	5.90 - 23.75	0.13 - 0.28	0.60	8.2	2.1 - 2.6	2.216	3°	Undefined
14	2	2.2 - 3.2	0.05 - 0.06	-	3.2	6.5 - 7.2	0.218	2°	Cascade
15	2	0.6 - 1.1	0.01 - 0.06	-	6.5	20.1 - 24.4	0.293	1°	Cascade
16	1	4.74	0.05	-	7.2	6.3	0.179	1°	Cascade
17	1	0.40	0.03	-	5.8	26.6	0.030	1°	Cascade
18	2	1.01 - 1.08	0.04 - 0.09	-	5.4	16.2 - 5.8	0.053	1°	Cascade
19	1	0.98	-	-	-	26.2	0.053	1°	Cascade
20	1	1.06	0.06	-	3.4	20.7	0.052	1°	Cascade
21	3	0.23 - 1.07	0.02 - 0.04	-	3.4	26.0	0.051	1°	Cascade
22	1	0.88	0.02	-	6.3	9.7	0.049	1°	Cascade
23	1	20.15	-	-	-	3.3	1.570	3°	Step-pool
24	1	9.98	-	-	-	4.4	0.519	2°	Cascade
25	1	6.63	0.05	-	7.5	9.8	0.130	2°	Cascade
26	1	7.76	0.08	-	12.75	7.7	0.142	2°	Cascade
27	1	1.70	0.05	-	5.5	8.7	-	-	Cascade
28	1	2.36	0.08	-	-	5.1	0.103	1°	Cascade
29	1	3.45	0.02	0.30	3.4	5.3	0.075	1°	Colluvial
30	1	0.95	0.11	-	3.2	23.5	0.026	1°	Cascade

Table 8 - Description of streamflow measurements with the current meter. 10* is the cross-section downstream, 10** the cross-section immediately upstream, and 10*** the cross-section immediately downstream of the cross-section used to measure streamflow with the dilution method. MD is the Maximum Depth, AD is the Average Depth and DBV is the Distance Between Verticals.

Cross-Section	Date	Mean streamflow [L s^{-1}]	Velocity [m s^{-1}]	Width [m]	MD [m]	AD [m]	DBV [m]	Area [km²]	Order [-]	Channel type
8	14/03/2017	8.7	0.03	1.5	0.25	0.23	0.3	1.136	3°	Cascade
4	10/04/2017	27.2	0.06	1.8	0.30	0.32	0.3	0.255	1°	Cascade
10*	14/03/2017	53.4	0.06	6.1	0.25	0.15	0.5	5.331	4°	Dune ripple
10**	05/07/2018	40.9	0.02	4.5	0.50	0.27	0.5	5.331	4°	Step-pool
10**	04/09/2018	410.0	0.15	4.5	0.67	0.41	0.5	5.331	4°	Step-pool
12	18/06/2020	6.0	0.04	1.2	0.21	0.12	0.2	2.216	3°	Undefined

4.3.1   Precision of streamflow measurements

We assessed the precision using 46 measurements. The percent error about the mean of multiple measurements ($error_P$) tends to decrease as Q_D increases (Figure 22 a and b). The first and third quartile of $error_P$ of all data were -5.0% and 4.7%, respectively, and the standard deviation was 14.7% (Figure 22b). The largest $error_P$ are close to 1 L s^{-1}.

Figure 22 - Precision assessment: (a) Percent error about the mean of multiple measurements, star (*) is the mean streamflow measurement and bars is the percent error about the mean for each cross-section. (b) Summary of the percent error about the mean of multiple measurements. The box indicates the 25th and 75th percentiles, the central mark indicates the median, and the whiskers extend to the most extreme data points not considered outliers. Outliers are plotted individually using the plus symbol (+).
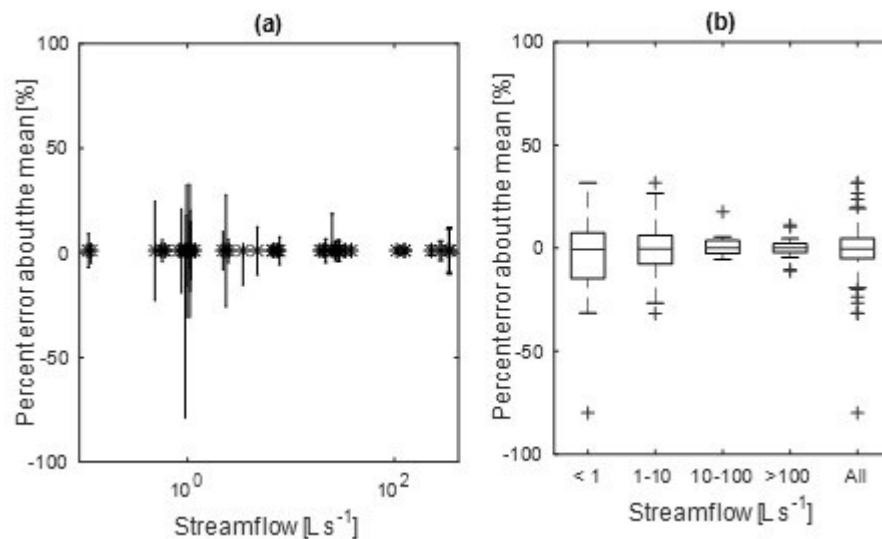
4.3.2   Accuracy of streamflow measurements

Comparison between dilution (Q_D) and current meter (Q_{CM}) data

In Table 9 the streamflows measured with the dilution method (QD) and the current meter (QCM) are compared for the six occasions (cf. Table 8) when both methods were used concurrently. Here we take QCM as the reference value. In six measurements QD was lower than QCM. The percent error compared to QCM (errorCM), which is taken as the reference streamflow here, ranged from 0.70% to 45.63%. The largest errorCM was for the lowest streamflow in RGC (Figure 11). Despite the small number of samples, these data are important, given the scarcity of streamflow measurements with more than one method in cross-sections in headwater streams under baseflow conditions.

Table 9 - Difference in streamflow obtained with the dilution method and the current meter. *error$_{CM}$* is the percent error compared to the reference streamflow which is taken here as the one obtained with the current meter.

Streamflow – Dilution [L s^{-1}]	Streamflow – Current meter [L s^{-1}]	*error$_{CM}$* [%]	Cross-section
5.90	6.03	2.28	13
6.00	6.35	5.57	12
7.33	8.70	15.77	8
19.13	19.98	4.25	10
27.05	27.24	0.70	4
38.31	40.90	6.33	10

Comparison between dilution (Q$_D$) and rating curve (Q$_{RC}$) data

In Table 10 the streamflows obtained with the dilution method (Q_D) and the rating curve (Q_{RC}) are compared for the nine occasions when both methods were used concurrently. Now Q_{RC} is taken as the reference value. The absolute percent error ranged from 1.30% to 42.37%, the median was 6.6%. The rating curve (Figure 23) was derived from measurements with the current meter between March 14, 2017 and September 12, 2018. After that date the cross-section was modified by a severe storm and we could not use the same rating curve.

Table 10 - Difference in streamflow measurement with the dilution method and the rating curve. error$_{RC}$ is the percent error compared to the reference streamflow which is taken here as the one obtained from the rating curve.

Streamflow – Dilution [L s^{-1}]	Streamflow – Rating curve [L s^{-1}]	*error$_{RC}$* [%]	Cross-section
19.14	21.96	12.86	10
28.98	27.37	5.85	10
33.04	33.47	1.30	10
38.31	40.27	4.86	10
125.55	121.94	2.96	10
227.00	371.18	38.84	10
280.00	299.85	6.62	10
294.00	396.89	25.92	10
337.45	237.02	42.37	10

Figure 23 - Rating curve derived from streamflow measurements with the current meter. Q_D is the streamflow measured with the dilution method and Q_{CM} is the streamflow measured with the current meter.
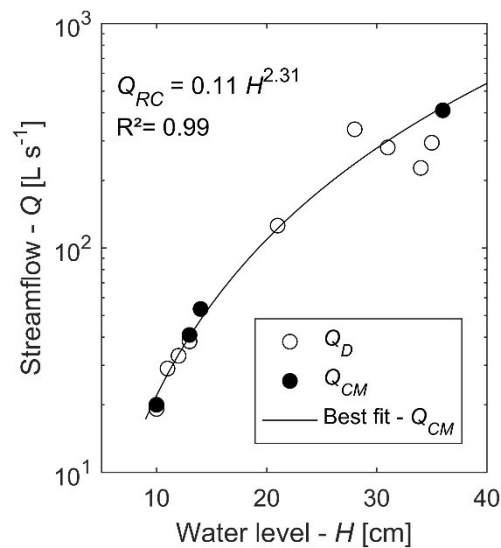
Streamflow and drainage area

The relationship between streamflow and drainage area can be derived by linear regression (Figure 24). All 55 measurements are fitted quite well by the same regression line ($R^2 = 0.68$). R^2 was ≥ 0.79 on all individual monitoring days. The measurements made to derive the rating curve were not considered.

Figure 24 - Relationship between streamflow and drainage area. Data are shown on a log-log scale to facilitate visualization.
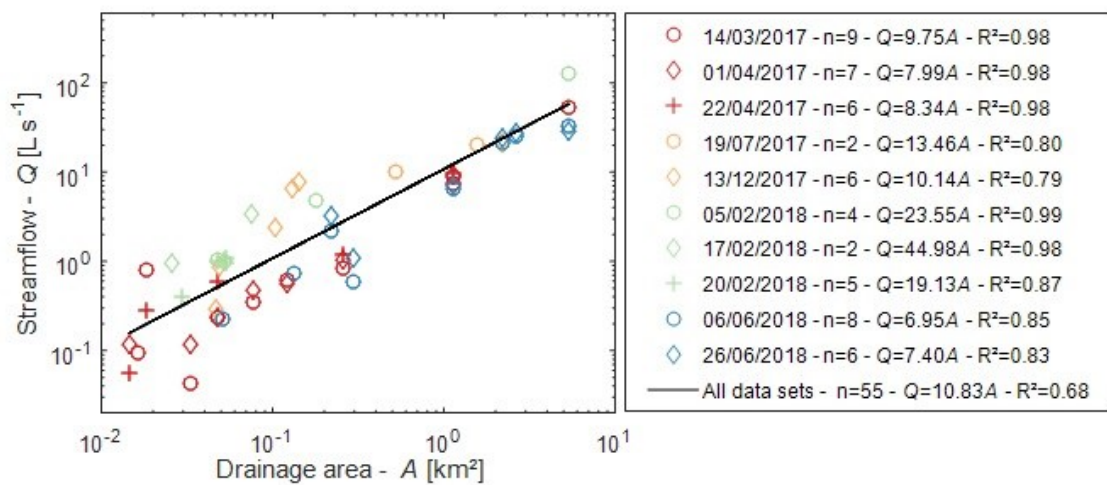
Flow velocity and streamflow

We measured the flow velocity 52 times, 43 times with the dilution method (v_D), and 9 times with the current meter (v_{CM}). There is a power-law relationship (see Equation 16) between v_D and Q_D (Figure 25 and Table 7) when the entire data set is considered. The regression lines for the current meter data (v_{CM}) and the data obtained with the dilution method (v_D) have a similar slope (b), but the intercept for the v_{CM} data (a) is about 100 m h^{-1} lower (Table 9) because the v_{CM} are lower than the v_D so that the regression line runs lower (Figure 25). When only cross-sections of first and second order streams are considered, it is not possible to verify a power-law relationship (Table 7).

Figure 25 - Relationship between streamflow and flow velocity.
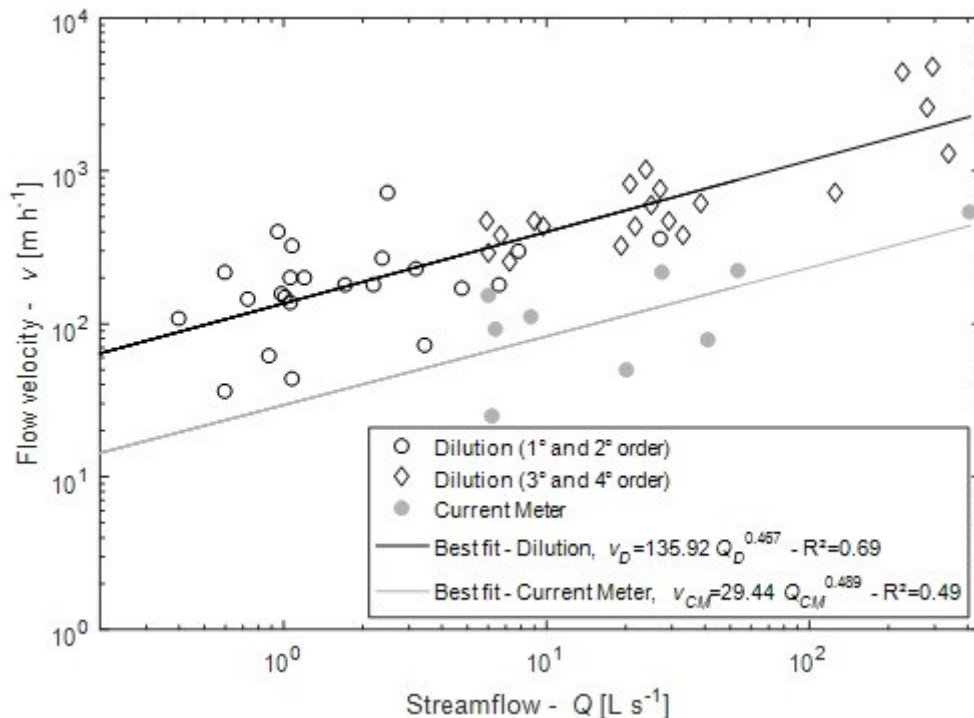
Our dilution method data lie above or among the data from other studies, while our current meter data lie below them (Figure 26). We can see in Table 7 that the values of the regression parameters are inside the range found in other studies. All values for a and b in Table 11 have a p-value < 0.05.

Table 11 - Values of the parameters *a* and *b* in power-law regressions (Equation 11) between streamflow (L s^{-1}) and flow velocity (m h^{-1}). n is the number of data points in the regression, R² reflects the goodness of fit, PLW stands for Peri Lake Catchment.

Study	*a*	*b*	n	R²
D'Angelo *et al.* (1993)	195.0	0.21	22	0.6
Morrice *et al.* (1997)	53.8	0.52	17	0.9
Edwardson *et al.* (2003)	101.0	0.29	31	0.4
Wondzell *et al.* (2007)	4.6	1.78	5	0.9
Bergstrom *et al.* (2016)	336.0	0.18	16	0.6
PLEC (Current meter)	29.4	0.47	9	0.5
PLEC (Dilution 1° and 2° order)	145.5	0.28	23	0.1
PLEC (Dilution 3° and 4° order)	115.4	0.53	20	0.7
PLEC (Dilution)	135.9	0.49	43	0.7

Figure 26 - Relationship between flow velocity and streamflow for a wide range of stream sizes and channel morphologies from several streams. Adapted from Wondzell, Gooseff, and McGlynn (2007). PLW stands from Peri Lake Experimental Catchment, D for dilution method and CM for current meter.
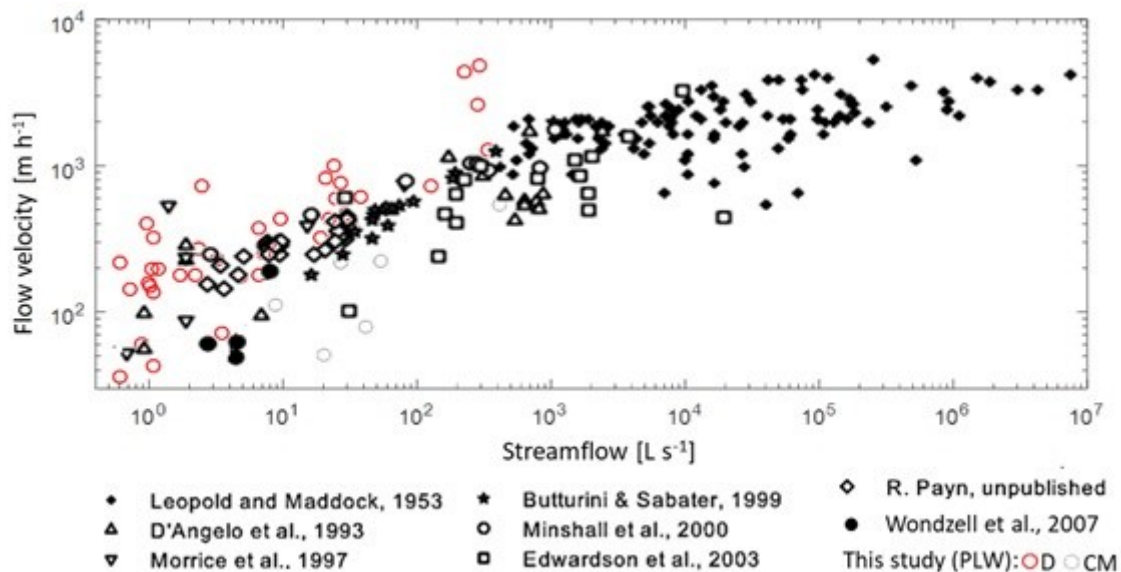
4.4 DISCUSSION

4.4.1 Choice of the streamflow measurement method

Here we discuss some particularities observed in the field for each method. All channels where the volumetric method was used are first order and mostly colluvial channels.

The main problem related to the use of this method in natural channels is that it is only feasible for small volumes and that all the water of the cross-sections must flow to the same point.

Concerning the slug dilution method, Day (1976) recommends a distance of 25 times the width of the channel so that there is a complete mixing of the tracer in the water. However, the method assumes that the mixing length should be straight with no pools. We noticed that there are pools between intervals smaller than 25 times the width of the channel in cascade and step-pool channels, which led us to adopt shorter distances. According to Montgomery and Buffington (1997), step-pool has a pool every 4 times the width of the channel, and cascade has a pool less than 1 time the width of the channel. However, in our study we noticed that this relationship varies with the flow. We observed that the lower the streamflow, the greater the number of pools in the channels. For example, in cross-section 4 (Figure 11) the distance between two pools is 6.3 meters with a streamflow of 1.19 L s^{-1}. When the streamflow was 27.05 L s^{-1}, the distance between pools increased to 9.7 meters.

On June 18, 2020, streamflow was measured in the driest conditions in the catchment encountered during this work. In this campaign the minimum velocity required for the propeller of the current meter to rotate was reached in just 2 of the 14 verticals. Therefore, Q_{CM} was probably below the actual streamflow.

The dilution method was the most appropriate to use in headwater stream because: (i) the irregular channel geometry and turbulent flow conditions ensure the complete mixing of the tracer in the water, while they do not allow the use of the volumetric or current meter method; (ii) streamflow measurements using the dilution method took us on average twenty minutes, while the current meter took us one hour per measurement, and (iii) the equipment used in the dilution method is easier to transport and has a lower cost when compared to the current meter. Also, (Davids *et al.*, 2019) concluded that the dilution method yields the most accurate measurements among streamflow measurement methods with low cost and low technical complexity.

4.4.2   Precision and accuracy errors

In our data set streamflow measurements with the dilution method at lower water levels had less spread dispersion around the rating curve than measurements at higher levels (Figure 23). According to Mcmillan, Krueger, and Freer (2012) the confidence bounds of the rating curve have typical values of 50–100% for low flows, 10–20% for medium or high (in-

bank) flows, and a single estimate of 40% for out of bank flows. In our data set there is less uncertainty in the rating curve at lower flow rates, different from what is indicated in the review article of Millan *et al.* (2012). Besides, using the dilution method makes it is possible to measure streamflow even at low water levels, where sometimes it is not possible to use a current meter. Because the dilution method showed good results for low streamflow measurements, the use of the dilution method could improve the derivation of the rating curve at low flows.

Day (1976) found a percent error about the mean of duplicates and triplicates (*error$_P$*) in the dilution method of up to $10 - 20\%$, although such percentages were infrequent. The most probable *error$_P$* were, however, considerably less, ranging from about 4 to 7%. In Day (1976) streamflow between 130 and 6110 L s^{-1} was measured, while our streamflow varied between 0.11 and 340 L s^{-1}. Even with the difference in scale between streamflow, the *error$_P$* were in the same order of magnitude.

With the current meter, *error$_P$* may range from 0.3 to 2.8% (Smoot; Carter, 1968a), or from 1.4 to 5.1% (Schneider; Smoot, 1976). In the studies of Smoot and Carter (1968) and Schneider and Smoot (1976) the *error$_P$* is inversely proportional to Q_{CM}, as in our results.

Hudson and Fraser (2002) estimated the *error$_{RC}$* of streamflow measurements with the dilution method and found it to be 5.5% on average in a stream with a drainage area of 8.6 km². The *error$_{RC}$* of our values was on average 9.0% in a stream with a drainage area of 5.3 km². Hence, the values from our study are similar to those of Hudson and Fraser (2002).

In general, the values found in the literature indicate that the *error$_{RC}$* (Clow; Fleming, 2008; Hudson; Fraser, 2002) is smaller than the error when comparing two measurement methods (Benischke; Harum, 1990; Bjerve; Grosterrud, 1980; Davids *et al.*, 2019; Gees, 1990; Kite, 1989). The opposite occurred with the data from our study. When we consider *error$_{CM}$* and *error$_{RC}$* together the errors are between 3.3 and 19.4% for the first and third percentile.

Other work in the literature found similar measurement errors (Figure 27), even in streams with higher streamflow. Figure 27 shows the relative errors as (i) the RMSE of the rating curve (Clow; Fleming, 2008; Hudson; Fraser, 2002); (ii) the average of the percent error compared to a reference streamflow (Benischke; Harum, 1990; Bjerve; Grosterrud, 1980; Davids *et al.*, 2019) and; (iii) the most probable percent error compared to reference streamflow (PLEC – this study; Benischke; Harum, 1990; Bjerve; Grosterrud, 1980; Gees, 1990; Kite, 1989).

Figure 27 - Variation of absolute percent error compared to reference streamflow from the literature. The squares indicate the average of maximum and minimum percentage error and maximum and minimum streamflow, the whiskers extend to the most extreme data points of streamflow and percent error. Where PLW is Peri Lake Experimental Catchment
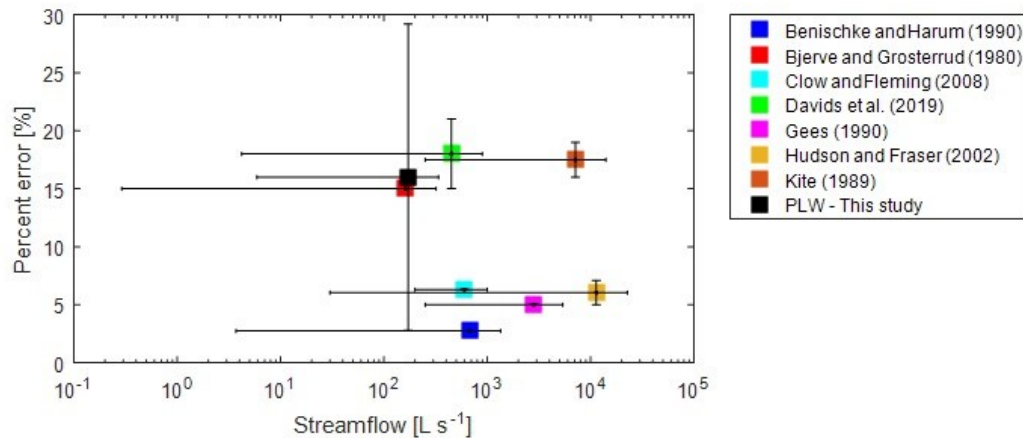
Relationship between streamflow and flow velocity

The velocity is not uniform across stream networks, because of differences in fluvial geometry (Leopold; Maddock, 1953). The headwater drainage network in our study area is formed mainly by cascade channels where there is a great variation in velocity between cross-sections which change between fast flow and pools. The velocity measured using the dilution method represents an average velocity in the mixing length, while the velocity measured with the current meter represents the velocity of a single cross-section. The choice of the streamflow monitoring cross-section might overestimate the average velocity of the stream when the dilution method is used, since the cross-section is chosen so that there is enough turbulence to ensure complete mixing. On the other hand, the cross-sections chosen to measure streamflow with the current meter must have a sufficient water level to support the operation of the device and this occurs only in cross-sections where the flow is slower. Using the current meter and dilution simultaneously to calculate the velocity is the ideal approach to characterize the flow velocity in the drainage network.

It was not possible to verify a general relationship between velocity and streamflow in first and second order streams under baseflow conditions. One explanation could be that there are two mechanisms that control flow velocity: (i) hydrodynamic dispersion, which occurs within the individual flow channel, and (ii) geomorphological dispersion, which changes

according to the geometry of the network (Rinaldo; Marani; Rigon, 1991). Both dispersion coefficients increase with increasing stream order (White *et al.*, 2004). If same order streams of a catchment have similar hydraulic patterns, this indicates the velocity must be similar in streams of the same order.

4.5   CONCLUSION

We found that the dilution was the best measuring method for the cascade morphology which we found in most of our headwaters. The dilution method is efficient even at low water levels, where the current meter cannot be used. The precision of the dilution measurements was around ±5.0% with a standard deviation of 14.7%. The error compared to a reference streamflow ranged from 0.7 to 45.6%. Precision and accuracy are in the same order of magnitude found in the literature for higher streamflows.

The relationship between streamflow and the drainage area is linear. The baseflow of the cross-sections is related to the characteristics of the drainage area and the exchange between the stream and the soil. It was possible to verify the power-law relationship between velocity and streamflow for the data set only when fourth order streams were considered. As can be expected, the first and second order streams are more heterogeneous in geometry and flow velocity. We recommend the use of more than one measurement method in these streams.

Although the accuracy of measured streamflow for first and second order streams has been estimated, knowing the magnitude of absolute errors for these streams is still a challenge. Our results can be applied to improve the quantification of streamflow in headwaters and further constrain the uncertainty estimation in rainfall-runoff modeling. We hope that this work will encourage further research involving streamflow measurements in headwater streams under baseflow conditions.

5. GEOLOGY TRUMPS TOPOGRAPHY: HOW DIABASE DIKES AFFECT SPATIAL DISTRIBUTION OF BASEFLOW

This chapter presents a version of the paper to be submitted to Hydrological Processes: INNOCENTE DOS SANTOS, C.; KLAUS, J.; CHAFFE, P. L. B. Geology trumps topography: How diabase dikes affect spatial distribution of baseflow.

ABSTRACT

The storage and release of groundwater during baseflow are controlled by both topography and geology. Although dikes can act as pathways or barriers to groundwater flow, it is still unclear how diabase dikes specifically interfere in the baseflow patterns. In this study, we investigate how diabase dikes impact baseflow patterns in a small catchment characterized by granite and diabase dikes. To do this, we conducted synoptic campaigns to measure baseflow and collected water samples to analyze $\delta^{18}O$ in 25 nested subcatchments of southern Brazil subtropical Peri Lake Experimental Catchment (19 km²), with areas ranging from 0.02 to 5.33 km², including 12 subcatchments characterized by the presence of diabase dikes. Our investigation included three analyses: Scaling of baseflow, Spearman correlations and multiple linear regression between landscape characteristics (area, mean elevation, mean slope, and percentage of granite) and baseflow (specific baseflow and $\delta^{18}O$). Our results indicate that the percentage of granite is the best predictor of specific baseflow in subcatchments characterized by both diabase dikes and granite, while mean elevation is the primary predictor for subcatchments without diabase dikes. Specific baseflow is found to be independent of area. Additionally, we observed elevation effects in $\delta^{18}O$ just in subcatchments without dikes, where streamflow $\delta^{18}O$ becomes heavier with increasing catchment area. The role of topography varies depending on the underlying geology, emphasizing the need for a deeper understanding of how geology influences baseflow patterns.

5.1 INTRODUCTION

Baseflow is sustained by groundwater stored in the soil, regolith, and bedrock (Egusa *et al.*, 2016; Segura *et al.*, 2019). The amount and sources of baseflow in a single stream is highly dependent on how different subsurface storages store and release water as a result of geology, topography, and land cover (Asano *et al.*, 2020; Fan *et al.*, 2019; Iwasaki; Nagasaka; Nagasaka, 2021; Pfister *et al.*, 2017). What different compartments and flow paths connect and disconnect to the stream also plays a major role in streamflow generation and related catchment transit times and streamflow intermittency (Antonelli *et al.*, 2020; Briggs *et al.*, 2022; Glaser *et al.*, 2021; Rodriguez; Klaus, 2019). The answer to where and how baseflow is generated is key for understanding and predicting the hydrological response and biogeochemical cycles of catchments under global change (Bergstrom *et al.*, 2016; Blöschl *et al.*, 2019; Buttle; Greenwood; Gerber, 2015; Garcia *et al.*, 2023; Iwasaki; Nagasaka; Nagasaka, 2021). Yet, we lack studies evaluating the sources of baseflow and its spatial streams (Segura *et al.*, 2019). The sources of baseflow across heterogeneous hydrological landscapes remain largely unexplored

outside humid, temperate catchments. How landscape elements combine to drive differences in baseflow between headwater streams (Rodriguez; Benettin; Klaus, 2020) for different climate zones, biomes, and in differently evolved landscapes needs urgent attention.

Among the landscape elements driving spatio-temporal patterns of baseflow, geology is the primary factor influencing the sources of baseflow (e.g., deep or shallow), which in turn leads to variations in specific baseflow (discharge per unit drainage area during baseflow conditions (Iwasaki; Nagasaka; Nagasaka, 2021). It is commonly assumed that nearby catchments within the same homogeneous landscape show similar specific baseflow (Karlsen *et al.*, 2016). Specific baseflow has been observed to be rather uniform in small, nested catchments characterized by low-permeable bedrock as a result of similar precipitation and evapotranspiration and the uniform groundwater storage characteristics (Asano; Uchida, 2010; Lyon *et al.*, 2012; Woods; Sivapalan; Duncan, 1995). In catchments characterized by permeable bedrock, specific baseflow often increases with area (Ameli *et al.*, 2018; Kaule; Gilfedder, 2021). One of the principal reasons for this can be the contribution of out-of-catchment deep groundwater flow from headwater catchments to their larger parent catchment (Ameli *et al.*, 2018; Genereux; Wood; Pringle, 2002). In catchments with fractured bedrock, specific baseflow commonly decreases with catchment area (Floriancic *et al.*, 2019; Tetzlaff; Soulsby, 2008) as bedrock fractures in the headwaters store more groundwater compared to downstream areas (Asano *et al.*, 2020). Although the influence of geology on baseflow in various geological settings has already been detected, studies on spatial baseflow patterns in heterogeneous geological systems are limited. Among these settings are dike swarms that are present in crystalline and sedimentary landscapes (Bourke *et al.*, 2023; Cavalcante *et al.*, 2020). Dikes may alter groundwater flow by acting barrier-like (Comte *et al.*, 2017) or provide preferential groundwater flow along their strike (Senger *et al.*, 2015). This type of formation creates a heterogeneous geological structure, whose effects on groundwater are known, but how these effects are transmitted to baseflow patterns is poorly understood, requiring a greater understanding of the role of this geological heterogeneity in baseflow.

Geological characteristics alone are insufficient to fully predict baseflow patterns in small catchments (< 10 km²), where other factors such as topography may become important (Fan *et al.*, 2019). Topography can influence the amount of specific baseflow by controlling the flow paths of water from hillslopes to the streams (Bergstrom *et al.*, 2016; Jencso; McGlynn, 2011; Klaus; Jackson, 2018; McGuire *et al.*, 2005; Muñoz-Villers *et al.*, 2016; Nippgen *et al.*, 2011; Price, 2009; Unfried; Kis-Katos; Poser, 2022). High-relief catchments are usually

characterized by shorter groundwater flow paths than low-relief catchments (McGuire *et al.*, 2005; Muñoz-Villers *et al.*, 2016). In low-relief catchments, the water table follows - with few exceptions - the land surface topography, resulting in predictable and constant baseflow patterns (Ameli *et al.*, 2018). An indirect method for investigating groundwater flow paths is through the use of tracers, such as water isotopes. The isotopes in rainfall are attenuated by mixing in the catchments (Tetzlaff *et al.*, 2015). Smaller hillslopes, with relatively short flow paths, have less capacity to store water and dampen the stable isotopes in the water molecule (SWI) compared to larger hillslopes with high storage capacity (Singh; Emanuel; McGlynn, 2016).

Both the isotopic signature of baseflow and specific baseflow are influenced by a storage process, suggesting that they should exhibit similar patterns (Gabrielli, McDonnell e Jarvis, 2012; Singh, Emanuel e McGlynn, 2016). Nevertheless, in some catchments, the SWI of baseflow is scale-dependent, while specific baseflow is scale-independent (Floriancic *et al.*, 2019; Iwasaki; Nagasaka; Nagasaka, 2021; Lyon *et al.*, 2012; Peralta-Tapia *et al.*, 2015). In these catchments, it remains unclear which mechanism is responsible for specific baseflow and the SWI of baseflow. Iwasaki *et al.*, (2021) speculated, based in their study area, that heterogeneity of geology can alter groundwater flow pathways in ways that are not yet fully understood. Groundwater within fractured bedrock can clearly impact the hydrological dynamics of catchments, affecting water storage, discharge and chemical composition of baseflow (Fan *et al.*, 2019; Hayashi, 2020) in headwaters and larger catchments (Bloomfield; Allen; Griffiths, 2009; Cervi *et al.*, 2017; Frisbee *et al.*, 2011; Thiros *et al.*, 2023). While we know that groundwater dynamics are dominated by fractures in bedrock (Gabrielli; McDonnell; Jarvis, 2012; Oxtobeem; Novakowski, 2003), there is a lack of observational datasets that can accurately constrain bedrock groundwater processes which further complicates our ability to understand these systems (Thiros *et al.*, 2023).

The aim of this study is to evaluate how topography and the heterogeneity of the geology influence the spatial distribution of specific baseflow and baseflow isotopic composition in a drainage network within a catchment characterized by numerous fractures in extrusive volcanic rocks (granite) filled with intrusive volcanic rock, specifically diabase. To achieve this, we carried out synoptic campaigns measuring discharge and sampling streamflow for $\delta^{18}O$ during baseflow in the nested Peri Lake Experimental Catchment (PLEC) characterized by two distinct geological zones, one characterized by granite and the other by granite with diabase dikes. Our general hypothesis posits that increasing geological heterogeneity enhances variability in

groundwater flows, making specific baseflow and its $\delta^{18}O$ across the stream network less predictable based on topographic characteristics. More specifically, we sought answers to the following three research questions:

1. What is the spatial variability of specific baseflow and the baseflow isotopic composition within headwater catchments characterized by granite and diabase dikes?

2. Which physical characteristics of catchments, such as catchment area, mean slope, mean elevation, and percentage of granite, can be used to predict the spatial variability in stream network patterns of specific baseflow and baseflow isotopic composition?

3. What hydrological mechanisms are responsible for variations in stream network patterns of specific baseflow and baseflow isotopic composition, and how do the topographic and geological characteristics of catchments influence these mechanisms?

5.2   MATERIAL AND METHODS

5.2.1   Statistical analysis to evaluate the variability of specific baseflow and $\delta^{18}O$ across the landscape

We examine the relationship between landscapes and baseflow for two groups of subcatchments, with and without diabase dikes to determine the impact of geology on specific baseflow (qn) and $\delta^{18}O$ in relation to landscape characteristics. From baseflow measurement dataset we selected just data in subcatchments where we collected water for isotopes. Statistical analyses were performed using all qn samples from the dataset. Statistical analyses using $\delta^{18}O$ were conducted separately in three ways: i) for campaigns where samples were collected in at least 23 subcatchments (C3 and C5; cf. Table 3); ii) medians of each subcatchments, and iii) the entire dataset.

We employed two approaches to evaluate the relationship between landscapes and baseflow characteristics: Spearman correlation and Multiple Linear Regression (MLR). We normalized and standardized all independent and dependent variables (area, mean elevation, mean slope and percentage of granite; Table 1) for the analysis. We utilized the Box-Cox technique (Box; Cox, 1964) for normalization. Stepwise regression was employed for the MLR analysis. The decision to add or remove independent variables was based on the p-value obtained from an F-test of the change in the sum of squared errors resulting from adding or removing the term. The criterion for adding a term was a p-value < 0.05. To assess the

correlation between independent variables, we used the Variation Inflation Factor and considered a tolerance of less than 5 as acceptable, while values above indicated a multicollinearity problem (Pourtaghi e Pourghasemi, 2014).

5.2.2 Elevation effect on $\delta^{18}O$ values in baseflow

In nested subcatchments baseflow $\delta^{18}O$ values are mainly related to elevation (Asano *et al.*, 2020). This happens because lighter $\delta^{18}O$ tends to precipitate at higher elevations during rainfall events (Kern *et al.*, 2020). However, baseflow $\delta^{18}O$ values can also be related to other landscape characteristic (e.g. slope, geology), which act as indicators of deep grounwater (e.g., Segura *et al.* (2019), and Peralta-Tapia *et al.*, 2016). Consequently, we presume that in subcatchments where baseflow $\delta^{18}O$ values are not explained by elevation, part of the baseflow originates from deep groundwater.

To identify which landscape characteristics, indicate a local water storage, we investigate if there is a significant correlation between elevation and $\delta^{18}O$ values in baseflow in different sets of subcatchment categorized by geology (with or without diabase dikes) and topography. It is assumed that in groups where it is not possible to describe $\delta^{18}O$ values in baseflow through elevation, there is the presence of deep groundwater. The topography-based groups were determined using k-means clustering based on area and slope attributes. We opted for only two distinct groups for area and slope due to the limited number of studied subcatchments.

We assess the elevation effect by the linear correlation between elevation (*E*) and baseflow $\delta^{18}O$ values:

$$\delta^{18}O_{EF} = \delta^{18}O + \alpha E \tag{17}$$

where $\delta^{18}O_{EF}$ is $\delta^{18}O$ corrected by elevation effect, α is the angular coefficient of the linear correlation between $\delta^{18}O$ and E (‰/m). From this correlation, we used the angular coefficient between E and $\delta^{18}O$ values in baseflow to eliminate elevation effect from the dataset and verified the statistical analysis to evaluate how $\delta^{18}O_{EF}$ changes with landscape characteristics.

5.3 RESULTS

5.3.1 Spatial variability of normalized specific baseflow

The normalized specific baseflow qn ranged from 0.04 to 3.96 $Ls^{-1}km^{-2}/Ls^{-1}km^{-2}$. These differences exceed the errors and uncertainties of discharge measurements, which are estimated to be around 0.14 $Ls^{-1}km^{-2}/Ls^{-1}km^{-2}$. These differences are likely related to differences in storage capacities derived from various landscape characteristics.

For subcatchments with diabase dikes, the spatial variation of the qn does not follow any discernible pattern (Figure 28). However, the variation of qn appears to be related to the G in these subcatchments, which G showed a significant negative Spearman correlation with qn (-0.68) for a set of 22 sampless. MLR results were consistent with Spearman, in which G was the predictor of qn ($R^2 = 0.19$; Figure 29b).

Unlike what we found for subcatchments with diabase dikes, subcatchments characterized only by granite showed a noticeable spatial variation, with higher values of qn at higher elevations (i.e., area A of Figure 28a) and lower values of qn at lower elevations (i.e., area B of Figure 28a). Spearman correlation was consistent with this visual observation, in which A and E showed significant positive correlations with qn (0.49 and 0.72), for a set of 18 samples. However, E proves to be a better predictor of qn based on MLR results ($R^2 = 0.52$; Figure 29c). The maximum Variation Inflation Factor of the MLR analysis was below 5.

Figure 28 - Geologic map showing the pattern of baseflow: (a) normalized specific baseflow (qn); and (b) median of baseflow $\delta^{18}O$ values.
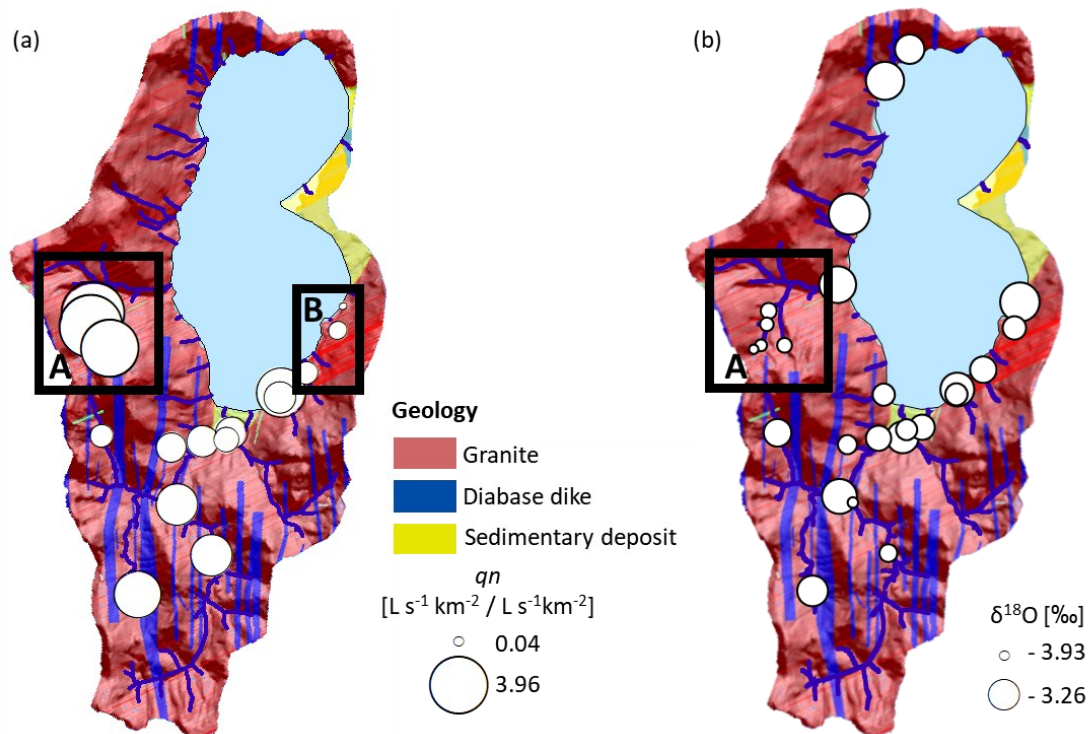
Figure 29 - Correlation between normalized specific baseflow (qn). (a) Spearman correlation, cells with thick borders indicate that there is a significant relationship. Blue color indicates positive correlation and red indicates negative. Color intensity indicates the strength of the correlation; (b) Multiple linear regression in subcatchments characterized by dike and granite; (c) Multiple linear regression in subcatchments characterized by granite; where Dike represents the dataset of subcatchments characterized by diabase dikes and granite, and Granite represents the dataset of subcatchment characterized just by granite, G is the percentage of granite, and E is the mean elevation. The index n indicates that the data set was normalized and standardized using the Box-Cox technique.

(a)

	Dike	Granite
Area	0.13	0.49
Elevation	0.17	0.72
Slope	-0.17	-0.41
Geology	-0.68	
	n = 22	n = 18

(b)
$\hat{qn}_n = -0.29\,G$
$R^2 = 0.19$

(c)
$\hat{qn}_n = 0.73\,E$
$R^2 = 0.52$

(d)

	Dike	Granite
Area	0.00	0.28
Elevation	-0.11	0.72
Slope	-0.06	-0.30
Geology	-0.49	
	n = 22	n = 21

(e)
$\hat{q}_n = 0.72\,E$
$R^2 = 0.51$
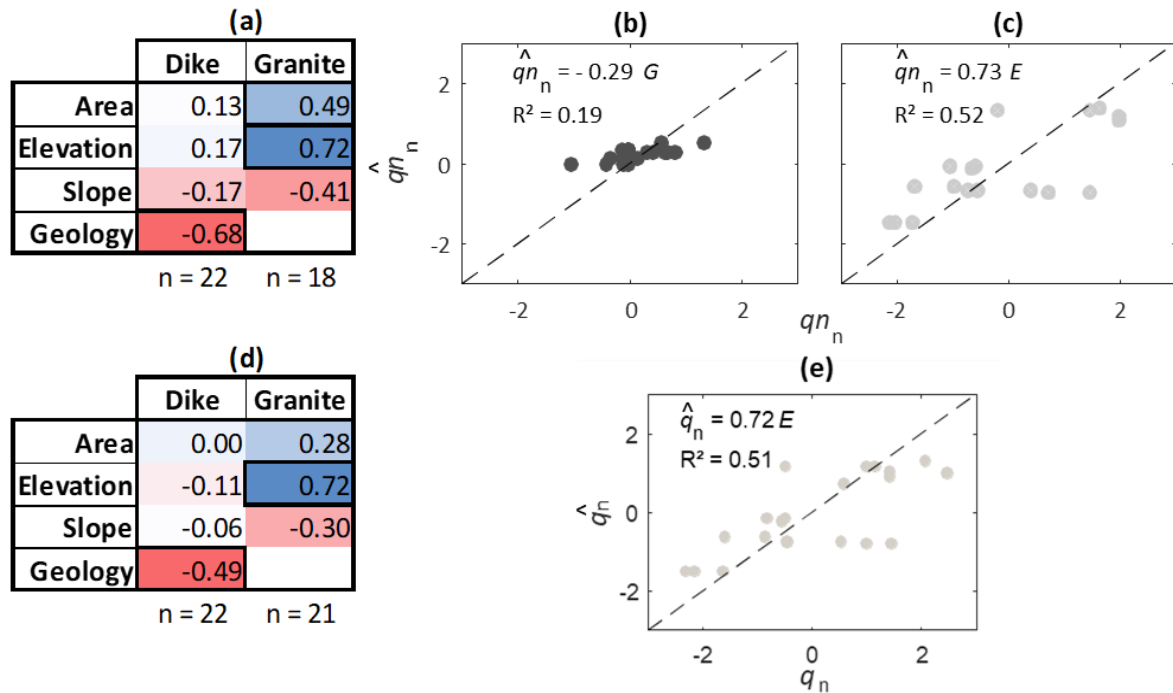
5.3.2 $\delta^{18}O$ in the water compartments of PLEC: spatio-temporal behavior

The observed weighted average $\delta^{18}O$ values in precipitation for the monitored period (from March to December 2018) was -3.26‰. This value is potentially biased to lighter values as the summer period (January, February) is missing from a full year of observation. However, the values are in line with the closest IAEA station (Rio Grande do Sul) that reported a -4.83‰ and the range (0‰ to -5.00‰) predicted by Gibson, Birks, and Edwards (2008) for the region. The average $\delta^{18}O$ of groundwater was -3.72‰ and lighter than the weighted average precipitation pointing towards preferential recharge of winter precipitation. When the PLEC was driest - assumed to be represented by the lowest observed baseflow in the campaigns – groundwater showed the largest difference to average precipitation with the lightest $\delta^{18}O$ values of -4.71‰ and -4.90‰ for W2 and W3 (Figure 11), respectively. In the other days, the values of $\delta^{18}O$ in groundwater were similar to values of $\delta^{18}O$ in baseflow.

Observed $\delta^{18}O$ values of the synoptic baseflow campaigns were consistently between the weighted average of precipitation and the $\delta^{18}O$ values of groundwater during the driest

conditions (Figure 30). The median $\delta^{18}O$ of baseflow for 25 subcatchments from the five synoptic campaigns ranged from -3.26‰ to 3.96‰ (Table 3). The values from subcatchment 16 (Table 3) were excluded from analyses because they likely experienced substantial fractionation by evaporation from an upstream pond, showing heavier isotope values compared to other samples with a median of -2.88‰.

Figure 30 - $\delta^{18}O$ of baseflow versus catchment area (log). The upper dashed line represents the amount-weighted rainfall $\delta^{18}O$, the lower dashed line represents the wells on the day with lowest baseflow of the campaigns. Each marker represents a median value of each subcatchment, the whiskers extend to the most extreme data points.
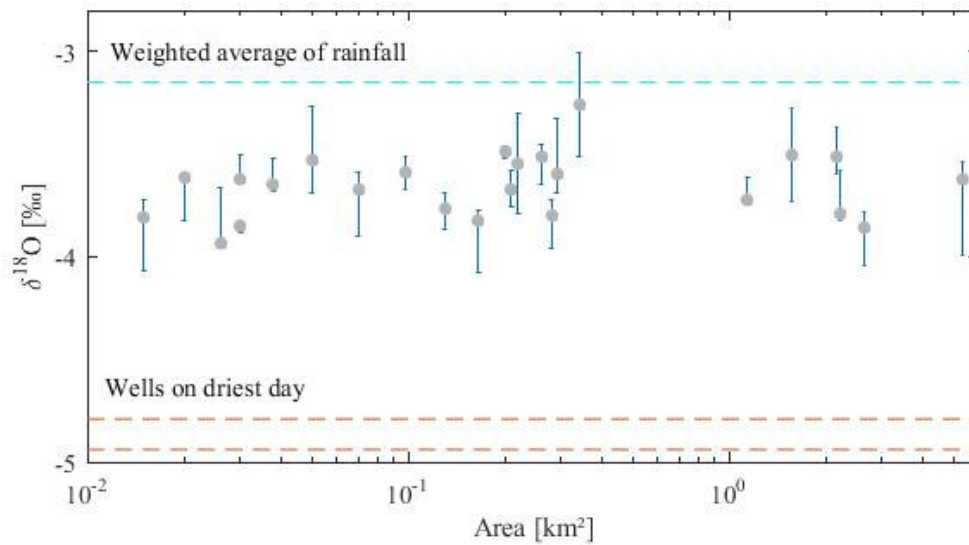
5.3.3 Spatial variability of $\delta^{18}O$ values in baseflow

We observed a clear spatial pattern of $\delta^{18}O$ values in baseflow during the synoptic sampling campaigns. The lighter values concentrated in the same area (i.e. area A of Figure 28b) characterized by higher elevation and homogeneous geology with the absence of diabase dikes. Other regions with a clear pattern in $\delta^{18}O$ values were not obviously visible. However, the evaluated landscape characteristics (area, elevation, slope, and geology) resulted in some organization of the spatial variability in $\delta^{18}O$ values especially when subcatchments were classified based on the presence and absence of diabase dikes.

In subcatchment with diabase dikes, we detected a significant Spearman correlation (ρ = 0.34) between slope and $\delta^{18}O$ of baseflow across all sampling campaigns. This positive correlation was observable also for individual and median of campaigns, however, it was not significant (Figure 31a). Other correlations were non-significant, however, mean elevation showed to be negatively correlated to $\delta^{18}O$ for the analysed samples. In subcatchments without diabase dikes, we found a significant negative Spearman correlation between elevation and

δ^{18}O values of baseflow for campaign 5 (ρ = -0.75), the median values (ρ = -0.58), and for all samples (ρ = -0.46) (Figure 31b). Further, δ^{18}O values were positively correlated to slope (Figure 31b), however significant only for the median of campaigns and across all sampling campaigns.

Figure 31 - Correlation between landscape and δ^{18}O values in baseflow. (a) Spearman correlation in subcatchments with dike. Cells with bold outlines indicate that there is a significant relationship, blue color indicates positive correlation, and red indicates negative correlation. The color intensity indicates the strength of the correlation; (b) Spearman correlation in subcatchments without dike, cells with thick borders indicate that there is a significant relationship. Blue color indicates positive correlation and red indicates negative. Color intensity indicates the strength of the correlation; (c) Multiple linear regression in subcatchments characterized by dike; (d) Multiple linear regression in subcatchments characterized by granite; where dike represented the dataset of subcatchments characterized by diabase dikes and granite, and Granite represents the dataset of subcatchment characterized just by granite, C3 is third campaign, C5 is fifth campaign. All of R² is R² adjusted. The index n indicates that the data set was normalized and standardized using the Box-Cox technique.

(a)

	C3	C5	Median	All
Area	0.10	-0.37	-0.25	-0.06
Elevation	-0.31	-0.49	-0.14	-0.17
Slope	0.27	0.56	0.52	0.34
Geology	-0.14	0.34	0.14	-0.04
	n = 11	n = 11	n = 12	n = 46

(b)

	C3	C5	Median	All
Area	0.35	0.10	0.34	0.25
Elevation	-0.41	-0.75	-0.58	-0.46
Slope	0.51	0.51	0.59	0.48
	n = 11	n = 13	n = 13	n= 40

(c) $\delta^{18}\hat{O}_n$ = 0.32 S R² = 0.12

(d) $\delta^{18}\hat{O}_n$ = 0.49 S R² = 0.23
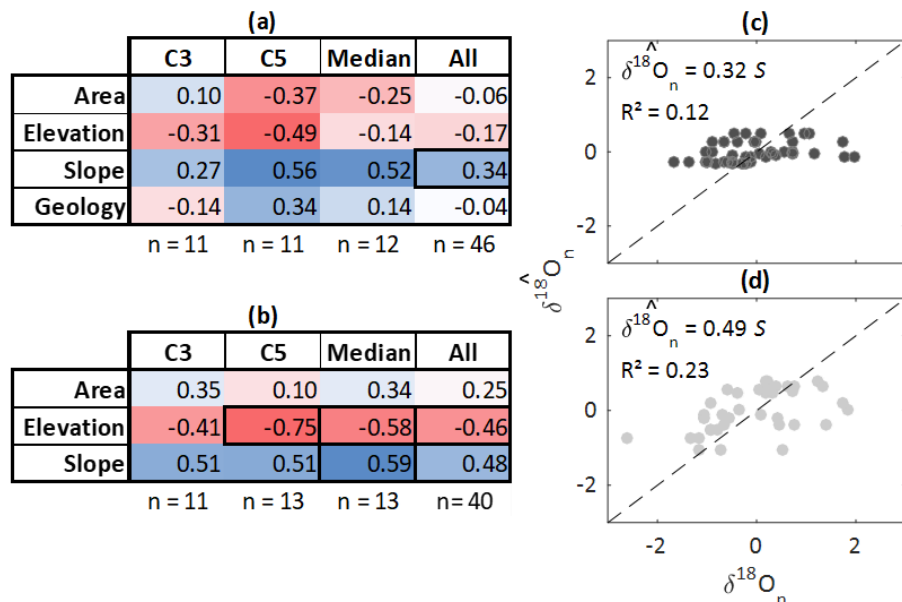
The results of our MLR analysis were consistent with the results of the Spearman correlation analysis. Slope was the predictor of baseflow δ^{18}O values with an adjusted R² of 0.12 for subcatchments with dikes (Figure 31c) and an adjusted R² of 0.23 for subcatchments without dikes (Figure 31d). Elevation, area, and geology coverage did not show to be significant. The maximum Variation Inflation Factor of the MLR was below 5.

5.3.3.1   Elevation effect on δ^{18}O in baseflow

We verified the correlation between elevation and δ^{18}O values in baseflow in different sets of subcatchments classified by topography and geology. This was done to determine whether the δ^{18}O values in baseflow is due because of the elevation effect or if it is also

influenced by deep groundwater. The k-means classification for further analysis of the elevation effect separated the subcatchment (a) based on area at 0.1 km² with 16 subcatchments that are larger and 9 that are smaller and (b) based on slope at 18° with 12 steeper and 13 flatter subcatchments. There are 12 subcatchments with diabase dike and 13 without.

We found a significant negative correlation and thus an elevation effect on $\delta^{18}O$ of baseflow for the synoptic fifth campaign (Figure 32b; $\delta^{18}O = -3.34‰ - 0.007‰\ E$, with E being elevation in m.asl.), median values of subcatchments (Figure 32c; $\delta^{18}O = -3.35‰ - 0.0017‰\ E$), and all samples (Figure 32d; $\delta^{18}O = -3.38‰ - 0.0016‰\ E$) in subcatchments smaller than 0.1 km². Samples from the third campaign did not show a significant elevation effect, nor did an elevation effect appear in the larger subcatchments. We observed a significant negative correlation between $\delta^{18}O$ and elevation in subcatchments with a sloper lower than 18° for the fifth campaign (Figure 32f; $\delta^{18}O = -3.40‰\ -0.0014‰\ E$), the median values of subcatchments (Figure 32g; $\delta^{18}O = -3.32‰\ -0.0016‰\ E$), and all samples (Figure 8h; $\delta^{18}O = -3.32‰ - 0.0016‰\ E$). We again did not observe an elevation effect in the third campaign nor in subcatchments with a slope above 18°. We also observed a significant elevation effect in subcatchments with diabase dikes with a negative linear correlation for the fifth synoptic campaign (Figure 32j; $\delta^{18}O = -3.34‰ - 0.0015‰\ E$), the median values of subcatchments (Figure 32k; $\delta^{18}O = -3.33‰\ -0.0014‰\ E$), and the entire dataset (Figure 32l); $\delta^{18}O = -3.36‰ - 0.0013‰\ E$). No significant correlation was detected for the third campaign nor for subcatchments with diabase dikes.

The angular coefficient of the linear correlation between elevation and $\delta^{18}O$ values in baseflow was consistent with those found in the literature for streamflow water in humid catchments (Tripti *et al.*, 2019). We used the value 0.0016‰/m as α at Equation 17 to calculate $\delta^{18}O_{EF}$. After we eliminated the elevation effect from $\delta^{18}O$ values in baseflow. Spearman correlation between $\delta^{18}O_{EF}$ values in baseflow and landscape characteristics (Figure 33) were different from Spearman correlation between $\delta^{18}O$ values in baseflow and landscape characteristics (Figure 31). In subcatchment without diabase dikes, we detected a significant Spearman correlation between area and $\delta^{18}O_{EF}$ values in baseflow across median ($\rho = -0.56$) and all sampling campaigns ($\rho = -0.36$) (Figure 33b). It was not possible to observe any other significant Spearman correlation between $\delta^{18}O_{EF}$ and landscape characteristics and predict $\delta^{18}O_{EF}$ in baseflow using MLR.

Figure 32 - Mean elevation of the subcatchments versus $\delta^{18}O$ of baseflow. (a), (e) and (i) Data from third campaign; (b), (f) and (j) Data from fifth campaign; (c), (g) and (k) Data from median values; (d), (h) and (l) Data from all samples. Dark blue represents subcatchments with drainage areas larger than 0.1 km², light blue, smaller. Brow represents catchments with mean slopes bigger than 18°, yellow slopes smaller. Dark gray represents subcatchments with diabase dikes , light gray subcatchments without diabase dikes. Just linear regression with p-value < 0.05 is shown. R^2 is R^2 adjusted.
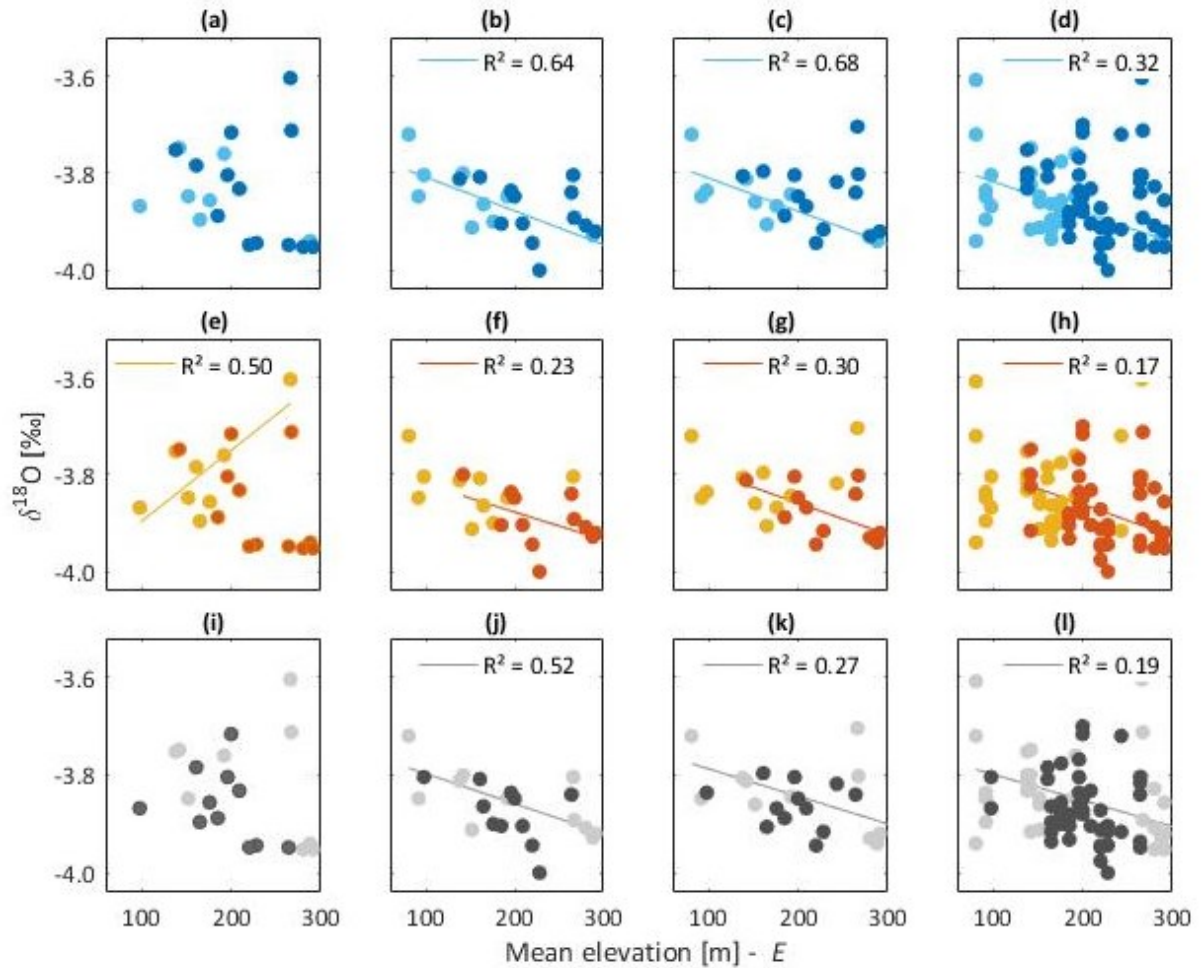
Figure 33 - Correlation between landscape and $\delta^{18}O_{EF}$ values in baseflow. (a) Spearman correlation in subcatchments with dike. Cells with bold outlines indicate that there is a significant relationship, blue color indicates positive correlation, and red indicates negative correlation. The color intensity indicates the strength of the correlation; (b) Spearman correlation in subcatchments without dike, cells with thick borders indicate that there is a significant relationship. Blue color indicates positive correlation and red indicates negative.

(a)

	C3	C5	Median	All
Area	0.45	0.09	0.00	0.06
Slope	-0.14	0.05	0.24	0.19
Geology	-0.28	0.16	-0.06	-0.07
	n = 11	n = 11	n = 12	n = 46

(b)

	C3	C5	Median	All
Area	0.37	0.36	0.56	0.36
Slope	0.04	-0.41	0.24	0.15
	n = 11	n = 13	n = 13	n = 40

5.3.4 Scatter in the relationship between area and baseflow

In general, the variability of normalized specific baseflow and specific baseflow decreases as subcatchment area increases (Figure 34a and Figure 34b). It is noticeable from a moving window that above 1 km² the standard deviation of normalized specific baseflow and of specific baseflow significantly decreases (Figure 34b and Figure 34d). This decrease in variability results in a characteristic "funnel" shape, where the range of specific baseflow narrows as area increases. This funnel is centered around the average specific baseflow across the PLEC, approximately 6 Ls^{-1}km^{-2}. However, this "funnel" shape was not observed for $\delta^{18}O_{EF}$ and $\delta^{18}O$ values in baseflow, as their variability does not decrease with increasing subcatchment area (Figure 34e, Figure 34f, Figure 34g and Figure 34h). Even above 1 km², the data show the same variability as in small subcatchments.

Spearman analysis revealed a significant positive correlation between area and normalized specific baseflow in subcatchments without dikes ($\rho = 0.49$) (Figure 29a). Furthermore, in subcatchments without dikes, there was a linear relationship between area and $\delta^{18}O_{EF}$ values in baseflow, where these values increased by 0.23‰ per square kilometer, the same was not observed in $\delta^{18}O$. In subcatchments with dikes or across all subcatchments was not observed a significant correlation between area and baseflow ($\delta^{18}O_{EF}$, $\delta^{18}O$, q and qn).

Figure 34 - Scale dependence of baseflow. (a) area versus normalized specific baseflow (qn); (b) area versus standard deviation of samples of qn from a moving window of 0.2 km²; (c) area versus specific baseflow (q); (d) area versus standard deviation of samples of q from a moving window of 0.2 km²; (e) area versus δ18OEF; (f) area versus standard deviation of samples of δ18OEF from a moving window of 0.2 km²; (g) area versus δ18O;; and (h) area versus standard deviation of samples of δ18O from a moving window of 0.2 km². Dark gray represents subcatchments characterized by granite and diabase dikes. Light gray represents subcatchments characterized by granite. The size of blue marks is relative to sample size ranging from 5 to 47.
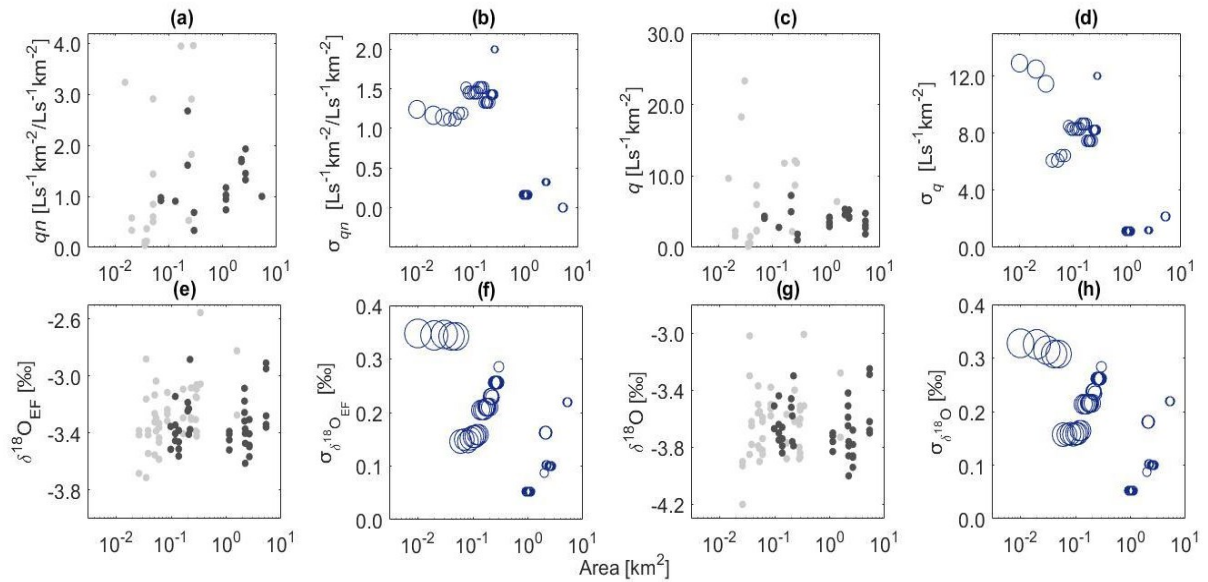
5.4 DISCUSSION

The spatial data of *qn* and $\delta^{18}O$ values in baseflow offer insights into hydrological processes and shed light on the capacity of catchments to store and release water to the streams during baseflow. The relationship between baseflow (specific baseflow and $\delta^{18}O$ values in baseflow) and subcatchment characteristics reveals the influence of geology and topography on storage dynamics during low flows.

5.4.1 Landscape streams of normalized specific baseflow

We believe that the observed spatial variability of *qn* is derived from differences in storage capacities among subcatchments, once that precipitation and evapotranspiration are very similar in the entire Peri Lake Experimental Catchment. We are confident that the spatial variation is not caused by errors and uncertainty of discharge measurements. Previous studies have reported similar spatial variability in *qn* (factor of 99 between maximum and minimum values). For instance, Woods *et al.* (1995) documented differences of up to a factor of 100 between maximum and minimum in the specific baseflow among subcatchments ranging from 0.08 km² to 10.00 km². Asano *et al.* (2020) found around a factor of 15 between maximum and

minimum in the specific baseflow for subcatchments ranging from 0.05 km² to 10.48 km², while Lyon *et al.* (2012) reported an approximately factor of 2 between maximum and minimum in the specific baseflow for subcatchments ranging from 0.12 km² to 10.00 km².

In our dataset, the variance damping occurred after 1 km², agreeing with other studies (e.g. Lyon et al., 2012; Woods; Sivapalan; Duncan, 1995) that reported that the variance of *qn* damped with the increase of drainage area, and *qn* turned constant after 1 km². This phenomenon arises due to the fact that the spatial variability of hydrological responses in catchments larger than 1 km² is less pronounced compared to that observed in hillslopes (Uchida *et al.*, 2005) and in PLEC, the presence of dikes did not change this phenomenon. Despite that in subcatchments larger than 1 km² it is still possible to notice a factor of 2 between maximum and minimum values of *qn*.

During baseflow, the high spatial heterogeneity of *qn* could be derived from differences in groundwater flow influenced by the hydraulic gradient of groundwater (Zimmer; Gannon, 2018). In this context, catchments with steep terrain generally exhibit a higher groundwater hydraulic gradient than those with gentle slopes, leading to lower baseflow (Kuentz *et al.*, 2017; Staudinger; Weiler; Seibert, 2015; Zimmer; Gannon, 2018), suggesting a negative correlation between slope and *qn*. However, Sayama *et al.* (2011) found the opposite trend, indicating that catchments with steeper slopes tend to have higher baseflow due to increased storage capacity. In the case of the Peri Lake Experimental Catchment (PLEC), the soil is thinner in areas with steeper slopes compared to those with gentler slopes. Consequently, we cannot expect to observe the same pattern as reported by Sayama *et al.* (2011). Despite this, in PLEC, there isn't a significant statistical correlation between slope and *qn*. One possible explanation for our failure to detect the influence of slope on *qn* could be that geological factors govern the flow path of groundwater. The correlation between other landscape (area and elevation) characteristics and *qn* differed between subcatchments with diabase dikes and those without diabase dikes, indicating differences in groundwater storage and release processes influenced by geological variations.

5.4.1.1 *Presence of diabase dikes impact the specific baseflow patterns*

Our observations indicate that the geological composition of subcatchments with diabase dikes is an important factor for predicting *qn*. These findings could be explained based on geological age. Older catchments tend to produce less baseflow directing more water through the shallow subsurface and as overland flow (Troch *et al.*, 2015). As granite is older than

diabase, subcatchments with a higher percentage of diabase dikes compared to granite, showed a higher *qn*. This observation is consistent with other studies, where an increase in the age of volcanic bodies and progressive erosion leads to a shallower main groundwater flow path (Asai; Satake; Tsujimura, 2009). As a result, Quaternary catchments demonstrate higher specific baseflow compared to Tertiary catchments (Asano *et al.*, 2020; Iwasaki; Nagasaka; Nagasaka, 2021; Tague; Grant, 2004), indicating a potential influence on groundwater flow trajectories contingent upon geological age. However, beyond the geological age, the hydrological process that controls baseflow patterns is related to the hydraulic characteristics of the geology.

Concerned with hydraulic properties, the permeability of diabase dikes is higher than that of granite allowing more flux of water. As a result, we anticipated a negative correlation between percentage of granite and *qn*, which is consistent with our findings. Some studies on landslides in neighboring regions of PLEC support our results. These studies have suggested that the presence of diabase dikes increases infiltrability and water percolation in hillslopes, making them one of the principal causes of landslides (Frederico, 2019; Salum, 2019; Silva, 2019).

Additionally, there is a geological factor that eludes measurement — the percentage of fractures in the bedrock. Based on the geological formation of the PLEC, we hypothesize the existence of fractures in the bedrock, facilitating preferential groundwater flow paths. According to (Gnann *et al.*, 2021), fractured bedrocks typically harbor local aquifers, resulting in catchments with higher baseflow values. In the PLEC, the geological composition of granite with diabase dikes is shaped by a series of tabular facies architecture-dominated flows, initially simple flows, followed by basalt flows with rubbly pahoehoe morphology (Florisbal *et al.*, 2018), configuring a fractured bedrock with established preferential flow paths. Even when the bedrock consists of a single lava flow, less complex than PLEC, the distribution of permeability within the lava is influenced by factors such as lava flow deposition and joint formation (Dafny; Burg; Gvirtzman, 2006). Thus, we anticipate the presence of fractured bedrock, however we cannot estimate the impact on that in each subcatchment.

5.4.1.2 *The fractured aquifer around the lake might be the reason why normalized specific baseflow is correlated to elevation*

Our observations indicate that elevation, in subcatchments dominated by granite, is a significant factor in predicting *qn*. We found that subcatchments with lower elevations exhibit

lower flows, which is contrary to our expectations based on soil properties and previous studies. Based on our wells, Peri Lake Experimental Catchment has relatively shallow soil (~2.5 m) in lower areas and even shallow soil in higher areas (~1 m). This led us to anticipate higher specific baseflow in lower areas due to their presumed greater soil storage capacity. Previous studies have reported that higher areas serve as groundwater recharge zones, while lower areas act as groundwater discharge zones (Winter, 1999). For instance, Ameli *et al.* (2018) discovered that 50% of recharge within the headwaters discharges into lower streams in a 2.80 km² catchment, defining it as the out-of-catchment groundwater flow contribution from a headwater to a lower-elevation stream. (Hwang *et al.*, 2012) studied water availability in catchments ranging from 0.08 to 1.43 km² and found a strong correlation with elevation, indicating greater lateral hydrologic connectivity at higher elevations than at lower ones. Asano *et al.* (2020) emphasize that lateral connection depends on bedrock hydraulic conductivity capacity, leading to higher specific baseflow in low streams in catchments characterized by permeable bedrock.

We believe that the correlation between elevation and *qn* reflects the hydraulic connectivity of the fractured bedrock surrounding the lake (Figure 10e). It is possible that these lower areas directly deliver groundwater to the lake instead of to the streams, as observed in other study areas by Winter (1999) and (Winter, Rosenberry e Labaugh, 2003), which may explain why lower subcatchments have lower *qn*. However, we did not observe significant correlation between elevation and *qn* in subcatchments with dikes, probably because in our experimental design we have more subcatchments characterized by the presence of diabase dikes in higher areas.

5.4.2 $\delta^{18}O$ values indicating that baseflow is a mixing of water from precipitation and from local water storage

Isotope data obtained through synoptic surveys can be employed to investigate the impact of various water sources and hydrological processes on baseflow patterns (Chen *et al.*, 2023). The differences between $\delta^{18}O$ values in baseflow among the nested subcatchments should be explained by elevation effect and $\delta^{18}O$ values in local water storage (Segura *et al.*, 2019; Peralta-Tapia *et al.*, 2016). We believe that there is local water storage in PLEC because elevation explains just 12% of the $\delta^{18}O$ values in baseflow in PLEC. In subcatchment with diabase dikes elevation is not even significantly correlated with $\delta^{18}O$ values in baseflow. Slope is a better predictor of $\delta^{18}O$ values in baseflow than elevation independently of geology characterization. This leads us to believe that the $\delta^{18}O$ values in baseflow are derived from

precipitation and water that has been damped in local storage. As a result of the damping, $\delta^{18}O$ groundwater is more depleted than rainfall $\delta^{18}O$ (Singh, Emanuel e McGlynn, 2016); (Peralta-Tapia *et al.*, 2015). In PLEC, on the driest day among the campaigns the $\delta^{18}O$ values in groundwater were depleted in relation to the weighted average $\delta^{18}O$ values in rainfall. However, in PLEC, we believe that local storage has not a larger capacity to dampen rainfall, or, local storage has a low contribution to baseflow, because $\delta^{18}O$ values in baseflow are more similar to $\delta^{18}O$ values in rainfall than $\delta^{18}O$ values in groundwater on the day with the lowest baseflow among the campaigns.

The limited ability to dampen the rainfall could be related to the size of the groundwater flow path, which catchments with shorter groundwater flow paths have less capacity to dampen the rainfall $\delta^{18}O$ signal (Singh; Emanuel; McGlynn, 2016) and baseflow reflect recent rainfall (Gentile *et al.*, 2023; Iwasaki; Nagasaka; Nagasaka, 2021). Maxwell *et al.* (2016) found that in humid regions, where there is more precipitation than evapotranspiration, the average groundwater flow path to streams is shorter compared to arid regions. According to Ameli *et al.* (2018) and (Garcia *et al.*, 2023), shorter groundwater flow path is found in high-relief catchments than in low-relief catchments. A priori we expected a short groundwater flow path in PLEC, once that is classified as a humid subtropical climate and 50% of subcatchments have slope greater than 18°, thus our findings align with our expectations. At PLEC, steeper subcatchments have $\delta^{18}O$ values in baseflow depleted in relation to the $\delta^{18}O$ of rainfall.

5.4.2.1   *Variability of $\delta^{18}O$ values in baseflow in subcatchments with diabase dikes does not decrease with area because of the differences in local storage among subcatchments*

We expected that the same landscape characteristics that were related to *qn* would also be linked to the $\delta^{18}O$ values of baseflow, given that both we supposed that both are associated with the water sources and storage capacity. However, contrary to the findings for *qn*, *G* is not a predictor of $\delta^{18}O$ values in baseflow, and the variability of $\delta^{18}O$ values in baseflow did not decrease with area in subcatchments with diabase dikes as *qn*.

Fischer *et al.* (2015) studied nested subcatchments characterized by sedimentary bedrock and found a decrease in the variability of baseflow SWI values in nested subcatchments from 0.2 km². One possible explanation for the lack of decrease in the variability of baseflow $\delta^{18}O$ values with area is that the analyzed subcatchments with diabase dikes have more

heterogeneous groundwater flow paths than the subcatchments studied by (Fischer *et al.*, 2015).

Furthermore, the elevation effect $\delta^{18}O$ values of baseflow was not detectable in subcatchments with diabase dikes, indicating that there are differences in local storage between those subcatchments. According to Iwasaki *et al.* (2021), in volcanic catchments like PLEC, groundwater moves beyond the drainage divide, which can alter the relationship between any topographic characteristic and $\delta^{18}O$ values in baseflow.

5.4.2.2 $\delta^{18}O$ values in baseflow has a higher variability but becomes heavier as one increases area in subcatchments without diabase dikes

In subcatchments without diabase dikes it is possible to notice elevation effect and indicating that in these subcatchments the water in the streams has lower inputs from local water storage (e.g. Segura et al., 2019). After the elevation effect is dropped out in $\delta^{18}O$ values of baseflow and calculated $\delta^{18}O_{EF}$, although presented a large variability of $\delta^{18}O_{EF}$ with area, the area had significant ranking correlation with $\delta^{18}O_{EF}$ – positive correlation. The same positive correlation occurred with Singh *et al.* (2016) – two metamorphic catchments 0.13 and 0.15 km²; and Fischer *et al.* (2015) – sedimentary flysch catchment 4.25 km², in which baseflow SWI becomes heavier as one moves from the channel head towards the outlet. According to Singh *et al.* (2016) this occurred because smaller hillslopes have limited water storage capacity, thus reducing their ability to dampen the rainfall $\delta^{18}O$ signal through mixing, unless at the channel head. Nevertheless, in a larger metamorphic catchment (68 km²), the baseflow $\delta^{18}O$ value is inversely proportional to area (Peralta-Tapia *et al.*, 2015), because of the regional groundwater inputs. However, the correlation between baseflow $\delta^{18}O$ values and catchment area is not dependent of the study area scale, because Chen *et al.* (2023), even studying a nested subcatchment of 7415 km², found lighter baseflow $\delta^{18}O$ values at smaller subcatchments.

5.4.3   Conceptual hydrological model of local water storage, groundwater flow path and specific baseflow

While it is widely accepted that subsurface hydrogeologic properties and land surface conditions influence groundwater fluxes, these processes often exhibit spatial heterogeneity, and their impacts on headwaters remain uncertain (Gardner *et al.*, 2020; Tague; Grant, 2004; Welgus; Abiye, 2022). Once that $\delta^{18}O$ of baseflow and *qn* are related to the water sources and

storage capacity, we expected that the same catchment characteristics would be correlated with both, but we did not find such a correlation. Other studies have reported variations in spatial patterns between specific baseflow and stream water chemistry (Egusa *et al.*, 2019); Floriancic *et al.*, 2019).

In summary, our main findings regarding the relationship between *qn* and landscape characteristics suggest that geology is a more critical factor than topography for predicting baseflow. In subcatchments with dikes, the percentage of granite serves as the best predictor of *qn*. In subcatchments without dikes, the elevation emerges as the primary predictor. In both cases, *qn* is linked not to topography but to geology. The *qn* is related to age of the bedrock body and hydraulic properties of bedrock, where subcatchments with more percentage of diabase dike deliver more water to the streams during baseflow (Figure 35a). Second, in subcatchments without dikes, the connection to geology is related to release capacity. This is because areas near the lake, located in low-lying regions, feature a fractured aquifer. We presume that groundwater in these areas drains directly into the lake (Figure 35b).

Patterns of baseflow $\delta^{18}O$ values reveal the capacity to dampen $\delta^{18}O$ of rainfall through mixing, which is closely related to the local water storage. In subcatchments without dikes, only areas near the channel head have sufficient storage capacity to dampen rainfall $\delta^{18}O$ (Figure 35b). Diabase dikes are shallower than granite, and the fractures in the granite create more complex and unpredictable flow pathways and local water storage, which causes the variability of $\delta^{18}O$ values in baseflow not to decrease with area (Figure 35a). Geology cannot be disregarded when predicting $\delta^{18}O$ and *qn*. The greater the complexity of the geology, the more challenging it becomes to predict the spatial patterns of baseflow.

Figure 35 - Conceptual model based on results from patterns of specific baseflow and streamflow $\delta^{18}O$.
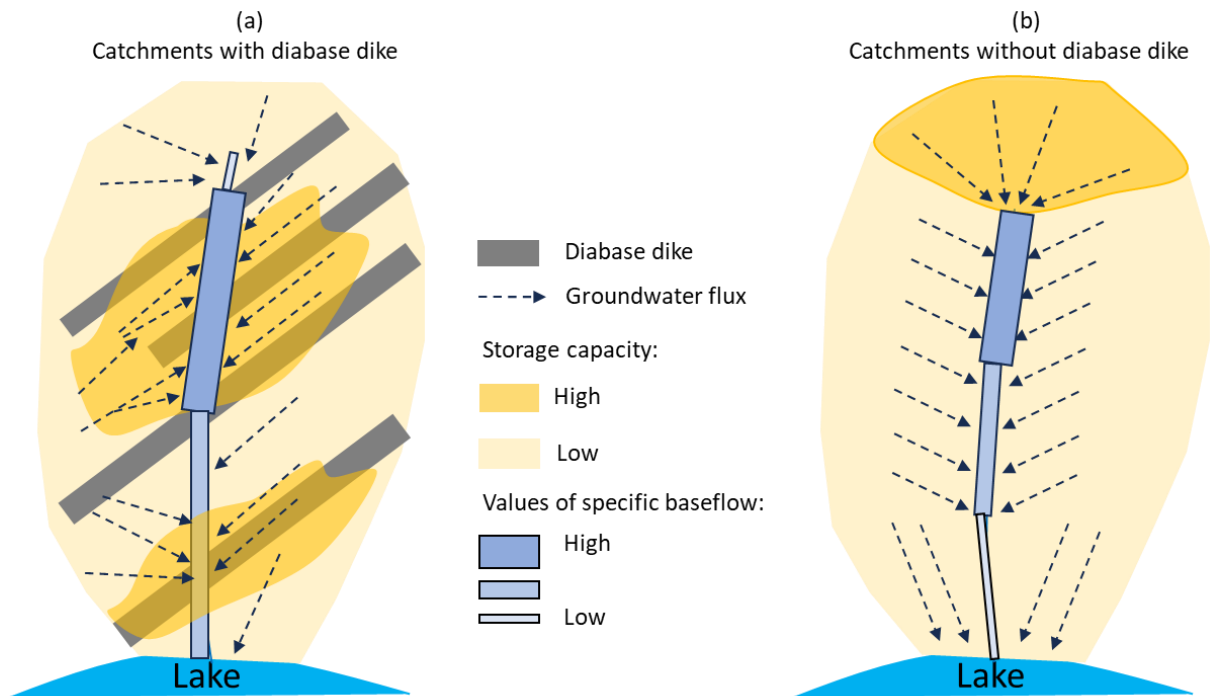
5.5 CONCLUSION

We studied how topography and varied geology affect the distribution of baseflow and $\delta^{18}O$ values in a drainage network within a catchment characterized by granite and diabase rock. Our general hypothesis posits that increasing geological heterogeneity enhances variability in groundwater flows, making normalized specific baseflow and its $\delta^{18}O$ across the stream network less predictable based on topographic characteristics. More specifically, we sought answers to three research questions, which will be described and answered: i) What is the spatial variability of specific baseflow and the baseflow isotopic composition within headwater catchments characterized by granite and diabase dikes? ii) Which physical characteristics of catchments, such as catchment area, slope, elevation, and geology, can be used to predict the spatial variability in stream network patterns of specific baseflow and baseflow isotopic composition?; and iii) What hydrological mechanisms are responsible for variations in stream network patterns of specific baseflow and baseflow isotopic composition, and how do the topographic and geological characteristics of catchments influence these mechanisms?

Noticeable spatial patterns are evident in subcatchments characterized by granite only, with higher normalized specific baseflow and lighter $\delta^{18}O$ values at higher elevation streams. However, no spatial patterns are observed in subcatchments with diabase dikes, where the complexity of the geology makes it challenging to notice some patterns.

Geology is a more critical factor than topography for predicting normalized specific baseflow. In subcatchments with diabase dikes, the percentage of granite is the best predictor of normalized specific baseflow, while in subcatchments without dikes, elevation is the primary predictor. Subcatchments with more diabase dikes deliver more water to streams during baseflow. In subcatchments without dikes, geology affects the release capacity, especially in low-lying areas near the lake with fractured aquifers, where groundwater likely drains directly into the lake. The effect of progressive isotopic depletion of precipitation on $\delta^{18}O$ values in baseflow is only noticeable in subcatchments without dikes, and $\delta^{18}O$ values in baseflow cannot be explained by elevation in subcatchments with diabase dikes. This indicates that the heterogeneity of the geology translates into heterogeneity of groundwater flow paths.

The main hydrological mechanisms that alter the patterns of water availability and $\delta^{18}O$ values during baseflow is the movement of groundwater that feeds the streams. Diabase dikes have a greater storage capacity and create preferential pathways for water to the streams, resulting in subcatchments with dikes having higher normalized specific baseflow. Meanwhile, the increased geological complexity makes the groundwater flow paths more complex, affecting the $\delta^{18}O$ values in baseflow.

This study demonstrates that to fully comprehend the hydrological cycle at small scales under baseflow conditions, it is essential to move beyond questions of scale dependence and topography, and consider geology as the primary controlling factor. In future studies, it is imperative to focus on fundamental small-scale hydrological mechanisms, including the influx of bedrock groundwater and the movement of water through various layers, including soil, regolith, and bedrock. Gathering this information will require field surveys, mapping, the use of subsurface sensing techniques, and the implementation of physical models.

6. EXPLORING ROLE OF GEOLOGY THROUGH PARFLOW CALIBRATION USING SHORT-TIME RAINFALL-RUNOFF AND BASEFLOW CAMPAINGS

This chapter presents a version of the paper to be submitted to Journal of Hydrology: INNOCENTE DOS SANTOS, C.; KLAUS, J.; CHAFFE, P. L. B. Does dikes matter and ow to parametrized them?

ABSTRACT

The control over storage and discharge of groundwater is influenced by both topography and geology. While diabase dikes may serve as pathways or barriers to groundwater movement, the precise impact of diabase dikes on baseflow patterns remains uncertain. Especially in the Global south where long-term records are scarce. Our focus was investigating how diabase dikes impact baseflow patterns in a small subtropical catchment in Southern Brazil using integrated hydrologic platform ParFlow-CLM to simulate hourly 15 m gridded data validated with short-time monitoring and snapshot campaigns to measure baseflow in 9 streams (areas ranging from 0.02 to 5.33 km²). We evaluated ParFlow-CLM in two different scenarios, one represented the real conditions of catchment, with subsurface heterogeneous and the other with homogeneous subsurface. Our results suggests that streamflow generation, patterns of streamflow and drainage dynamics are controlled by subsurface proprieties. This approache is important to the advance of the hydrologic science in catchments with poorly gauged.

6.1 INTRODUCTION

Understanding the controls of streamflow spatial distribution continues to be a challenge (Fan *et al.*, 2019). Climate drivers are easily perceptive, which means that high precipitation and drought translates into a pattern of high and very low streamflow (Floriancic *et al.*, 2022; Tague; Grant, 2004). However, in small scale, under homogeneous climate conditions, there is a considerable streamflow spatial variability that cannot be explained (Asano *et al.*, 2020; Floriancic *et al.*, 2019, 2022; Karlsen *et al.*, 2016; Lyon *et al.*, 2012). Soil structure and geological formation control the water storage in the catchment and groundwater flow routing (Cervi *et al.*, 2017; Glaser *et al.*, 2020; Maxwell *et al.*, 2016; Pfister *et al.*, 2017). The most influential hydrogeological control is the type (Asano *et al.*, 2020; Tetzlaff; Soulsby, 2008) and position of the catchment bedrock (Iwasaki; Nagasaka; Nagasaka, 2021). The number, width, inclination, and persistence of fractures in the bedrock play a fundamental role in groundwater paths (Iwasaki; Nagasaka; Nagasaka, 2021; Oxtobeem; Novakowski, 2003; Tetzlaff; Soulsby, 2008). In South America and Africa's coastal regions, it is very common to find a complex geology characterized by extrusive fractured bedrock (e.g., granite) filled by intrusive rocks (e.g., diabase dike). The diabase dike, being shallower, can act as a groundwater barrier and change fracture patterns. Despite that, hydrological model studies have not captured the role of

geology in the groundwater, as they often assume homogeneous impermeable bedrock. Here we focus on the effect of the presence of diabase to understand the role of the geology in the streamflow patterns, during baseflow and storm conditions, and the stream network dynamics.

During baseflow, the sources are mainly groundwater and subsurface water, coming from bedrock and soil layers (Egusa *et al.*, 2016). Thus, we expected that geology play a crucial function during baseflow conditions, and studies have confirmed this (e.g., (Asano *et al.*, 2020; Iwasaki; Nagasaka; Nagasaka, 2021; Pfister *et al.*, 2017), which reflect in stream network dynamics (Godsey; Kirchner, 2014; Whiting; Godsey, 2016). In catchments characterized by permeable bedrock, it is possible to notice that there is groundwater out-of-catchment from a headwater catchment to its larger parent catchment (Ameli *et al.*, 2018; Genereux; Wood; Pringle, 2002; Kaule; Gilfedder, 2021), which translates to the specific baseflow rate increasing with catchment area (Asano *et al.*, 2020). In contrast, in impermeable bedrock, specific baseflow could be independent of catchment area (Lyon *et al.*, 2012; Uchida; Asano, 2010) because all areas of the catchments are releasing an equal amount of water to the streams, generating the same specific baseflow. In catchments with fractured bedrock, some studies found that specific baseflow decreases with catchment area (e.g. Floriancic et al., 2019b; Tetzlaff; Soulsby, 2008b). However, it remains unclear which mechanism is responsible for the scaling relationship of specific baseflow in catchments with fractured bedrock in small catchments, particularly regarding how small catchments can store more water than larger ones (Iwasaki; Nagasaka; Nagasaka, 2021).

While the patterns of baseflow are clearly affected by geology, runoff generation is usually estimated just considering the drainage shape and land cover (Beven, 2020; Bhunya *et al.*, 2011; Rigon *et al.*, 2016; Singh; Mishra; Jain, 2014). There are three main documented processes to describe runoff generation (McDonnell, 2013): saturation excess overland flow (Dunne; Black, 1970), infiltration excess overland flow (Horton, 1933), and subsurface stormflow (Hursh; Brater, 1941). Infiltration excess occurs in urban areas, while saturation excess and subsurface storm flow are "two sides of the same coin" (McDonnell, 2013), described as the process of "fill-spill". This process refers to storing water in a landscape unit through vertical and lateral additions. The storage, known as "fill", continues until it reaches a critical level and generates runoff, or "spill" (McDonnell *et al.*, 2021). Underground characteristics, such as porosity, soil depth, and hydraulic conductivity (Ks), will determine the space and the velocity in the water will fill before spill. Generally, Ks gradually decreases, and water tables are formed in the deeper layer (Godsey; Elsenbeer; Stallard, 2004). When Ks

decreases fast, the superficial layers of soil may promote the formation of a shallow, suspended, and temporary water table (Saffarpour *et al.*, 2016). At some hillslopes, depressions at the soil-bedrock interface are the key to lateral flow generation, where connectivity of a thin transient saturated zone was a precondition for lateral flow generation at the hillslope scale (Tromp-van Meerveld; McDonnell, 2006). Diabase dike formation in the granite have commonly fractures on the granite that can work as reservoirs and preferential paths that might modify the fill-spill process, which should reflect in stream network dynamics (Mutzner et al., 2016; Perez, A. B. A. et al., 2020b). However, it is almost impossible to parameterize the geology to represent those fractures in a physical model.

Although we expected to notice that streamflow spatial patterns, under baseflow and storm conditions, and stream network dynamics are affected by presence of fractured rocks and diabase dikes, it is not easy to capture this effect from field measurements. It is unrealistic to expect most research groups to install or maintain field work infrastructure (Tauro *et al.*, 2018), especially in developing countries, where long-term records are scarce (Burt; McDonnell, 2015; Wohl *et al.*, 2012). An alternative is to use a field-modeling approach, using limited field data, as snapshot campaigns, and virtual experiments with different scenarios (e.g. Ameli et al., 2018b; Sayama; McDonnell, 2009; Weiler; McDonnell, 2004). ParFlow-CLM is a perfect choice to investigate the diabase dike effect in the streamflow patterns once it simulates the surface and subsurface flow using Richard's equation (Kollet; Maxwell, 2008; Maxwell; Miller, 2004; Maxwell, 2009; Maxwell; Kollet, 2008). ParFlow-CLM has been expanded to include the coupling of surface and subsurface flow, allowing for the comprehensive simulation of hillslope runoff and channel routing in a fully integrated manner (Gilbert; Maxwell, 2017). ParFlow-CLM is an open-access integrated model, and it has been tested on the various surface and groundwater problems in large domains ($6.3x106$ km^2) (Maxwell *et al.*, 2016), and small catchments (38.5 ha) (Fang *et al.*, 2016).

In this study, we tested geologic scenarios at Ribeirão Grande Catchment to investigate the role of diabase dike on spatial distribution of streamflow. Our study area is a subtropical catchment characterized by granite, and diabase dike. Granite with a diabase dike is considered fractured bedrock, particularly in the vicinity of the dike. Our investigation is using data from field snapshot campaigns, short-time rainfall-runoff series, and virtual experiments using ParFlow.

Our research questions are:

1. Can information from snapshot baseflow campaigns be useful to validate the baseflow of an integrated hydrology model that simulates surface and subsurface flow?

2. Can the geology and soil parameters be set up in the ParFlow model to accurately predict hourly flow for four months?

3. How does heterogeneity on geology influence the patterns of streamflow?

4. How does heterogeneity on geology influence the streamflow network dynamics?

6.2   MATERIAL AND METHODS

6.2.1   Parflow parametrization of the subsurface for different scenarios

ParFlow is a grid-based, fully integrated physical hydrology model capable of simulating groundwater surface water interactions in complex and heterogeneous domains using Richard equation 3D (Maxwell, 2009). We used the digital elevation model (SDS, 2013) with a resolution of 15 x 15 m to represent our domain. The extents of the simulation domain were based on Ribeirão Grande Catchment (RGC) regions. Regions that did not drain into RGC were excluded from the active domain of the computational grid. The RGC domain was discretized into 168 rows and 279 columns. The vertical discretization of the model used a variable thickness where the thickness of each of the 20 layers increased with depth from the surface. The layer thicknesses, from bottom to top, were 5, 1, 1, 0.5, 0.5, 0.5, 0.5, 0.5, 0.25, 0.1, 0.05, 0.05, 0.02, 0.01, 0.01, 0.003, 0.002, 0.002, 0.002, 0.001 m for a total thickness of 10 m.

We defined two scenarios. Scenario 1 (S1) corresponds to real geology based on the geologic map from the Department of Geoscience of University of Santa Catarina (Figure 36; UFSC, 2018). In S1, the geology composition is a mixture between granite and diabase, with different soil depth based on field experiments (Figure 18) and four different subsurface zones (granite, residual granite soil, diabase, and residual diabase soil; Figure 18g). The values of porosity for S1 were based on Oliveira, Bim, and Espindola (2012) and Pecapedra and Oliveira (2016) (Table 12). The hydraulic conductivity of the soil was defined based on field measurements on Figure 18. Based on porosity the hydraulic parameters were defined based on Rosetta dataset. For S1, we chose to characterize the values of granite and diabase within the suggested range of Oliveira, Bim, and Espindola (2012), which varies from 0.036 m/h to 3.6 10^{-7} m/h for granite and from 0.36 m/h to 3.6 10^{-4} m/h to diabase. Scenario 2 (S2) has a homogeneous subsurface where there is no difference between soil and bedrock, the hydraulic

conductivity is the weighted average (based on S1; Table 12). In both scenarios the manning value is 0.04 s m$^{-1/3}$.

Figure 36 - Different geologic scenarios to verify the effect of geology in the streamflow scaling relationship. Scenario 1 represents the real geology.
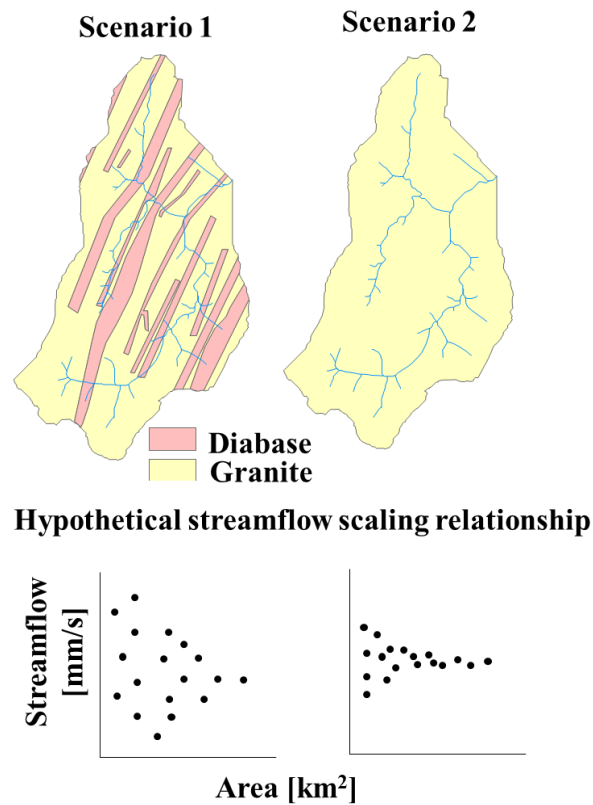
Table 12 – Geological information used to set up ParFlow. S1 is Scenario 1, S2 is Scenario 2, K is hydraulic conductivity, Ø is the porosity, α is a Van Genuchen parameter related to the inverse of the air entry suction, n is a Van Genuchen parameter related to the pore-size distribution, Θr and Θs are Van Genuchen parameters, residual and saturated water content, respectively.

| | | K | Ø | α | Θr | Θs | n | H |
		[m h^{-1}]	[-]	[cm^{-1}]	[cm³cm^{-3}]	[cm³cm^{-3}]		[m]
S1	Residual granite soil	0.690	0.430	0.270	0.088	0.430	1.210	0.50 - 3.00
	Residual diabase soil	1.050	0.470	0.140	0.093	0.470	1.320	0.20 - 2.80
	Granite	0.004	0.100	0.004	0.010	0.100	1.500	9.50 - 7.00
	Diabase	0.036	0.150	0.013	0.010	0.150	1.514	9.80 - 7.20
	S2	0.180	0.185	0.050	0.026	0.185	1.455	10

For each scenario, we predicted the scaling relationship of streamflow during both baseflow, and storm conditions based on literature findings (Figure 36). Regarding baseflow to the catchment area, "drainage ratio method" is commonly used to estimate the baseflow in ungauged catchments (Archfield; Vogel, 2010). Specific baseflow is the discharge divided by

the catchment area. Nearby catchments in the same landscape are often assumed to have similar specific baseflow (q). This seems to be applied to areas above 1 or 2 km² (e.g. (Egusa *et al.*, 2016; Lyon *et al.*, 2012; Uchida; Asano, 2010; Woods; Sivapalan; Duncan, 1995). However, fractured bedrock plays a role in groundwater in flow paths, changing the storage capacity and the connections between different compartments (Thiros *et al.*, 2023). In S1, we expected dispersion of baseflow in small catchments (area < 2 km²) due to changes in storage capacity caused by the dikes. Nevertheless, as the drainage area increases, baseflow stabilizes (Woods; Sivapalan; Duncan, 1995). In S2, with a homogeneous subsurface, we expected a small dispersion between small catchments if compared to S1 (e.g. Ameli et al., 2018b; Genereux; Wood; Pringle, 2002b; Kaule; Gilfedder, 2021b). The residual soil of granite is deeper and has a lower hydraulic conductivity than the residual soil of diabase. Therefore, in S1, where there are diabase dikes, there will be a higher flow rate during rainfall in catchments with higher percentages of dikes, while in S2, with homogeneous geology, the flow rate will be related only to the topography of the catchment.

6.2.2 Evaluation of integrated groundwater–land surface–overland flow model (ParFlow-CLM)

The simulation was conducted in one hour time steps for 4 months (Figure 20). A spin-up phase with duration of one year was conducted with an initial condition. For each scenario the spin-up was evaluated until a steady-state flow field was achieved. Spin-up was done by running the simulations for 8640 hours (about 1 year) with overland flow enabled to allow the system to reach steady-state for the fully coupled surface-subsurface flow system with. The initial water table was 1 m from the surface. A comparison was always made between the final output and one 5000 hours earlier to confirm the steady-state flow field, and simulations were continued as needed until steady behavior was obtained. The total change in volumetric water content integrated over the entire domain between the last two hours was always less than 1%. ParFlow was evaluated by short-time meteorological data and rainfall-runoff data of P1 and P2. We validated the accuracy of spin-up with discharge measurements during baseflow.

From ParFlow, we just used pressure-head information. ParFlow estimated pressure-head in each step to solve Richards's equation:

$$S(p)S_s \frac{\partial p}{\partial t} - \frac{\partial(S(p)\rho(p)\emptyset)}{\partial t} - \nabla(K(p)\rho(p)(\nabla p - \rho(p)\vec{g})) = Q, in\ \Omega \qquad (18)$$

where p is pressure-head [L], K is the hydraulic conductivity tensor [L T^{-1}]; S_s is the specific storage [L^{-1}]; Ø is the porosity [-]; S is the relative saturation [-]. Density and viscosity are constant. S are estimated using the Van Genuchen equation as presented in Maxwell et al (2013). We evaluate the performance of the ParFlow at the P1 and P2 by objective function Kling–Gupta efficiency (KGE). We used only data from P1 and P2 below 1 m³/s to calculate the KGE because the maximum discharge measured to estimate ratting curve was around 1 m³/s.

To use the CLM, the land cover was determined to be uniform, Evergreen Broadleaf Forest. Evapotranspiration was adjusted to only 10% of the evapotranspiration estimated by the CLM, this adjustment is due to the fact that the CLM is designed to estimate evapotranspiration on a larger scale. When the CLM was considered, without adjustments, the catchment was without streamflow most of the time in both scenarios, even though there were four months in which the accumulated precipitation was ~1200 mm. As the research questions of this chapter does not include the performance of evapotranspiration, the results were not presented.

The Juwels supercomputer from the Jülich Supercomputing Center (JSC) was used to run ParFlow-CLM. The model was run using one node (99 processors), where the domain was divided into 10 parts in the x direction, 9 parts in the y direction and one part in the z direction.

6.3   RESULTS

6.3.1   Spin-up

The spin-up process aids in achieving a steady state of the model from the initial conditions such that the transient effects from initial conditions do not significantly affect the results. In RGC, a steady state was achieved within 43 and 33 days for Scenario 1 (S1) and Scenario 2 (S2) respectively. Whereas S1 is characterized by diabase dike and granite, S2 is characterised by homogeneous subsurface. During the spin-up phase, both groundwater flow and surface water flow stabilized simultaneously for S2. The formation of the entire drainage network coincided with the day the water table reached the surface, with no further fluctuations in subsurface storage (Figure 37). The groundwater flow and surface water flow stabilized simultaneously for S2 but stabilization for S1 began from day 25 until 43. Although surface

storage continued to increase, streams were formed way before the subsurface storage stabilized (Figure 37e). In S2, it is evident that both surface storage and the formation of the drainage network are directly influenced by subsurface storage (Figure 37)

Once the subsurface storage reaches its capacity, the drainage network forms, and surface storage stabilizes accordingly. The same is not observed in cases of greater heterogeneity. Nevertheless, we can observe a linear correlation between subsurface storage and both the number of active drainage cells and discharge at the outlet (Figure 38a,c). While the spin-up process does not directly reflect drainage network fluctuations due to ongoing catchment filling, the observed linear correlation between the drainage network (Figure 38b) is consistent with fieldwork-based drainage network mapping (e.g. Godsey; Kirchner, 2014; Whiting; Godsey, 2016), where the active drainage network can be an indication of how much water is available in the catchment in surface and subsurface storage (Figure 38a,b).

The influence of the geological layer on vertical infiltration and lateral groundwater flow significantly contribute to the differences in time taken to achieve the steady state. This influence affects the drainage networks, surface storage and discharge dynamics. The heterogeneity within the geological layer in S1 could also lead to the formation of preferential flow paths, particularly sensitive to significant changes in soil properties. Diabase dikes and residual soil of diabase, characterized by higher hydraulic conductivity, caused areas with granite to establish drainage networks earlier than those with diabase. This preferential flow path, resulting from differences in hydraulic conductivity, caused a delay in reaching steady state. The drainage network formed at the end of the spin-up process is similar, but not identical, between these two scenarios (Figure 37d,e). The number of drainage cells active is bigger in the S2.

The discharge showed small variability across the two scenarios (Figure 39a). In general, the discharge in the stream network is smaller in S1 than in S2 (Figure 39a) except for cross-section 11 (Table 13). This is because greater hydraulic conductivities in the surface layers of the soil cause the catchment to have less discharge in a steady state. The differences between both simulated discharges are 12.77% for the outlet, 20.75% for P2, and 12.77% for P1 (Figure 39), and the errors in relation to observed in S1 for P1 and P2 were on the order of 50%; for the same catchments, the error for S2 was on the order of 75%. The error in relation to observed at the outlet was -10% in relation to S1 and 3% in relation to S2. The biggest differences between observed and simulated, reaching more than 400%, are in the smallest discharge (Figure 39), which corresponds to the smallest catchments. Although we tried to

represent subsurface heterogeneity, this representation was not sufficient to simulate discharge correctly in small catchments, but as the catchment becomes larger, it is easier to correctly simulate discharge.

Figure 37 – Spin-up of Ribeirão Grande Catchment at the ParFlow for different geological scenarios. (a) Subsurface storage variation in the time; (b) Surface storage variation in the time; (c) Number of drainage cell active in the time; (d) Drainage network in different days in RGC parametrized with homogeneous geology; (e) Drainage network in different days in RGC parametrized with heterogeneous geology.
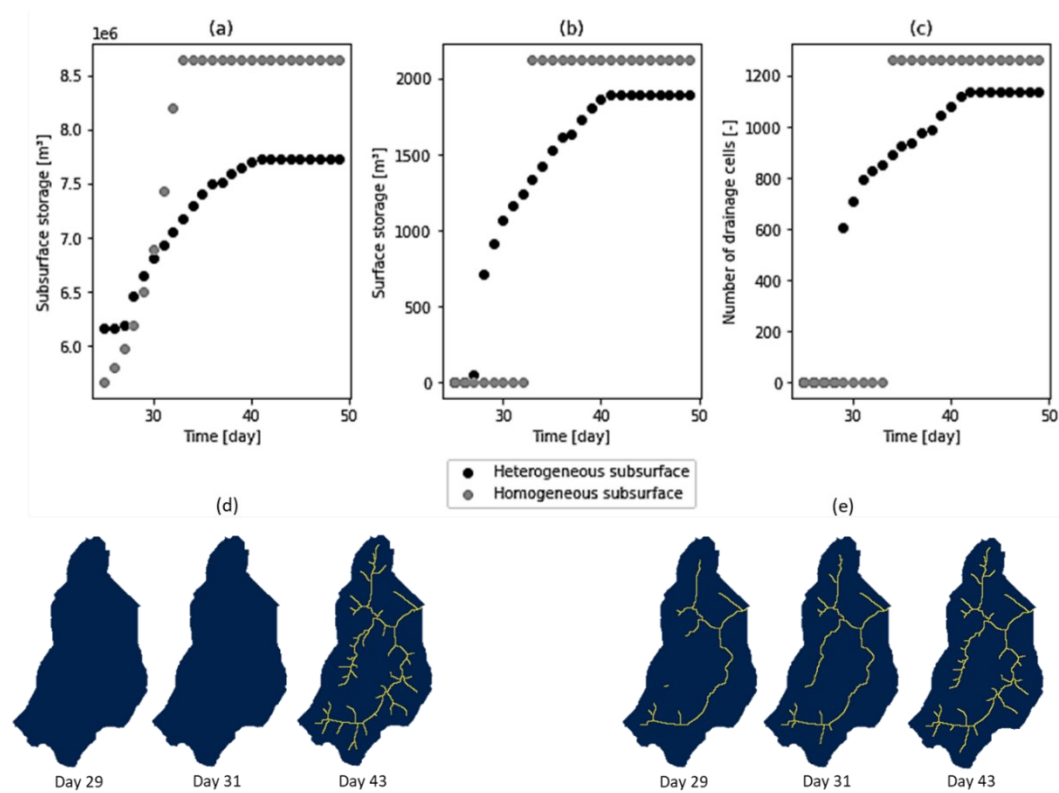
Figure 38 – Controls of number of drainage cells of RGC at ParFlow for Scenario 1 during spin-up. (a) Subsurface storage; (b) Surface storage; and (c) Discharge.
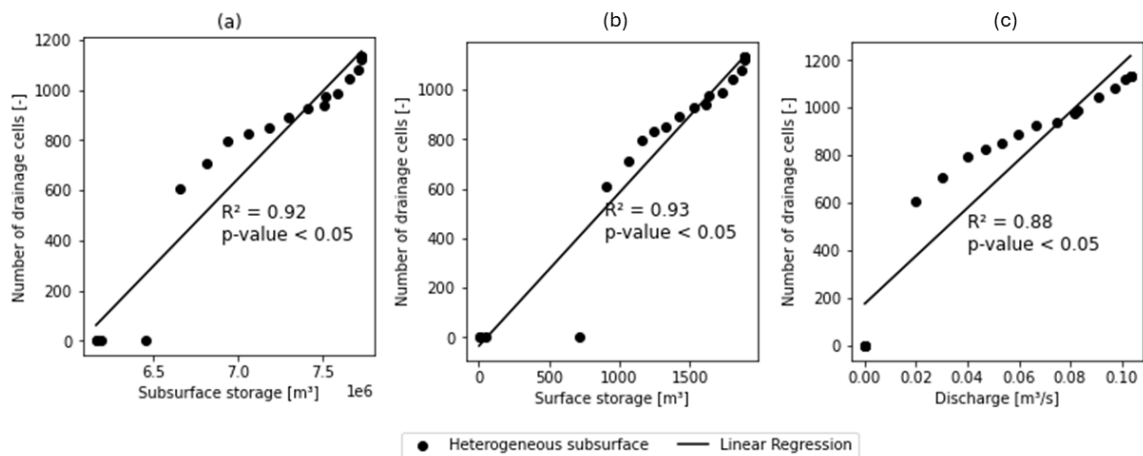
Table 13 – Monitored and simulated cross-section, where CS is cross-section, number is the number of observations, S1 is Scenario 1 and S2 is Scenario2.

CS	Number	Mean observation [m³/s]	Simulated S1 [m³/s]	Simulated S2 [m³/s]	Error S1 [%]	Error S2 [%]	Diference S1 and S2 [%]
11	1	0.00073	0.00390	0.00370	434.25	406.85	-5.13
12	5	0.02500	0.05500	0.06500	120.00	160.00	18.18
13	2	0.02100	0.04400	0.05500	109.52	161.90	25.00
14	2	0.00270	0.00480	0.00760	77.78	181.48	58.33
15	2	0.00110	0.00081	0.00086	-26.36	-21.82	6.17
22	2	0.00080	0.00120	0.00120	50.00	50.00	0.00
P1	7	0.03100	0.04700	0.05300	51.61	70.97	12.77
P2	4	0.03600	0.05300	0.06400	47.22	77.78	20.75
Outlet	15	0.12800	0.11398	0.13173	-10.96	2.91	15.58

Figure 39 – Discharge during spin-up of RGC at ParFlow for different geological scenarios. (a) Discharge in the time; and (b) Observed discharge at end of Spin up versus simulated discharge in subcatchments of RGC during baseflow.
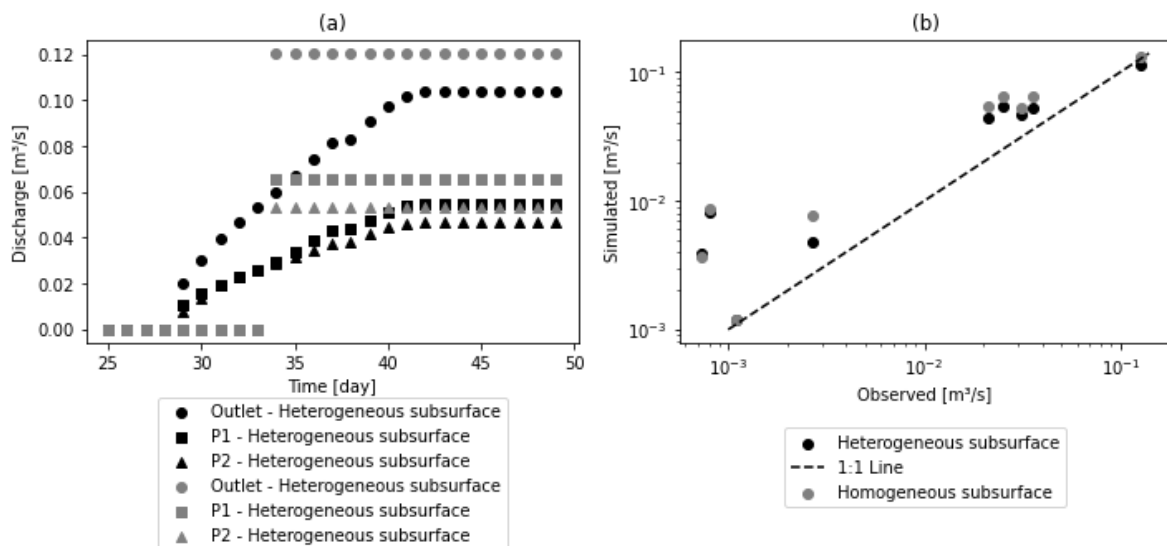
6.3.2 Parflow-CLM performance

The simulated streamflow of the two scenarios (S1 – Heterogeneous subsurface; S2 – Homogeneous subsurface), compared to hour data series of measurements at the P1 and P2 (Figure 40) represents the capability of the ParFlow-CLM simulate the streamflow generation. It took a seven days to run the S1 and three days to run the S2. Neither scenario adequately captured the general trend of observations, especially regarding peaks that are not precisely captured by either of them. For S1, KGE were 0.43 and 0.36 for the P1 and P2 respectively and 0.22 and -0.10 for the P1 and P2 respectively for S2. The low performance of the models may be related to a large volume of precipitation, which was atypical even for the study region, which is humid subtropical, where it was around 300 mm per month.

Figure 40 – Comparison of simulated discharge on Parflow-CLM. (a) Cross section P1; and (b) Cross section P2. Where homogeneous and heterogeneous is referent to the subsurface.
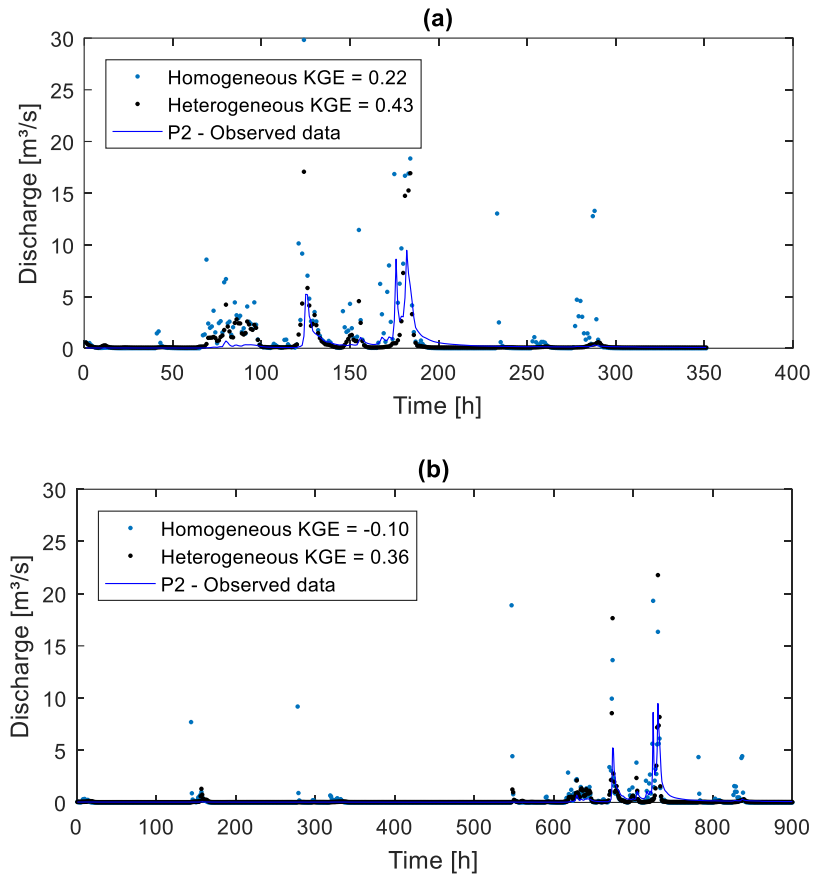
In Figure 40, S2 showed a greater variation in streamflow than in S1 thus more sensitive to precipitation and causing the RGC to become saturated and dry out very quickly. These fluctuations across time were observed in surface storage (Figure 41b) and the number of drainage cells (Figure 41c) but were not observed in subsurface storage (Figure 41a), where the values remained almost constant throughout the period for S2. For S1, after an initial increase at time 600, they never decreased to the initial conditions.

Figure 41 – Variation on time of the (a) subsurface storage (b) surface storage and (c) number of drainage cell, across entire domain (Ribeirão Grande Catchment) for heterogeneous subsurface (scenario 1) and homogeneous subsurface (scenario 2).
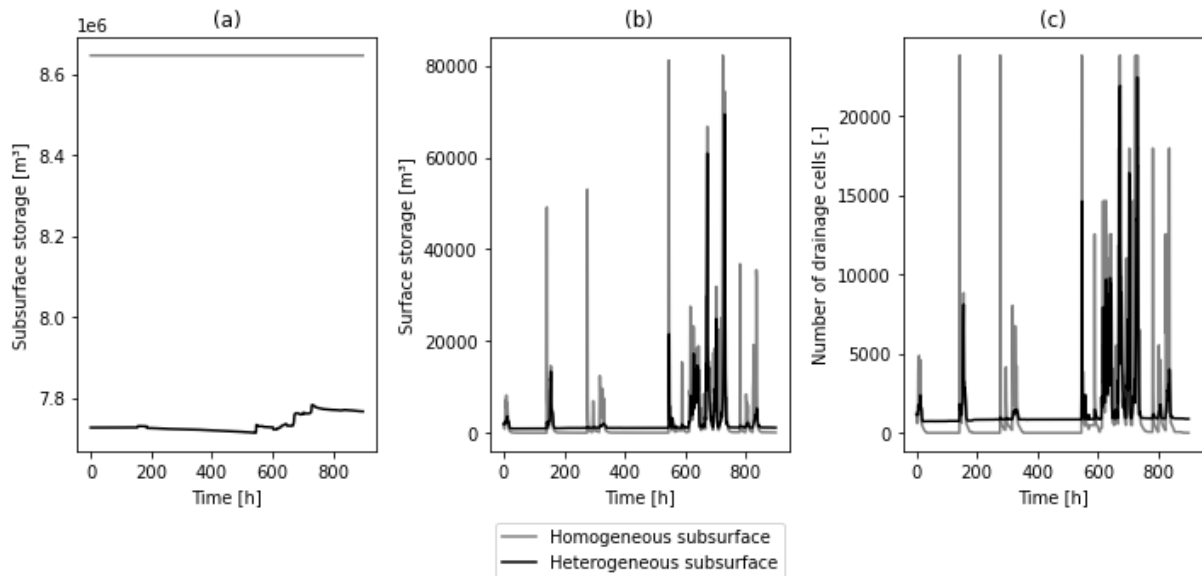
We expected that the subsurface storage would primarily control the drainage network for both S1 and S2. However, the results show that there is no linear correlation between the number of drainage cells and subsurface storage for S1, as evidenced by a noticeable gap between 7.74 and 7.75 x 10^6 m³ (Figure 42d). This gap is attributed to a heavy rainfall event at hour 671, which caused an increase in the volume of stored water that remained high until the end of the period (Figure 42d). Interestingly, in the S2, a threshold of subsurface storage of 880 x 10^6 m³ is necessary to activate drainage cells and generate discharge in the catchment (Figure 42a). Above this threshold, the number of active drainage cells increases rapidly, though not linearly with subsurface storage. In contrast, the heterogeneous scenario does not show a similar threshold effect.

Figure 42 – Correlation between the hydrological variables for the two scenarios, homogeneous subsurface (a;b;c) and heterogeneous subsurface (d;e;f): (a) Number of drainage cell versus subsurface storage for homogeneous subsurface; (b) Number of drainage cell versus surface storage for homogeneous subsurface; (c) Number of drainage cell versus discharge heterogeneous subsurface; (d) Number of drainage cell versus subsurface storage for heterogeneous subsurface; (e) Number of drainage cell versus surface storage for heterogeneous subsurface; and (f) Number of drainage cell versus discharge heterogeneous subsurface.
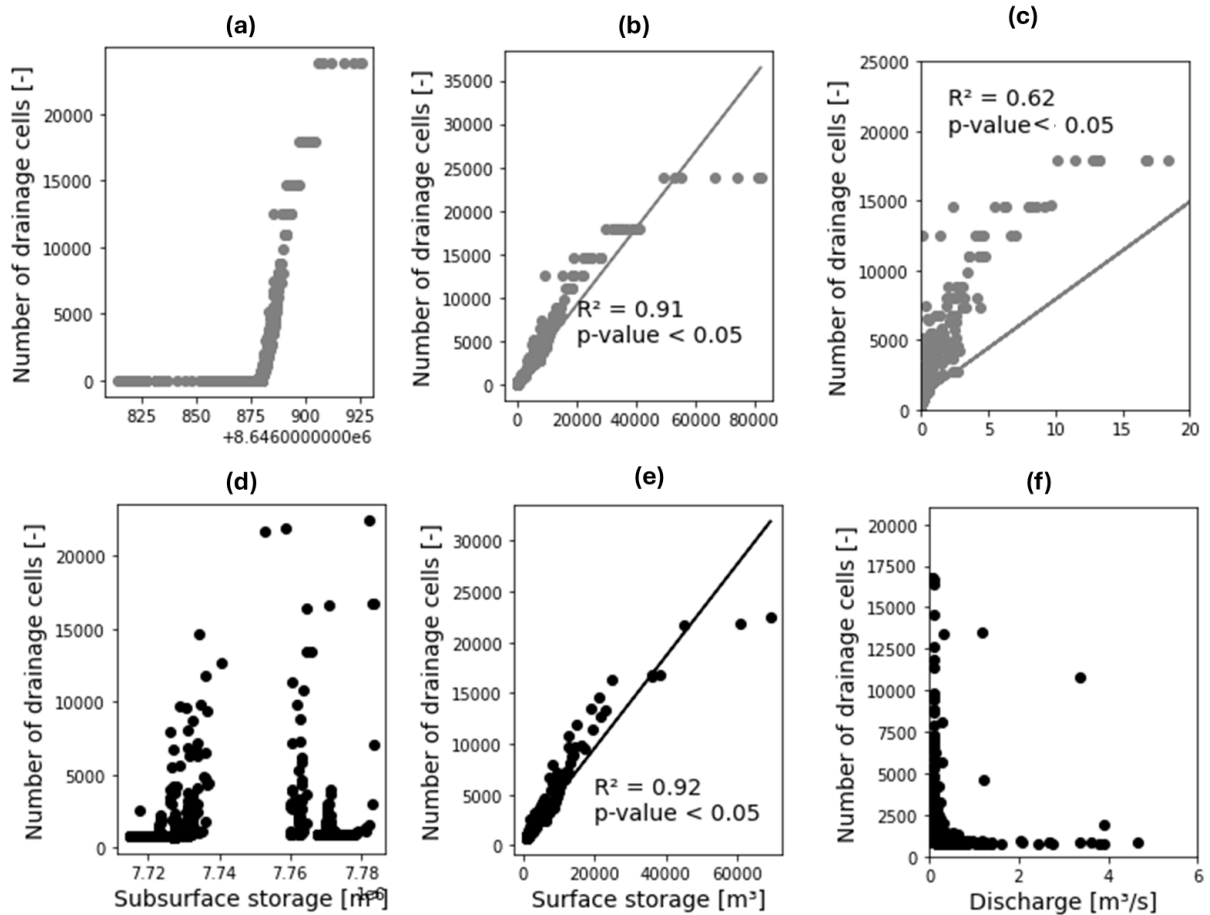
In contrast to subsurface storage, surface storage shows a linear relationship with the activation of drainage in both scenarios. It is possible to observe a linear relationship between the number of drainage cells and surface storage (Figure 42f). In the S2 the maximum number of active cells is higher than S1 (22000), reaching 25000. This increase is due to the inactivity of cells located above the granite in the S1. In both scenarios when surface storage reaches about 40000 m³, the number of drainage cells stabilizes.

As subsurface storage, discharge is linearly related to the activation of the drainage in S2 (Figure 42c). In S2, even at low discharges, many cells are draining water. This occurs because we consider a threshold of 0.001 m.c.a. for a cell to be considered as part of the drainage network. This water level at the outlet is equivalent to 1×10^{-5} m³/s. As seen in the Spin-up (Figure 37c), all the drainage is active at the same time, which can mean that many of the matrix cells can be part of the drainage at low discharge.

6.3.3   Streamflow patterns and stream network dynamics

The relationship between area and specific discharge in different states of catchment saturation is different among S1 and S2 (Figure 43). In S1, for lower discharges, specific discharge decreases with the area until reaching 2.9 m³/s, then remains constant with the area, and the data variability also slightly decreases. Outliers for lower discharges tend to be higher values of specific discharge, whereas, for higher discharges, outliers are lower values. In S2, when discharge at the outlet is 0.03 m³/s, the entire catchment experiences no surface runoff, with no active drainage network, and data variability is lower compared to S1 for all discharges. The area at which specific discharge starts to become constant is approximately 0.5 km² for S2, while for S1, this constant area value is only noticeable at the highest discharge of 6.06 m³/s and is also around 0.5 km². The standard deviation for S1 are 4.1, 3.6, 3.9, 3.4, 3.2 and 2.9 m/s km² from the dry to wet condition while 0, 0, 0.04, 0.45, 0.51, 0.72, 1.13 m/s km² for S2.

The drainage networks differ between the two scenarios, as do their dynamics (Figure 44). For lower discharges, the drainage network in S1 is denser, whereas for higher discharges, the opposite is observed. At a discharge of 6.06 m³/s, the drainage network covers the entire catchment, with virtually all cells experiencing pressures greater than 0.001 km. In S1, particularly for the three highest discharges, blue areas are noticeable in the bottom right corner of the catchment, indicating regions devoid of drainage networks. These areas correspond to granite concentrations without diabase dikes.

Figure 43 – Scale dependence of streamflow in different conditions. Where Q is discharge at the outlet of RGC based on the ParFlow-CLM simulation using Scenario 1.
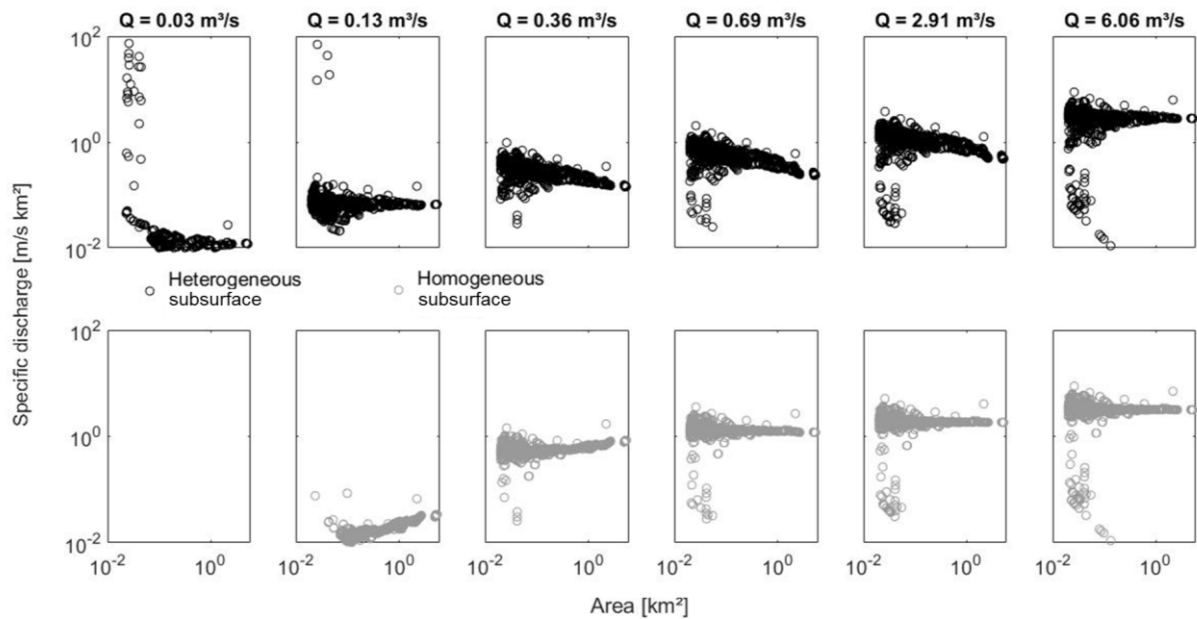
Figure 44 – Stream network dynamics under different saturation conditions for two different scenarios on ParFlow-CLM scenario 1 (Heterogeneous subsurface) and scenario 2 (Homogeneous subsurface). Yellow represents the stream network while blue represents the hillslopes.
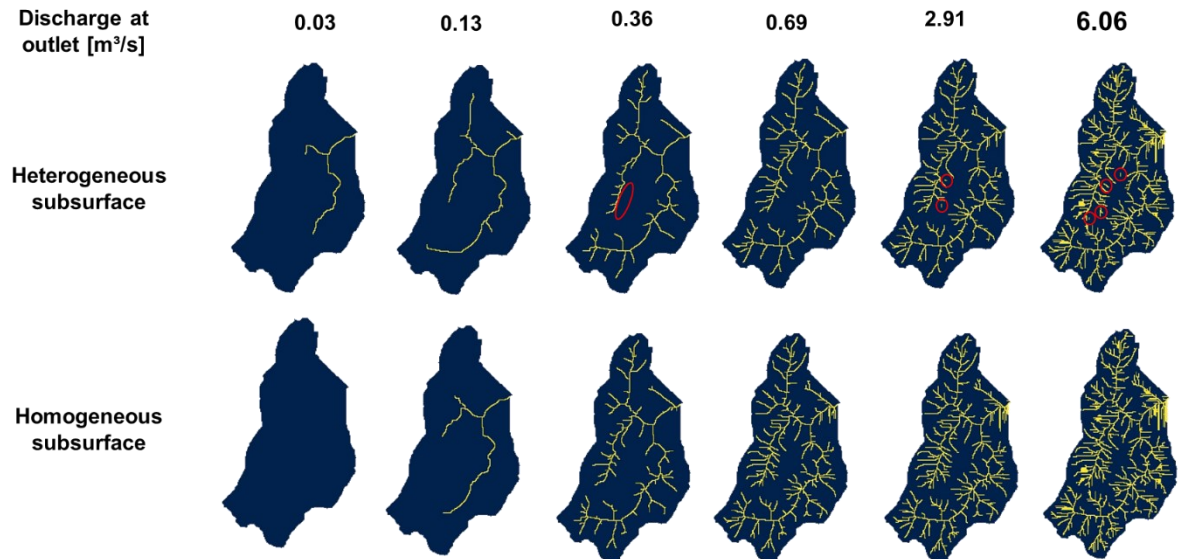
6.4   DISCUSSION

6.4.1   Spin-up observations coupled with baseflow campaigns can serve as valuable tools for comprehending subsurface water flows

Spin-up allows that models to reach a steady-state condition, where the various components of the hydrological system stabilize, besides that the spin-up period also allows us to gain insights into the identification of model behaviour (Engdahl, 2024). It is possible to notice the dynamics of the catchment during spin-up, and it serves as an opportunity to compare simulated results with observed data, assessing the accuracy of model predictions, and identifying areas where improvements may be needed (Beven, 2012). While running four months of ParFlow-CLM in S2 took three entire days to spin up from one year, spending 6 hours provided information that could be compared to catchment data during baseflow. From the spin-up period, it is possible to verify the spatial distribution of the discharge and the active drainage network in the whole catchment. However, generally, studies with models validate the data just using data from the outlet, which could be a mistake; in our case, errors were minimized at higher discharge, giving the impression that the model is representative of the behaviour of the catchment, when in fact it is not. Therefore, it is essential that the models are spatially validated at the time of spin-up if the goal is to understand the patterns of the hydrological process.

In S1 it was possible to capture drainage formation of granite areas before diabase dikes areas despite their location within the same catchment. This suggested that baseflow stream water from a granite area was sustained by greater amounts of groundwater due to higher bedrock permeability in the diabase areas. It has been parameterized that diabase has a higher bedrock permeability than granite.

6.4.2   Variability of the discharge in the time is related to streamflow generation

Geology influences the variability of discharge over time. In the cross-sections P1 and P2, it can be observed that in the scenario with homogeneous subsurface, there is a greater variation, with a quick response and significant disturbance in the catchment during storms events, and at the end of rainfall, the streams dry up. This same variation is not noted in the scenario with S1, where a greater portion of rainfall infiltrates and is gradually released during inter-event periods, baseflow. The variability of discharge is related to differences in the streamflow generation process between these two scenarios.

Under homogeneous geology, it is possible to notice the saturation excess overland flow (Dunne; Black, 1970) or infiltration excess overland flow (Horton, 1933) when rainfall intensity exceeds the infiltration capacity of the soil because of the saturation or rainfall

intensity, leading to surface runoff. This phenomenon is described as a quick and direct response to rainfall. In our case, we refer to saturated soil because the storage did not change over time (Figure 41a), all subsurface areas have the same hydraulic properties, with a hydraulic conductivity of 0.072 m h-1 (72 mm h-1). The rainfall intensity ranged from 0.02 to 48.2 mm h-1, that means, the rainfall intensity never exceeds the hydraulic conductivity.

Under heterogeneous geology, we identified as subsurface stormflow (Dunne; Black, 1970) as the mechanism responsible for streamflow generation, explaining the delayed response of streamflow to storm events. According to this concept, a portion of the rainfall infiltrates into the soil and moves laterally through the subsurface, bypassing the soil matrix and reaching the stream quickly as subsurface flow. This process is often associated with the presence of preferential flow paths, such as macropores or fractures, which facilitate rapid water movement through the subsurface. It is interesting to note that while it is not possible to parameterize fractures in ParFlow, the parametrization of diabase dikes was sufficient to describe the preferential flow path. Additionally, by parameterizing different layers for soil and geology, the low permeability of the granite and diabase ensures that the stream will have baseflow in the streams between events.

The spatial heterogeneity was so significant that the model represented two distinct streamflow generation models. This is not a novel finding; other studies have also demonstrated this using Darcy-Richards models (e.g. Hopp; McDonnell, 2009; Meerveld; Weiler, 2008). The interface between soil and bedrock is fundamental for well represent the water flow at the catchment, because lateral subsurface stormflow is observed solely under conditions where relatively cohesive zones of saturation are established at the interface between soil and bedrock (Hopp; McDonnell, 2009; Tromp-van Meerveld; McDonnell, 2006). As there is no interface between soil and bedrock in the homogeneous scenario, there are no different thresholds to be reached for the parts of the catchment to connect, the entire catchment has only one threshold for streamflow activation. In this way, the concept of fill-spill would have only one threshold for the homogeneous scenario and four different thresholds for the heterogeneous scenario. The threshold in the case of a homogeneous scenario is easily detectable; once storage reaches 880 x 10^6 m³, cells begin to drain water onto their surface. Yet, it is not possible to define threshold in the heterogeneous subsurface.

Getting data at a good resolution to adequately represent this heterogeneity explicitly can be challenging, generally the catchments has just a few soil test and the data is extrapolated for whole catchment (Clark *et al.*, 2017). However, what matters most is that the heterogeneity

is represented sufficiently to capture its control over streamflow generation. Knowing the exact configuration of storage areas is not necessary to simulate their filling and spilling. Nonetheless, with a good geospatial representation of bedrock topography could be enough to correctly simulate observed runoff (Meerveld; Weiler, 2008) and this can also be observed with our results.

The results showed that greater storage capacity does not translate into an active catchment for longer, since the homogeneous scenario always has greater storage, but there is no water available in the streams between events. The main difference among the scenarios was the contribution of baseflow to total streamflow. The presence of baseflow plays a crucial role in maintaining the memory of catchment and sustaining streamflow during dry periods. Baseflow, derived from groundwater discharge, provides a continuous supply of water to streams even when there is no direct rainfall input. One of the primary ways catchment memories influences the response to climate change is through its impact on streamflow dynamics. Catchments with high memory, characterized by significant storage capacities in soils, groundwater, and surface water bodies, are better equipped to buffer the effects of short-term climate variability (Sutanto; Van Lanen, 2022). Our results suggest that memory in humid catchments is related to differences between the hydraulic characteristics of layers; a layer with a high infiltration and percolation capacity close to the surface captures water that is directed to the lower layers that store the water and slowly release it into the streams. Thus, catchment can sustain streamflow during dry periods by releasing water stored in geology, thereby mitigating the impacts of droughts on water availability.

6.4.3 Increased subsurface heterogeneity translates into greater variability of specific streamflow data

The observation that specific discharge decreases with increasing catchment area and then becomes relatively constant aligns with findings from previous studies (Lyon *et al.*, 2012; Uchida *et al.*, 2005; Woods; Sivapalan; Duncan, 1995) with both scenarios, homogeneous or heterogeneous subsurface. This pattern is often attributed to the increasing contribution of regional groundwater relative to local groundwater as catchment size increases (Asano *et al.*, 2020). In our data geology, the variability of specific baseflow is different in both scenarios, with the same topography but with different geology characterization. Geology has been found to exert a greater impact on differences in streamflow generation between nested catchments

during baseflow, while topography exerts a greater impact during storm flow periods (Pfister *et al.*, 2017). This is expected because the recharge and release of bedrock groundwater are primarily governed by geological factors (Pfister *et al.*, 2017), our results showed that even during storm conditions geology influences streamflow.

The decrease in data variability with increasing discharge observed is consistent with the concept of hydrological connectivity. As discharge increases, the network of flow paths becomes more connected, leading to more predictable and consistent flow patterns (Dohman; Godsey; Hale, 2021). The presence of outliers maybe due to various factors such as localized differences in soil properties (Egusa *et al.*, 2019), land use (Lyon *et al.*, 2012), or geological (Iwasaki; Nagasaka; Nagasaka, 2021) features that influence flow pathways and storage capacities within the catchment. For example, dikes can act as hydraulic barriers within the subsurface geological structure (Cavalcante *et al.*, 2020). This can prevent groundwater from moving past the dike, leading to increased water accumulation and the formation of pools on the surface above the dike. Such pools might be more persistent due to consistent groundwater outflow to the surface (Bourke *et al.*, 2023). In our virtual study, all the characteristics of the catchment (land use and topography) are the same, just the subsurface changes between both scenarios, however, the standard deviation of the specific discharge just decreases in the scenario with heterogeneous subsurface while for homogeneous subsurface increases. This shows that the interference of topography on discharge increases for wetter conditions and that of geology on discharge increases for drier conditions. However, geology plays an important role even for wetter conditions since the standard deviation of S1 is greater than S2 for all saturation conditions.

6.4.4   The shape of the drainage network depends on the topography, but its activation depends on the geology

Mapping the drainage network in different states of catchment saturation can be a challenge in catchment covered by dense forest, such as in this study area, and this type of virtual experiment is very valuable for understanding the dynamics of the drainage network. Apparently, the drainage networks for both scenarios are similar, following the logic that the contributing area is the decisive factor for the drainage network, as demonstrated in APPENDIX D. Contribution area is related to topography, not to geology. Nevertheless, the activation areas

in each saturation state are related to the flow generation process, which is influenced by geology.

The observed variation in drainage network density between S1 and S2 is consistent with the influence of subsurface heterogeneity on flow pathways and connectivity within catchments (Dohman; Godsey; Hale, 2021). Previous studies have demonstrated that geological factors can significantly affect the spatial distribution of drainage networks (Bourke *et al.*, 2023; Mutzner *et al.*, 2016). There are two primary ways in which dikes can affect discontinuous streamflow. Firstly, providing preferential groundwater flow along their strike (Senger *et al.*, 2015), which are characterized by their significant contributions to surface flow. Secondly, dikes can alter groundwater flow by acting barrier-like (Comte *et al.*, 2017) and create variability in how streams exchange groundwater or the hyporheic zone. We parameterize diabase as being closer to the surface than granite and more permeable than granite but lower than granite residual soil. Therefore, it is expected to see these two effects (preferential flow path and barrier) in the drainage network. At storm conditions, we noticed granite areas without overland flow (or drainage), this occurs because of the difference between permeability. Granite and other substrates with low permeability tend to result in decreased surface runoff and a less dense drainage network compared to more permeable materials (Comte *et al.*, 2017), influencing the number of drainage cells.

Initially, we expected that subsurface storage would be a primary determinant in controlling the drainage network (Hofer *et al.*, 2011) for both scenarios, however it is not the first controller. For heterogeneous subsurface scenario, there was a lack of a linear correlation between the number of drainage cells and subsurface storage. In contrast, the homogeneous scenario exhibits a clearer, though non-linear, relationship between subsurface storage and drainage activation, with a specific threshold (880×10^6 m³) required to activate the drainage network. This follows the fill-spill hypothesis, where after reaching a storage threshold, the cell transforms into a drainage cell (Tromp-van Meerveld; McDonnell, 2006). Surface storage and discharge is related to drainage by linear correlation in both scenarios, unlike the more complex effects of subsurface storage. This suggests that surface storage could be a more reliable indicator of drainage network behavior and should be considered in hydrological modeling and water management practices (Cazorzi *et al.*, 2013).

6.5   CONCLUSION

A distributed physical hydrological model used in two different scenarios (ParFlow) highlights the influence of subsurface heterogeneity on streamflow generation and drainage network dynamics. Our main conclusions from analyses of steady-state (spin-up) and non-steady-state model observations, combined with baseflow campaigns and short rainfall-runoff data series are as follows:

- The data from baseflow camapings was useful for check if after the spin-up, the model represents a good starting point for simulations. The results underline the necessity of spatial validation to avoid misleading conclusions about model accuracy based solely on outlet data.

- A geospatial representation of bedrock topography and surface topography could be sufficient to increase the quality of the simulations, from homogeneous to heterogeneous geologic scenarios.

- The subsurface characteristics influence how the models represents the streamflow generation. The streamflow generation is characterized by saturation excess overland flow for homogeneous scenario and subsurface stormflow for heterogeneous scenario. These changes affect our perception of streamflow generation that affect water availability, especially during baseflow, and the dynamics of the drainage network. It also shows that greater subsurface storage, or storage capacity, does not necessarily result in a greater amount of water available in streams.

- The drainage cells do not follow a pattern that totaly follows topography in the heterogeneous scenario, and the specific baseflow presents more variability than homogeneous scenario. This occurs due to differences in permeability and must be accurately represented to estimate correct spatial patterns in a catchment.

This research provides compelling evidence that understanding geological heterogeneity is fundamental to accurately modeling and managing water flow in catchments. It emphasizes the need for integrating detailed geological and spatial hydrological data to better predict streamflow. The insights from this study are crucial for developing strategies to enhance the sustainability and resilience of water resources in diverse geological settings.

7. GENERAL CONCLUSIONS

The objective of this thesis is to analyze the influence of landscape structures on streamflow generation in the Peri Lake Experimental Catchment (PLEC) through baseflow campaigns. The baseflow campaigns showed a significant spatial variability in specific baseflow and $\delta^{18}O$ values in baseflow. The spatial variation is greater than the errors derived from discharge measurements. These differences in specific discharge are related to variations in storage and release of water, which are controlled by the subsurface part of the catchment during baseflow. The prediction of baseflow patterns is challenging due to the complex geology of the catchment. In subcatchments with dikes, the percentage of granite serves as the best predictor of specific baseflow. In subcatchments without dikes, the elevation emerges as the primary predictor. In both cases, specific baseflow is linked to geology and not topography. The specific baseflow is related to age of the bedrock body and hydraulic properties of bedrock, where subcatchments with more percentage of diabase dike deliver more water to the streams during baseflow. Also, in subcatchments without dikes, the connection to geology is related to release capacity especially in areas near the lake, located in low-elevated regions, feature a fractured aquifer. We presume that groundwater in these areas drains directly into the lake.

Patterns of $\delta^{18}O$ values in baseflow show that subsurface can change the $\delta^{18}O$ from rainfall by mixing. In areas without dikes, channel head have more water coming from deep groundwater. Because diabase dikes are shallower than granite, they create more complex and unpredictable water flow paths and storage areas. This complexity means that $\delta^{18}O$ values in baseflow do not decrease as the area increases. The complexity of the geology is key to predicting both $\delta^{18}O$ and baseflow, with more complex geological structures making it harder to predict baseflow pattern. Virtual experimental physical-based models (ParFlow) can provide insights into how subsurface heterogeneity can change streamflow patterns in different saturation states.

Our steady-state and non-steady-state simulations, coupled with baseflow campaigns and short rainfall-runoff data series, demonstrated that geospatial representations of bedrock and surface topography can substantially increase the simulation quality. The models of streamflow generation differ between the scenarios (homogeneous and heterogeneous subsurface): saturation excess overland flow in homogeneous and subsurface stormflow in heterogeneous. These differences affect water availability during baseflow and alter drainage network dynamics. Notably, greater subsurface storage does not necessarily correlate with

increased water availability in streams, and in heterogeneous scenarios, drainage cells display greater variability without following a landscape pattern, due to differences in permeability.

This research underscores the importance of moving beyond scale dependence and topography to focus on geology as the primary controlling factor in understanding the hydrological cycle at small scales. It highlights the importance of using detailed geological and hydrological data to improve streamflow predictions. Future studies should explore small-scale water processes, like how groundwater moves through bedrock and how water travels through soil and other underground layers. Achieving this will require extensive field surveys, mapping, subsurface sensing techniques, and the application of physical-based models. The findings are vital for creating strategies that make water resources more sustainable and resilient across different geological environments.

8. REFERENCES

ADJI, Tjahyo Nugroho *et al.* Spatial and temporal hydrochemistry variations of karst water in Gunung Sewu, Java, Indonesia. **Environmental Earth Sciences**, [*s. l.*], v. 76, n. 20, p. 1–16, 2017.

AJAMI, Hoori; MCCABE, Matthew F.; EVANS, Jason P. Impacts of model initialization on an integrated surface water-groundwater model. **Hydrological Processes**, [*s. l.*], v. 29, n. 17, p. 3790–3801, 2015.

AJMAL, Muhammad *et al.* Investigation of SCS-CN and its inspired modified models for runoff estimation in South Korean watersheds. **Journal of Hydro-Environment Research**, [*s. l.*], v. 9, n. 4, p. 592–603, 2015. Disponível em: http://dx.doi.org/10.1016/j.jher.2014.11.003.

ALEXANDER, Richard B; SMITH, Richard A; SCHWARZ, Gregory E. Effect of stream channel size on the delivery of nitrogen to the Gulf of Mexico. **Nature**, [*s. l.*], v. 403, n. 6771, p. 758–761, 2000.

ALI, Geneviève *et al.* A comparison of wetness indices for the prediction of observed connected saturated areas under contrasting conditions. **Earth Surface Processes and Landforms**, [*s. l.*], v. 39, n. 3, p. 399–413, 2014.

ALLEN, Gerald R.; LIU, Guangdong. IHACRES Classic: Software for the Identification of Unit Hydrographs and Component Flows. **Ground Water**, [*s. l.*], v. 49, n. 3, p. 305–308, 2011. Disponível em: http://doi.wiley.com/10.1111/j.1745-6584.2011.00814.x.

AMELI, A. A. *et al.* Groundwater subsidy from headwaters to their parent water watershed: A combined Field-Modeling approach. **Water Resources Research**, [*s. l.*], v. 54, n. 7, p. 5110–5125, 2018.

ANDERSON, M. G.; BURT, T. P. Automatic monitoring of soil moisture conditions in a hillslope spur and hollow. **Journal of Hydrology**, [*s. l.*], v. 33, n. 1–2, p. 27–36, 1977.

ANTONELLI, Marta *et al.* Saturated areas through the lens: 2. Spatio-temporal variability of streamflow generation and its relationship with surface saturation. **Hydrological Processes**, [*s. l.*], v. 34, n. 6, p. 1333–1349, 2020.

ARAGUÁS-ARAGUÁS, L.; FROEHLICH, K.; ROZANSKI, K. Deuterium and oxygen-18 isotope composition of precipitation and atmospheric moisture. **Hydrological Processes**, [*s. l.*], v. 14, n. 8, p. 1341–1355, 2000.

ARCHFIELD, S. A.; VOGEL, R. M. Map correlation method: Selection of a reference streamgage to estimate daily streamflow at ungaged catchments. **Water Resources Research**, [*s. l.*], v. 46, n. 10, p. 1–15, 2010.

ASAI, Kazuyoshi; SATAKE, Hiroshi; TSUJIMURA, Maki. Isotopic approach to understanding the groundwater flow system within an andesitic stratovolcano in a temperate humid region: case study of Ontake volcano, central Japan. **Hydrological Processes**, [*s. l.*], v. 23, n. 4, p. 559–571, 2009.

ASANO, Yuko *et al.* An increase in specific discharge with catchment area implies that bedrock infiltration feeds large rather than small mountain headwater streams. [*s. l.*], p. 1–19, 2020.

ASANO, Yuko; UCHIDA, Taro. Is representative elementary area defined by a simple mixing of variable small streams in headwater catchments?. **Hydrological Processes**, [*s. l.*], v. 24, n. 5, p. 666–671, 2010.

BÁRDOSSY, András *et al.* The master transit time distribution of variable flow systems. **Water Resources Research**, [*s. l.*], v. 35, n. 1, p. 1–10, 1999.

BARTHOLD, Frauke K. *et al.* How many tracers do we need for end member mixing analysis (EMMA)? A sensitivity analysis. **Water Resources Research**, [*s. l.*], v. 47, n. 8, p. 1–14, 2011.

BATISTA, Karina Romariz. Sertão do Peri: um olhar etnográfico. **PerCursos**, [*s. l.*], v. 5, n. 2, 2006.

BENISCHKE, R.; HARUM, T. Determination of discharge rates in turbulent streams by salt tracer dilution applying a microcomputer system. Comparison with current meter measurements. **Hydrology in mountainous regions I**, [*s. l.*], n. 193, p. 215–221, 1990.

BERGSTROM, Anna *et al.* Watershed structural influences on the distributions of stream network water and solute travel times under baseflow conditions. **Hydrological Processes**, [*s. l.*], v. 30, n. 15, p. 2671–2685, 2016.

BERNARD, M. An approach to determinate stream flow. **Transactions of the American Society of Civil Engineers**, [*s. l.*], v. 100, p. 347–362, 1935.

BERNARDARA, P.; DE MICHELE, C.; ROSSO, R. A simple model of rain in time: An alternating renewal process of wet and dry states with a fractional (non-Gaussian) rain intensity. **Atmospheric Research**, [*s. l.*], v. 84, n. 4, p. 291–301, 2007.

BEVEN, Keith. A history of the concept of time of concentration. **Hydrology and Earth System Sciences Discussions**, [*s. l.*], p. 1–28, 2020.

BEVEN, Keith. **Rainfall-Runoff Modelling**. Chichester, UK: John Wiley & Sons, Ltd, 2012. Disponível em: http://doi.wiley.com/10.1002/9781119951001.

BEVEN, Keith. The hydrological response of headwater and sideslope areas. **Hydrological Sciences Bulletin**, [*s. l.*], v. 23, n. 4, p. 419–437, 1978.

BEVEN, K. J.; KIRKBY, M. J. A physically based, variable contributing area model of basin hydrology. **Hydrological Sciences Bulletin**, [*s. l.*], v. 24, n. 1, p. 43–69, 1979.

BHADRA, A. *et al.* Development of a geomorphological instantaneous unit hydrograph model for scantily gauged watersheds. **Environmental Modelling & Software**, [*s. l.*], v. 23, n. 8, p. 1013–1025, 2008. Disponível em: https://linkinghub.elsevier.com/retrieve/pii/S1364815207002034.

BHUNYA, P. K. *et al.* Comparison between Weibull and gamma distributions to derive synthetic unit hydrograph using Horton ratios. **Water Resources Research**, [*s. l.*], v. 44, n. 4, 2008. Disponível em: http://doi.wiley.com/10.1029/2007WR006031.

BHUNYA, P.K. *et al.* Suitability of Gamma, Chi-square, Weibull, and Beta distributions as synthetic unit hydrographs. **Journal of Hydrology**, [*s. l.*], v. 334, n. 1–2, p. 28–38, 2007. Disponível em: http://linkinghub.elsevier.com/retrieve/pii/S0022169406005075.

BHUNYA, P. K. *et al.* Synthetic unit hydrograph methods: a critical review. **The Open Hydrology Journal**, [*s. l.*], v. 5, n. 1, p. 1–8, 2011.

BHUNYA, P. K.; SINGH, P. K.; MISHRA, S. K. Fréchet and chi-square parametric expressions combined with Horton ratios to derive a synthetic unit hydrograph. **Hydrological Sciences Journal**, [*s. l.*], v. 54, n. 2, p. 274–286, 2009. Disponível em: http://www.tandfonline.com/doi/abs/10.1623/hysj.54.2.274.

BIRKEL, Christian *et al.* Headwaters drive streamflow and lowland tracer export in a large-scale humid tropical catchment. **Hydrological Processes**, [*s. l.*], n. February, p. 3824–3841, 2020.

BJERVE, L; GROSTERRUD, O. Discharge Measurements by a New-Formed Relative Salt-Dilution Method in Small Turbulent Streams. **Nordic Hydrology**, [*s. l.*], p. 121–132, 1980.

BLOOMFIELD, J. P.; ALLEN, D. J.; GRIFFITHS, K. J. Examining geological controls on baseflow index (BFI) using regression analysis: An illustration from the Thames Basin, UK. **Journal of Hydrology**, [*s. l.*], v. 373, n. 1–2, p. 164–176, 2009.

BLÖSCHL, G. *et al.* Twenty-three unsolved problems in hydrology (UPH)–a community perspective. **Hydrological Sciences Journal**, [*s. l.*], v. 64, n. 10, 2019.

BOTTER, Gianluca; BERTUZZO, Enrico; RINALDO, Andrea. Transport in the hydrologic response: Travel time distributions, soil moisture dynamics, and the old water paradox. **Water Resources Research**, [*s. l.*], v. 46, n. 3, p. 1–18, 2010.

BOTTER, Gianluca; RINALDO, Andrea. Scale effect on geomorphologic and kinematic dispersion. **Water Resources Research**, [*s. l.*], v. 39, n. 10, 2003.

BOURKE, Sarah A. *et al.* A hydrological framework for persistent pools along non-perennial rivers. **Hydrology and Earth System Sciences**, [*s. l.*], v. 27, n. 3, p. 809–836, 2023.

BOX, G. E. P.; COX, D. R. An Analysis of Transformations. **Journal of the Royal Statistical Society: Series B (Methodological)**, [*s. l.*], v. 26, n. 2, p. 211–243, 1964.

BRIGGS, Martin A *et al.* Bedrock depth influences spatial patterns of summer baseflow, temperature and flow disconnection for mountainous headwater streams. **Hydrology and Earth System Sciences**, [*s. l.*], v. 26, n. 15, p. 3989–4011, 2022.

BRUNNER, Manuela I. *et al.* Uncertainty Assessment of Synthetic Design Hydrographs for Gauged and Ungauged Catchments. **Water Resources Research**, [*s. l.*], v. 54, n. 3, p. 1493–1512, 2018.

BRUTSAERT, W. **Hydrology: an introduction. 3rd ed**. [*S. l.: s. n.*], 2008-. ISSN 1098-6596.

BURT, T. P.; MCDONNELL, J. J. Whither field hydrology? The need for discovery science and outrageous hydrological hypotheses. **Water Resources Research**, [*s. l.*], v. 51, n. 8, p. 5919–5928, 2015. Disponível em: http://doi.wiley.com/10.1002/2014WR016839.

BUTTLE, J. M.; GREENWOOD, W. J.; GERBER, R. E. Spatiotemporal patterns of baseflow metrics for basins draining the Oak Ridges Moraine, southern Ontario, Canada. **Canadian Water Resources Journal**, [*s. l.*], v. 40, n. 1, p. 3–22, 2015.

CAMACHO SUAREZ, V. V. *et al.* Understanding runoff processes in a semi-arid environment through isotope and hydrochemical hydrograph separations. **Hydrology and Earth System Sciences**, [*s. l.*], v. 19, n. 10, p. 4183–4199, 2015.

CARLOTTO, T.; CHAFFE, P. L.B. Master Recession Curve Parameterization Tool (MRCPtool): Different approaches to recession curve analysis. **Computers and Geosciences**, [*s. l.*], v. 132, n. June, p. 1–8, 2019. Disponível em: https://doi.org/10.1016/j.cageo.2019.06.016.

CAUDURO, F.A.; DORFMAN, R. **Manual de ensaios de laboratório e de campo para irrigação e drenagem.** Firsted. Porto Alegre: PRONI/ IPH-UFRGS, 1986.

CAVALCANTE, Felipe Lisbona *et al.* Well productivity in the Ponta Grossa dike Swarm, Brazil: An integrated study with magnetic data inversion and clustering analysis of model solutions. **Journal of Hydrology**, [*s. l.*], v. 588, n. May, p. 125079, 2020. Disponível em: https://doi.org/10.1016/j.jhydrol.2020.125079.

CAVALLINI, Fabio. Computing the unit hydrograph via linear programming. [*s. l.*], v. 19, n. 9, p. 1285–1294, 1993.

CAZORZI, Federico *et al.* Drainage network detection and assessment of network storage capacity in agrarian landscape. **Hydrological Processes**, [*s. l.*], v. 27, n. 4, p. 541–553, 2013.

CERVI, F. *et al.* Perennial springs provide information to predict low flows in mountain basins. **Hydrological Sciences Journal**, [*s. l.*], v. 62, n. 15, p. 2469–2481, 2017. Disponível em: https://doi.org/10.1080/02626667.2017.1393541.

CHAPMAN, T.; MAXWELL, A. Baseflow separation-comparison of numerical meth- ods with tracer experiments. **Hydrological and Water Resources Symposium. Institution of Engineers Australia, Hobart**, [*s. l.*], p. 539–545, 1996.

CHEN, Lei *et al.* Event-based nonpoint source pollution prediction in a scarce data catchment. **Journal of Hydrology**, [*s. l.*], v. 552, p. 13–27, 2017.

CHEN, Yingbing *et al.* New method to calculate the dynamic factor–flow velocity in Geomorphologic instantaneous unit hydrograph. **Scientific Reports**, [*s. l.*], v. 9, n. 1, p. 1–13, 2019.

CHEN, Ke *et al.* Synoptic water isotope surveys to understand the hydrology of large intensively managed catchments. **Journal of Hydrology**, [*s. l.*], v. 623, n. November 2022, p. 129817, 2023.

CHENG, Qiuming *et al.* GIS modeling for predicting river runoff volume in ungauged drainages in the Greater Toronto Area, Canada. **Computers and Geosciences**, [*s. l.*], v. 32, n. 8, p. 1108–1119, 2006.

CHOW, V.T. Hydrologic determination of waterway areas for the design of drainage structures in small drainage basins. **Engineering Experiment Station Bulletin**, [*s. l.*], v. 462, p. 104, 1962.

CHRISTOPHERSEN, Nils *et al.* Modelling streamwater chemistry as a mixture of soilwater end-members — A step towards second-generation acidification models. **Journal of Hydrology**, [*s. l.*], v. 116, n. 1–4, p. 307–320, 1990.

CISNEROS VACA, César; VAN DER TOL, Christiaan; GHIMIRE, Chandra Prasad. The influence of long-term changes in canopy structure on rainfall interception loss: A case study in Speulderbos, the Netherlands. **Hydrology and Earth System Sciences**, [*s. l.*], v. 22, n. 7, p. 3701–3719, 2018.

CLARK, C. O. Storage and the unit hydrograph. **Proceedings of the American Society of Civil Engineers.**, [*s. l.*], p. 1333–1360, 1945.

CLARK, Martyn P. *et al.* The evolution of process-based hydrologic models: Historical challenges and the collective quest for physical realism. **Hydrology and Earth System Sciences Discussions**, [*s. l.*], n. January, p. 1–14, 2017.

CLOW, David W.; FLEMING, Andrea C. Tracer gauge: An automated dye dilution gauging system for ice-affected streams. **Water Resources Research**, [*s. l.*], v. 44, n. 12, p. 1–11, 2008.

COE, M. T. *et al.* The effects of deforestation and climate variability on the streamflow of the Araguaia River, Brazil. **Biogeochemistry**, [*s. l.*], v. 105, n. 1, p. 119–131, 2011.

COHN, Timothy A.; KIANG, Julie E.; MASON, Robert R. Estimating Discharge Measurement Uncertainty Using the Interpolated Variance Estimator. **Journal of Hydraulic Engineering**, [*s. l.*], v. 139, n. 5, p. 502–510, 2013.

COLLISCHONN, Walter *et al.* Hydraulic Causes for Basin Hydrograph Skewness. **Water Resources Research**, [*s. l.*], p. 1–16, 2017. Disponível em: http://doi.wiley.com/10.1002/2017WR021543.

COMTE, JC *et al.* Effect of volcanic dykes on coastal groundwater flow and saltwater intrusion: A field-scale multiphysics approach and parameter evaluation. **Water Resources Research**, [*s. l.*], v. 53, n. 3, p. 2171–2198, 2017.

CONDON, Laura E.; MAXWELL, Reed M. Implementation of a linear optimization water allocation algorithm into a fully integrated physical hydrology model. **Advances in Water Resources**, [*s. l.*], v. 60, p. 135–147, 2013.

COOKE, Ciara D.; BUTTLE, James M. Assessing basin storage: Comparison of hydrometric- and tracer-based indices of dynamic and total storage. **Hydrological Processes**, [*s. l.*], v. 34, n. 9, p. 2012–2031, 2020.

CROLEY, Thomas E. Gamma synthetic hydrographs. **Journal of Hydrology**, [*s. l.*], v. 47, n. 1–2, p. 41–52, 1980. Disponível em: http://linkinghub.elsevier.com/retrieve/pii/0022169480900463.

CUDENNEC, Christophe. On width function-based unit hydrographs deduced from separately random self-similar river networks and rainfall variability. Discussion of "Coding randon self-similar river networks and calculating geometric distances: 1. General methodology" and "2. App. **Hydrological Sciences Journal**, [*s. l.*], v. 52, n. 1, p. 230–237, 2007.

DAFNY, Elad; BURG, Avi; GVIRTZMAN, Haim. Deduction of groundwater flow regime in a basaltic aquifer using geochemical and isotopic data: The Golan Heights, Israel case study. **Journal of Hydrology**, [*s. l.*], v. 330, n. 3–4, p. 506–524, 2006.

D'ANGELO, D. J. *et al.* Transient Storage in Appalachian and Cascade Mountain Streams as Related to Hydraulic Characteristics. **Journal of the North American Benthological Society**, [*s. l.*], v. 12, n. 3, p. 223–235, 1993.

DAVIDS, Jeffrey C. *et al.* Citizen science flow-an assessment of simple streamflow measurement methods. **Hydrology and Earth System Sciences**, [*s. l.*], v. 23, n. 2, p. 1045–1065, 2019.

DAY, D. G. Drainage density changes during rainfall. **Earth Surface Processes**, [*s. l.*], v. 3, n. 3, p. 319–326, 1978.

DAY, Terry J. Observed mixing lengths in mountain streams. **Journal of Hydrology**, [*s. l.*], v. 35, n. 1–2, p. 125–136, 1977.

DAY, Terry J. On the precision of salt dilution gauging. **Journal of Hydrology**, [*s. l.*], v. 31, n. 3–4, p. 293–306, 1976.

DE ALMEIDA, Isabel Kaufmann *et al.* Estimation on time of concentration of overland flow in watersheds: A review. **Geociencias**, [*s. l.*], v. 33, n. 4, p. 661–671, 2014.

DE LAVENNE, A.; BOUDHRAÂ, H.; CUDENNEC, C. Streamflow prediction in ungauged basins through geomorphology-based hydrograph transposition. **Hydrology Research**, [*s. l.*], v. 46, n. 2, p. 291–302, 2015.

DI LAZZARO, Michele. Regional analysis of storm hydrographs in the Rescaled Width Function framework. **Journal of Hydrology**, [*s. l.*], v. 373, n. 3–4, p. 352–365, 2009. Disponível em: http://dx.doi.org/10.1016/j.jhydrol.2009.04.027.

DINGMAN, S L. **Physical hydrology**. Waveland ped. [*S. l.: s. n.*], 2015.

DOHMAN, J. M.; GODSEY, S. E.; HALE, R. L. Three-Dimensional Subsurface Flow Path Controls on Flow Permanence. **Water Resources Research**, [*s. l.*], v. 57, n. 10, p. 1–18, 2021.

DOOGE, James. A General Theory of the Unit Hydrograph. **Journal of Geophysical Research**, [*s. l.*], v. 64, n. 2, p. 241–256, 1959.

DOOGE, J C I. Linear theory of hydrologic systems. **Technical Bulletin**, [*s. l.*], v. 1468, n. 1468, p. 1–337, 1973.

DOYLE, Martin W. *et al.* Effective discharge analysis of ecological processes in streams. **Water Resources Research**, [*s. l.*], v. 41, n. 11, p. 1–16, 2005.

DUNKERLEY, David L. Evaporation of impact water droplets in interception processes: Historical precedence of the hypothesis and a brief literature overview. **Journal of Hydrology**, [*s. l.*], v. 376, n. 3–4, p. 599–604, 2009.

DUNKERLEY, David. Intra-event intermittency of rainfall: an analysis of the metrics of rain and no-rain periods. **Hydrological Processes**, [*s. l.*], v. 29, n. 15, p. 3294–3305, 2015.

DUNNE, Thomas; BLACK, Richard D. Partial Area Contributions to Storm Runoff in a Small New England Watershed. **Water Resources Research**, [*s. l.*], v. 6, n. 5, p. 1296–1311, 1970. Disponível em: http://doi.wiley.com/10.1029/WR006i005p01296.

ECKHARDT, K. How to construct recursive digital filters for baseflow separation. **Hydrological Processes**, [*s. l.*], v. 19, n. 2, p. 507–515, 2005. Disponível em: http://doi.wiley.com/10.1002/hyp.5675.

EDWARDSON, Kenneth J. *et al.* The hydraulic characteristics and geochemistry of hyporheic and parafluvial zones in Arctic tundra streams, north slope, Alaska. **Advances in Water Resources**, [*s. l.*], v. 26, n. 9, p. 907–923, 2003.

EGUSA, Tomohiro *et al.* Contrasting Patterns in the Decrease of Spatial Variability With Increasing Catchment Area Between Stream Discharge and Water Chemistry. **Water Resources Research**, [*s. l.*], v. 55, n. 8, p. 7419–7435, 2019.

EGUSA, Tomohiro *et al.* Quantifying aggregation and change in runoff source in accordance with catchment area increase in a forested headwater catchment. **Hydrological Processes**, [*s. l.*], v. 30, n. 22, p. 4125–4138, 2016.

EMBRAPA. Solos de Santa Catarina: Boletim de Pesquisa e Desenvolvimento n°46. [*s. l.*], p. 745, 2004.

ENGDAHL, Nicholas B. Impacts of Permeability Uncertainty in a Coupled Surface-Subsurface Flow Model Under Perturbed Recharge Scenarios. **Water Resources Research**, [*s. l.*], v. 60, n. 3, p. e2023WR035975, 2024.

EVANS, Ian S. An integrated system of terrain analysis and slope mapping. | Request PDF. **Final report on grant DA-ERO-591-73-G0040**, [*s. l.*], 1980.

EVARISTO, Jaivime; JASECHKO, Scott; MCDONNELL, Jeffrey J. Global separation of plant transpiration from groundwater and streamflow. **Nature**, [*s. l.*], v. 525, n. 7567, p. 91–94, 2015.

FAN, Y. *et al.* Hillslope Hydrology in Global Change Research and Earth System Modeling. **Water Resources Research**, [*s. l.*], p. 1–36, 2019.

FANG, Zhufeng *et al.* Scale dependent parameterization of soil hydraulic conductivity in 3D simulation of hydrological processes in a forested headwater catchment. **Journal of Hydrology**, [*s. l.*], v. 536, p. 365–375, 2016. Disponível em: https://linkinghub.elsevier.com/retrieve/pii/S0022169416301251.

FERGUSON, Ian M. *et al.* Effects of root water uptake formulation on simulated water and energy budgets at local and basin scales. **Environmental Earth Sciences**, [*s. l.*], v. 75, n. 4, p. 1–15, 2016.

FISCHER, Benjamin M.C. *et al.* Contributing sources to baseflow in pre-alpine headwaters using spatial snapshot sampling. **Hydrological Processes**, [*s. l.*], v. 29, n. 26, p. 5321–5336, 2015.

FISCHER, Benjamin M.C.; VAN MEERVELD, H. J.(Ilja); SEIBERT, Jan. Spatial variability in the isotopic composition of rainfall in a small headwater catchment and its effect on hydrograph separation. **Journal of Hydrology**, [*s. l.*], v. 547, p. 755–769, 2017.

FLEISCHMANN, Ayan S. *et al.* On river-floodplain interaction and hydrograph skewness. **Water Resources Research**, [*s. l.*], v. 52, n. 10, p. 7615–7630, 2016. Disponível em: http://doi.wiley.com/10.1002/2016WR019233.

FLORAM. **MONA da Lagoa do Peri 38 anos**. [*S. l.: s. n.*], 2019.

FLORIANCIC, Marius G. *et al.* A multi-scale study of the dominant catchment characteristics impacting low-flow metrics. **Hydrological Processes**, [*s. l.*], v. 36, n. 1, p. 1–18, 2022.

FLORIANCIC, Marius G. *et al.* Spatial variability in specific discharge and streamwater chemistry during low flows: Results from snapshot sampling campaigns in eleven Swiss catchments. **Hydrological Processes**, [*s. l.*], v. 33, n. 22, p. 2847–2866, 2019.

FONTES, Maria Luiza S. *et al.* Dynamics of planktonic prokaryotes and dissolved carbon in a subtropical coastal lake. **Frontiers in Microbiology**, [*s. l.*], v. 4, n. APR, p. 1–9, 2013.

FREDERICO, Felipe Golin. Retroanálise do deslizamento de encosta, associado à presença de dique, ocorrido na rodovia SC-401, Florianópolis/SC. [*s. l.*], 2019.

FREEMAN, Mary C.; PRINGLE, Catherine M.; JACKSON, C. Rhett. Hydrologic connectivity and the contribution of stream headwaters to ecological integrity at regional scales. **Journal of the American Water Resources Association**, [*s. l.*], v. 43, n. 1, p. 5–14, 2007.

FRISBEE, Marty D. *et al.* Streamflow generation in a large, alpine watershed in the southern Rocky Mountains of Colorado: Is streamflow generation simply the aggregation of hillslope runoff responses?. **Water Resources Research**, [*s. l.*], v. 47, n. 6, 2011.

GABRIELLI, C. P.; MCDONNELL, J. J.; JARVIS, W. T. The role of bedrock groundwater in rainfall-runoff response at hillslope and catchment scales. **Journal of Hydrology**, [*s. l.*], v. 450–451, p. 117–133, 2012.

GAD, Mohamed A. A useful automated rainfall-runoff model for engineering applications in semi-arid regions. **Computers and Geosciences**, [*s. l.*], v. 52, p. 443–452, 2013.

GANDOLFI, C.; BISCHETTI, G. B. Influence of the drainage network identification method on geomorphological properties and hydrological response. **Hydrological Processes**, [*s. l.*], v. 11, n. 4, p. 353–375, 1997.

GARCIA, Roberto D. *et al.* Spatial and temporal patterns in the chemistry of temperate low order Andean streams: effects of landscape gradients and hydrology. **Aquatic Sciences**, [*s. l.*], v. 85, n. 4, p. 1–15, 2023.

GARDNER, W. Payton *et al.* A numerical investigation of bedrock groundwater recharge and exfiltration on soil mantled hillslopes. **Hydrological Processes**, [*s. l.*], v. 34, n. 15, p. 3311–3330, 2020.

GARRETT, Krista K.; WOHL, Ellen E. Climate-invariant area–slope relations in channel heads initiated by surface runoff. **Earth Surface Processes and Landforms**, [*s. l.*], v. 42, n. 11, p. 1745–1751, 2017.

GEES, A. Flow measurement under difficult measuring conditions: field experience with the salt dilution method. **Hydrology in mountainous regions I**, [*s. l.*], n. 193, p. 255–262, 1990.

GENEREUX, David P.; WOOD, Sharon J.; PRINGLE, Catherine M. Chemical tracing of interbasin groundwater transfer in the lowlandrainforest of Costa Rica. **Journal of Hydrology**, [*s. l.*], v. 258, n. 1–4, p. 163–178, 2002.

GENTILE, Alessio *et al.* Towards a conceptualization of the hydrological processes behind changes of young water fraction with elevation: A focus on mountainous alpine catchments. **Hydrology and Earth System Sciences**, [*s. l.*], v. 27, n. 12, p. 2301–2323, 2023.

GERRITS, A. M.J.; PFISTER, L.; SAVENIJE, H. H.G. Spatial and temporal variability of canopy and forest floor interception in a beech forest. **Hydrological Processes**, [*s. l.*], v. 24, n. 21, p. 3011–3025, 2010.

GIBSON, J. J.; BIRKS, S. J.; EDWARDS, T. W.D. Global prediction of δA and δ2H-δ18O evaporation slopes for lakes and soil water accounting for seasonality. **Global Biogeochemical Cycles**, [*s. l.*], v. 22, n. 2, p. 1–12, 2008.

GIBSON, J. J.; BIRKS, S. J.; MONCUR, M. C. Stable isotope data (oxygen-18 and deuterium) from surveys of lakes, wetlands, rivers, and input waters across the South Athabasca Oil Sands region, Alberta, 2007–2009. **Data in Brief**, [*s. l.*], v. 22, p. 781–786, 2019.

GILBERT, James M.; MAXWELL, Reed M. Examining regional groundwater-surface water dynamics using an integrated hydrologic model of the San Joaquin River basin. **Hydrology and Earth System Sciences**, [*s. l.*], v. 21, n. 2, p. 923–947, 2017.

GLASER, Barbara *et al.* Intra-catchment variability of surface saturation - Insights from physically based simulations in comparison with biweekly thermal infrared image observations. **Hydrology and Earth System Sciences**, [*s. l.*], v. 24, n. 3, p. 1393–1413, 2020.

GLASER, Barbara *et al.* Sources of Surface Water in Space and Time: Identification of Delivery Processes and Geographical Sources With Hydraulic Mixing-Cell Modeling. **Water Resources Research**, [*s. l.*], v. 57, n. 12, 2021.

GNANN, Sebastian J. *et al.* Including Regional Knowledge Improves Baseflow Signature Predictions in Large Sample Hydrology. **Water Resources Research**, [*s. l.*], v. 57, n. 2, p. 1–22, 2021.

GODSEY, S; ELSENBEER, H; STALLARD, R. Overland flow generation in two lithologically distinct rainforest catchments. **Journal of Hydrology**, [*s. l.*], v. 295, n. 1–4, p. 276–290, 2004.

GODSEY, S. E.; KIRCHNER, J. W. Dynamic, discontinuous stream networks: Hydrologically driven variations in active drainage density, flowing channels and stream order. **Hydrological Processes**, [*s. l.*], v. 28, n. 23, p. 5791–5803, 2014.

GOTTSCHALK, Lars; WEINGARTNER, Rolf. Distribution of peak flow derived from a distribution of rainfall volume and runoff coefficient, and a unit hydrograph. **Journal of Hydrology**, [*s. l.*], v. 208, n. 3–4, p. 148–162, 1998.

GRANT, Gordon E.; DIETRICH, William E. The frontier beneath our feet. **Water Resources Research**, [*s. l.*], p. 1–5, 2017.

GRAY, Don M. Synthetic unit hydrographs for small watersheds. **Journal of the Hydraulics Division**, [*s. l.*], v. 4, p. 33–54, 1961.

GREGORY, K. J.; WALLING, K. J. The variation of drainage density within a catchment. **International Association of Scientific Hydrology. Bulletin**, [*s. l.*], v. 13, n. 2, p. 61–68, 1968.

GRIEVE, Stuart W.D. *et al.* Controls on Zero-Order Basin Morphology. **Journal of Geophysical Research: Earth Surface**, [*s. l.*], v. 123, n. 12, p. 3269–3291, 2018.

GRIMALDI, Salvatore *et al.* Flow time estimation with spatially variable hillslope velocity in ungauged basins. **Advances in Water Resources**, [*s. l.*], v. 33, n. 10, p. 1216–1223, 2010. Disponível em: http://dx.doi.org/10.1016/j.advwatres.2010.06.003.

GRIMALDI, S. *et al.* Time of concentration: a paradox in modern hydrology. **Hydrological Sciences Journal**, [*s. l.*], v. 57, n. March 2015, p. 217–228, 2012.

GRIMALDI, Salvatore; PETROSELLI, Andrea. Avons-nous encore besoin de la formule rationnelle ? Une méthode empirique alternative pour l'estimation du débit de pointe dans les petits bassins et les bassins non jaugés. **Hydrological Sciences Journal**, [*s. l.*], v. 60, n. 1, p. 67–77, 2014. Disponível em: http://dx.doi.org/10.1080/02626667.2014.880546.

GRIMALDI, S.; PETROSELLI, A.; NARDI, F. A parsimonious geomorphological unit hydrograph for rainfall-runoff modelling in small ungauged basins. **Hydrological Sciences Journal**, [*s. l.*], v. 57, n. 1, p. 73–83, 2012.

GUSWA, Andrew J. *et al.* Advancing ecohydrology in the 21st century: A convergence of opportunities. **Ecohydrology**, [*s. l.*], v. 13, n. 4, p. 1–14, 2020.

HAYASHI, Masaki. Alpine Hydrogeology: The Critical Role of Groundwater in Sourcing the Headwaters of the World. **Groundwater**, [*s. l.*], v. 58, n. 4, p. 498–510, 2020.

HAYHOE, Shelby J. *et al.* Conversion to soy on the Amazonian agricultural frontier increases streamflow without affecting stormflow dynamics. **Global Change Biology**, [*s. l.*], v. 17, n. 5, p. 1821–1833, 2011.

HENKLE, Jameson E.; WOHL, Ellen; BECKMAN, Natalie. Locations of channel heads in the semiarid Colorado Front Range, USA. **Geomorphology**, [*s. l.*], v. 129, n. 3–4, p. 309–319, 2011. Disponível em: http://dx.doi.org/10.1016/j.geomorph.2011.02.026.

HEWLETT, John D. Soil moisture as a source of base flow from steep mountain watersheds. **Dept. of Agriculture**, [*s. l.*], v. 132, p. 20, 1961.

HEWLETT, John D.; HIBBERT, Alden R. Moisture and energy conditions within a sloping soil mass during drainage. **Journal of Geophysical Research**, [*s. l.*], v. 68, n. 4, p. 1081–1087, 1963.

HOFER, Markus *et al.* Modelling subsurface drainage pathways in an artificial catchment. **Physics and Chemistry of the Earth**, [*s. l.*], v. 36, n. 1–4, p. 101–112, 2011.

HOOPER, Richard P.; CHRISTOPHERSEN, Nils; PETERS, Norman E. Modelling streamwater chemistry as a mixture of soilwater end-members - An application to the Panola Mountain catchment, Georgia, U.S.A. **Journal of Hydrology**, [*s. l.*], v. 116, n. 1–4, p. 321–343, 1990.

HOPP, L.; MCDONNELL, J. J. Connectivity at the hillslope scale: Identifying interactions between storm size, bedrock permeability, slope angle and soil depth. **Journal of Hydrology**, [*s. l.*], v. 376, n. 3–4, p. 378–391, 2009. Disponível em: http://dx.doi.org/10.1016/j.jhydrol.2009.07.047.

HORTON, Robert E. Drainage-basin characteristics. **Transactions, American Geophysical Union**, [*s. l.*], v. 13, n. 1, p. 350, 1932.

HORTON, Robert E. Erosional development of streams and their drainage basins; Hydrophysical approach to quantitative morphology. **Bulletin of the Geological Society of America**, [*s. l.*], v. 56, n. 3, p. 275–370, 1945.

HORTON, Robert E. The Role of infiltration in the hydrologic cycle. **Transactions, American Geophysical Union**, [*s. l.*], v. 14, n. 1, p. 446, 1933. Disponível em: http://doi.wiley.com/10.1029/TR014i001p00446.

HORTON, J. H.; HAWKINS, R. H. Flow path of rain from the soil surface to the water table. **Soil Science**, [*s. l.*], v. 100, n. 6, p. 377–383, 1965.

HRACHOWITZ, M *et al.* A decade of Predictions in Ungauged Basins (PUB)— a review. **Hydrological Sciences Journal – Journal des Sciences Hydrologiques**, [*s. l.*], v. 58, n. 6, p. 1198–1255, 2013.

HRACHOWITZ, Markus *et al.* Transit times - the link between hydrology and water quality at the catchment scale. **WIREs Water**, [*s. l.*], 2016.

HROMADKA, T. V. A unit hydrograph rainfall-runoff model using Mathematica. **Environmental Modelling and Software**, [*s. l.*], v. 15, n. 2, p. 151–160, 2000.

HUDSON, Roberto; FRASER, John. Alternative methods of flow rating in small coastal streams. **Forest Research**, [*s. l.*], v. 2, n. January, p. 1–6, 2002.

HURSH, C. R.; BRATER, E. F. Separating storm-hydrographs from small drainage-areas into surface- and subsurface-flow. **Transactions, American Geophysical Union**, [*s. l.*], v. 22, n. 3, p. 863, 1941. Disponível em: http://doi.wiley.com/10.1029/TR022i003p00863.

HWANG, Taehee *et al.* Ecosystem processes at the watershed scale: Hydrologic vegetation gradient as an indicator for lateral hydrologic connectivity of headwater catchments. **Water Resources Research**, [*s. l.*], v. 48, n. 6, p. 1–16, 2012.

IMBRIE, J; MCLNTYRE, A; MIX, A. **Climate and Geosciences**. [*S. l.: s. n.*], 1989.

IWASAKI, Kenta; NAGASAKA, Yu; NAGASAKA, Akiko. Geological Effects on the Scaling Relationships of Groundwater Contributions in Forested Watersheds. **Water Resources Research**, [*s. l.*], v. 57, n. 7, p. 1–20, 2021.

JAKEMAN, A.J.; LITTLEWOOD, I.G.; WHITEHEAD, P.G. Computation of the instantaneous unit hydrograph and identifiable component flows with application to two small upland catchments. **Journal of Hydrology**, [*s. l.*], v. 117, n. 1–4, p. 275–300, 1990. Disponível em: https://linkinghub.elsevier.com/retrieve/pii/002216949090097H.

JANUS, Tomasz *et al.* Multicriteria land cover design in multi-sector systems via coupled distributed land and water management models. **Journal of Hydrology**, [*s. l.*], v. 620, n. PB, p. 129294, 2023.

JENCSO, Kelsey G. *et al.* Hydrologic connectivity between landscapes and streams: Transferring reach- and plot-scale understanding to the catchment scale. **Water Resources Research**, [*s. l.*], v. 45, n. 4, 2009.

JENCSO, Kelsey G.; MCGLYNN, Brian L. Hierarchical controls on runoff generation: Topographically driven hydrologic connectivity, geology, and vegetation. **Water Resources Research**, [*s. l.*], v. 47, n. 11, 2011.

JOHSNTONE, D; CROSS, W. P. **Elements of applied hydrology**. First Edtied. New York: The Ronald Press Company: [*s. n.*], 1949.

KARLSEN, R. H. *et al.* The assumption of uniform specific discharge: unsafe at any time?. **Hydrological Processes**, [*s. l.*], v. 30, n. 21, p. 3978–3988, 2016.

KAULE, Robin; GILFEDDER, Benjamin S. Groundwater Dominates Water Fluxes in a Headwater Catchment During Drought. **Frontiers in Water**, [*s. l.*], v. 3, n. August, p. 1–14, 2021.

KERN, Zoltán *et al.* Isotopic "altitude" and "continental" effects in modern precipitation across the Adriatic-Pannonian region. **Water (Switzerland)**, [*s. l.*], v. 12, n. 6, 2020.

KIRCHNER, James W. A double paradox in catchment hydrology and geochemistry. **Hydrological Processes**, [*s. l.*], v. 17, n. 4, p. 871–874, 2003.

KIRKBY, M. J. Tests of the random network model, and its application to basin hydrology. **Earth Surface Processes and Landforms**, [*s. l.*], v. 1, n. 3, p. 197–212, 1976.

KIRKBY, MJ. Tests of the random network model, and its application to basin hydrology. **Earth Surface Processes**, [*s. l.*], v. 1, n. August 1975, p. 197–212, 1976. Disponível em: http://onlinelibrary.wiley.com/doi/10.1002/esp.3290010302/abstract.

KITE, Geoff. An extension to the salt dilution method of measuring streamflow. **International Journal of Water Resources Development**, [*s. l.*], v. 5, n. 1, p. 19–24, 1989.

KITE, Geoff. Computerized streamflow measurement using slug injection. **Hydrological Processes**, [*s. l.*], v. 7, n. 2, p. 227–233, 1993.

KLAUS, Julian; JACKSON, C. Rhett. Interflow Is Not Binary: A Continuous Shallow Perched Layer Does Not Imply Continuous Connectivity. **Water Resources Research**, [*s. l.*], v. 54, n. 9, p. 5921–5932, 2018.

KOLLET, Stefan J.; MAXWELL, Reed M. Capturing the influence of groundwater dynamics on land surface processes using an integrated, distributed watershed model. **Water Resources Research**, [*s. l.*], v. 44, n. 2, p. 1–18, 2008.

KONDOLF, G. Mathias; PIÉGAY, Hervé. **Tools in fluvial geomorphology**. Seconded. Oxford: Wiley, 2016. Disponível em: https://onlinelibrary.wiley.com/doi/book/10.1002/0470868333.

KUENTZ, Anna *et al.* Understanding hydrologic variability across Europe through catchment classification. **Hydrology and Earth System Sciences**, [*s. l.*], v. 21, n. 6, p. 2863–2879, 2017.

LAGARIAS, Jeffrey C. *et al.* Convergence Properties of the Nelder--Mead Simplex Method in Low Dimensions. **SIAM Journal on Optimization**, [*s. l.*], v. 9, n. 1, p. 112–147, 1998. Disponível em: http://epubs.siam.org/doi/10.1137/S1052623496303470.

LEE, Kwan Tun *et al.* A window-based inquiry system for design discharge based on geomorphic runoff modeling. **Computers and Geosciences**, [*s. l.*], v. 32, n. 2, p. 203–211, 2006.

LEOPOLD, L. B. Downstream change of velocity in rivers. **American Journal of Science**, [*s. l.*], v. 251, p. 606–624, 1953.

LEOPOLD, L. B.; MADDOCK, Thomas Jr. The Hydraulic Geometry of Stream Channels and Some Physiographic Implications. **Geological Survey Professional Paper 252**, [*s. l.*], p. 1–57, 1953.

LIANG, Wei Li; CHAN, Meng Chun. Spatial and temporal variations in the effects of soil depth and topographic wetness index of bedrock topography on subsurface saturation generation in a steep natural forested headwater catchment. **Journal of Hydrology**, [*s. l.*], v. 546, p. 405–418, 2017.

LITTLEWOOD, Ian G.; CROKE, Barry F. W. Data time-step dependency of conceptual rainfall—streamflow model parameters: an empirical study with implications for regionalisation. **Hydrological Sciences Journal**, [*s. l.*], v. 53, n. 4, p. 685–695, 2008. Disponível em: http://www.tandfonline.com/doi/abs/10.1623/hysj.53.4.685.

LLOYD, C.R; MARQUES, A.De O. Spatial variability of throughfall and stemflow measurements in Amazonian rainforest. **Agricultural and Forest Meteorology**, [*s. l.*], v. 42, n. 1, p. 63–73, 1988.

LOHSE, Kathleen A. *et al.* Interactions Between Biogeochemistry and Hydrologic Systems. **Annual Review of Environment and Resources**, [*s. l.*], v. 34, n. 1, p. 65–96, 2009.

LYNE, V.; HOLLICK, M. Stochastic Time-Variable Rainfall-Runoff Modelling. **Institute of Engineers Australia Perth**, [*s. l.*], p. 89–93, 1979.

LYON, Steve W. *et al.* Specific discharge variability in a boreal landscape. **Water Resources Research**, [*s. l.*], v. 48, n. 8, p. 1–13, 2012.

MACHADO, José Luiz Flores. **Mapa Hidrogeológico Do Estado De Santa Catarina**. [*S. l.: s. n.*], 2013.

MAXWELL, Reed M. Coupled Surface-Subsurface Modeling across a Range of Temporal and Spatial Scales. **Vadose Zone Journal**, [*s. l.*], v. 8, n. 4, p. 823–824, 2009. Disponível em: http://doi.wiley.com/10.2136/vzj2009.0117.

MAXWELL, Reed M *et al.* The imprint of climate and geology on the residence times of groundwater. **Geophysical Research Letters**, [*s. l.*], v. 43, n. 2, p. 701–708, 2016. Disponível em: https://onlinelibrary.wiley.com/doi/10.1002/2015GL066916.

MAXWELL, Reed M.; KOLLET, Stefan J. Quantifying the effects of three-dimensional subsurface heterogeneity on Hortonian runoff processes using a coupled numerical, stochastic approach. **Advances in Water Resources**, [*s. l.*], v. 31, n. 5, p. 807–817, 2008. Disponível em: https://linkinghub.elsevier.com/retrieve/pii/S0309170808000201.

MAXWELL, R. M.; MILLER, N. L. On the development of a coupled land surface and groundwater model. **Developments in Water Science**, [*s. l.*], v. 55, n. PART 2, p. 1503–1510, 2004.

MCCUEN, Richard H. Uncertainty Analyses of Watershed Time Parameters. **Journal of Hydraulic Engineering**, [*s. l.*], v. 14, n. 5, p. 490–498, 2009.

MCDONNELL, Jeffrey J. A Rationale for Old Water Discharge Through Macropores in a Steep, Humid Catchment. **Water Resources Research**, [*s. l.*], v. 26, n. 11, p. 2821–2832, 1990.

MCDONNELL, Jeffrey J. Are all runoff processes the same?. **Hydrological Processes**, [*s. l.*], v. 27, n. 26, p. 4103–4111, 2013.

MCDONNELL, Jeffrey J. Beyond the water balance. **Nature Geoscience**, [*s. l.*], v. 10, n. 6, p. 396, 2017.

MCDONNELL, Jeffrey J. *et al.* Fill-and-Spill: A Process Description of Runoff Generation at the Scale of the Beholder. **Water Resources Research**, [*s. l.*], v. 57, n. 5, p. 1–13, 2021.

MCDONNELL, Jeffrey J.; BEVEN, Keith. Debates-The future of hydrological sciences: A (common) path forward? A call to action aimed at understanding velocities, celerities and residence time distributions of the headwater hydrograph. **Water Resources Research**, [*s. l.*], v. 50, n. 6, p. 5342–5350, 2014. Disponível em: http://doi.wiley.com/10.1002/2013WR015141.

MCGUIRE, K. J. *et al.* The role of topography on catchment-scale water residence time. **Water Resources Research**, [*s. l.*], v. 41, n. 5, p. 1–14, 2005.

MCGUIRE, Kevin J.; MCDONNELL, Jeffrey J. A review and evaluation of catchment transit time modeling. **Journal of Hydrology**, [*s. l.*], v. 330, n. 3–4, p. 543–563, 2006.

MCMILLAN, Hilary *et al.* How uncertainty analysis of streamflow data can reduce costs and promote robust decisions in water management applications. **Water Resources Research**, [*s. l.*], v. 53, n. 7, p. 5220–5228, 2017.

MCMILLAN, Hilary *et al.* Impacts of uncertain river flow data on rainfall-runoff model calibration and discharge predictions. **Hydrological Processes**, [*s. l.*], v. 24, n. 10, p. 1270–1284, 2010.

MCMILLAN, Hilary; KRUEGER, Tobias; FREER, Jim. Benchmarking observational uncertainties for hydrology: Rainfall, river discharge and water quality. **Hydrological Processes**, [*s. l.*], v. 26, n. 26, p. 4078–4111, 2012.

MEERVELD, Ilja Tromp van; WEILER, Markus. Hillslope dynamics modeled with increasing complexity. **Journal of Hydrology**, [*s. l.*], v. 361, n. 1–2, p. 24–40, 2008.

MELO, Davi C.D. *et al.* The big picture of field hydrology studies in Brazil. **Hydrological Sciences Journal**, [*s. l.*], v. 65, n. 8, p. 1262–1280, 2020.

MERZ, Ralf; BLÖSCHL, Günter. A regional analysis of event runoff coefficients with respect to climate and catchment characteristics in Austria. **Water Resources Research**, [*s. l.*], v. 45, n. 1, p. 1–19, 2009.

MILLER, Matthew P. *et al.* The importance of base flow in sustaining surface water flow in the Upper Colorado River Basin. **Water Resources Research**, [*s. l.*], v. 52, n. 5, p. 3547–3562, 2016.

MILLER, O. M.; SUMMERSON, Charles H. Slope-Zone Maps. **Geographical Review**, [*s. l.*], v. 50, n. 2, p. 194, 1960.

MOCKUS, Victor. Use of storm and watershed characteristics in synthetic hydrograph analysis and application. **US Department of Agriculture, Soil Conservation Service, Latham, MD**, [*s. l.*], 1957.

MONTANARI, A. *et al.* "Panta Rhei-Everything Flows": Change in hydrology and society-The IAHS Scientific Decade 2013-2022. **Hydrological Sciences Journal**, [*s. l.*], v. 58, n. 6, p. 1256–1275, 2013.

MONTGOMERY, D R; BUFFINGTON, J M. Channel classification, prediction of channel response, and assessment of channel condition. **Washington State Department of Natural Resources Report**, [*s. l.*], n. TFW-SH10-93-002, p. 84, 1993.

MONTGOMERY, David R.; BUFFINGTON, John M. Channel-reach morphology in mountain drainage basins. **Bulletin of the Geological Society of America**, [*s. l.*], v. 109, n. 5, p. 596–611, 1997.

MONTGOMERY, D. R.; DIETRICH, W. E. Channel Initiation and the Problem of Landscape Scale. **Science**, [*s. l.*], v. 255, n. 5046, p. 826–830, 1992.

MONTGOMERY, D. R.; DIETRICH, W. E. Channel Initiation and the Problem of Landscape Scale. **Science**, [*s. l.*], v. 255, n. 5046, p. 826–830, 1992. Disponível em: https://www.sciencemag.org/lookup/doi/10.1126/science.255.5046.826.

MONTGOMERY, David R.; DIETRICH, William E. Source areas, drainage density, and channel initiation. **Water Resources Research**, [*s. l.*], v. 25, n. 8, p. 1907–1918, 1989.

MONTGOMERY, David R.; DIETRICH, William E. Where do channels begin?. **Nature**, [*s. l.*], v. 336, n. 6196, p. 232–234, 1988.

MORRICE, John A. *et al.* Alluvial characteristics, groundwater-surface water exchange and hydrological retention in headwater streams. **Hydrological Processes**, [*s. l.*], v. 11, n. 3, p. 253–267, 1997.

MOSLEY, M. Paul. Streamflow generation in a forested watershed, New Zealand. **Water Resources Research**, [*s. l.*], v. 15, n. 4, p. 795–806, 1979.

MOTA, Aline de Almeida *et al.* Instalação de uma pequena bacia experimental florestal: estudo de caso da bacia do Rio Araponga. **Engenharia Sanitaria e Ambiental**, [*s. l.*], v. 22, n. 1, p. 73–80, 2017.

MOUSSA, Roger. Effect of channel network topology, basin segmentation and rainfall spatial distribution on the geomorphologic instantaneous unit hydrograph transfer function. **Hydrological Processes**, [*s. l.*], v. 22, n. 3, p. 395–419, 2008. Disponível em: http://jamsb.austms.org.au/courses/CSC2408/semester3/resources/ldp/abs-guide.pdf.

MUELLER, Jerry E. An Introduction to the Hydraulic and Topographic Sinuosity Indexes. **Annals of the Association of American Geographers**, [*s. l.*], v. 58, n. 2, p. 371–385, 1968. Disponível em: http://www.tandfonline.com/doi/abs/10.1111/j.1467-8306.1968.tb00650.x.

MUÑOZ-VILLERS, Lyssette E. *et al.* Factors influencing stream baseflow transit times in tropical montane watersheds. **Hydrology and Earth System Sciences**, [*s. l.*], v. 20, n. 4, p. 1621–1635, 2016.

MUTZNER, Raphaël *et al.* Field study on drainage densities and rescaled width functions in a high-altitude alpine catchment. **Hydrological Processes**, [*s. l.*], v. 30, n. 13, p. 2138–2152, 2016.

NADARAJAH, Saralees. Probability models for unit hydrograph derivation. **Journal of Hydrology**, [*s. l.*], v. 344, n. 3–4, p. 185–189, 2007. Disponível em: http://linkinghub.elsevier.com/retrieve/pii/S0022169407004040.

NASH, J. E. Systematic determination of unit hydrograph parameters. **Journal of Geophysical Research**, [*s. l.*], v. 64, n. 1, p. 111, 1959.

NASH, J. E. The form of the instantaneous unit hydrograph. **International Association of Scientific Hydrology**, [*s. l.*], v. 3, p. 114–121, 1957.

NIPPGEN, Fabian *et al.* Landscape structure and climate influences on hydrologic response. **Water Resources Research**, [*s. l.*], v. 47, n. 12, 2011.

NRCS. Part 630 Hydrology National Engineering Handbook Chapter 16 Hydrographs. **Engineering**, [*s. l.*], 2007.

O'CALLAGHAN, Hohn F; MARK, David M. The extraction of ordered vector drainage networks from elevation data. **Computer Vision, Graphics and Image Processing**, [*s. l.*], v. 47, n. 1, p. 45–58, 1989.

OLIVEIRA, Orlando Martini de; BIM, Rodrigo; ESPINDOLA, Murilo da Silva. Aspectos geotécnicos do escorregamento de encosta da rodovia SC-401/florianópolis. **Congr Bras Mecânica dos Solos e Eng Geotécnica**, [*s. l.*], 2012.

OXTOBEEM, Jaime P. A.; NOVAKOWSKI, Kent S. Ground water surface water interaction in a fractured rock aquifer. [*s. l.*], p. 1–23, 2003. Disponível em: http://jamsb.austms.org.au/courses/CSC2408/semester3/resources/ldp/abs-guide.pdf.

PALUCIS, M. C.; LAMB, M. P. What controls channel form in steep mountain streams?. **Geophysical Research Letters**, [*s. l.*], v. 44, n. 14, p. 7245–7255, 2017.

PAN, Tsung Y.; WANG, Ru Y. State space neural networks for short term rainfall-runoff forecasting. **Journal of Hydrology**, [*s. l.*], v. 297, n. 1–4, p. 34–50, 2004.

PEARCE, A. J.; STEWART, M. K.; SKLASH, M. G. Storm Runoff Generation in Humid Headwater Catchments: 1. Where Does the Water Come From?. **Water Resources Research**, [*s. l.*], v. 22, n. 8, p. 1263–1272, 1986.

PECAPEDRA, Luana Lenzi; OLIVEIRA, O M. Aplicação do modelo proposto por Khalili Khabbaz (1998) na previsão da resistência ao cisalhamento em função da sucção de solos tropicais do Brasil. *In*: , 2016. **XVIII Congresso Brasileiro de Mecânica dos Solos e Engenharia Geotécnica**. [*S. l.: s. n.*], 2016.

PEDROSO, Andreia; MANNICH, Michael. The uncertainties of synthetic unit hydrographs applied for basins with different runoff generation processes. **RBRH**, [*s. l.*], v. 26, 2021.

PERALTA-TAPIA, Andrés *et al.* Scale-dependent groundwater contributions influence patterns of winter baseflow stream chemistry in boreal catchments. **Journal of Geophysical Research: Biogeosciences**, [*s. l.*], v. 120, n. 5, p. 847–858, 2015.

PEREZ, A.B.A. *et al.* Connectivity of ephemeral and intermittent streams in a subtropical atlantic forest headwater catchment. **Water (Switzerland)**, [*s. l.*], v. 12, n. 6, 2020.

PEREZ, Alondra B A. **Densidade de drenagem e conectividade hidrológica em uma bacia de cabeceira na Lagoa do Peri**. 2019. 1–108 f. - Federal University of Santa Catarina, Florianópolis, 2019.

PFISTER, Laurent *et al.* Bedrock geology controls on catchment storage, mixing, and release: A comparative analysis of 16 nested catchments. **Hydrological Processes**, [*s. l.*], v. 31, n. 10, p. 1828–1845, 2017.

POURTAGHI, Zohre Sadat; POURGHASEMI, Hamid Reza. GIS-based groundwater spring potential assessment and mapping in the Birjand Township, southern Khorasan Province, Iran. **Hydrogeology Journal**, [*s. l.*], v. 22, n. 3, p. 643–662, 2014.

PRADHAN, Nawa Raj; OGDEN, Fred L. Development of a one-parameter variable source area runoff model for ungauged basins. **Advances in Water Resources**, [*s. l.*], v. 33, n. 5, p. 572–584, 2010.

PREFEITURA DE FLORIANÓPOLIS. **Mapa de uso e ocupação do solo**. [*S. l.*], [*s. d.*]. Disponível em: http://geo.pmf.sc.gov.br/. Acesso em: 18 dez. 2018.

PRICE, Roland K. An optimized routing model for flood forecasting. **Water Resources Research**, [*s. l.*], v. 45, n. 2, p. 1–15, 2009.

RAZAVI, Tara; COULIBALY, Paulin. Streamflow Prediction in Ungauged Basins: Review of Regionalization Methods. **Journal of Hydrologic Engineering**, [*s. l.*], v. 18, n. 8, p. 958–975, 2013.

RIGON, Riccardo *et al.* The geomorphological unit hydrograph from a historical-critical perspective. **Earth Surface Processes and Landforms**, [*s. l.*], v. 41, n. 1, p. 27–37, 2016.

RINALDO, Andrea; MARANI, Alessandro; RIGON, Riccardo. Geomorphological dispersion. **Water Resources Research**, [*s. l.*], v. 27, n. 4, p. 513–525, 1991.

ROBERTS, Michael C.; ARCHIBOLD, O. W. VARIATION OF DRAINAGE DENSITY IN A SMALL BRITISH COLUMBIA WATERSHED. **Journal of the American Water Resources Association**, [*s. l.*], v. 14, n. 2, p. 470–476, 1978.

RODRIGUEZ, Fabrice; ANDRIEU, Hervé; CREUTIN, Jean Dominique. Surface runoff in urban catchments: Morphological identification of unit hydrographs from urban databanks. **Journal of Hydrology**, [*s. l.*], v. 283, n. 1–4, p. 146–168, 2003.

RODRIGUEZ, Nicolas B.; BENETTIN, Paolo; KLAUS, Julian. Multimodal water age distributions and the challenge of complex hydrological landscapes. **Hydrological Processes**, [*s. l.*], v. 34, n. 12, p. 2707–2724, 2020.

RODRIGUEZ, Nicolas B.; KLAUS, Julian. Catchment Travel Times From Composite StorAge Selection Functions Representing the Superposition of Streamflow Generation Processes. **Water Resources Research**, [*s. l.*], v. 55, n. 11, p. 9292–9314, 2019.

RODRÍGUEZ-ITURBE, Ignacio; GONZÁLEZ-SANABRIA, Marcelo; BRAS, Rafael L. A geomorphoclimatic theory of the instantaneous unit hydrograph. **Water Resources Research**, [*s. l.*], v. 18, n. 4, p. 877–886, 1982. Disponível em: http://doi.wiley.com/10.1029/WR018i004p00877.

RODRÍGUEZ-ITURBE, Ignacio; VALDÉS, Juan B. The geomorphologic structure of hydrologic response. **Water Resources Research**, [*s. l.*], v. 15, n. 6, p. 1409–1420, 1979. Disponível em: http://doi.wiley.com/10.1029/WR015i006p01409.

ROSSO, Renzo. Nash Model Relation to Horton Order Ratios. **Water Resources Research**, [*s. l.*], v. 20, n. 7, p. 914–920, 1984. Disponível em: http://doi.wiley.com/10.1029/WR020i007p00914.

ROWLAND, Richard; INAMDAR, Shreeram; PARR, Thomas. Evolution of particulate organic matter (POM) along a headwater drainage: role of sources, particle size class, and storm magnitude. **Biogeochemistry**, [*s. l.*], v. 133, n. 2, p. 181–200, 2017.

SÁ, João H.M. **A Influência da vegetação no processo de interceptação da chuva em floresta de mata Atlântica**. [*S. l.: s. n.*], 2019.

SACKS, Laura A.; LEE, Terrie M.; SWANCAR, Amy. The suitability of a simplified isotope-balance approach to quantify transient groundwater-lake interactions over a decade with climatic extremes. **Journal of Hydrology**, [*s. l.*], v. 519, n. PD, p. 3042–3053, 2014.

SAFFARPOUR, Shabnam *et al.* Multiple runoff processes and multiple thresholds control agricultural runoff generation. **Hydrology and Earth System Sciences**, [*s. l.*], v. 20, n. 11, p. 4525–4545, 2016.

SALUM, Bernardo Raimundo. Levantamento dos condicionantes geológicos e geotécnicos de um talude rodoviário afetado por um deslizamento no bairro Saco Grande. [*s. l.*], 2019.

SANTOS, I. D. *et al.* **Hidrometria aplicada**. Curitiba: Instituto de Tecnologia para o desenvolvimento: [*s. n.*], 2001.

SANTOS, Gilberto F Dos; SILVA, Jose T N. Análise Ambiental da Lagoa do Peri. **Geosul**, [*s. l.*], p. 101–123, 1989.

SARAVANAN, S.; MANJULA, R. Geomorphology Based Semi-distributed Approach for Modeling Rainfall-runoff Modeling Using GIS. **Aquatic Procedia**, [*s. l.*], v. 4, n. Icwrcoe, p. 908–916, 2015.

SAYAMA, Takahiro *et al.* How much water can a watershed store?. **Hydrological Processes**, [*s. l.*], v. 25, n. 25, p. 3899–3908, 2011.

SAYAMA, Takahiro; MCDONNELL, Jeffrey J. A new time-space accounting scheme to predict stream water residence time and hydrograph source components at the watershed scale. **Water Resources Research**, [*s. l.*], v. 45, n. 7, p. 1–14, 2009.

SBROGLIA, Regiane Mara; BELTRAME, Ângela Da Veiga. O zoneamento, conflitos e recategorização do parque municipal da lagoa do Peri, Florianópolis/SC. **Boletim de Geografia**, [*s. l.*], v. 30, n. 1, p. 5–18, 2012. Disponível em: http://www.periodicos.uem.br/ojs/index.php/BolGeogr/article/view/11542.

SCHNEIDER, V. R.; SMOOT, G. F. Development of a standard rating for the Price Pygmy current meter: U.S. Geological. **Survey Journal of Research**, [*s. l.*], v. 4, n. 3, p. 293–297, 1976.

SCHUMM, S.A. Evolution of drainage systems and slopes in badlands at parth amboy, New Jersey. **Bulletin of the Geological Society of America**, [*s. l.*], v. 67, p. 507–648, 1956.

SECRETARY OF STATE FOR THE ECONOMIC AND SUSTAINABLE DEVELOPMENT (SDS). **Levantamento Aerofotogramétrico do Estado de Santa Catarina**. Florianópolis: ENGEMAP, 2013.

SEGURA, Catalina *et al.* Climate, Landforms, and Geology Affect Baseflow Sources in a Mountain Catchment. **Water Resources Research**, [*s. l.*], v. 55, n. 7, p. 5238–5254, 2019.

SENGER, Kim *et al.* Fracturing of doleritic intrusions and associated contact zones: Implications for fluid flow in volcanic basins. **Journal of African Earth Sciences**, [*s. l.*], v. 102, p. 70–85, 2015.

SEO, Y.; PARK, S.-Y. Prediction of direct runoff hydrographs utilizing stochastic network models: a case study in South Korea. **Hydrology and Earth System Sciences Discussions**, [*s. l.*], v. 11, n. 10, p. 11247–11279, 2014.

SHEN, Xinyi *et al.* GDBC: A tool for generating global-scale distributed basin morphometry. **Environmental Modelling & Software**, [*s. l.*], v. 83, p. 212–223, 2016.

SHERMAN, L. K. Streamflow from rainfall by the unit-graph method. **Eng. News Record**, [*s. l.*], v. 108, p. 501–505, 1932.

SIDLE, Roy C. Field observations and process understanding in hydrology: Essential components in scaling. **Hydrological Processes**, [*s. l.*], v. 20, n. 6, p. 1439–1445, 2006.

SIDLE, Roy C. *et al.* Stormflow generation in steep forested headwaters: A linked hydrogeomorphic paradigm. **Hydrological Processes**, [*s. l.*], v. 14, n. 3, p. 369–385, 2000.

SILVA, Ricardo Souza Rosa. Retroanálise de um Deslizamento de Talude Ocorrido no Morro da Praia Mole/SC-406. [*s. l.*], 2019.

SILVEIRA, André. Fator de Pico para Hidrogramas Unitários Sintéticos Triangulares. **Revista Brasileira de Recursos Hídricos**, [*s. l.*], v. 21, n. 1, p. 46–52, 2016. Disponível em: http://www.abrh.org.br/SGCv3/index.php?PUB=1&ID=188&SUMARIO=5146.

SINGH, Krishan Piara. Nonlinear instantaneous unit-hydrograph theory. **Journal of the Hydraulics Division**, [*s. l.*], v. 90, p. 313–350, 1964.

SINGH, Sushil K. Transmuting Synthetic Unit Hydrographs into Gamma Distribution. **Journal of Hydrologic Engineering**, [*s. l.*], v. 5, n. 4, p. 380–385, 2000. Disponível em: http://ascelibrary.org/doi/10.1061/%28ASCE%291084-0699%282000%295%3A4%28380%29.

SINGH, Vijay P.; CUI, Huijuan; BYRD, Aaron. Sediment Graphs Based on Entropy Theory. **Journal of Hydrologic Engineering**, [*s. l.*], v. 20, n. 6, p. C4014004, 2015.

SINGH, Nitin K.; EMANUEL, Ryan E.; MCGLYNN, Brian L. Variability in isotopic composition of base flow in two headwater streams of the southern Appalachians. **Water Resources Research**, [*s. l.*], v. 52, n. 6, p. 4264–4279, 2016.

SINGH, P.K.; MISHRA, S.K.; JAIN, M.K. A review of the synthetic unit hydrograph: from the empirical UH to advanced geomorphological methods. **Hydrological Sciences Journal**, [*s. l.*], v. 59, n. 2, p. 239–261, 2014. Disponível em: http://www.tandfonline.com/doi/abs/10.1080/02626667.2013.870664.

SIQUEIRA, Vinícius Alencar *et al.* Real-time updating of HEC-RAS model for streamflow forecasting using an optimization algorithm. **RBRH**, [*s. l.*], v. 21, n. 4, p. 855–870, 2016.

SKLASH, Michael G.; FARVOLDEN, Robert N. The role of groundwater in storm runoff. **Journal of Hydrology**, [*s. l.*], v. 43, n. 1–4, p. 45–65, 1979.

SKRZYPEK, Grzegorz *et al.* Estimation of evaporative loss based on the stable isotope composition of water using Hydrocalculator. **Journal of Hydrology**, [*s. l.*], v. 523, p. 781–789, 2015.

SMOOT, G. F.; CARTER, R. W. Are individual current meter ratings necessary?. **American Society of Civil Engineers Journal of the Hydraulics Division**, [*s. l.*], v. 94, p. 391–397, 1968.

SNYDER, Franklin F. Synthetic unit-graphs. **Transactions, American Geophysical Union**, [*s. l.*], v. 19, n. 1, p. 447, 1938. Disponível em: http://www.agu.org/pubs/crossref/1938/TR019i001p00447.shtml.

SOKOLOV, Sergei. Approximate technique for calculation the celerity of long wave in channels with complex cross section. **SN Applied Sciences**, [*s. l.*], v. 2, n. 2, p. 1–8, 2020. Disponível em: https://doi.org/10.1007/s42452-020-2018-7.

STAN, John T Van. **Precipitation Partitioning by Vegetation**. [*S. l.: s. n.*], 2020.

STAUDINGER, M.; WEILER, M.; SEIBERT, J. Quantifying sensitivity to droughts-an experimental modeling approach. **Hydrology and Earth System Sciences**, [*s. l.*], v. 19, n. 3, p. 1371–1384, 2015.

STEINMETZ, Alice Alonzo *et al.* Spatial discretization influence on flood modeling using unit hydrograph theory. **RBRH**, [*s. l.*], v. 24, 2019.

STRAHLER, Arthur N. Dynamic basis of geomorphology. **Bulletin of the Geological Society of America**, [*s. l.*], v. 63, n. 9, p. 923–938, 1952.

STUMPP, C. *et al.* Hydrological dynamics of water sources in a Mediterranean lagoon. **Hydrology and Earth System Sciences**, [*s. l.*], v. 18, n. 12, p. 4825–4837, 2014.

SUTANTO, Samuel Jonson; VAN LANEN, Henny A J. Catchment memory explains hydrological drought forecast performance. **Scientific reports**, [*s. l.*], v. 12, n. 1, p. 2689, 2022.

TAGUE, Christina; GRANT, Gordon E. A geological framework for interpreting the low-flow regimes of Cascade streams, Willamette River Basin, Oregon. **Water Resources Research**, [*s. l.*], v. 40, n. 4, p. 1–9, 2004.

TAURO, Flavia *et al.* Measurements and observations in the XXI century (MOXXI): Innovation and multi-disciplinarity to sense the hydrological cycle. **Hydrological Sciences Journal**, [*s. l.*], v. 63, n. 2, p. 169–196, 2018. Disponível em: https://doi.org/10.1080/02626667.2017.1420191.

TAYLOR, Arnold B.; SCHWARZ, Harry E. Unit-hydrograph lag and peak flow related to basin characteristics. **Transactions, American Geophysical Union**, [*s. l.*], v. 33, n. 2, p. 235, 1952. Disponível em: http://www.agu.org/pubs/crossref/1952/TR033i002p00235.shtml.

TETZLAFF, Doerthe *et al.* The essential value of long-term experimental data for hydrology and water management. **Water Resources Research**, [*s. l.*], p. 1–7, 2017.

TETZLAFF, Doerthe *et al.* Tracer-based assessment of flow paths, storage and runoff generation in northern catchments: A review. **Hydrological Processes**, [*s. l.*], v. 29, n. 16, p. 3475–3490, 2015.

TETZLAFF, D.; SOULSBY, C. Sources of baseflow in larger catchments - Using tracers to develop a holistic understanding of runoff generation. **Journal of Hydrology**, [*s. l.*],

v. 359, n. 3–4, p. 287–302, 2008. Disponível em: http://dx.doi.org/10.1016/j.jhydrol.2008.07.008.

THIROS, Nicholas E. *et al.* Constraining Bedrock Groundwater Residence Times in a Mountain System With Environmental Tracer Observations and Bayesian Uncertainty Quantification. **Water Resources Research**, [*s. l.*], v. 59, n. 2, 2023.

TODESCHINI, S.; PAPIRI, S.; CIAPONI, C. Stormwater quality control for sustainable urban drainage systems. **International Journal of Sustainable Development and Planning**, [*s. l.*], v. 9, n. 2, p. 196–210, 2014. Disponível em: http://www.witpress.com/doi/journals/SDP-V9-N2-196-210.

TODINI, E. Rainfall-runoff modeling - Past, present and future. **Journal of Hydrology**, [*s. l.*], v. 100, n. 1–3, p. 341–352, 1988.

TRIPTI, M. *et al.* Evidence of elevation effect on stable isotopes of water along highlands of a humid tropical mountain belt (Western Ghats, India) experiencing monsoonal climate. **Journal of Hydrology**, [*s. l.*], v. 573, n. December 2018, p. 469–485, 2019.

TROMP-VAN MEERVELD, H. J.; MCDONNELL, J. J. Threshold relations in subsurface stormflow: 2. The fill and spill hypothesis. **Water Resources Research**, [*s. l.*], v. 42, n. 2, 2006. Disponível em: http://doi.wiley.com/10.1029/2004WR003800.

TUREKIAN, Karl K. Marine geochemistry. *In*: STABLE ISOTOPES. [*S. l.: s. n.*], 2016. v. 52, p. IUGG237–IUGG244.

UCHIDA, Taro *et al.* Are headwaters just the sum of hillslopes? **Hydrological Processes**, [*s. l.*], v. 19, n. 16, p. 3251–3261, 2005.

UCHIDA, Taro; ASANO, Yuko. Spatial variability in the flowpath of hillslope runoff and streamflow in a meso-scale catchment. **Hydrological Processes**, [*s. l.*], v. 24, n. 16, p. 2277–2286, 2010. Disponível em: https://onlinelibrary.wiley.com/doi/10.1002/hyp.7767.

UFSC - UNIVERSIDADE FEDERAL DE SANTA CATARINA. **Mapa Geológico da Ilha de Santa Catarina**. Florianópolis: [*s. n.*], 2018. Disponível em: http://lmo.ufsc.br/mapa-geologico-da-ilha-de-santa-catarina/. Acesso em: 18 dez. 2018.

UNFRIED, Kerstin; KIS-KATOS, Krisztina; POSER, Tilman. Water scarcity and social conflict. **Journal of Environmental Economics and Management**, [*s. l.*], v. 113, n. March 2021, p. 102633, 2022.

UNIVERSIDADE FEDERAL DE SANTA CATARINA. **Mapa Geológico da Ilha de Santa Catarina**. Florianópolis: [*s. n.*], 2018.

USDA-NRCS. National Engineering Handbook Chapter 15, Time of Concentration. [*s. l.*], p. 1–15, 2010.

VAN LOON, A. F.; VAN HUIJGEVOORT, M. H.J.; VAN LANEN, H. A.J. Evaluation of drought propagation in an ensemble mean of large-scale hydrological models. **Hydrology and Earth System Sciences**, [*s. l.*], v. 16, n. 11, p. 4057–4078, 2012.

VAN MEERVELD, H. J. Ilja *et al.* Expansion and contraction of the flowing stream network changes hillslope flowpath lengths and the shape of the travel time distribution. **Hydrology and Earth System Sciences Discussions**, [*s. l.*], v. 2006, n. May, p. 1–18, 2019.

VOLPI, E. *et al.* Reservoir Effects on Flood Peak Discharge at the Catchment Scale. **Water Resources Research**, [*s. l.*], v. 54, n. 11, p. 9623–9636, 2018.

WALTHER, Bruno A; MOORE, Joslin L. The concepts of bias, precision and accuracy, and their use in testing the performance of species richness estimators, with a literature review of estimator performance. **Ecography**, [*s. l.*], v. 28, n. 6, p. 815–829, 2005.

WEILER, Markus; MCDONNELL, Jeff. Virtual experiments: A new approach for improving process conceptualization in hillslope hydrology. **Journal of Hydrology**, [*s. l.*], v. 285, n. 1–4, p. 3–18, 2004.

WELGUS, Marcja N.; ABIYE, Tamiru A. Surface water and groundwater interaction in the Vredefort Dome, South Africa: a stable isotope and multivariate statistical approach. **Environmental Monitoring and Assessment**, [*s. l.*], v. 194, n. 10, 2022. Disponível em: https://doi.org/10.1007/s10661-022-10164-y.

WEST, Mark J. Stereological methods for estimating the total number of neurons and synapses: issues of precision and bias. **Trends in Neurosciences**, [*s. l.*], v. 22, n. 2, p. 51–61, 1999.

WHITE, Amanda B. *et al.* Hydrodynamic and geomorphologic dispersion: Scale effects in the Illinois River Basin. **Journal of Hydrology**, [*s. l.*], v. 288, n. 3–4, p. 237–257, 2004.

WHITE, Timothy *et al.* **The Role of Critical Zone Observatories in Critical Zone Science**. [*S. l.*]: Elsevier B.V., 2015-. ISSN 09282025.v. 19

WHITING, John A.; GODSEY, Sarah E. Discontinuous headwater stream networks with stable flowheads, Salmon River basin, Idaho. **Hydrological Processes**, [*s. l.*], v. 30, n. 13, p. 2305–2316, 2016.

WILCOX, Andrew C. *et al.* Hydraulics, morphology, and energy dissipation in an alpine step-pool channel. **Water Resources Research**, [*s. l.*], v. 47, n. 7, p. 1–17, 2011.

WINTER, Thomas C. Relation of streams, lakes, and wetlands to groundwater flow systems. **Hydrogeology Journal**, [*s. l.*], v. 7, n. 1, p. 28–45, 1999.

WINTER, Thomas C.; ROSENBERRY, Donald O.; LABAUGH, James W. Where Does the Ground Water in Small Watersheds Come From?. **GroundWater**, [*s. l.*], v. 41, n. 7, p. 989–1000, 2003.

WOHL, Ellen *et al.* The hydrology of the humid tropics. **Nature Climate Change**, [*s. l.*], v. 2, n. 9, p. 655–662, 2012. Disponível em: http://www.nature.com/doifinder/10.1038/nclimate1556.

WOLFE, Brent B. *et al.* Carbon and Oxygen Isotope Analysis of Lake Sediment Cellulose: Methods and Applications. *In*: TRACKING ENVIRONMENTAL CHANGE USING LAKE SEDIMENTS. Dordrecht: Kluwer Academic Publishers, 1997. p. 373–400.

WOLOCK, David M. Effects of Subbasin Size on Topographic Characteristics and Simulated Flow Paths in Sleepers River Watershed, Vermont. **Water Resources Research**, [*s. l.*], v. 31, n. 8, p. 1989–1997, 1995.

WONDZELL, Steven M.; GOOSEFF, Michael N.; MCGLYNN, Brian L. Flow velocity and the hydrologic behavior of streams during baseflow. **Geophysical Research Letters**, [*s. l.*], v. 34, n. 24, p. 1–5, 2007.

WOOD, Eric F. *et al.* Effects of spatial variability and scale with implications to hydrologic modeling. **Journal of Hydrology**, [*s. l.*], v. 102, n. 1–4, p. 29–47, 1988.

WOODS, Ross A.; SIVAPALAN, Murugesu. A connection between topographically driven runoff generation and channel network structure. **Water Resources Research**, [*s. l.*], v. 33, n. 12, p. 2939, 1997.

WOODS, Ross; SIVAPALAN, Murugesu; DUNCAN, Maurice. Investigating the representative elementary area concept: An approach based on field data. **Hydrological Processes**, [*s. l.*], v. 9, n. 3–4, p. 291–312, 1995. Disponível em: http://doi.wiley.com/10.1002/hyp.3360090306.

YANG, Dawen; HERATH, Srikantha; MUSIAKE, Katumi. Development of a geomorphology-based hydrological model for large catchments. **PROCEEDINGS OF HYDRAULIC ENGINEERING**, [*s. l.*], v. 42, p. 169–174, 1998. Disponível em: http://joi.jlc.jst.go.jp/JST.Journalarchive/prohe1990/42.169?from=CrossRef.

YAO, Cheng *et al.* Improving the flood prediction capability of the Xinanjiang model in ungauged nested catchments by coupling it with the geomorphologic instantaneous unit hydrograph. **Journal of Hydrology**, [*s. l.*], v. 517, p. 1035–1048, 2014.

YOO, Chulsang *et al.* Method for Estimating Concentration Time and Storage Coefficient of the Clark Model Using Rainfall-Runoff Measurements. **Journal of Hydrologic Engineering**, [*s. l.*], v. 19, n. 3, p. 626–634, 2014.

ZIMMER, Margaret A.; GANNON, John P. Run-off processes from mountains to foothills: The role of soil stratigraphy and structure in influencing run-off characteristics across high to low relief landscapes. **Hydrological Processes**, [*s. l.*], v. 32, n. 11, p. 1546–1560, 2018.

ZOCH, Richmond. On the relation between Rainfall and Stream Flow. **Monthly weather review**, [*s. l.*], v. 96, n. 3, 1934.

APPENDIX A - DATASET

The database is available at the following address: https://drive.google.com/drive/folders/1Sk2yQotiWL5wHyDVYbcpr8VXUikzmJ1C?usp=sharing and is divided into nine directories described below:

1) Dados_horarios: Contains hourly hydrological variable data from Peri Lake Experimental Catchment from December 2015 to August 2020. The variables presented include temperature, humidity, radiation, pressure, precipitation, and the water levels of Ribeirão Grande and Peri Lake.

2) Curva_chave: Contains discharge and velocity measurements made at the outlet of the Ribeirão Grande Catchment used to estimate the rating curve. These measurements occurred between March 14, 2017, and October 4, 2018.

3) Nascentes_e_hidrografia: Contains data from springs monitored in the field, and the algorithm for drainage generation using the methodology proposed in APPEDIX D. It also contains shapefiles of different drainage networks and monitored springs.

4) SIG_Bruto: Contains the shapes of the Peri Lake Experimental Catchment from various sources, as well as the places of automatic monitoring.

5) Caracteristicas_da_Paisagem: Contains the algorithm and the output of this algorithm for calculating the physical characteristics of the sub-catchments of the Peri Lake Experimental Catchment.

6) Parametros_quimicos: Contains information on chemical parameters monitored during the baseflow of wells, the lagoon, and rivers. It also includes data on precipitation, throughfall, and stemflow.

7) Vazao_velocidade: Contains data on flow and velocity monitored during the baseflow.

8) Modelos_Hidrologicos_BHRG: Contains the algorithms of the hydrological models: HU and Tank Model, calibrated for the data series of the Ribeirão Grande Catchment.

9) Evapotranspiração: Contains the algorithms of the calibrated models of Penman-Monteith and Priestley-Taylor for potential evapotranspiration of slopes and lake evaporation in the watershed of Lagoa do Peri. It also includes the Hydrocalculator tool to estimate lake evaporation from isotopes.

APPENDIX B – PHYSICAL PARAMETERS OF THE CATCHMENTS

This appendix presents the products of the algorithm found in the database (Appendix A). In Figure 1B, the characteristics of each watershed were calculated, delineated from all the drainage points.

FigureB 1 – Physical characteristics analyzed of the catchments. Where: A is area, P is perimeter, O is order, L_{MS} is length of the main stream, L_w is length of the catchment, S_{MS} is slope of the main stream, R_C is circularity ratio, C_C is compactness coefficient, R_B is relief of the basin, F_F is shape factor, Dd is drainage density, H_M is median altitude, Si_{MS} is sinuosity of the main river, TWI is average topographic index, Flor Atlân is Atlantic forest.
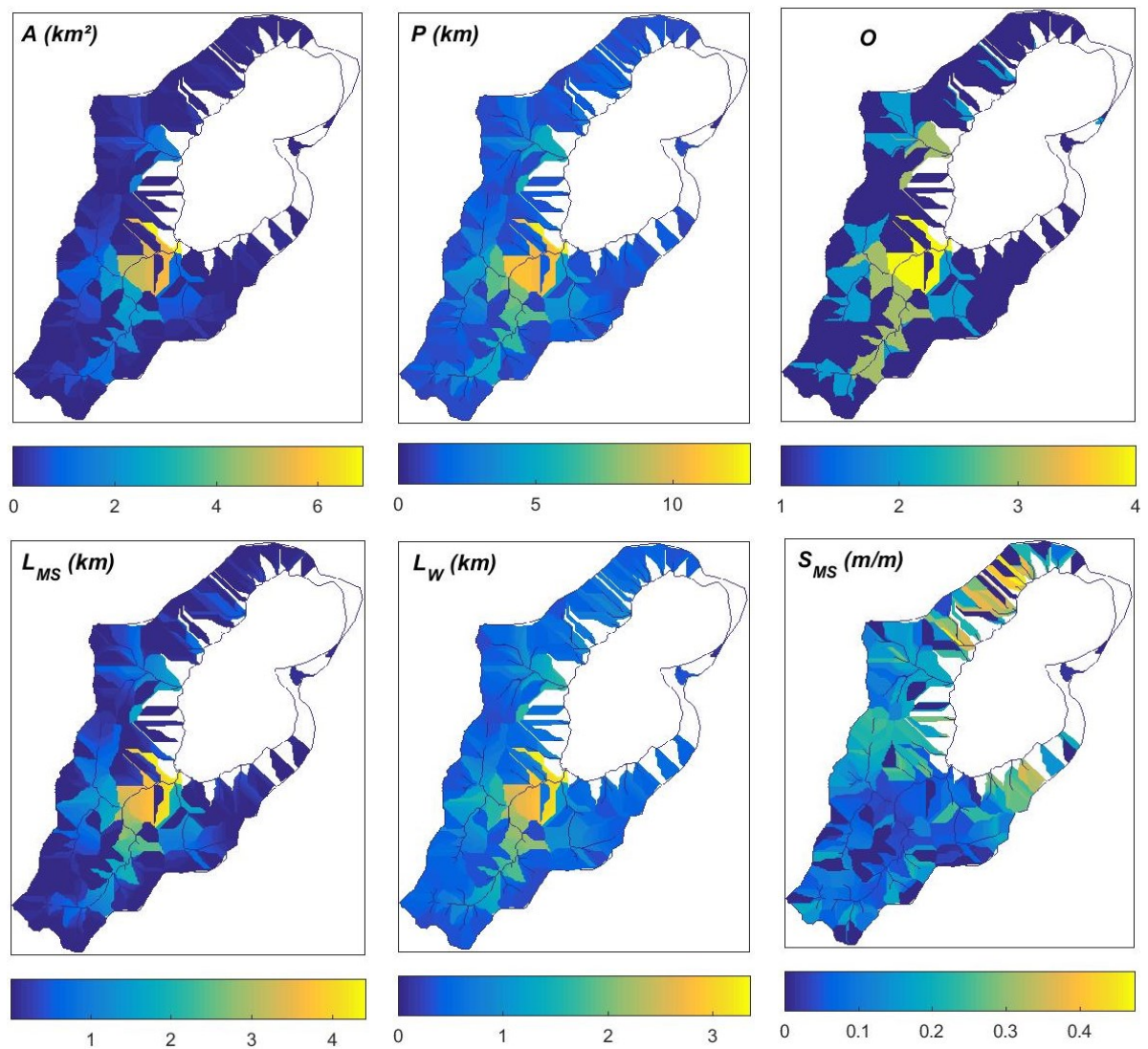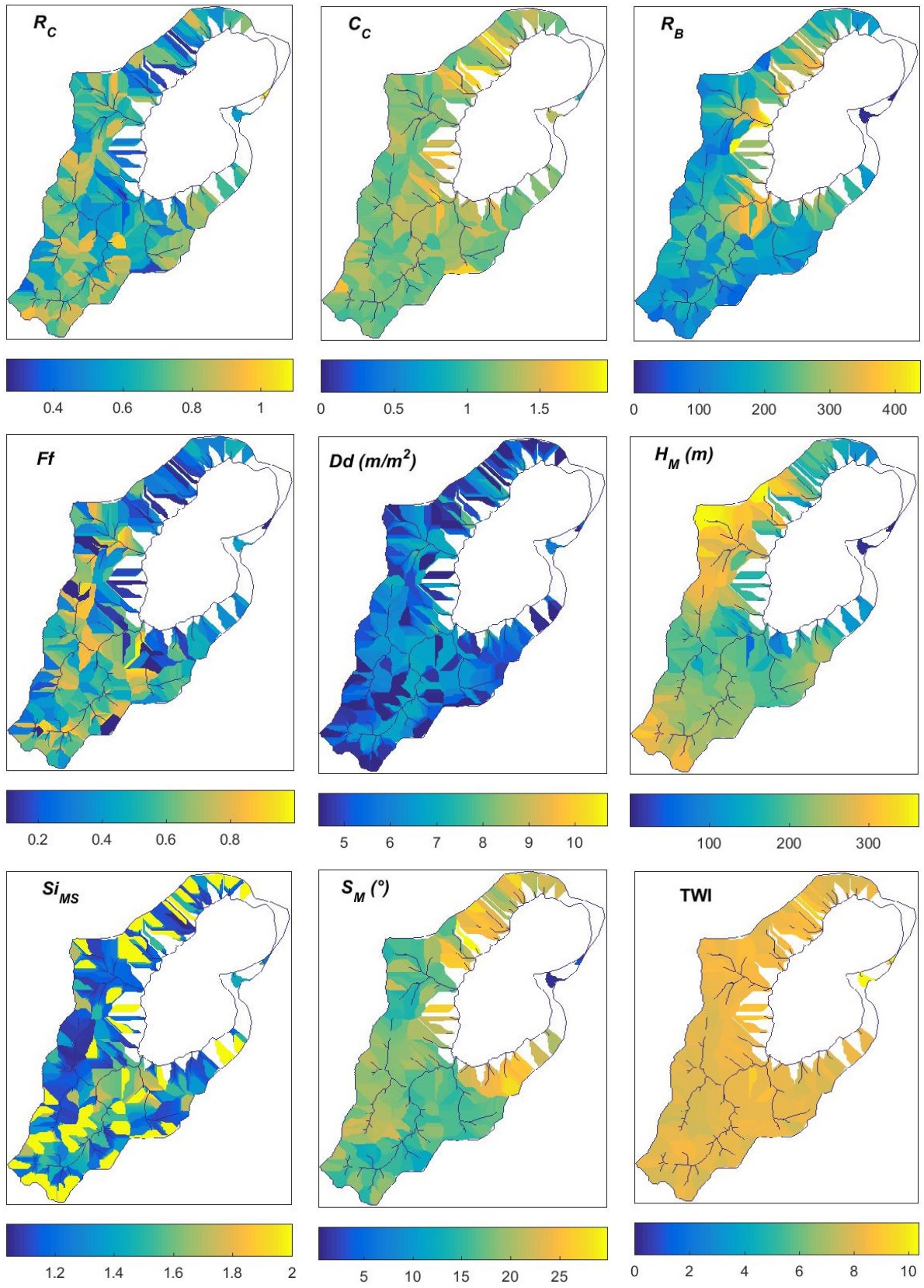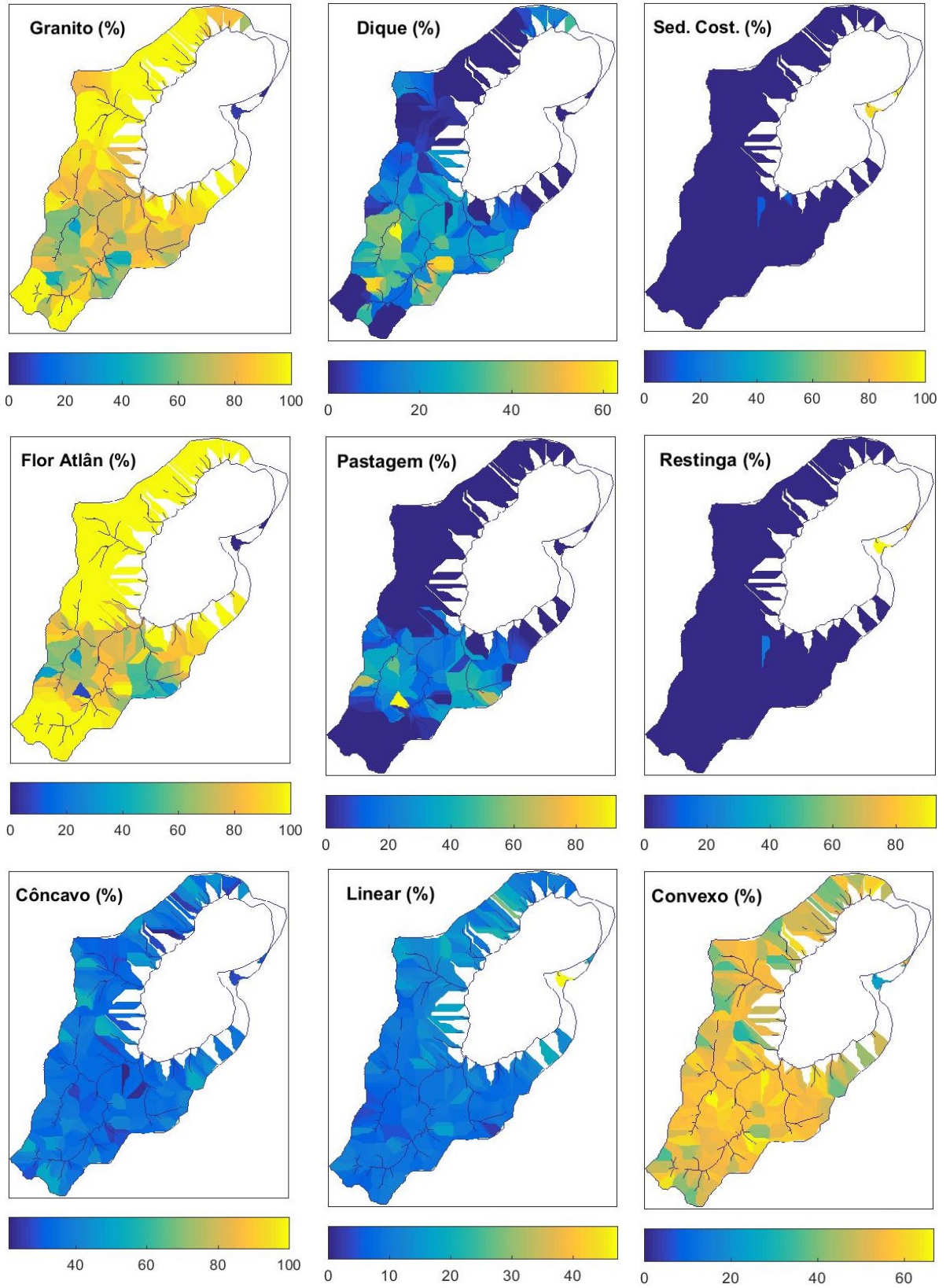
APPENDIX C - SUNHYT A TOOL FROM TRADTIONAL TO AN INNOVATIVE UNIT HYDROGRAPH MODEL BASED ON BASEFLOW MEASUREMENTS

ABSTRACT

Unit hydrographs (UH) are widely used in scientific research and engineering projects to simulate rainfall-runoff processes. There are four main approaches for calculating UH: the traditional, the conceptual, the probabilistic, and the geomorphological approaches. Most software designed to facilitate the estimation of UH is usually based on only one UH approach, limiting its applicability for scientific hypotheses testing. This paper presents the Synthetic Unit Hydrograph Tool (SUnHyT), which provides nine different UH models from the four main approaches used in UH applications and an innovation SUH that uses the relationship between discharge and velocity during baseflow in order to improve the estimation of the UH. SUnHyT is an open-source application that can be used intuitively through a graphical user interface. We tested the model in a case study that highlights the need for alternative approaches of UH when the traditional approach does not perform well. SUnHyT allows the estimation of design hydrographs in gauged and ungauged catchments and can be useful for hydrologists, water managers and decision-makers.

1C INTRODUCTION

Sherman (1932) theory for the unit hydrograph (UH) or instantaneous unit hydrograph, has become one of the most used theories for estimating storm runoff hydrographs (Todini, 1988). Even though more complex hydrological models are available, the UH is still used because it provides runoff estimates with few parameters that are easily determined using digital elevation models (Lee *et al.*, 2006; Singh; Mishra; Jain, 2014). UH has been used as model to estimate nonpoint pollution (Chen *et al.*, 2017; Todeschini; Papiri; Ciaponi, 2014), sediment discharge (Singh, Cui e Byrd, 2015), streamflow regionalization (De Lavenne; Boudhraâ; Cudennec, 2015; Littlewood; Croke, 2008; Razavi; Coulibaly, 2013; Seo; Park, 2014; Yao *et al.*, 2014), and flood prediction (Gad, 2013; Siqueira *et al.*, 2016).

The different approaches used to calculate the UH shape are divided into four main classes (Singh; Mishra; Jain, 2014; Figure C1): (i) traditional or empirical; (ii) conceptual; (iii) probabilistic; and (iv) geomorphological. The traditional approach, also known as the synthetic unit hydrograph (SUH), uses physical characteristics related to the stream network and

hydraulic properties to predict floods in ungauged catchments (Bernard, 1935; Gottschalk; Weingartner, 1998; Mockus, 1957). The conceptual UH is based on a reservoir analogy (Clark, 1945; Dooge, 1973; Nash, 1959) or a linear cascade of reservoirs (Nash, 1957) that represents a complex hydrologic system. The probabilistic approach uses probability density functions (PDF), e.g., the two-parameter gamma distribution, to approximate the shape of the UH (e.g. Bhunya et al., 2008; Bhunya; Singh; Mishra, 2009; Croley, 1980; Nadarajah, 2007; Singh, 2000). The geomorphological instantaneous unit hydrograph (GIUH) unifies traditional and conceptual classes by considering catchments as a hydrologic system composed of streams (e.g. (Rodríguez-Iturbe; Valdés, 1979; Rosso, 1984). Another perspective of GIUH comes from the idea of using the maximum information from digital elevation models, where the instantaneous unit hydrograph is derived from the definition of a width function (Kirkby, 1976), under the hypothesis of constant celerities throughout the network (Rigon et al., 2016). This UH is known as the width function instantaneous unit hydrograph (WFIUH).

The applicability of one of the most common approaches is usually justified based on the limitations of other methods. For example, the most traditional model (i.e., Mockus, 1957b) uses the time of concentration, which is a highly subjective parameter (Beven, 2020), and estimation of the time of concentration can differ by up to 500% (Grimaldi *et al.*, 2012). The conceptual and probability classes are black box models, their parameters cannot be directly related to catchment characteristics, and therefore, their application is limited to ungauged catchments. On the other hand, the GIUH has been widely applied in scientific research, but the velocity parameters used in those models are usually interpreted as velocities and travel times of the water in overland flow when they should be related to wave celerity (Beven, 2020). The last developments offer a solution using WFIUH and estimate the hillslope velocities cell by cell through physical equations (Grimaldi; Petroselli; Nardi, 2012; Grimaldi *et al.*, 2010; Grimaldi; Petroselli, 2014). However, the flow velocity of hillslopes tends to be overestimated using physical equations (e.g. Darcy–Weisbach formula, Manning's formula) (Grimaldi *et al.*, 2010).

HEC-HMS (USACE, 2001) is one of the most popular computer software based on UH theory using traditional UH approaches for hydrograph design. There are other tools based on linear programing (Cavallini, 1993; Hromadka, 2000), instrumental variables (Allen; Liu, 2011; Jakeman; Littlewood; Whitehead, 1990), and geomorphological approach (Bhadra *et al.*, 2008; Lee *et al.*, 2006; Yang; Herath; Musiake, 1998). The most suitable UH approach depends on each catchment runoff generation process. Although the UH is indicated for catchments

whose runoff generation process is Hortonian, the HU has been used in catchments with different runoff generation (Pedroso; Mannich, 2021). The uncertainty of UH is around 50% for ungauged catchments (Brunner *et al.*, 2018), peak flow can be overestimated by up to 60 times in some catchments (Pedroso; Mannich, 2021) and errors can reach up to 137% using traditional and conceptual HU approaches (Steinmetz *et al.*, 2019).

There is a need to combine different classes of UH into an easy-to-use computational tool for scientific and engineering applications. These UH models in unified software encourage users to employ a joint method approach in order to verify the uncertainty inherent in rainfall-runoff models. In addition, the tool simplifies the process of identifying the UH model that is best suited for any specific application.

In this chapter, we develop the Synthetic Unit Hydrograph Tool – SUnHyT. We implemented nine UH models in the tool: two traditional (Mockus, 1957; Snyder, 1938) known as SCS; two conceptual (Nash, 1957; Zoch, 1934); two probabilistic (two-parameter log-normal distribution - TwoParLn and two-parameter gamma distribution - TwoParGamma); and four geomorphologic (two based on Laws of Horton - Rodríguez-Iturbe and Valdés (1979), and Rosso (1984); and two based on width function – Kirkby (1976) and IWVVTTF - Inflow Weighted, Variable Velocity, Travel Time Functions). IWVVTTF approach is an innovative proposal using the width function modified by Bergstrom *et al.* (2016) to use in catchments during baseflow periods. Here we and adding a term, which is the relationship between celerity and velocity, considering the kinematic wave that occurs during rainfall-runoff event. After presenting SUnHyT, we apply this tool to a case study in Ribeirão Grande Catchment and we verify the performance of each UH model for rainfall-runoff simulation.

Figure C 1- Main UH models, where q_p is the peak flow, t_b is the base time, t_{lag} is the time between rainfall gravity center and the hydrograph peak, t_p is the peak time, t_r is the recession time, t_c is the concentration time, β is a product of peak rate flow, k is the storage coefficient, n is the number of reservoirs, α is a function of t/t_p, R_L is the stream lengths law, R_B is the bifurcation law, R_A is the law of stream areas, v is the average peak flow velocity or characteristic velocity.
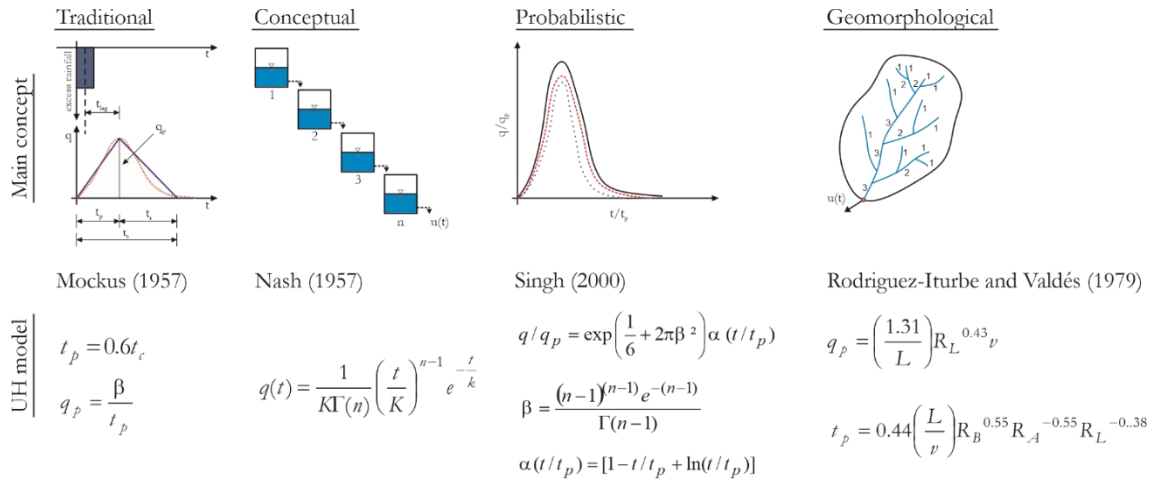
Sherman (1932) developed the Unit Hydrograph (UH) based on the assumption that the catchment responds linearly to rainfall (Dooge, 1973). Considering surface runoff as a linear function of effective rainfall (Snyder, 1938), the resulting hydrograph is expressed by the convolution integral in Equation 1C.

$$Q(t) = A \int_0^t q(t - \tau) * P_{ef}(\tau) d\tau \tag{1C}$$

where $Q(t)$ is surface runoff per time unit [L³ T⁻¹], A is drainage area, q is the unit hydrograph, P_{ef} [L] is the effective precipitation and τ [T] is travel time (Volpi *et al.*, 2018).

Initially, HU was treated as a histogram whose ordinates were unknown parameters to be determined (Beven, 2012), and calibration was impossible with the available rainfall-runoff data at that time. Zoch (1934) proposed a conceptual UH (Figure 1C) with just one parameter, which describes catchment behavior as a reservoir and assumes that the stream is dry when the rain began (Equation 2C).

$$q(t) = q_0 e^{-\frac{t}{k}} \tag{2C}$$

where q_0 [L T⁻¹] represents the initial runoff and k [T⁻¹] is the linear storage coefficient. However, this situation does not occur very often in nature and Nash (1957) increased the complexity of the model to get closer to the real rainfall-runoff hydrograph. Nash (1957) assumed that a stream system is equivalent to a series of linear reservoirs, where discharge is

proportional to storage, with the downstream input corresponding to the upstream output (Equation 3C).

$$q(t) = \frac{1}{k\Gamma(n)} e^{\frac{-t}{k}} \left(\frac{t}{k}\right)^{n-1} \tag{3C}$$

where n [-] is the number of reservoirs and Γ is the density gamma function. Thus, the form of the UH, controlled by the number of reservoirs (n) and linear storage coefficient (k), can be obtained by the convolution of upstream inflow with the downstream linear reservoir. This process, repeated n times, corresponds to a density gamma function (Γ). Nash (1957) reservoir system was further developed by Dooge (1959), who conceptualized the catchment response in terms of a succession of reservoirs and channels represented in a time-area curve, where each reservoir drained one catchment subdivision. Singh (1964) considered the catchment as a series of two reservoirs with different storage coefficients.

The major issue with conceptual models (Figure C1) is that their parameters cannot be estimated without measured data. On the other hand, they consolidated the idea that UH could be described by the behavior of the composition of reservoirs, whose shape is similar to a probability density function (PDF). This conclusion led to new UH developments based on its association with PDF (Figure C1). Nadarajah (2007) implemented nine PDFs to represent the UH. One example is the two-parameter lognormal distribution (Equation 4C).

$$q(t) = \frac{1}{\sqrt{2\pi}\sigma t} e^{\left(-\frac{(\ln t - \mu)^2}{2\sigma^2}\right)} \tag{4C}$$

where σ [-] and μ [-] are parameters of the PDF function. Another example is the two parameters gamma distribution that results in the same mathematical formulation of Nash (1957) and has been widely adopted (e.g., Bhunya et al., 2008, 2007; Singh, 2000).

The conceptual and probabilistic UH models showed that it is possible to describe the rainfall-runoff process using UH. Nevertheless, it is only possible to establish the UH shape in catchments with rainfall-runoff data. The aim of going beyond this limitation has led to the so-called synthetic UH, which links the main components of UH to catchment characteristics, in order to make UH predictable based on catchment characteristics.

There are three main components of synthetic UH: (i) peak time, representing the moment when most of the catchment is generating outflow; (ii) peak flow, the outflow at the moment of peak time; and (iii) base time, the total duration of the UH. The traditional UH (as

classified by Singh, Mishra, and Jain (2014) determines the shape of the UH (i.e., base time, peak discharge, and peak time) on the basis of empirical relations derived from data on several catchment characteristics. Snyder (1938) derived a UH based on Equations 5C, 6C and 7C.

$$t_p = C_t (LL_c)^{0.3} \tag{5C}$$

$$q_p = 2.78 \left(\frac{A_W C_P}{t_p} \right) \tag{6C}$$

$$t_b = 3 + 3 \left(\frac{t_p}{24} \right) \tag{7C}$$

where t_p [T] is peak time, q_p [L³ T⁻¹] is peak flow, t_b [T] is base time, C_t and C_p are dimensionless constants, A_W is the drainage area [L²], L [L] is the mainstream length, L_c [L] is the distance from the catchment outlet to a point on the main stream nearest to the center of the catchment area [km].

Peak time and peak flow are closely related to the stream network, main stream length, slope, and catchment centroid (Snyder, 1938; Taylor; Schwarz, 1952). Moreover, Mockus (1957) stated that t_p and q_p are a function of the time of concentration (t_c), an attribute that can be calculated via empirical formulas (Grimaldi *et al.*, 2012) (Equations 8C and 9C).

$$t_p = 0.6 t_c \tag{8C}$$

$$\frac{q(t)}{q_p} = e^m \left[\left(\frac{t}{t_p} \right)^m \right] \left[e^{\left(-m \left(\frac{t}{t_p} \right) \right)} \right] \tag{9C}$$

where *m* is a dimensionless variable [-]; and t_c is the time of concentration [T].

These traditional UH can be described by a PDF using the gamma distribution (Equation 30) (Singh, 2000), as shown in equations (Equations 10C and 11C).

$$n = \frac{7}{6} + 2\pi\beta^2 \tag{10C}$$

$$k = \frac{t_p}{n - 1} \tag{11C}$$

where β [-] is a factor governing the shape of the dimensionless UH and varies for each model (e.g., β is $1.09 C_P$ for the Snyder model). Since the area under the PDF is guaranteed to be unity, it is not required to calculate t_b.

Motivated by the idea of predicting UH in ungauged catchments, Rodriguez-Iturbé and Valdés (1979) established a geomorphologic unit hydrograph (GIUH), in which only the parameters related to flow velocity need to be estimated. GIUH considers that rainfall randomly

falling in a catchment follows a predetermined path according to the contribution area. Rodríguez-Iturbe and Valdés (1979) proposed the time for the water at each point of the catchment to reach the outlet where q_p, t_p and β depend on Horton's laws (Equations 12C, 13C and 14C).

$$q_p = \frac{1,31}{L} Rl^{0,43} v \tag{12C}$$

$$t_p = \frac{0,44L}{v} \left(\frac{Rb}{Ra}\right)^{0,55} Rl^{-0,38} \tag{13C}$$

$$\beta = 0.584 \left(\frac{Rb}{Ra}\right)^{0,55} Rl^{0.05} \tag{14C}$$

where Rb [-] is the bifurcation ratio, Rl [-] is the length ratio, Ra [-] is the area ratio and L [L] is the length of the mainstream, v [L T^{-1}] is the hydrodynamic factor flow velocity.

Rosso (1984) unified aspects first introduced by Nash (1957) and Rodríguez-Iturbe and Valdés (1979) to create a UH model that estimates the number of reservoirs and linear storage coefficient using geomorphological data (Equation 15C and Equation 16C).

$$n = 3.29 \left(\frac{Rb}{Ra}\right)^{0.78} Rl^{0.07} \tag{15C}$$

$$k = 0.70 \left(\frac{Ra}{RbRl}\right)^{0.48} \frac{L}{v} \tag{16C}$$

Several other models have been derived since. Rodríguez-Iturbe, González-Sanabria, and Bras (1982) suggested a UH concept that varies depending on the intensity and duration of effective rainfall.

GIUH can be estimated using the Horton's laws (Rodríguez-Iturbe; Valdés, 1979) or using the width function (Kirkby, 1976), known as the width function instantaneous unit hydrograph (WFIUH). The width function represents the distribution of distances upstream from the outlet, which can be normalized by the total area to obtain a probability distribution function. The product of the distance and flow velocity corresponds to travel time. Flow velocity in the catchment can be divided into hillslope velocity and stream velocity (Rigon *et al.*, 2016). The WFIUH can be estimate using Equations 17C, 18C and 19C.

$$T_{r \to o} = \sum_{i=r}^{0} T_i = \sum_{i=r}^{0} \frac{x_i}{v_r} \tag{17C}$$

$$T_{h \to r} = \sum_{i=h}^{0} T_i = \sum_{i=r}^{0} \frac{x_i}{v_h} \tag{18C}$$

$$q(t) = T_{r \to o} + T_{h \to r} \tag{19C}$$

where $T_{r \to o}$ [T] is the travel time of the water in the stream network to outlet, $T_{h \to r}$ [T] is the travel time on the hillslope to the stream, x is the position of the cell and v_r [L T^{-1}] is the median velocity of water in the stream and v_h [L T^{-1}] is the median velocity of water on the hillslope. The latest developments of WFIUH reach a calibration-free configuration with one parameter (WFIUH-1par) constraining the channel velocity to the time of concentration or to the lag time and estimate the hillslope velocities cell by cell through physical equations (Grimaldi; Petroselli; Nardi, 2012; Grimaldi *et al.*, 2010; Grimaldi; Petroselli, 2014). However, the flow velocity tends to be overestimated using physical equations (e.g. Darcy–Weisbach formula, Manning's formula) (Grimaldi *et al.*, 2010).

Here we proposed a new GIUH based on IWVVTTF from Bergstrom *et al.* (2016), where we can estimate the variation of velocity based in the correlation between catchment area and discharge (Equation 20C) and discharge and flow velocity (Equation 6C). Through this Equation 20 and Equation 5C the travel time of the water could be estimated in each stream cell of the DEM:

$$T_{r \to o} = \frac{c}{v_r} \sum_{i=r}^{O} \frac{L_c(i)}{a_{vQ}(qA(i))^{b_{vQ}}} \tag{20C}$$

where A is the area draining at each point, q is the specific discharge, a_{vQ} and b_{vQ} are regression constants determined by Eq. 15 and c is celerity. The relationship between c and v_r can be taken as 5/3 (McDonnell; Beven, 2014) in the case of rectangular sections.

Therefore, in this SUH, both types of velocity – hydraulic (related to the channel shape) and geomorphological (related to the drainage network shape) (e.g. (White *et al.*, 2004) – are considered when calculating a variable velocity with discharge throughout the drainage network.

2C THE SYNTHETIC UNIT HYDROGRAPH TOOL - SUNHYT

SUnHyT is a tool implemented in the MATLAB programming language and contains a graphical user interface (GUI) that facilitates UH determination by providing nine different methods: Snyder (1938), Mockus (1957), Zoch (1934), Nash (1957), two-parameter log-

normal, two-parameter gamma distribution, Rodríguez-Iturbe and Valdés (1979), Rosso (1984), and width function-based geomorphological UH based on Kirkby (1976) and IWVVTTF approach. Snyder (1938) and Rodríguez-Iturbe and Valdés (1979) models are applied to the probabilistic theory introduced by Singh (2000).

Table 14C - The input and output for each UH model in the calibration module. Where TwoParLn is two-parameter log normal distribution, TwoParGamma is two-parameter gamma distribution, R-R is a rainfall-runoff event [mm – m³/s], A [km²] is drainage area, L is the mainstream length [km], Lc is the distance from the catchment outlet to a point on the main stream nearest to the center of the catchment area [km], t_c is the time of concentration [dt], Ct, Cp, σ, μ, β, α are dimensionless constants, n [-] is the number of reservoirs, a dimensionless parameter, and k [L T^{-1}] is the unit of time-related to reservoir decay, FAC is a raster of flow accumulation and FDR is a raster of flow direction, DEM is digital elevation model, tr is the threshold of cells to define drainage, v is the hydrodynamic factor flow velocity [m dt^{-1}], v_r is the median velocity of water in the stream [m dt^{-1}] and v_h is the median velocity of water in the hillslope [m dt^{-1}]. dt is the temporal resolution of the input data.

UH model	Equation	Calibration-Input	Calibration-Output
Snyder (1938)	5C, 6C, 7C, 10C and 11C	R-R, A, L, Lc	C_t, C_p
Mockus (1957)	8C and 9C	R-R, A	t_c
Zoch (1934)	2C	R-R, A	k
Nash (1957)	3C	R-R, A	n, k
TwoParLn	4C	R-R, A	σ, μ
TwoParGamma	3C	R-R, A	γ, α
Rodríguez-Iturbe and Valdés (1979)	10C, 11C, 12C, 13C and 14C	R-R, A, Rb, Rl, Ra and L	v
Rosso (1984)	15C and 16C	R-R, A, Rb, Rl, Ra and L	v
Kirkby (1976)	17C, 18C and 19C	R-R, A, FAC and FDR derived from DEM and tr	v_r, v_h
IWVVTTF	20C	R-R, A, FAC and FDR	c/v

Three modules are available for using the tool: (i) calibration; (ii) validation; and (iii) ungauged. In the calibration and validation modules, the user needs to input rainfall-runoff data. In the calibration module, different inputs are required for each model, as shown in Table 1C. Flow accumulation (FAC) and flow direction (FDR) files in .txt format should be created by the user from the DEM.

To determine the hydrograph from the UH, it is necessary to determine the amount of rainfall that drains from the catchment through runoff. In this regard, SUnHyT is equipped with

resources for separating baseflow and surface runoff in a hydrograph. Three numerical flow separation filters are provided within the tool: (i) Lyne and Hollick (1979), (ii) Chapman and Maxwell (1996), and (iii) Eckhardt (2005). Digital filters and mathematical formulations for numerical filters are presented in Carlotto and Chaffe (2019). The constant baseflow option can be used for the ungauged method. Alternatively, for the intermittent stream, it is possible to use the tool without considering the baseflow.

Effective rainfall, a key parameter for estimating UH, is determined by Curve Number(e.g. Ajmal et al., 2015), which consists of two main components t: initial abstraction (*Ia*) [L] and curve number (*CN*) [-]. *Ia* is defined as the rainfall of an event that falls before the direct runoff starts. *CN* calibration is performed by conducting a mass balance, where all effective rainfall is converted into direct runoff. If there is no rainfall-runoff data, the tool supports the estimation of effective precipitation using the curve number method parameters, which are associated with soil type, soil cover, and saturation state. These parameters can be calibrated using data from neighboring gauged catchments (e.g. Cheng et al., 2006).

After defining the effective rainfall, a matrix with the effective rainfall is generated to perform the convolution operation, as explained by Cavallini (1993). To determine this matrix, it is necessary to determine the base time of the hydrograph. The base time is determined as the time interval between the beginning and end of the surface runoff in the calibration and validation module. In the ungauged module, the user must determine the base time.

The UH is calibrated using the D'Errico (2023) search algorithm based on Lagarias et al. (1998). The algorithm aims to find the lowest possible value for an operation. We employed an objective function (OF) inspired by the Nash-Sutcliffe equation. While Nash-Sutcliffe values range from one to minus infinite, our function varies from minus one to infinite (Equation 21C).

$$\text{OF} = -\frac{\sum_{t=1}^{T}(Q_m^t - Q_O^t)^2}{\sum_{t=1}^{T}\left(Q_O^t - \overline{Q_O}\right)^2} \tag{21C}$$

where Q_0 is the mean of observed runoff, and Q_m is modeled runoff. Q_O^t is observed discharge at time t. The output parameters are the ones that better respond to an objective function.

2.1C GRAPHICAL USER INTERFACE

SUnHyT is composed of the main GUI that provides the choice of methods for separating hydrographs and creating unit hydrographs (UH). In the GUI, the three modules are available to perform the procedures. Each module includes features for viewing and saving results, with

a GUI that allows the user to choose the visualization mode (graphs or spreadsheet), location, and format to save the data (.txt (text file) or .xlsx (Excel files)). The sub-windows that are part of the GUI are shown in Figure C 2.

A – **General parameters**: These are mandatory inputs used in all UH methods. The catchment area must be in square kilometers and the time interval (*dt*) must be given in seconds (e.g. if the data was monitored with a time interval of 1 hour then dt is 3600 s).

B – **Baseflow separation methods:** It provides methods for baseflow hydrograph separation, and it is an optional procedure. When selected, the checkbox enables the Combobox to display the available options.

C – **Unit hydrograph methods (UH)**: In this section, a Combobox displays all UH methods, and the user must choose one of them.

D – **Selection of procedures to be performed**: There are three procedures are available, and the user must select at least one of them: (i) calibration, (ii) validation, and (iii) ungauged.

E – **Next button**: Clicking this button registers the entered information and opens a new window where the user can input parameters based on the chosen methods and actions. If more than one action is selected, the window will open in the following order: calibration, validation and ungauged.

F – **Data input**: In this panel there are the buttons that allow the user to enter the precipitation and streamflow data, and also the information of flow accumulation and flow direction, when necessary. In the calibration and validation windows, the "Event data" button allows the user to locate and open the .txt file containing the event, with two columns consisting, precipitation and streamflow data. In the "Ungauged" window, the "Event data" button allows to enter precipitation data for a period when there is no monitored streamflow data. The "Flow accumulation" and "Flow direction" buttons will only be visible when Kirkby's method or IWVVTTF is selected. These buttons allow you to locate and open the flow accumulation and flow direction data previously made by the user with a digital elevation model suitable for the study area. These files must be written in ASCII format in a .txt file. The structure of the data files can be verified in the test cases that are available with SUnHyT.

G – **Baseflow parameters**: the parameter entry will only be available if a hydrograph separation method has been selected. Otherwise, the parameter input panel will be identified as "not applicable". For the Eckhardt method, the input boxes for parameters a and BFI will be enabled. For other methods, only the parameter a will be necessary.

H – **Physical and geomorphological properties**: This panel is related to physical and geomorphological properties of the catchment. When Snyder method is selected, the input values for the physical properties of the catchment will be enabled (2 inputs). In the case of Rodriguez-Iturbé and Rosso, the inputs for the geomorphological properties of the catchment are enabled (4 inputs). For the other methods, these properties are not required, and the parameter inputs will remain disabled and with the identification "not applicable".

Figure C 2- The graphical user interface of the calibration, validation, ungauged, and data visualization and saving modules available at SUnHyT. Identified with letters are the components of the GUI.
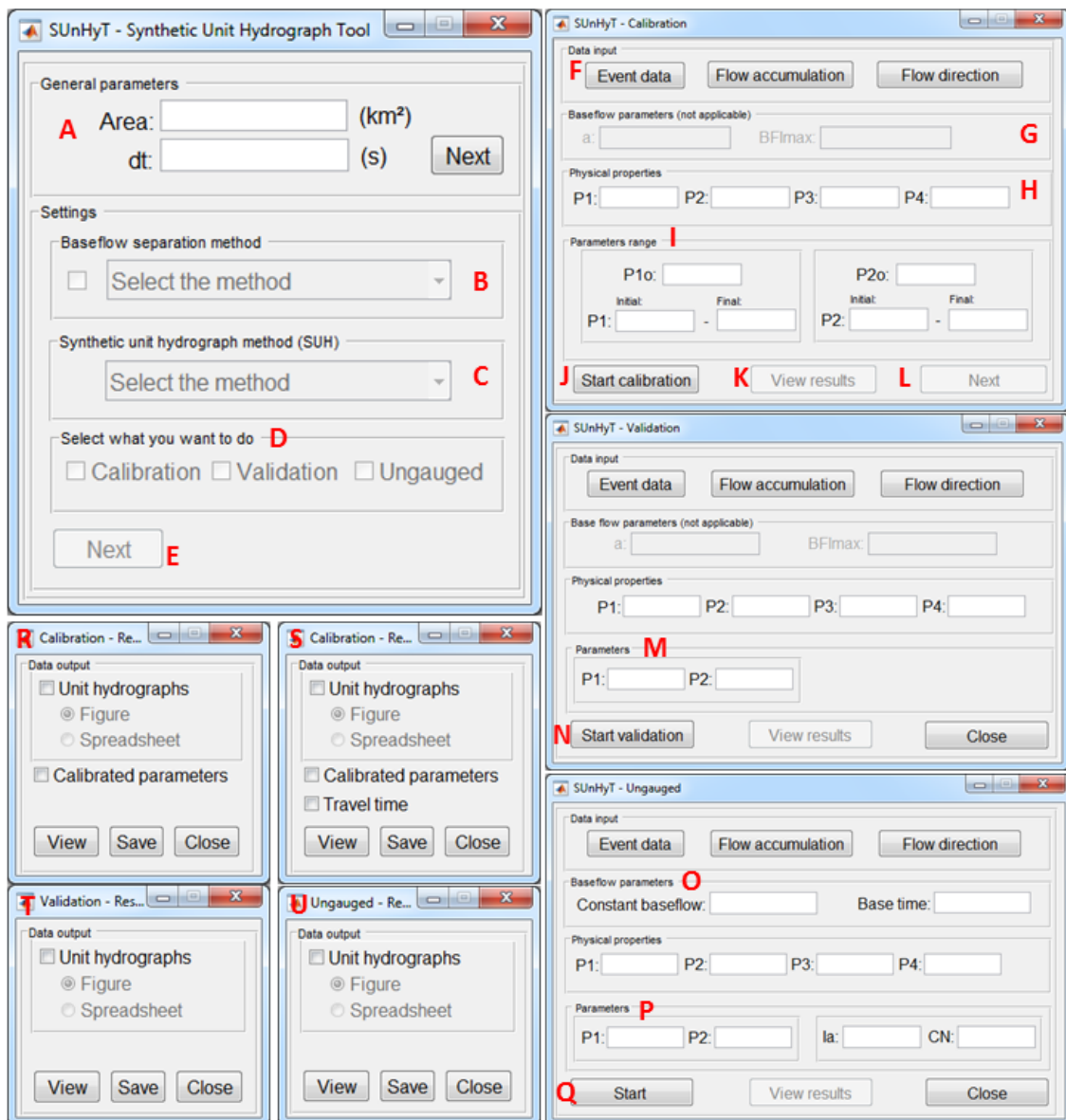
I – **Parameters range**: This section is for setting the parameters range calibration. In addition to defining the calibration range, the user must also specify an initial value for each parameter.

Help texts are provided if the user hovers the mouse cursor over the parameter name. Table 15C displays the common values used or found in the literature for each parameter.

J – **Start calibration**: Clicking on this button initiates the calibration process. When the calibration is completed, the "View Results" and either "Next" or "Close" buttons will be enabled. For the Kirkby method, the user will be prompted to define a threshold corresponding to the minimum number of cells for the formation of the drainage network.

K – **View results**: This button opens the window for viewing and saving the results. The preview window and its features will be presented in items R, S, T, and U.

L – **Next or close button**: In the calibration and validation windows, the "Next" button appears when there are subsequent procedures (e.g., it appears in the calibration window if both calibration and validation procedures are selected). The "Close" button appears when no further procedures are needed.

M – **Validation parameters**: Enter the validation parameters. If the calibration procedure has been completed, the validation parameters will be auto filled.

N – **Start validation**: This button will start the parameter validation process. When the calibration is finished, the "View Results" and "Next" buttons will be enabled.

O – **Baseflow parameters**: In the synthetic unit hydrograph estimation window for periods without streamflow monitoring ("Ungauged"). The baseflow parameters consist of: "Constant baseflow" and "Base time". If you do not have a value for the constant baseflow then enter the value zero to disregard the baseflow and obtain a unit hydrograph with streamflow starting at zero. The base time is around 1.6 times the time of concentration (USDA-NRCS, 2010). We recommend that the user chooses the base time greater than this value.

Table 15C - Common values used or found in the literature for each parameter. Where TwoParLn is two-parameter log-normal distribution, TwoParGamma is two-parameter gamma distribution, t_c [T] is the time of concentration, C_t, C_p, σ, μ, γ, α are dimensionless constants, n [-] is the number of reservoirs, a dimensionless parameter, and k [T^{-1}] is the unit of time related to reservoir decay, v [L T^{-1}] is the hydrodynamic factor flow velocity, v_r [L T^{-1}] is the median velocity of water in the stream and v_h[L T^{-1}] is the median velocity of water in the hillslope.

UH model	Parameters	Initial-Final	Literature-based	Catchment area [km²]
Snyder (1938)	C_t	0.65 – 2.20	Silveira (2016); Singh *et al.* (2014); Snyder (1938).	0.25 - 25000
	C_p	0.31 – 1.22		
Mockus (1957)	t_c	Time of concentration (e.g. Fang *et al.*, 2008; Kirpich, 1940)	NRCS (2007)	5.20 - 11.14
	m	0.50 – 6.00		
Zoch (1934)	k	1.0 – 10.00	-	< 1
Nash (1957)	n	1.00 – 5.86	Bhunya *et al.* (2008)	114 - 350
	k	2.12 – 10.00 h^{-1}		
TwoParLn	σ	$\sigma > 0$	Nadarajah (2007)	
	μ	$-\infty < \mu < +\infty$		
TwoParGamma	γ	$\gamma > 0$	Nadarajah (2007)	
	α	$\alpha > 0$		
Rodríguez-Iturbe and Valdés (1979)	v	1.0 – 5.0 m s^{-1}	Rodríguez-Iturbe *et al.* (1979); (Moussa, 2008)	1 - 3024
Rosso (1984)	v	0.1 – 10.0 m s^{-1}	Rosso (1984); Chen et al., (2019b)	5 - 1719
Kirkby (1976)	v_r	1.27 – 2.42 m s^{-1}	Di Lazzaro (2009b); Rigon *et al.* (2016); Grimaldi *et al.* (2012b)	10 - 4116
	v_h	0.009 – 0.033 m s^{-1} (10 to 100 times smaller than v_r)		
IWVVTTF	c/v	0.50 – 5.00	-	

P – **Parameters**: In the "Ungauged" mode window, it is necessary to inform the Initial abstraction *Ia* (defined as the rainfall of an event that falls before the direct runoff starts) and Curve Number (CN). If the user wants to provide effective rainfall instead of using the CN method, the user should define CN equal to 100 and *Ia* equal to 0, this will define that all of the input rainfall will be effective rainfall. When the calibration process is applied for an event with the monitored streamflow to obtain parameters to estimate the unit hydrograph for a period without monitored streamflows, the parameters *Ia*, CN and others will be filled in automatically.

Q – **Start button**: This button starts the process of estimating the UH from a precipitation event in the "Ungauged" mode.

R – **Visualization of calibration results**: This is the window for viewing and saving the calibration results. To view the results (Unit Hydrographs), the user can choose between a graphical view (by checking the Figure option) and a spreadsheet (by checking the spreadsheet option). It is also possible to view basic statistics of the calibration of the parameters in the form of graphs that show the evolution of the objective function values. To save the results, the user must check which data to save (Unit hydrograph, Calibrated parameters, and others). During

the saving process, messages will appear to inform the user which results are being saved, allowing confirmation or cancellation of the save process. To proceed with saving the results, the user must confirm and specify the location and filename for the saved files.

S – **Visualization of calibration results (Kirkby's method)**: The results display window of the Kirkby method offers the same viewing and saving options as other methods, with an additional feature that allows users to view water travel times in the stream and on the hillslopes. The procedures for saving the calibration results and statistics are the same as those for other methods.

T – **Visualization of validation results**: The resources for viewing and saving validation results, as well as the procedures for these tasks, are the same as those described in sections R and S.

U – **Visualization of ungauged results**: The resources and procedures for viewing and saving results in 'Ungauged' mode are the same as those presented in topics R and S above.

2.3C SUNHYT CASE STUDY: RIBEIRÃO GRANDE CATCHMENT

The physical characteristics of RGC, as detailed in Table 16C, were calculated using the digital elevation model provided by the Santa Catarina Department for Sustainable Development (SDS/SC) with one-meter spatial resolution (SDS, 2013).

In this case, all three modules of the tool, "Calibration", "Validation", and "Ungauged", were used. Two events were selected as input data (the events are available with the program). All UH models were used for this analysis. Two events were selected, 'event_calibration.txt' was used for calibration, and 'event_validation.txt' was used for validation. Hypothetical precipitation was utilized to estimate the hydrograph in the "Ungauged" module.

Table 16C - Ribeirão Grande catchment physical parameters. Where A [km^2] is the area, L [km] is the main stream length, Lc [km] is the distance from the catchment outlet to a point on the main stream nearest to the center of the catchment area, Rb [-] is Horton law of stream number, Rl [-] is the law of stream length, Ra [-] is the law of stream areas.

A	L	L_c	Rl	Rb	Ra
5.30	3.15	2.11	2.14	3.98	4.17

The digital baseflow filter by Eckhardt (2005) was selected with the following parameters: $a = 0.995$ and BFI = 0.80. For UH calibration, the initial, maximum and minimum

values chosen for the parameters were respectively: 1000, 10 and 10000 m h^{-1} for v_r, and 10, 100 and 1000 m h^{-1} for v_h. The optimal value was 6108 m h^{-1} or 1.69 m s^{-1} (v_r) and 48 m h^{-1} or 0.01 m s^{-1} (v_h) (

C). The water travel time is longer on the hillslope than on the stream (Figure 4c).

Figure C 3 shows that calibration and validation processes resulted in a good fit with the observed data. When calibrating and validating all models, it is evident that no class (traditional, conceptual, probabilistic, or geomorphological) outperformed the others in either calibration or validation, as indicated in Table 17C.

The poorest calibration results were obtained for the conceptual model proposed by Zoch (1934). This was expected because Zoch (1934) considers that the catchment is just one reservoir, whereas Nash (1957) views it as a collection of reservoirs. This catchment can be represented as 1.28 reservoirs and decay of 2.63 h (Table 17C). Despite sharing the same theoretical foundation, the calibration of the velocity parameter 'v' varied between Rosso (1984) and Rodriguez-Iturbé (1979) (Table 17C).

We measured discharge and velocity 43 times in 21 cross-sections of PLEC. Velocities ranged from 0.01 to 1.33 m s^{-1} and discharges from 0.12 to 337.5 L s^{-1}. With these discharge measurements, we were able to establish the relationship between stream velocity and discharge as Bergstron *et al.* (2016). Based on this relationship, the median velocity during the peak is 0.64 m s^{-1}. Kirkby (1976) model overestimated the velocity of the stream (1.69 m s^{-1}), while hillslope velocity was very low (0.01 m s^{-1}). It is possible that the velocity of the stream is overestimated to compensate for the velocity in the hillslope. Rosso (1984) and Rodriguez-Iturbé and Valdes (1979) didn't perform well, even though Rosso (1984) estimated a coherent hydrodynamic factor flow velocity (0.77 m s^{-1}). Regarding the IWVVTTF model, the value of c/v was coherent, and the results are discussed in the section 7.3.2.

Figure C 3 - Calibration and validation of the UH. a) Rainfall-runoff event calibrated using UH based in width function. b) Calibration parameters of UH based in width function. c) Rainfall-runoff event validated using UH based in width function. d) Travel time simulated by using UH based in width function.
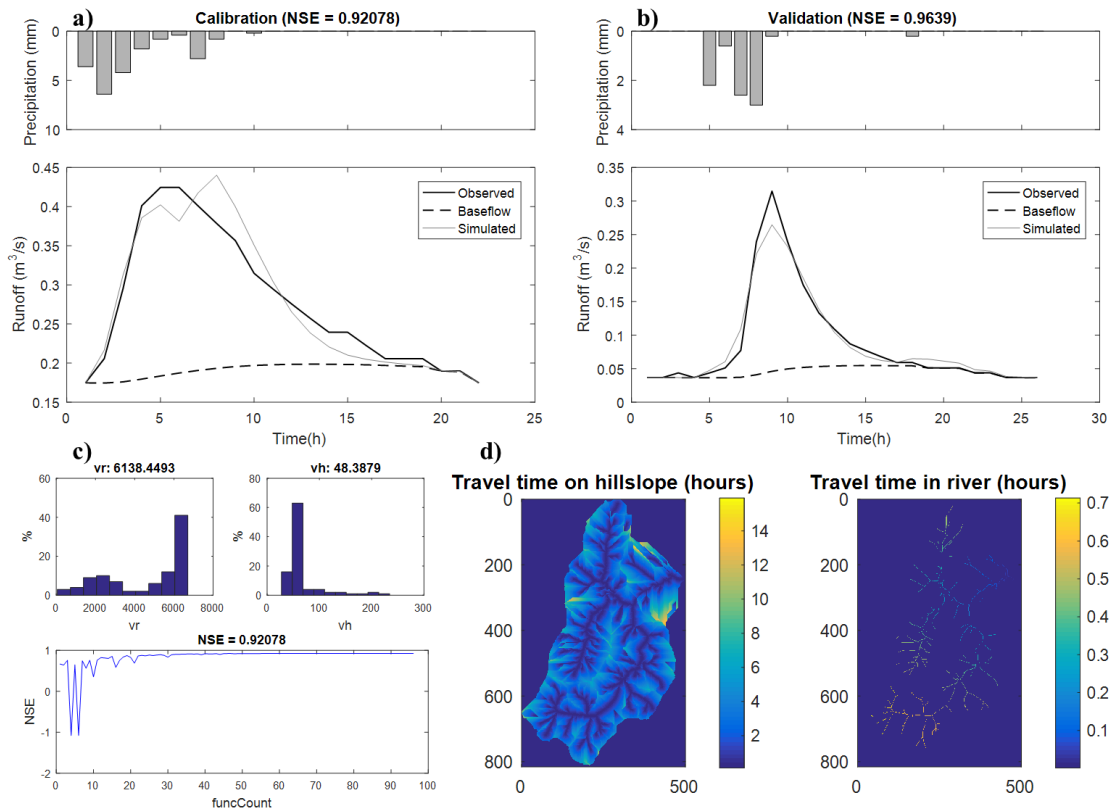

In traditional models the values were not consistent with what was expected. The parameters of the Snyder (1938) model are out of the literature references (Table 15C). While the time of concentration of Mockus (1957) is longer than that calculated by time of concentrations formulas: Kirpich (1940): 0.35 h; Chow (1962): 0.68 h; Johsntone and Cross (1949): 1.35 h; and Dooge (1973b): 0.95 h.

Nash (1957), TwoParLn and TwoParGamma have performed well, as these models are conceptual or probabilistic, there is no parameter related to the physical characteristics of the catchment. When using the tool in the "Ungauged" module, it is possible to verify the impact that the parameters cause on the design hydrograph. For example, a design hydrograph is shown using the parameters calibrated for the case study (Figure C 4a) with Mockus (1957). The calibrated time of concentration is 3.6 hours, the peak flow is 0.32 m^3 s^{-1}, and the duration of the event is 26 h (Figure C 4b). If the time of concentration were 10 hours, the peak flow would be lower, 0.25 m^3 s^{-1}, and the event duration would be larger, 41 hours. Conversely, if the time of concentration is reduced to 1 hour, the peak flow would increase to 0.43 m^3 s^{-1}, and the event duration would be shorter, at 16 hours.

Table 17C - Calibration (Cal) and validation (Val) results. Where TwoParLn is two-parameter log normal distribution, TwoParGamma is two parameter gamma distribution, t_c is the time of concentration, C_t, C_p, σ, μ, γ, α are dimensionless constants, n is the number of reservoirs, a dimensionless parameter, and k is the unit of time related to reservoir decay, v is the hydrodynamic factor flow velocity, v_r is the median velocity of water in the stream and v_h is the median velocity of water in the hillslope.

UH	Parameters	Cal Nash	Val Nash
Snyder (1938)	C_p = 0.43 C_t = 0.13	0.95	0.92
Mockus (1957)	t_c = 3.59 h m = 1.74	0.92	0.96
Zoch (1934)	k = 3.31 h^{-1}	0.83	0.80
Nash (1957)	n = 1.28 k = 2.63 h^{-1}	0.92	0.95
TwoParLn	σ = 0.65 μ = 1.11	0.92	0.96
TwoParGamma	γ = 2.63 α = 1.28	0.92	0.96
Rodriguez-Iturbé and Valdes (1979)	v = 0.10 m s^{-1}	0.85	0.82
Rosso (1984)	v = 0.77 m s^{-1}	0.85	0.82
Kirkby (1976)	v_r = 1.69 m s^{-1} v_h = 0.01 m s^{-1}	0.95	0.96
IWVVTTF	c/v = 1.1	0.88	0.86

Figure C 4 - Simulation of designed hydrographs: a) The interface of the Ungauged module with the calibrated parameters of the Mockus model. b) Design hydrograph to calibrated parameters in a). c) Design hydrograph to calibrated parameters but with the time of concentration (tc) set to 10 hours. d) Design hydrograph to calibrated parameters but with a time of concentration (tc) as 1 hour.
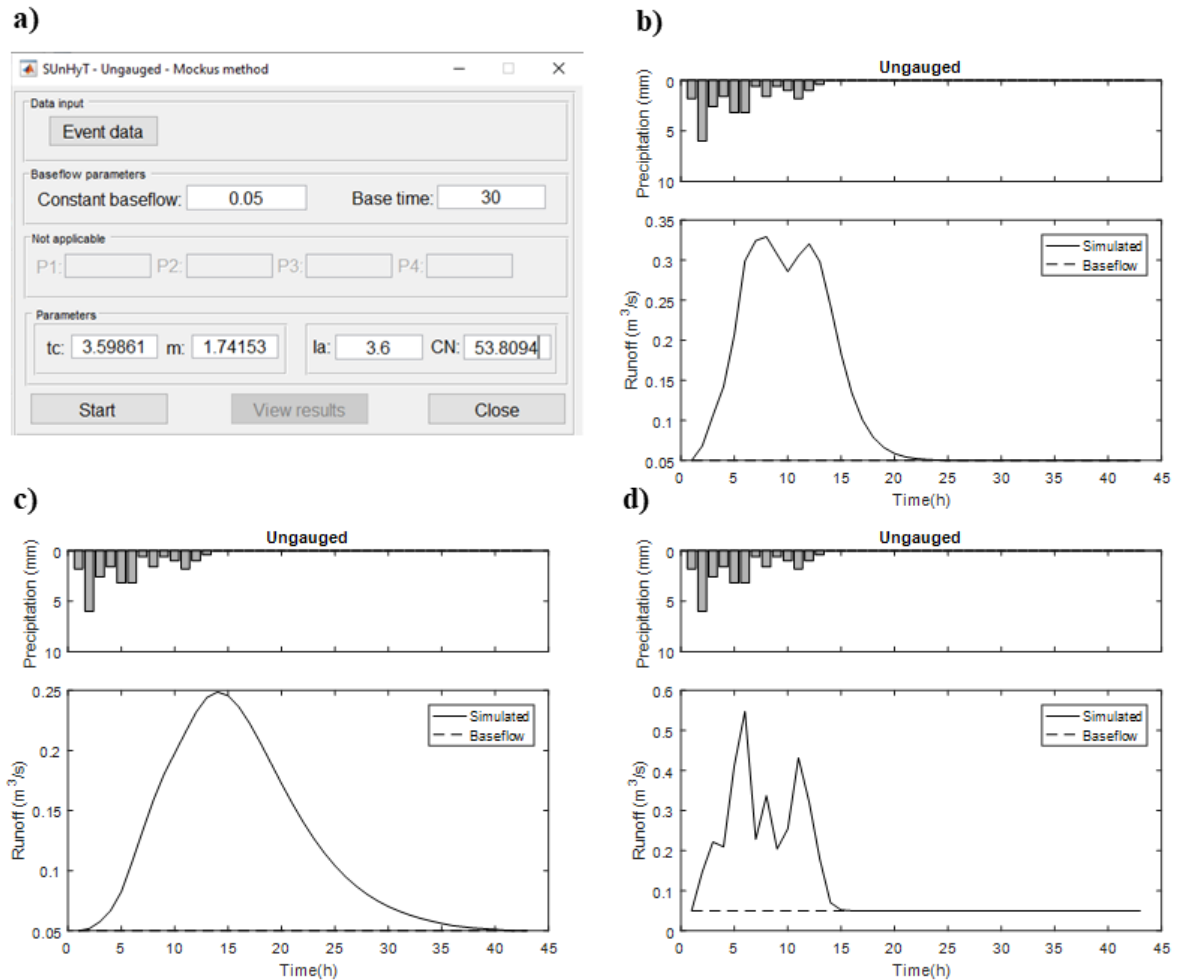

3.1.1 IWVVTTF performance

Here we brought 11 events calibrations IWVVTTF models to RGC (Figure C 5 and Table 17C). In order to select well-defined events for a temporal discretization of one hour, only events where the peak flow was at least 0.2 mm (380 L s^{-1}) were selected. The events ranged from 5.4 to 132.0 mm of precipitation. Most of the drainage network consists of cascade and step-pool sections, characterized by quick flow between rocks and pools, where the water moves much slower. During stream velocity monitoring, the velocity in pools was estimated using a micro-propeller, and in cascade cross-sections, by dilution method. The parameters a_{vQ} and b_{vQ} differ between measurements with the micro-propeller and dilution. The parameters were used based on measurements by current meter in cross-sections with slope less than 4°

and on the dilution-based equation for slopes of cross-section greater than 4°. The value of 4° was defined based on field section observations, cross-referenced with terrain slope data.

Figure C 5 - Calibration of IWVVTTF model using events from the Ribeirão Grande catchment in the year 2016. Each event is enumerated.
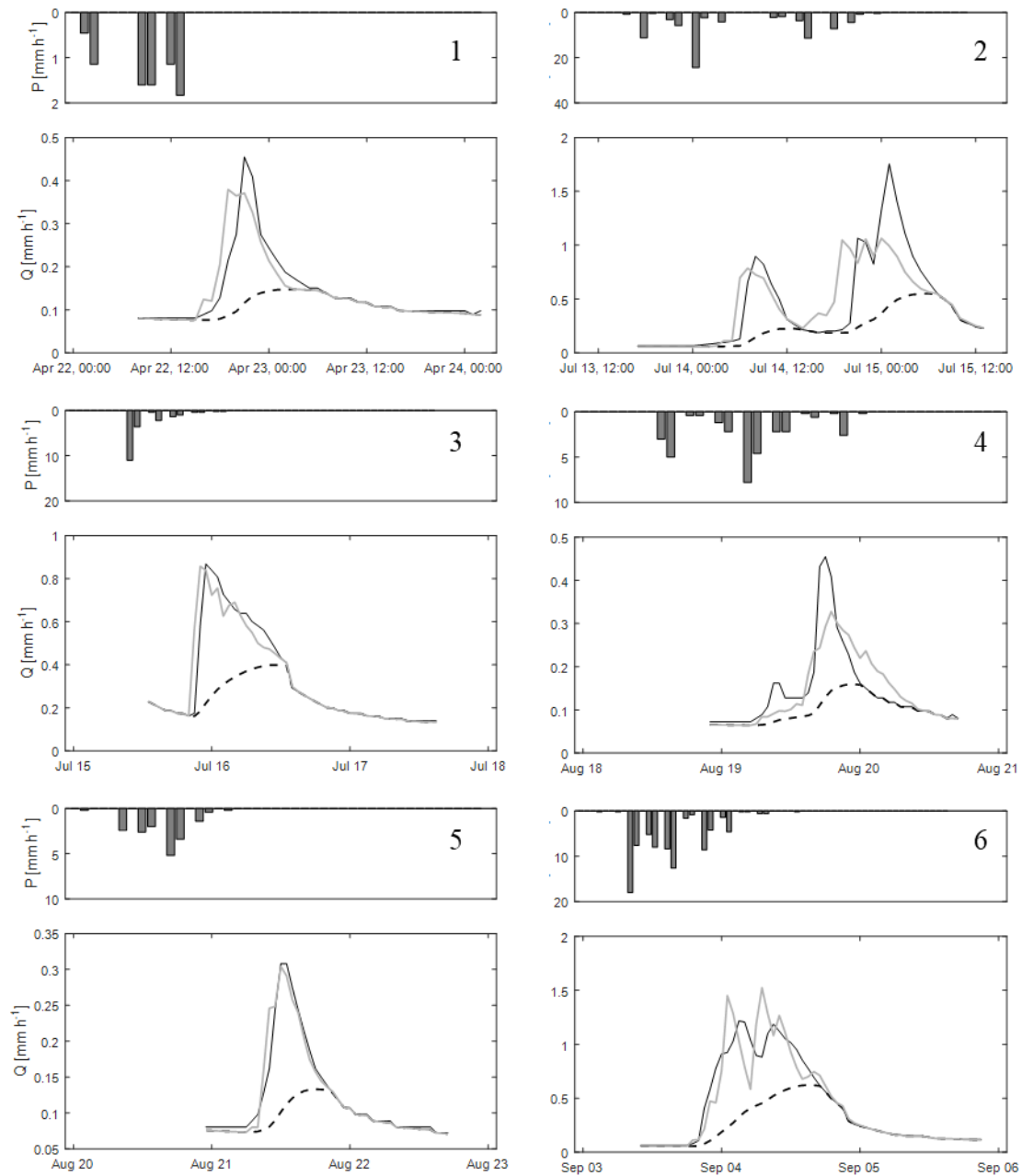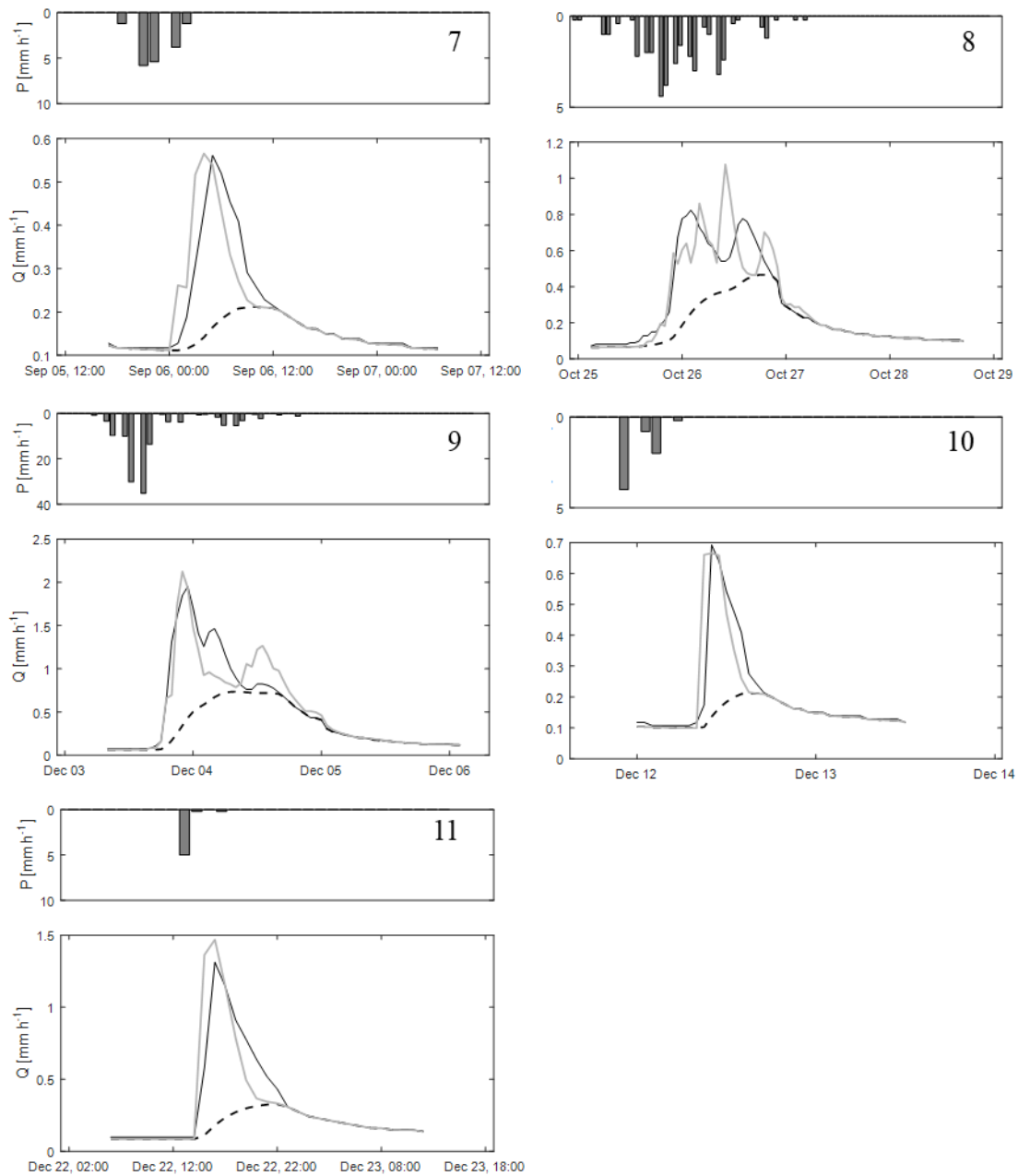
The largest event was event 10 (Figure C 5 and Table 5C), was 132 mm, occurring after 15 rainless days. December 2016 was a very wet month, with 230 mm of precipitation. Base low between rainfall events was around 190 L s⁻¹, while for the rest of the series, it was around 100 L s⁻¹. During this period, events 9, 10, and 11 occurred.

Table 5C – Informações sobre os eventos calibrados por três modelos de hidrograma unitário geomorfológico. Onde Q_P é vazão de pico, P_T é precipitação total, P_E é precipitação efetiva, c/v é celeridade sobre velocidade, IW-VV-TTF *Inflow Weighted, Variable Velocity, Travel Time Functions.*

| Event	Q_P [mm h⁻¹]	P_T [mm]	P_E [mm]	IWVVTTF	
				c/v	Nash
1	0,4	7,8	1,5	1,6	0,87
2	1,7	84,6	9,6	1,2	0,68
3	0,9	20,8	4,7	1,2	0,93
4	0,4	32,8	1,8	2,1	0,71
5	0,3	17,8	1,2	1,7	0,92
6	1,2	83,2	10,5	1,0	0,86
7	0,6	17,4	1,9	1,3	0,95
8	0,8	37,0	7,9	1,0	0,69
9	1,9	132,0	12,5	1,2	0,73
10	0,7	7,0	2,1	1,3	0,65
11	1,3	5,4	4,2	1,1	0,69

In Event 2 (Figure C 5), it's possible to notice three flow peaks, which are increasing, however, during the precipitation, the intensity is decreasing. During the event, there's a 6-hour period without rain, and when it starts raining again, it seems that the catchment doesn't respond to the first four precipitation impulses, which may indicate that the catchment storage capacity has been replenished within 6 hours. The same is observed in Event 4 (Figure 5C), where apparently the last impulse isn't responded to by the catchment, even though surface runoff is still occurring. It's interesting to highlight that studies on interception loss suggest that the minimum inter-event time (the minimum time between events for the canopy to dry out) is 6 hours (Bernardara; De Michele; Rosso, 2007; Dunkerley, 2015; Stan, 2020), and this might be related to precipitation storage capacity, rendering the CN methodology inadequate for events with long intervals without precipitation.

In Events 8 and 9 (Figure C 5), the IWVVTTF fail to represent the last precipitation events of the event because they assume the catchment is fully saturated when apparently, the catchment regains its storage capacity during the event. One hypothesis for these phenomena is the canopy's capacity, as a reservoir, to dry out rapidly. Therefore, in these cases, it's not the IWVVTTF that misrepresents the rainfall-runoff process, but rather the effective rainfall isn't distributed correctly by the CN.

The highest rainfall intensities, where at least one precipitation impulse exceeded 10 mm h-1, occurred in Events 2, 6, and 9. Ignoring the flaws in defining effective precipitation, we see that the IWVVTTF is damped as effective precipitation increases (Figure 6C), which is exactly the opposite of what is expected because it's expected that the higher the precipitation, the higher the specific discharge and the higher the velocity/celerity in streams (Equation 16).

The extent to which the input of energy into the channel due to precipitation causes the velocity in the channels to be higher than the celerity is unknown, especially for irregular sections (Sokolov, 2020), as is the case with natural channels, especially cascade-type channels (Montgomery; Buffington, 1993). The results showed an interesting factor; apparently, the increase in energy in the streams, causing the kinematic wave, is more noticeable in small events, where the flow velocity in streams reaches twice the velocity during baseflow (Figure C 7), and from 5 mm of effective precipitation, the c/v seems to stabilize between 1 and 1.25, for rectangular sections, regardless of the water depth, the value is always 1.66 (Sokolov, 2020).

Figure C 6 - IWVVTF calibrated for eleven events of the Ribeirão Grande Catchment. The origin of each hydrograph is in the volume of effective precipitation.
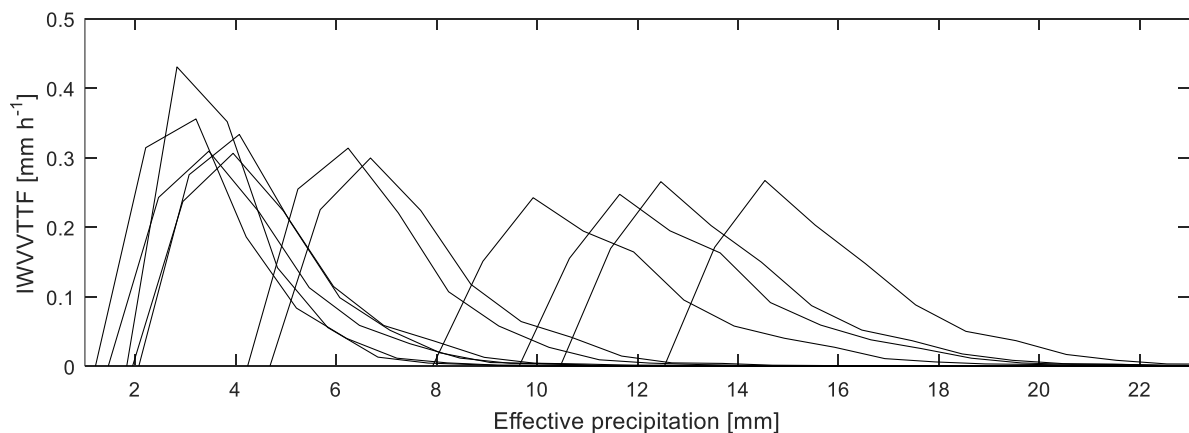
Collischonn *et al.* (2017) showed that celerity increases rapidly with discharge, so the hydrograph tends to have a positive skewness, as we strongly see a skewness trend in the IWVVTTF up to 8 mm of effective precipitation. However, Fleischmann et al. (2016) demonstrated that there's a decline in celerity as water spills over from the channel, and this decline in celerity can produce a tendency for negative skewness. No IWVVTTF exhibits negative skewness, but it was observed that the positive skewness was damped. It's known that at the outlet, there's an extrapolation from the channel from a discharge of 1.2 mm h^{-1}, which occurs in Events 2, 6, 9, and 11, all events from 4 mm of effective precipitation onwards.

However, little can be affirmed about this since it's a single section, and the IWVVTTF is calculated as the result of multiple sections.

Figure C 7 - Relationship between effective precipitation (P_E) and the ratio between celerity and water velocity in the channels (c/v).
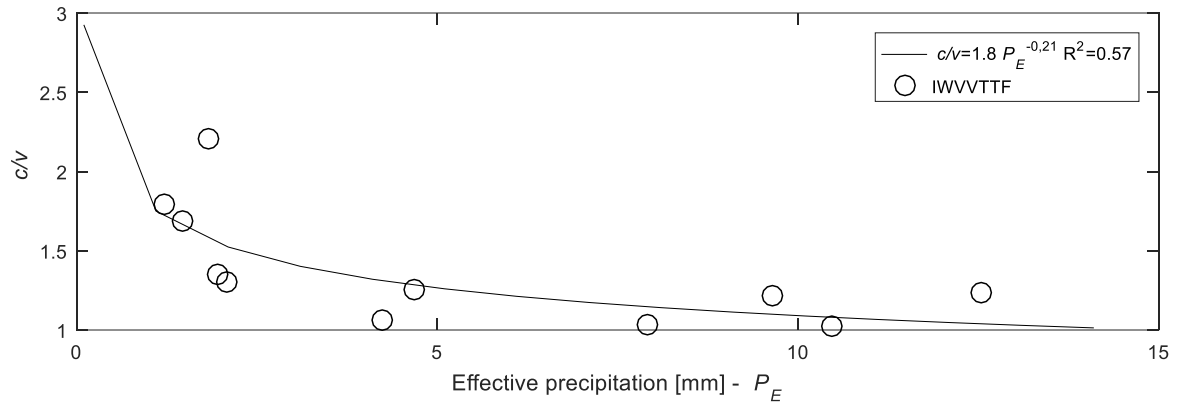
4C CONCLUSION

The Synthetic Unit Hydrograph Tool – SUnHyT implements ten different UH models from four different classes: traditional, conceptual, probabilistic, and geomorphological. SUnHyT can be used intuitively through a graphical user interface, developed in the MATLAB. This tool combines a wide range of UH methods into one user-friendly tool, with the potential to enhance the use of various UH theories and models within the academic, research, and engineering communities. The ungauged module, in addition to estimating hydrographs in ungauged catchments, also provides the user with the experience of being able to visually check the impact of each parameter of UH on the storm hydrograph.

In the study case, we tested the most robust synthetic unit hydrograph for rainfall-runoff simulation in a subtropical forest. All UH perform well, but the advantage of the GIUH and WFIUH is that the parameters have a clear interpretation with respect to flow velocity. A suitable WFIUH approach for understanding and application in ungauged catchments, could certainly be employed, and SUnHyT, as an open tool, provides the foundation for exploring this issue. We highlight the importance of testing the performance of multiple UH models to ensure adequate performance in rainfall-runoff modeling.

SUnHyT is a valuable tool for hydrologists, engineers, researchers, and decision-makers in water management. It integrates multiple UH approaches, promoting the adoption of ensemble methods to address the inherent uncertainty in rainfall-runoff models. Additionally, the calibration tool simplifies the process of identifying the most suitable UH model for a specific application.

APPEDIX D – SLOPE-AREA RELATIONSHIPS FOR THE ANALYSIS OF EPHEMERAL AND PERENNIAL DRAINAGE NETWORKS

ABSTRACT

The drainage network is a key component for estimating rainfall-runoff hydrographs, and its study during baseflow can provide information about groundwater dynamics. In this study, the ephemeral and perennial drainage network was estimated based on field data and three models that utilize accumulated area and local slope. This work also illustrates how the choice of drainage network can impact the geomorphological unit hydrograph. Geomorphological parameters of the drainage networks in the catchment of Peri Lake Experimental Catchment, a coastal catchment containing a lake surrounded by hillslopes, were analysed. The drainage network density generated by groundwater is approximately 20% of the drainage network when surface runoff occurs. During rainfall, the catchment can increase the Strahler order by up to two times.

1D INTRODUCTION

The drainage network is dynamic, and its extent varies with the seasons (dry and wet) and individual rainfall events. Channels can expand due to increased surface runoff or rising groundwater levels. After rainfall events, baseflow is observed, consisting of groundwater from the water table or soil profile (Egusa *et al.*, 2016; Peralta-Tapia *et al.*, 2015). This dynamic of the drainage network alters the connectivity (and disconnection) between compartments and influences the transport of water, nutrients, and sediment in the catchment (Godsey; Kirchner, 2014; Perez *et al.*, 2020; Whiting; Godsey, 2016). Correct determination of the expansion and contraction of the drainage network can aid in understanding groundwater dynamics on slopes (Godsey; Kirchner, 2014). Additionally, the drainage network is widely used in hydrological models, such as in the case of geomorphological unit hydrographs (Bhunya *et al.*, 2008; Botter; Rinaldo, 2003; Rigon *et al.*, 2016; Rodríguez-Iturbe; González-Sanabria; Bras, 1982).

At the catchment scale, springs follow a potential relationship between area and slope (Montgomery; Dietrich, 1992; Montgomery; Dietrich, 1988). Given this potential relationship, models based on joint thresholds of area and slope have been developed, such as Montgomery and Dietrich (1992). Furthermore, the extent of the drainage network depends on landscape characteristics, such as soil depth, slope, drainage area, and the saturation state (Godsey; Kirchner, 2014; Perez *et al.*, 2020; Whiting; Godsey, 2016).

Drainage is usually determined using fixed area thresholds for the entire terrain due to landscape equilibrium suggested by Montgomery and Foufoula-Georgiou (1993). However, several studies have shown that a single threshold for drainage identification may not exist at the catchment scale (Garrett; Wohl, 2017; Grieve *et al.*, 2018; Henkle; Wohl; Beckman, 2011; Mutzner *et al.*, 2016). In this chapter, three methods of automatic drainage network extraction based on area and local slope thresholds were investigated to assess the spatial variability of the channel network. A model based on the potential relationship between area and slope was also proposed. The effect of using different drainage networks on the rescaled width function and geomorphological characteristics of the Peri Lake Experimental Catchment was examined.

2D MATERIALS AND METHODS

The first model used to extract the drainage network (D-M1) defines the springs as the cells in the digital elevation model, which follows the equation:

$$S = aA^b \tag{1D}$$

where S is local slope [°], A is area [m²], and a and b are parameters determined using the set of mapped springs in the field. Then, drainage is determined as the flow paths that extend from the sources to the outlet.

Area and slope thresholds are widely used in the literature for drainage network determination and are defined as 'classic approaches' (Gandolfi; Bischetti, 1997; O'Callaghan; Mark, 1989). The drainage network can be extracted by identifying cells with values greater than the area and slope thresholds. To determine the threshold, the formula proposed by Montgomery and Dietrich (1992) was used:

$$\text{Treshold} = AS^k \tag{2D}$$

where k is equal to 2, as proposed by Montgomery and Dietrich (1992). The values of A and S are defined based on the medians of the maximum values among the mapped springs. Medians were tested because, theoretically, it is a value that well represents the dataset. The maximum values were tested because at Mutzner *et al.* (2016), these values better represented the field-mapped drainage than median values. The model that uses medians is called D-M2, and the one that uses maximum values is called D-M3.

To choose the best drainage network generation model, we examined how many times the calculated drainage network overestimated or underestimated the true drainage network.

This verification was based on points mapped in the field, where it is known whether there is or isn't ephemeral or perennial drainage.

In order to verify the difference between drainage networks, we assessed drainage density, Strahler order, length of the longest stream, and the Rescaled Width Function (RWF, Rigon *et al.*, 2016). The RWF is defined by the equation:

$$\tau(x, y) = \frac{L_h(x, y)}{u_h} + \frac{L_c(x, y)}{u_c} \tag{3D}$$

where τ is the theoretical time for each cell to the outlet, L_c is the flow path through the streams, and L_h is the distance from the hillslope to the channel. The parameters u_h and u_c are the hillslope and streams velocities. u_h and u_c control the wave propagation related to celerity and should not be confused with water velocities that control water transport under baseflow conditions (McDonnell; Beven, 2014). The RWF corresponds to a geomorphological unit hydrograph, obtained by normalizing τ for each cell by the total number of cells.

3D RESULTS

The set of springs mapped in the field exhibits a different relationship between drainage area (*A*) and local slope (*S*) for channels active during baseflow and channels active through surface runoff (Figure 3a). This difference decreases as the area increases. In other words, springs with low slope and a large drainage area are more stable and do not change position during precipitation. Groundwater springs have a larger area compared to surface runoff springs, where the medians were 15.802 and 948 m² respectively (Figure D 1 a,b and c). The opposite occurs concerning slope, with medians of 37 for active springs with surface runoff and 30° for active springs with baseflow. The median of the accumulated area considering all springs is 1.574 m², and the local slope is 35°.

The drainage network for D-M1, both for groundwater and surface runoff, was generated using the equation presented in Figure D 1a. Limits for active drainage generation during base low of 15.802 and 66.219 m² and 30 and 19° were used when employing models D-M2 and D-M3. To define the drainage network during surface runoff, values of 948 and 4.257 m² and 37 and 30°, respectively, were used.

The difference in drainage density in the network generated by groundwater is about 20% of the drainage density when surface runoff occurs. Additionally, for methods D-M1 and

D-M2, the Strahler order of the catchment increases from 4 to 6, while for D-M3, it increases from 4 to 5. This is expected since D-M3 is more restrictive regarding the points that can be considered drainage. There is no significant difference in the length of the longest stream.

The points checked in the field to analyze the effectiveness of the models are presented in Figure D 2. The model that overestimated the drainage network the least was D-M3, but it was also the one that underestimated the most (Table 1D), meaning that this model likely represents a drainage network smaller than the actual drainage network. However, there are many overestimated points in the other models, so D-M3 was considered the most realistic model.

L_h is the distance from the hillslope to the stream, as shown in Figure D 3 for the different generated drainage networks. Distances were normalized by the greatest distance from the slope to the stream found for the D-M3 network during base flow (Lh,max = 1080 m). The mean, maximum, and standard deviations for the different extraction methods are listed in Figure 40. The denser the drainage network, the shorter the distance from the hillslope to the stream. The highest standard deviation occurs in less dense networks.

The Rescaled Width Functions (RWF) are presented in Figure D 4 for three hypothetical cases with different celerities on the slopes. As expected, the peak height decreases, and the peak moment delays as the slope velocity decreases. This factor is more visible for less dense drainage networks (D-M3).

As expected, the RWF becomes more attenuated as slope celerity decreases (Rigon *et al.*, 2016), tending not to have a positive asymmetry, a factor more observed in the D-M3 model, where there is a less dense drainage network. In events in catchments without a lake, the asymmetry of the RWF is likely to be positive (Mutzner *et al.*, 2016). The difference in peak time in different models is more noticeable when there is a significant difference between stream and hillslope celerities.

Figure D 1 - Drainage networks generated from the proposed methodology: (a) Relationship between area and slope of springs mapped in the field; (b) Variation of the area and slope of the set of springs mapped in the field. In each boxplot, the central mark indicates the median, and the lower and upper edges of the box indicate the 25th and 75th percentiles, respectively. The whiskers extend to the most extreme data points not considered outliers; (d) Active groundwater drainage network and active surface runoff drainage network using three different methodologies (D-M1, D-M2, D-M3); (e) Width function plotted for each drainage network generated using three different methodologies.
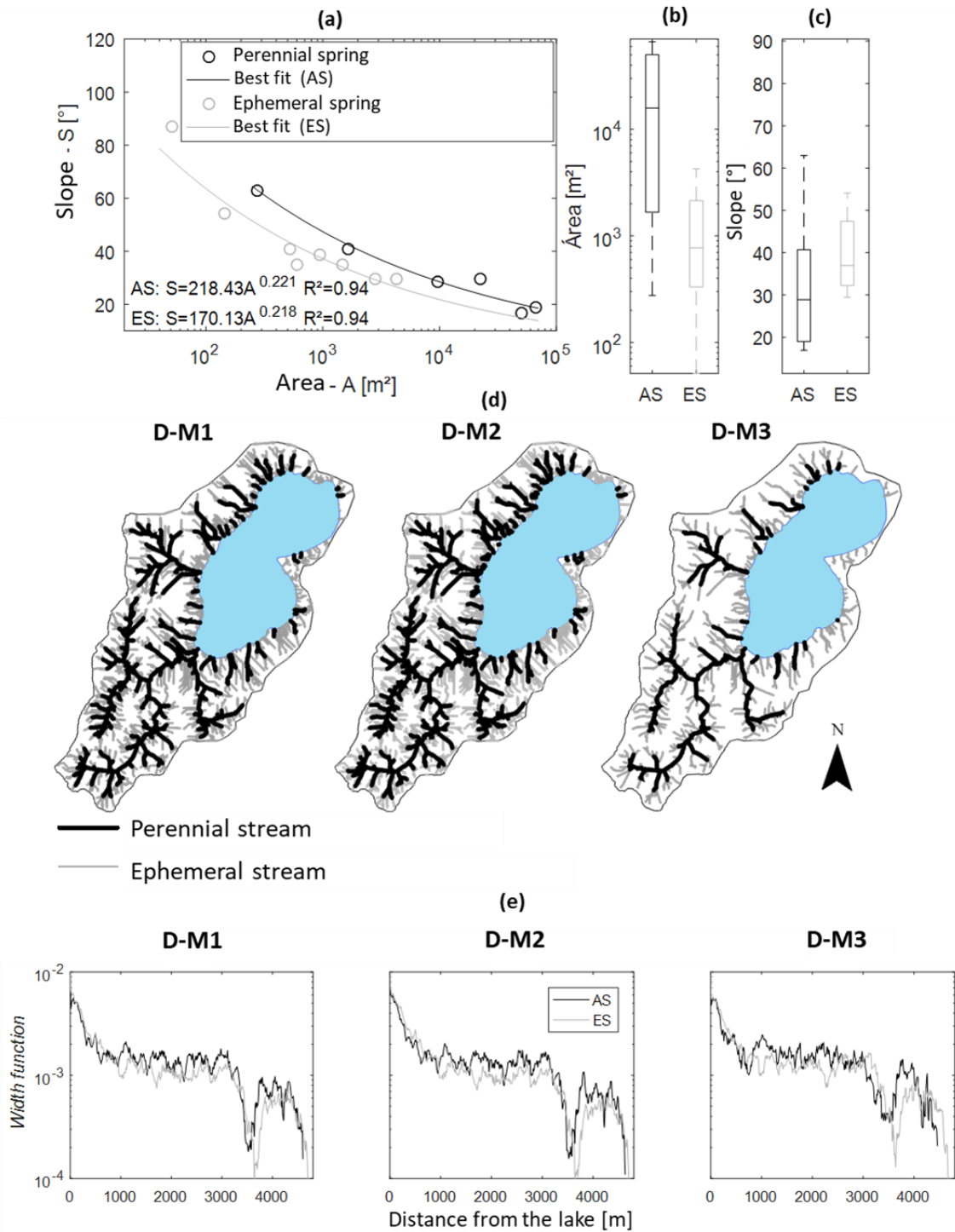
Table 18D – Drainage network characteristics. Where AS is perennial drainage and ES is ephemeral drainage.

Method	Type of drainage	Drainage density [km/km²]	Order	Length of the longest stream [km]	Underestimated channels	Overestimated channels
D-M1	AS	3.18	4	4.60	1	4
	ES	15.56	6	4.77	0	15
D-M2	AS	3.81	4	4.63	0	5
	ES	19.96	6	4.78	0	16
D-M3	AS	1.55	4	4.46	10	0
	ES	6.81	5	4.67	1	0

Figure D 2 - Points checked to validate drainage network generation models.
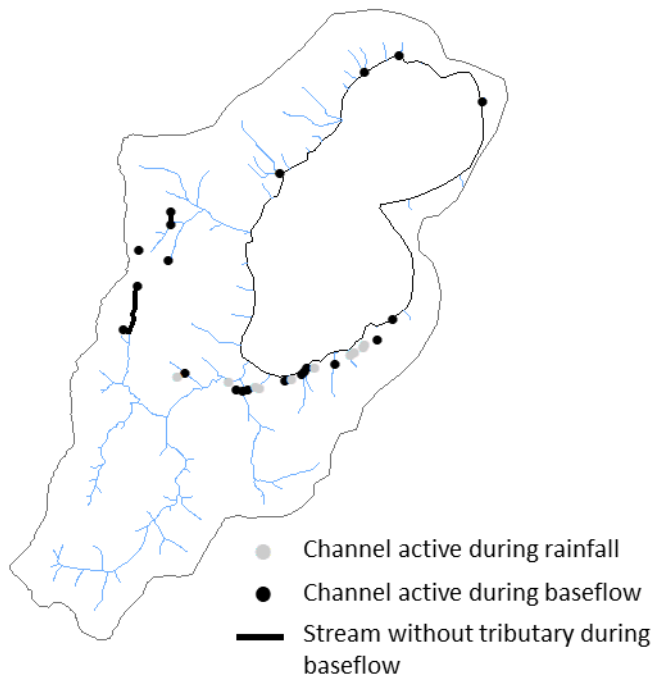
Figure D 3- Distance from the hillslope to the stream for different drainage network generation models. Where L_h is the distance from the hillslope to the stream, $L_{h,máx}$ is the maximum distance from the slope to the stream, σ is the standard deviation, AS is active drainage with groundwater, ephemeral drainage, and ES is active drainage with surface runoff, perennial drainage.
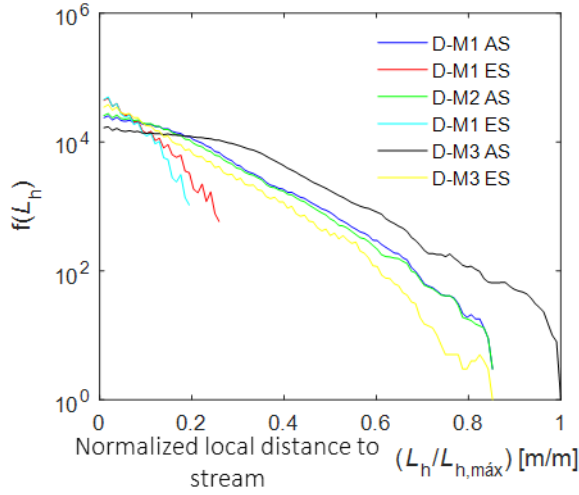
	L_h [m]	σ [m]	$L_{h,máx}$ [m]
D-M1 AS	129,1	126,6	927,8
D-M1 ES	56,5	58,2	282,8
D-M2 AS	118,9	122,9	927,8
D-M2 ES	49,4	46,5	212,1
D-M3 AS	193,4	158,8	1080,5
D-M3 ES	87,0	108,8	920,7

Figure D 4 - Rescaled width function with different velocities for the hillslope (u_h): (a) u_h is 0,20 m s^{-1}; (b) u_h is 0,10 m s^{-1} e; (c) u_h is 0,04 m s^{-1}.
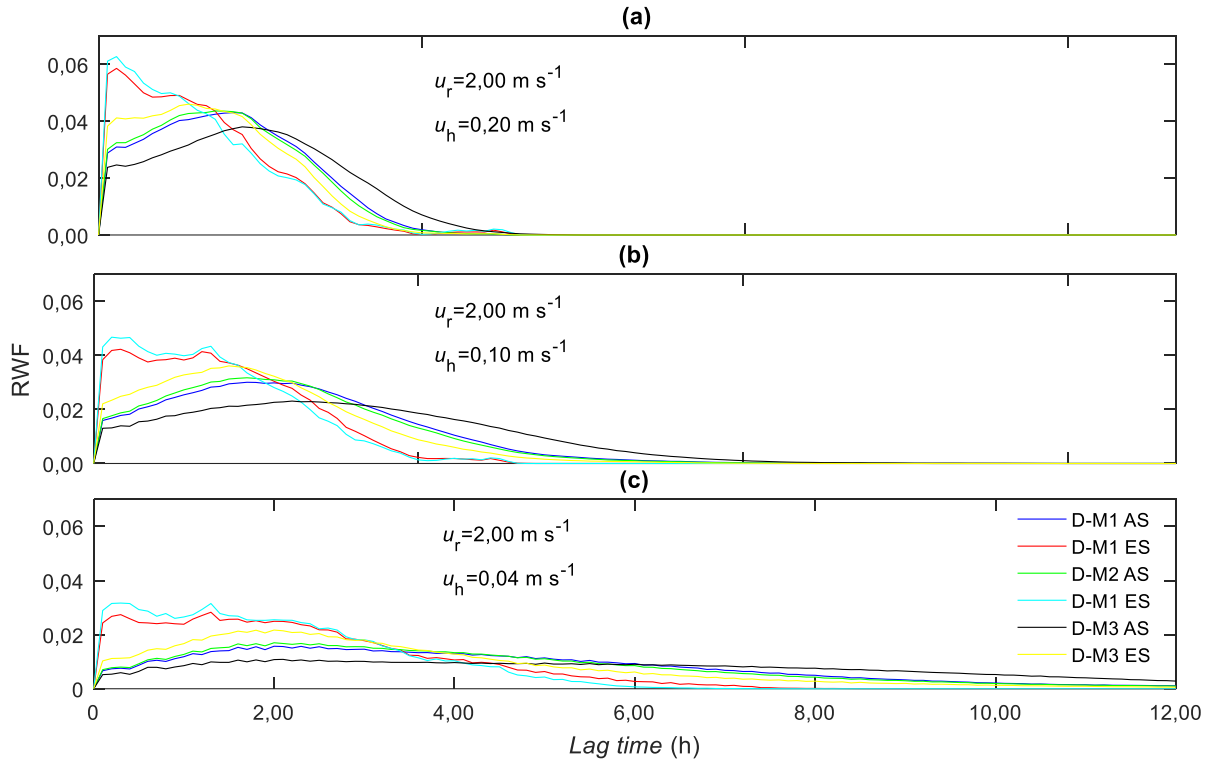
4D DISCUSSION

It is evident that groundwater springs require different conditions to emerge compared to surface runoff springs, confirming that initiation processes are of a different nature (Henkle; Wohl; Beckman, 2011; Montgomery; Dietrich, 1989). Groundwater springs have lower values of local slope compared to surface runoff springs, but local slope alone is not a sufficient criterion to differentiate the two spring groups (Mutzner *et al.*, 2016). Slope environments, such as the case of all monitored springs, are challenging to represent, in part because it is difficult to define the beginning of each channel and because the processes of surface runoff generation that lead to channel formation are complex and dependent on soil characteristics (Perez *et al.*, 2020). Given the high variability in area and slope of the springs, our results confirm that a single threshold for spring identification may not exist, even at the catchment scale (Garrett; Wohl, 2017; Grieve *et al.*, 2018; Henkle; Wohl; Beckman, 2011; Mutzner *et al.*, 2016).

The observed drainage density in the field is quite heterogeneous. The slopes to the east of the catchment have many ephemeral streams, and this was satisfactorily represented by the models since models employing slope and area as criteria for spring occurrence were used. Methods using the median slope and area of the monitored springs overestimated the drainage network, and the thresholds that would represent a drainage network more similar to reality should be higher than the median of the mapped springs.

Regardless of the method used, the generated drainage network density is higher than in literature works, even during baseflow (Godsey; Kirchner, 2014; Mutzner *et al.*, 2016; Whiting; Godsey, 2016). This is because in hillslopes, where there is a higher slope, less drainage area is needed for the formation of a channel. Much of the land draining to the lake consists of steep hillslopes, affecting the shape of the width function (Figure D 1e). Typically, the width function has a shape similar to a logarithmic probability density function (Cudennec, 2007; Di Lazzaro, 2009; Mutzner *et al.*, 2016). In other words, many channels would be at a short distance from the lake. The difference in $f(L_h)$ in different models (Figure D 3) is greater than in the width function (Figure D 1), so the impact of choosing the drainage network seems to be more crucial in small catchments, where slope displacement is predominant.

The Rescaled Width Function (RWF) is sensitive to drainage network generation methods. The largest discrepancies between RWF are from the model that generates a less dense drainage network. There is a significant difference between the RWF generated for groundwater

and surface water drainage networks, which can affect hydrological modelling. It is likely that methods using area and slope as extraction criteria tend to underestimate the distances between the slope and the channel since these methods are valid assuming landscape equilibrium (Mutzner *et al.*, 2016), which is not the case on hillslopes (Garrett; Wohl, 2017; Henkle; Wohl; Beckman, 2011; Perez *et al.*, 2020).

5D CONCLUSION

In this Appedix, we analysed the influence of different drainage networks on common geomorphological parameters, such as the distance from the hillslope to the stream and the rescaled width function. Springs were mapped in the field. We compared different active drainage networks with baseflow or surface runoff, obtained with three methods based on the slope and accumulated area of the mapped springs. The results indicate that the drainage network generation model using the largest drainage area and steepest hillslope among the mapped springs as thresholds was the most realistic. The difference in drainage density in the network generated by groundwater is always, regardless of the method, about 20% of the drainage density when surface runoff occurs. For all methods, the catchment increases by at least one Strahler order when compared to drainage with ephemeral or only perennial streams.

This study can help understand how catchment drainage expands under the effect of rainfall and connects hillslopes to streams through overland flow. Additionally, it showed how the choice of different drainage generation models can affect the geomorphological unit hydrograph.